# MECHANISMS OF DISSOLVED Zn AND Cu RETENTION BY MUSSEL SHELLS IN A RAPID-FLOW STORMWATER TREATMENT SYSTEM.

A thesis submitted in partial fulfilment of the requirements for the degree of Master of Water Resource Management

By

Rachel Anne Skews.

Waterways Centre for Freshwater Management

University of Canterbury

Christchurch, New Zealand

2021

# ABSTRACT

Dissolved zinc ($Zn_{diss}$) and copper ($Cu_{diss}$) are a threat to aquatic life, but continue to enter urban waterways largely via stormwater passing over the roofing and cladding materials ubiquitous in the urban environment. Typical stormwater treatment is aimed at removing particulates, so a retrofittable inline downpipe device was developed (the Storminator™) to remove dissolved metals from roof runoff prior to it reaching the stormwater network. The device with its waste seashell media inside had previously been shown to be effective at removing $Zn_{diss}$ and $Cu_{diss}$ (>80% removal for both metals), but the mechanisms of removal were unconfirmed.

Research into metal retention mechanisms by biogenic calcium carbonate ($CaCO_3$) such as seashells had so far been limited to higher metal concentration solutions and longer contact times than are relevant to the Storminator™ system. In addition to this, modelling to predict removal mechanisms carried out prior to this research was largely confined to mathematical correlation, with no basis in potential geochemical causal pathways. Therefore, this study aimed to determine the dominant Zn and Cu removal mechanisms occurring in a Storminator™ style system, using geochemical modelling to augment chemical and spectroscopic methods of analysis.

Geochemical models, such as PHREEQC, can predict when a mineral will be oversaturated in a given solution, or adsorbed to a surface such as hydrous ferric oxide (HFO), by balancing known thermodynamic equations for their formation. Therefore, predictions of how much $Zn_{diss}$ or $Cu_{diss}$ could be removed from solution by those mechanisms were made using PHREEQC. These predictions were validated against $Zn_{diss}$ and $Cu_{diss}$ reductions measured in flow-through column experiments, and evidence of either mechanism was sought through analysis of used shells. Shells which had been exposed to high loads of Zn or Cu were subjected to a sequential extraction procedure (SEP), which is designed to release elements bound in one specific chemical phase at a time. The shells were also analysed by scanning electron microscopy coupled with energy dispersive X-ray (SEM-EDS), to look for evidence of precipitates or adsorption by visual identification of particulates and elemental concentration mapping.

Flow-through column results showed reductions of 73%–97% for $Zn_{diss}$ and 55%–82% for $Cu_{diss,}$ for concentrations typical of roof runoff, and that ranged over 2 orders of magnitude ($Zn_{diss} \approx$ 0.3–3 mg/L, $Cu_{diss} \approx$ 0.5–3 mg/L). PHREEQC geochemical modelling suggested that no stable Zn minerals were predicted to form at the measured pH, while $Cu_{diss}$ could have been reduced by up to 99% by precipitation of Cu hydroxide carbonate minerals. Further PHREEQC modelling suggests there was insufficient HFO present for adsorption onto this mineral to be a dominant removal mechanism for Zn or Cu.

The sequential extraction of used seashell media released the largest proportions of Zn from the “carbonate” fraction. Cu was predominantly released from both the “carbonate” and “Fe oxides” fractions, though it appeared that larger proportions of Cu and Zn were released in the “Fe oxides” fractions when total Cu or Zn concentrations on the shell were low.

SEM-EDS analyses of used media rarely highlighted ‘hotspots’ of high concentrations of Zn or Cu, instead generally showing low levels uniformly spread through the shell structures. The rare SEM-EDS analyses where Zn was concentrated in visible particles were of shells that had been exposed to high

initial Zn concentrations (27 mg/L Zn), and these appeared to be either hydrozincite (a Zn hydroxycarbonate) or a Zn/Na/Al/Si based compound.

Results suggest that adsorption to the calcium carbonate shell surface dominates removal mechanisms for Zn, and that the formation of surface precipitates is likely where influent Zn concentrations are high. The formation of Cu hydroxycarbonates is likely to be the dominant mechanism for $Cu_{diss}$ removal, though the relative importance of aqueous precipitation of such minerals, and their formation on the shell surface via adsorption to the $CaCO_3$, was less clear. The role of adsorption to other surfaces, such as organic material, HFO and aluminosilicates, in the removal $Zn_{diss}$ and $Cu_{diss}$ appeared to increase in importance as dissolved Zn and Cu concentrations decreased.

Implications for the optimisation of a Storminator™ type device include: maximising the shell surface area by minimising the shell fragment size, and increasing the runoff retention time within the device. However, these will be constrained by the hydraulic conductivity requirements of the inline system. Results suggest that the lifespan of the device is likely to be limited by operational factors rather than the availability of adsorption sites, so estimations of lifespan should be based on future field trials. Extension of the device lifespan may be possible by re-packing, or by regeneration of the media with EDTA or a low concentration weak acid, which should be investigated in further study.

# ACKNOWLEDGEMENTS

I am incredibly grateful for the support, guidance and encouragement from many people, without whom I could not have completed this thesis:

My chemistry and main supervisor Jenny Webster-Brown, for your unwavering faith in my abilities, for your detailed, considered and always constructive feedback, and for the friendly and open discussion we could have.

My engineering supervisors Frances Charters, Aisling O'Sullivan and Tom Cochrane, for your friendly support, willingness to include me in the team, and to put me in touch with whatever support I needed, for the variety of feedback styles, and the opportunity to contribute to a wider team project.

The Waterways administrator 'Camp Mother' Suellen Knopick, for your enthusiasm and personal care for all of us postgraduate students. In spite of the many bureaucratic and personal hurdles we faced it was never too much trouble for you to help us onto the right path.

The senior lecturers and other postgraduate students in Waterways, for your willingness to share and discuss your thoughts at our group sessions or outside it. In particular Marlese Fairgray for imparting what tips on modelling and sequential extractions she could before departing after her own PhD.

The technical staff of the Environmental Lab in the CNRE Peter McGuigan and Aude Thierry, for your positive and practical guidance (on science and life!), shared stories, and for building my experimental columns. The Waterways technical staff John Revell, for your guidance in tricky chemical analyses and chats about the whole chemistry thing.

The Hydroeco group at the Civil and Natural Resources Engineering (CNRE) department, in particular Will Heffernan and Elise Howe for some used shells and associated data from their accelerated loading experiments, and Forrest Bilek, Sergio Hansen and Julian Maranan for assistance with sampling field columns and provision of real roof runoff.

Technical staff at the Chemistry department Nathan Alexander and Rob Stainthorpe, for your assistance with or running of the IC and ICP-MS, and in the Mechanical Engineering department Shaun Mucalo for operation of the SEM-EDS.

Funding for the completion of this thesis was gratefully received from the Waterways Centre for Freshwater Management Masters Scholarship, and the University of Canterbury Masters Scholarship.

My friends, old and new and too many to name, for your genuine interest in what I was doing, in many cases your personal understanding of what I was going through, and regardless, your encouragement to achieve what I think important in life.

Finally, and crucially, my parents Pam and Terry, and my brother Mark, for raising me to have such confidence in myself that I can achieve whatever I set my mind to, for being open to a chat whenever, and for your support through the life change that is quitting full time work and making the most of 4 years of part time study/part time work.

# TABLE OF CONTENTS

## LIST OF FIGURES

## LIST OF TABLES

# 1 INTRODUCTION

Urban waterways hold important aesthetic and ecological values, as well as forming an integral part of the wellbeing of communities from a cultural perspective. This holistic value of a water body to the indigenous communities of New Zealand, for example, is recognised in NZ freshwater legislation as Te Mana o te Wai (National Policy Statement for Freshwater Management (NPS-FM), 2020). That framework derives from Te Ao Māori (the Māori worldview) that the holistic health of the community is linked to the holistic health of the water (NPS-FM, 2020). However, these values are degraded in urban waterways by the very process of urbanisation (Liu et al., 2015b). Rain falling on impervious surfaces becomes runoff, and the increased area of impervious surface concomitant with urbanisation means that the overall volume of stormwater (runoff from all sources) is increased as it cannot dissipate through the ground (Liu et al., 2015b). The ecosystem health, cultural and aesthetic values of the urban waterways which form the receiving environment for this stormwater are therefore threatened by potential flooding and erosion of stream and road banks. Those same values are also threatened by the chemical quality of runoff, which is mainly impacted by the introduction of contaminants from the surfaces the rain comes in contact with along its drainage pathway.

Organic carbon and nutrients (nitrogen and phosphorus) arise from degrading plant matter, animal waste, and fertiliser, and large quantities of suspended sediment can be washed into stormwater in relatively short time periods from soils, cement and bricks from the construction industry (Liu et al., 2015b). Polyaromatic hydrocarbons (PAHs) are emitted from vehicles via brake and tyre degradation and exhaust emissions, as are zinc (Zn) and copper (Cu) (Charters et al., 2016; Egodawatta et al., 2013; Liu et al., 2015b; Mancinelli et al., 2015). However corrosion of galvanised or copper roof, guttering, and cladding material is the key source of Zn and Cu (respectively) in runoff (Brown & Peake, 2006; Charters et al., 2016; Liu et al., 2015b; Mancinelli et al., 2015).

These contaminants reduce the ability of the aquatic ecosystem to thrive, whether by direct toxicity, eg. ecotoxic heavy metals, or by alteration of the habitat, eg. nutrients promoting algal blooms which block light and alter dissolved oxygen (DO) concentrations (Simon, 2002). Where the health of the aquatic ecosystem declines, the cultural and aesthetic value of the waterway declines too, so a reduction in contaminants reaching urban waterways supports a range of values and uses for the waterways. Therefore, it is critical to reduce the contaminant load in runoff that reaches the waterways.

## 1.1 METAL CONTAMINANTS IN ROOF RUNOFF

There are several heavy metals that are commonly present in urban stormwater (for example zinc (Zn), copper (Cu), lead (Pb), cadmium (Cd)), but Zn and Cu are of particular concern due to their ubiquitous presence in urban areas and their toxicity in the aquatic environment (ANZG, 2019; Davis et al., 2001; Liu et al., 2015b; Makepeace et al., 1995). While runoff from roading and particular industrial land uses contribute Zn and Cu to the total urban stormwater load, roof runoff on its own can contribute very high concentrations to the stormwater, and so has been the subject of specific study.

In a review of >70 international studies on runoff quality that included roof runoff specifically, Göbel et al. (2007) identified 5–15 studies (specific number not reported) that included data for roofs specifically made of Zn or with Zn gutters and/or downpipes. From this data they calculated a maximum event mean total Zn concentration of 4800 µg/L, and average concentrations of 6000 and 1851 µg/L for runoff from Zn roofs and Zn gutters/downpipes respectively. Davis et al. (2001) reported mean total Zn concentrations in runoff from institutional or commercial roofs of 1100 µg/L (Maryland, USA), and McIntyre et al. (2019) reported up to 809 µg/L total Zn in runoff from Zincalume® roofing (Washington, USA). From galvanised roofs in Christchurch, NZ, Wicke et al. (2014) reported maximum total Zn concentrations of 7900 µg/L in first flush runoff. Charters et al.'s 2016 study reported a maximum total Zn concentration of 1970 µg/L in runoff from galvanised roofing and a mean of 397 µg/L, which placed local (Christchurch, NZ) Zn roof runoff concentrations generally in the low to mid-range internationally. However, Charters et al. (2021) report total Zn concentrations of up to 56000 µg/L from uncoated Zn roofing that is >25 years old. This showed that exceptionally high Zn concentrations may be leached from old, deteriorated Zn roofing, and this correlation between older (originally coated) roofing and higher metal leaching is also supported by the studies by Wicke et al. (2014) and McIntyre et al. (2019).

Göbel et al. (2007) extracted average total Cu concentrations of 2600 µg/L in runoff from copper roofing from the 5-15 relevant studies in their review (specific number not reported). For runoff from institutional roofs Davis et al. (2001) reported mean total Cu concentrations of 5000 µg/L, while McIntyre et al. (2019) reported a maximum total Cu concentration of 2250 µg/L from copper roofing and even up to 549 µg/L from roofing that incorporated CCA treated wood (copper chromated arsenate). For runoff from copper roofing in Christchurch, NZ, Charters et al. (2016) reported total Cu concentrations of up to 7860 µg/L, with a mean of 1663 µg/L, while Wicke et al. (2014) reported even higher concentrations in first flush runoff, of up to 13800 µg/L.

### 1.1.1 COMPARISON WITH RECEIVING WATER Zn AND Cu LIMITS

While there is no standard defining maximum allowable contaminant concentrations in runoff in NZ, general guideline values for the protection of aquatic species in NZ waterways do exist (ANZG, 2019, an online updated database founded on previous guidelines known as ANZECC (2000)), and a regional council may set their own contaminant limits for ecological protection of the waterways in its region which receive the runoff.

The ANZG guidelines offer trigger values for toxicants at four levels of ecosystem protection, the 95% (of species protected) level being identified as the ideal target for "highly disturbed ecosystems" such as urban waterways (ANZG, 2019). The concentrations of Zn and Cu that would allow for this 95% protection in freshwater are 8.0 and 1.4 µg/L respectively (ANZG, 2019). Environment Canterbury (2019) in its Land and Water Regional Plan (LWRP) has set limits of 15 and 1.8 µg/L for Zn and Cu respectively in spring-fed urban plains waterways, such as those throughout Christchurch, which was the location of the study sites in the 2016 and 2021 Charters et al. studies.

There are several caveats to comparing runoff concentrations with receiving water contaminant limits, the first being that runoff will be diluted upon entering the receiving waterway. Comparison to the guideline or limit values should also be based on bioavailable concentrations (eg dissolved), and ANZG guidelines may also be adjusted by site specific alkalinity measurements, in recognition of the role

alkalinity plays in reducing the bioavailability of a metal (ANZG, 2019). However, where necessary total metal concentrations can be used as a start point, and it should also be noted that a change in water quality parameters could induce the release of previously less bioavailable forms, so comparison with total concentrations may be pertinent in some cases (ANZG, 2019; Mancinelli et al., 2015).

Notwithstanding the caveats, comparison of runoff concentrations with ecological protection limits can give a useful insight into the environmental toxicity of the runoff. Even when using the higher of the two limits for either metal for comparison, the roof runoff Zn and Cu concentrations reported above are up to 3 orders of magnitude above those limits. This suggests that the roof runoff has Zn and Cu in potentially ecologically damaging concentrations, and this will be of greater concern where there is a higher proportion of copper and zinc based roofs, particularly where these roofs are older.

### 1.1.2 METAL SPECIATION

The speciation of the metal has a large impact on its toxicity in the environment, with dissolved or weakly complexed species being more bioavailable than particulate or strongly bound species. The form of the metal also influences what removal techniques may be effective, so for these two reasons an understanding of the metal speciation and what impacts this is critical.

Metal concentrations are commonly divided into two forms: dissolved, and particulate (sediment bound and precipitated). It is important to note that there is sometimes overlap between dissolved and particulate forms. There can be large fractions of sediment that are sizes very close to the 0.45 µm upper limit for what is considered dissolved (Andral et al., 1999). Nonetheless these smaller particles require different processes to remove them than those designed for larger, settleable particles so the distinction remains useful (Stumm & Morgan, 1995)

#### DISSOLVED

Zn and Cu in roof runoff are predominantly present in a dissolved form, although compared to Zn Cu is likely to have a lower proportion of its total concentration present as a dissolved form (Athanasiadis et al., 2004; Charters et al., 2021; Pennington & Webster-Brown, 2008). Stormwater that includes runoff from other surfaces such as roads can have much lower proportions of dissolved Zn and Cu compared to particulate (Charters et al., 2021; Mancinelli et al., 2015).

The category of dissolved metals includes a number of forms, from free ions to metal complexes with a variety of ligands, to colloids (Gnecco et al., 2008; Guéguen & Dominik, 2003; Stumm & Morgan, 1995).

Free metal ions are also known as hydrated metal ions, due to the water molecules that complex the metal when in an aqueous solution (Gnecco et al., 2008). These metals are considered truly dissolved and are the most bioavailable form, and hence the most toxic in the aquatic environment (Gnecco et al., 2008).

Carbonates, oxides, and hydroxides are common ligands available in natural waters, and form sparingly soluble metal complexes (Stumm & Morgan, 1995). If the concentration of the complex exceeds its saturation limit the metal oxide/hydroxide/carbonate may precipitate from solution, and thus partition to the particulate phase. However considering the relatively low concentrations of metals in roof runoff (typically µg/L), these minerals may not exceed their saturation concentration in

this context. They would therefore remain in a dissolved form, albeit a strongly complexed one that is considered less bioavailable than other dissolved forms (Stumm & Morgan, 1995). The metals may form complexes with other ligands (such as phosphate or sulphate), and the same distinction between particulate and dissolved forms based on saturation applies, though these ligands tend to have much higher saturation concentrations and so are more likely to be present in a dissolved form.

Colloids that pass through a 0.45 µm filter are also considered dissolved and remain suspended in the water column for extended periods of time, though their behaviour can be more difficult to define as given enough time they may aggregate and start showing behaviour closer to that of a particulate (Guéguen & Dominik, 2003).

Each metal will show a different preference for the dissolved species that dominates, as well as being influenced by the characteristics of the water (Gnecco et al., 2008; Mancinelli et al., 2015). Cu often forms complexes with fulvic acids (being a dissolved form of organic carbon), or carbonates (Gnecco et al., 2008; Mancinelli et al., 2015). Zn however is often found as $Zn^{2+}$, or in a less preferred complex with sulphate (Gnecco et al., 2008).

#### PARTICULATE

Studies detailing the particulate metal fraction in roof runoff specifically are rare, as the predominant form of Zn or Cu in this matrix is dissolved. However newer research by Charters et al. (2021) reported higher percentages of particulate Zn and Cu in roof runoff than other studies (up to 35%), and that the partitioning varies depending on the roof type. So, it is worthwhile considering the form and behaviour of the particulate metal forms, which could include: metal fragments and other corrosion products from the degradation of the roof; sediment bound (adsorbed) forms; and precipitated particles.

Insight into how the particulate metal fraction in roof runoff may behave could be offered by studies into the behaviour of metal fraction in other urban stormwater. That smaller particles have a larger specific surface area is well known, and this therefore has implications for heavy metal adsorption (Liu et al., 2015b). The particle size also influences transport, of the sediment and therefore the heavy metals, due to the smaller particles having lower sedimentation speeds thus making them more mobile (Andral et al., 1999; Liu et al., 2015b). Large proportions of sediment in stormwater have been found to be very fine and have the larger proportion of metals attached to them: Herngren et al. (2006) and Gunawardana et al. (2014) found most bound metals were bound to sediment <150µm, and Gunawardana et al. (2014) found this to make up 70% of road deposited sediment; Andral et al. (1999) calculated that approximately 75% by weight of sediment was from particles <50µm, and found 90% of Cu and Zn bound to particles <100µm. Therefore we can see that sediment bound metals are nonetheless likely to be highly mobile.

As explained above, metals may also partition to the particulate phase by forming low solubility complexes with ligands they encounter in the runoff, and precipitating out of solution. This is more likely to result in precipitation (as opposed to a strongly complexed dissolved compound) in water with a raised pH or alkalinity (ANZG, 2019; Sansalone & Buchberger, 1997; Wicke et al., 2012).

### 1.1.3 INFLUENCES ON METAL SPECIATION

As the dissolved species of metals are more bioavailable and difficult to remove than particulates, treatment of a water to remove metals typically centres on facilitating the transition of the metal from

a dissolved to particulate form. There are two main pathways to achieve this: adsorption to a solid surface; and precipitation. The main influences on adsorption and saturation (the prerequisite for precipitation) are therefore discussed below.

## ADSORPTION TO A SURFACE

Adsorption of a metal to sorbent can refer to numerous mechanisms including ion exchange (replacement of ion attached to or within a sorbent), chemisorption (addition of ion attached to sorbent), and surface precipitation (formation of precipitates on the sorbent surface, as opposed to in the bulk liquid, also known as micro precipitation) (Robalds et al., 2016). In many literature papers the terms are confused (Robalds et al., 2016), however on a broader scale these mechanisms are all generally discussed as concurrent processes in stormwater treatment and are influenced by similar physico-chemical parameters (Dierkes et al., 2006; Kammerer et al., 2011; Volesky, 2001).

Given the tendency to adsorb to sediment discussed above, it follows that increased sediment concentrations, particularly of smaller (but not less than 0.45 µm) particles, can promote metal partitioning to the particulate phase.

The key parameter that influences adsorption, whether to a suspended particle in the water or to a surface the stormwater comes into contact with, is the type(s) of functional group(s) available on the surface of the sorbent (Demirbas, 2008; Volesky, 2001). Oxic natural sediments typically contain oxygen (O) bearing functional groups, such as —OH and —COOH, that metals can form complexes with (such as —OM where M is a metal) (Stumm & Morgan, 1995). Oxides of iron (Fe), manganese (Mn), aluminium (Al), and silicon (Si) constitute a high proportion of natural sediments and when in aqueous solution their surfaces are covered with —OH groups making them important adsorbing surfaces (Stumm & Morgan, 1995). Organic carbon sources such as naturally occurring humic and fulvic acids can also contribute to the adsorption capacity of a sediment with surface groups such as —COOH, and other C-O based groups (Stumm & Morgan, 1995).

An important consideration regarding the availability of adsorption sites for metal binding on a surface is that it varies with pH. As can be seen from the example equilibrium below (where ≡ denotes an attachment to a surface), the lower the pH the more the equilibrium will be driven towards protonated functional groups, and therefore away from the adsorbed metal form (metals in the particulate phase) and towards an ionic aqueous form (metals in the dissolved phase) (Stumm & Morgan, 1995).

$$\equiv OH + M^{2+} \leftrightarrow \equiv OM^{+} + H^{+}$$

Additionally, the concentration of the metal ion in solution will also impact on the direction of the equilibrium reaction, and therefore on the amount of metal adsorbed to the surface or dissolved in solution (Abdulaziz & Musayev, 2017). Where metal ions are adsorbed to the surface in close proximity this can create an increase in their local concentration, and if this surpasses the saturation concentration for a metal complex then surface precipitation of that complex may occur.

This is a competitive reaction so where multiple ions (metal or otherwise) are present, and each with a different equilibrium constant for its reaction with the surface group, different metals will be complexed with the surface groups to a different extent (Abdulaziz & Musayev, 2017). The length of time a solution remains in contact with the sorbent is another factor that can influence adsorption as thermodynamic equilibrium may not occur instantaneously.

Finally it is worth noting that the redox conditions at the surface-water interface can also influence the form of the surface functional groups, and thus the attraction between the surface and a metal (Stumm & Morgan, 1995).

#### SATURATION- PRECIPITATION

As discussed earlier a dissolved complex may partition to the particulate phase via precipitation, if the concentration of that complex exceeds its saturation concentration. The degree of saturation of a complex is controlled by the equilibrium equation for its formation, for example in the equation below. It shows that an increase in pH, ie. an increase in the concentration of $OH^-$, would drive the equilibrium towards the formation of the hydroxide product so long as sufficient free metal ions were also present. Hence, the dissolved concentrations of both the metal and the ligand influence the degree of saturation with respect to their complex.

$$M^{2+}_{(aq)} + OH^-_{(aq)} \leftrightarrow M(OH)_{2\,(s\ or\ aq)}$$

Similarly to adsorption, the presence of other ligands and metals creates competition, and also increases the number of complexes (often referred to as minerals in natural systems) that could form. Therefore, the complete chemical composition of the water can influence the types of complexes that may form, their degree of saturation, and therefore the possibility of metals precipitating out of solution.

It is not only the metal composition of stormwater that can be influenced by the surfaces over which the stormwater flows (as mentioned earlier), but other components as well: pH and alkalinity are notable examples of parameters that can be raised by the stormwater passing over concrete which is ubiquitous in urban settings (Gnecco et al., 2008; Sansalone & Buchberger, 1997; Wicke et al., 2012).

## 1.2 METAL REMOVAL METHODS

Whether in natural or manmade (including wastewater and stormwater treatment) systems, heavy metals can be removed from waters via mechanisms requiring varying degrees of active resource or energy input. To cope with the volume and physical spread of stormwater, its treatment needs to be largely passive so only those that require minimal ongoing input are discussed below.

### 1.2.1 SEDIMENTATION

Stormwater treatment usually includes a method of slowing water flow to increase water retention time, possible via numerous structures such as wetlands, sedimentation ponds, rain gardens, and swales, all of which encourage sedimentation (Fletcher et al., 2013; Liu et al., 2015a). Where metals are predominantly present as a particulate, for example in road runoff, sedimentation can make large reductions in metal concentrations in the stormwater, particularly as retention times increase (Carpenter et al., 2014; Mancinelli et al., 2015). However this method is unlikely to produce a significant reduction in dissolved metal concentrations, so is less suitable for treating roof runoff.

### 1.2.2 FILTRATION

Filtration is another method of removing the particulate phase of the metal. In many stormwater treatment systems the filter is soil and is termed infiltration, for example in swales or rain gardens

where the water percolates downwards and the soil filters out the particulates (Dierkes et al., 2006; Fletcher et al., 2013). It can also be a method of reducing the dissolved phase if other (chemical) mechanisms occur within a filtration bed, such as precipitation and adsorption (these are discussed separately).

### 1.2.3 BIO-UPTAKE

Plants uptake nutrients through their roots from the surrounding soil and water, and as the binding sites for these nutrients are not specific enough to exclude toxic metals, where present these are taken up into the plant tissues (Stumm & Morgan, 1995; Weiss et al., 2006). This can be effective for the removal of dissolved metals, and this removal pathway is taken advantage of in wetlands where large spaces of growing plants and a long hydraulic retention time are key parts of the system.

### 1.2.4 PRECIPITATION

In passive stormwater treatment systems, concrete surfaces, waste shellfish shells and calcareous soils (eg incorporated in a rain garden), have been credited with raising the pH and alkalinity of passing water, thus promoting the precipitation of metal carbonates and hydroxides from dissolved metal ions (as described earlier) (Davies et al., 2010; Dierkes et al., 2006; DiLoreto et al., 2016; Du et al., 2011; Good et al., 2014; Plassard et al., 2000; Uster et al., 2015). Precipitation can take place in the bulk solution based solely on dissolved ligand concentrations, though it has also been suggested that precipitation can occur on the surface of sorbents such as activated carbon (Reed et al., 1994).

### 1.2.5 ADSORPTION

As stormwater flows over impervious surfaces it can pick up sediment/particulates that become suspended, and there are several types of this suspended sediment that can provide favourable adsorption sites for metals.

Clays present in soil sediments have aluminol and silanol groups that make good sorption sites for heavy metals (Stumm & Morgan, 1995). Organic carbon present as humic and fulvic acids in soil sediment can act as the sorbent, with its hydrophilic oxygen containing surface groups that favour heavy metal adsorption (Mancinelli et al., 2015; Shim et al., 2001). Oxygen containing surface groups are also provided on Fe hydroxide particulates (section 1.1.3), which can be expected to be present in urban stormwater from the corrosion of steel building materials (Asahi, 2014; Kajimura, 2014; Stumm & Morgan, 1995).

Common stormwater treatment systems, such as detention ponds and wetlands, largely rely on metals already being adsorbed to suspended sediment and that sediment being trapped in the system (Christchurch City Council, 2012). However there is acknowledgment that they may facilitate direct adsorption of dissolved metals to humic substances in the soil, or via transfer from a biofilm (Christchurch City Council, 2012). It should also be noted that the release of humic and fulvic acids from soil can also decrease the pH, and therefore promote the (re)dissolution of previously adsorbed metals (Good et al., 2012).

## 1.3 THE USE OF ALKALINE BIOSORBENTS TO REMOVE METALS

In recent years the use of biogenic $CaCO_3$, such as mussel, oyster, snail, shrimp, arca, and crab shells, has gained attention as an effective biosorbent for heavy metals in wastewaters and stormwater, with the added advantage of using a waste material from the seafood industry (for but a few examples see Dahiya et al., 2008; Good et al., 2014; Hossain & Aditya, 2015; Londono-Zuluaga et al., 2019; McCauley et al., 2009; Wu et al., 2014). Mussel shells in particular have been found to reduce dissolved metal concentrations by 87%-99% in treatment systems for acid mine drainage (DiLoreto et al., 2016; Uster et al., 2015). However, this is a concentrated waste stream and the predominant contaminant metals are Fe and Al, so direct applicability of results to Cu and Zn in roof runoff treatment should not be assumed.

In a stormwater context, a report prepared for Auckland Regional Council by Craggs et al. (2010) identified crushed mussel shells as both a common waste product from the New Zealand commercial shellfish industry, and a promising media for retention of heavy metals from stormwater when incorporated into rain gardens. In the published literature, Good et al. (2014) investigated the impact of mussel shells on the removal of Cu and Zn from stormwater, via shell addition to topsoil in a series of large laboratory rain gardens. They found that total Zn removal could be up to 80%, though Cu at most only 55%, and for both they were more effectively removed when the ratio of mussel shell to soil was higher. For the output of the rain gardens the authors calculated hardness adjusted trigger values based on the ANZECC (2000) guidelines, and found the effluent concentrations of Zn to be below the 90% trigger values for the higher (1:1) ratio mussel shell:soil mixtures. Cu still exceeded the trigger values but by far less in the higher ratio mixture.

Given the ecologically very high concentrations of Zn and Cu in roof runoff specifically, and the promising results from using mussel shells as a filter medium, removal of these metals was targeted in the design of a retrofittable inline downpipe filtration device packed with mussel shells, designed by researchers at the University of Canterbury (T. Cochrane, A. O'Sullivan, and F. Charters) and trademarked as the Storminator™. The efficacy demands of this device are unique among stormwater treatment systems, as they are designed to allow real-time roof drainage in a wide range of storm intensities, only allowing for contact times of seconds to a few minutes at most, not the long hydraulic residence times which give a typical treatment system more time to reach optimum removal (hours-days). In addition to this, the size of the device and amount of filtration media within is limited by the requirement to be retrofittable into a guttering system. Nonetheless these devices show promise, having achieved dissolved Zn and Cu reductions of 93%-99% and >90% respectively in laboratory conditions, and 81%-97% and 85%-98% respectively in field experiments, all of these experiments having been conducted using hydraulic retention times and device configurations relevant to real world operational requirements (Gregoire, 2018).

### 1.3.1 PROPOSED METAL RETENTION MECHANISMS

In the stormwater context research as above, mechanisms for Zn and Cu removal have been suggested, but not studied in detail. Good et al. (2014) proposed adsorption and filtration as mechanisms, based on an observed relation between hardness/pH buffering and metal removal. Craggs et al. (2010) suggested that ion exchange (adsorption) was the dominant mechanism, based on Ca concentrations released, though also observed the shells turning green on contact with a Cu

solution which indicated the formation of a Cu precipitate. Gregoire (2018) suggested that metal removal was related to an increasing pH, which facilitates adsorption and precipitation.

Biogenic $CaCO_3$ based biosorbents' interaction with solutions of higher concentrations of metals (in the mg/L range, rather than the µg/L range more typical of roof runoff), and with longer contact times between the sorbent and solution (than is practical for the Storminator™ design context), have been the subject of more thorough investigation. Some have focused specifically on their use in treating acid mine drainage (AMD) (for example DiLoreto et al., 2016; McCauley et al., 2009; Uster, 2015), while others have focused on a more generic 'wastewater' with other dominant metal ions like lead (Pb), cadmium (Cd) or nickel (Ni) (for example Belova et al., 2014; Hossain & Aditya, 2015; Zhou et al., 2017). Some however have included Zn and/or Cu in their more generic wastewater matrix and so further detail on their experimental contexts is provided in Table 1-1 and Table 1-2.

Due to the key differences in experimental context their findings cannot be assumed directly relevant to the Storminator™ context. Nonetheless they are explored below to further define gaps in the current literature, and to provide guidance on mechanisms that may apply in the inline downpipe treatment context.

### PRECIPITATION

Dissolution of the calcareous layer in the shells raises the alkalinity of the water and provides a source of carbonate and hydroxide to encourage metal precipitation, which can also improve the physical filtration. These precipitates have been seen via molecular imaging and analysis techniques on other shellfish shells, though only some were identified as specific minerals (Table 1-1 and Table 1-2): scanning electron microscopy (SEM), electron dispersive X-ray (EDS), X-ray diffraction (XRD)).

In the AMD context, several authors have found mussel shells to be more effective than traditional limestone at raising alkalinity, and postulate this is due to more rapid dissolution of the shells (McCauley et al., 2009; Uster et al., 2015). Reactive surface area, size and shape of the grains, and the specific mix of calcium carbonate polymorphs that make up the shells (aragonite vs calcite) have been suggested as reasons for the rapid dissolution (McCauley et al., 2009; Uster et al., 2015). Limestone is calcite, while the $CaCO_3$ polymorph present in mussel shells can be up to 90% aragonite depending on the species of mussel (Ben Shir et al., 2013; Cubillas et al., 2005). As aragonite is more soluble than calcite this leans credibility to their suggestions, and validates the concept in the stormwater context (Stumm & Morgan, 1995). Interestingly though, Good et al. (2014) did not find a reduced grain size to offer improved metal retention as the previous factors should suggest, which could imply that the alkalinity rise is not the sole mechanism at work.

It should be noted that in the studies in Table 1-1 and Table 1-2 that identified precipitates, they were surface/micro precipitates, which has been defined above as a form of adsorption, rather than precipitation of salts from dissolved ions in the bulk solution.

**Table 1-1: Summary of relevant data from previous studies into the mechanisms of Zn or Cu retention by seashells.**

| Shell/$CaCO_3$ polymorph | Metal: concentration (Single/mixed solution) Contact time | Proposed mechanism of metal retention (mineral if identified) | Evidence | Reference |
|---|---|---|---|---|
| Cockle / aragonite | **Zn**: 0.85–69.3 mg/L (mixed) 72 hours | Surface precipitation (hydrozincite) | SEM-EDS XRD | Köhler et al. (2007) |
| Razor clam / aragonite Oyster / calcite | **Zn**: 200–1000 mg/L (mixed) 48–96 hours | Surface precipitation (hydrozincite) | SEM XRD Geochemical modelling | Du et al. (2011) |
| | | Chemisorption | Pseudo second order model fit | |
| Crab / calcite | **Zn**: 4.39 mg/L **Cu**: 5.14 mg/L (mixed) 1 hour | Micro-precipitation | SEM-EDS | Vijayaraghavan et al. (2010) |
| Mixed bivalves / aragonite | **Zn**: 6.54–1,962 mg/L (single) 24 hours | Adsorption Surface precipitation (hydrozincite) | XRD Ca ion release Intra-particle diffusion model fit | Egerić et al. (2018) |
| | **Cu**: 6.35–635 mg/L (single) 24 hours | Complexation Ion exchange | XRD Ca ion release | |

**Table 1-2: Summary of relevant data from previous studies into the mechanisms of Cu retention by seashells. * study did not report the $CaCO_3$ polymorph, polymorph inferred to be calcite from Wu et al. (2014), Du et al. (2011) and Zhou et al. (2017).**

| Shell/$CaCO_3$ polymorph | Metal: concentration (Single/mixed solution) Contact time | Proposed mechanism of metal retention (mineral if identified) | Evidence | Reference |
|---|---|---|---|---|
| Oyster / calcite | **Cu**: 5–100 mg/L (single) 24 hours | Monolayer adsorption (<30 mg/L initial concentration) Adsorption/surface precipitation (> 30 mg/L initial concentration) | Langmuir isotherm fit Freundlich isotherm fit | Wu et al. (2014) |
| Anadara inaequivalvis / aragonite | **Cu**: 20–100 mg/L (single) 2.5–60 minutes | Surface precipitation (CaCu compounds) | SEM XRD | Bozbaş and Boz (2016) |
| | | Metal-carbonate bond formation | FTIR | |
| | | Monolayer chemisorption | Langmuir isotherm, and pseudo second order kinetic model fit | |
| Oyster / calcite* | **Cu**: 50 mg/L (mixed) 10–720 minutes | Ion exchange / complexation | SEM First order kinetic model fit | Shin et al. (2014) |
| Oyster / calcite | **Cu**: 20–400 mg/L (mixed) 24 hours | Micro-precipitation | SEM | Xu et al. (2019) |
| | | Monolayer adsorption | Langmuir isotherm, and pseudo second order kinetic model fit Intra-particle diffusion model fit | |

#### ADSORPTION

The structure of the mussel shell is much like a brick and mortar arrangement, where the bricks are calcium carbonate (contributing the alkalinity as above), and the mortar is a layer of organic matter (Jacob et al., 2008). The calcium carbonate surface itself can provide O bearing surface groups, while the organic matter has chitin (a polysaccharide) and acidic proteins, which provide nitrogen (N) and further O bearing functional groups favoured by Zn and Cu for complexation (Levi-Kalisman et al., 2001; Papadimitriou et al., 2017; Shim et al., 2001; Stumm & Morgan, 1995). The shells also have an outer proteinaceous layer (periostracum) which provides more O and N surface functional groups where metal adsorption could take place (Zhao & Waite, 2005). Studies in the context of alkaline biosorbents have focused solely on potential adsorption to the shell surfaces, and thus have not included the potential role of particulates as adsorbing surfaces, such as the Fe or clay oxides/hydroxides that may be present in an urban runoff.

In addition to the adsorption based (surface/micro) precipitation noted above, several authors reported evidence of other mechanisms of adsorption to shells (metal-carbonate bond formation, chemisorption, ion exchange and complexation) using a variety of techniques: SEM; XRD; Fourier transform infrared spectroscopy (FTIR); fit to the Langmuir isotherm; fit to the pseudo second order kinetic model; and Ca ion release correlation with metal removal (Table 1-1 and Table 1-2).

### 1.3.2 MODELLING

In addition to the experimental observations, many studies attempt to model metal retention by the sorbent to give a wider potential applicability of their results (Table 1-1 and Table 1-2). How well the Langmuir or Freundlich isotherms fit the data is commonly discussed as an explanation for how the adsorbed metal concentration changes with change in solution metal concentration, as well as suggesting the mechanism of metal retention. The Langmuir isotherm assumes a homogenous surface upon which the adsorbate forms a monolayer, while the Freundlich isotherm allows for heterogeneous surfaces and the formation of multiple adsorbate layers which can lead to surface precipitation (Ho et al., 2017). Fit with both isotherms has been reported for Cu and Zn in different conditions (Table 1-1 and Table 1-2), but of particular note is Wu's (2014) study which reported a switch in best fit based on initial Cu concentration: Langmuir at lower concentrations vs Freundlich at higher concentrations, indicating that the mechanism of retention changed with changing initial concentraiton.

Fit with kinetic models has also been investigated to explain and predict the rate of adsorption and suggest which mechanisms may be at play. The pseudo first order kinetic model differentiates between the transfer of the [metal] ion from the solution to the adsorbing surface, and physical or chemical adsorption to the surface, as controlling mechanisms (Shin et al., 2014). The pseudo second order kinetic model assumes that adsorption (in the wider sense) is controlled by chemisorption, while the intra-particle diffusion model suggests how crucial intra-particle diffusion is in controlling adsorption (Du et al., 2011; Egerić et al., 2018). Each have been cited as evidence towards the identification of dominant mechanisms of Cu or Zn adsorption to shells (Table 1-1 and Table 1-2).

In acknowledgement of the many parameters that can influence adsorption and the often non-linear relationships between them, Egerić et al. (2018) created a General Regression Neural Network model to predict which parameters influenced retention the most. They concluded that the initial metal

concentration and its covalent radius impacted retention the most, but did not infer from this what mechanisms were occurring.

The common element of all these models is that they are purely mathematical models based on correlations between experimental data, and while they have been able to adequately explain the data from the authors' studies, they incorporate no consideration of potential geochemical causal pathways, and so should be subject to higher scrutiny if predictions are to be made for a different context. Indeed Craggs et al. (2010) note that there is no theoretically valid basis for the use of Langmuir and/or Freundlich isotherms where precipitation is occurring (as well as adsorption), as is potentially the case with these biosorbents. Du et al. (2011) however did include the use of the geochemical model MINTEQ in their study, to investigate whether any Zn minerals were predicted to be oversaturated in their study solutions, and therefore if precipitation of any such mineral could be expected to remove Zn from the dissolved phase.

## 1.4 GAPS IN THE LITERATURE

As noted in 2012 by Clark and Pitt, *"most of the stormwater literature does not address on a fundamental level the interaction of the treatment processes with the stormwater pollutants"* (pg 6716), and the comment in a review of crustacean based biosorbents by Londono-Zuluaga et al. in 2019 suggests this has not changed since: *"few efforts have been made to improve or explain the mechanisms behind adsorption of heavy metal ions"* (pg. 759). These comments expose a gap in the literature, for the use of a predictive model based on existing understanding of geochemical speciation.

Comparison of the experimental contexts of the few mechanistic studies carried out to date, with the operational context for which the Storminator™ is designed, exposes two further key gaps in the literature: the contact time between the metal solution and the sorbent in existing studies is minutes-hours, whereas the contact time allowed in an inline downpipe system may only be seconds in order for the system to be hydraulically useful; and the concentrations of metals used in existing studies were orders of magnitude higher than those typically expected of roof runoff.

Suspended solids concentrations are typically low in roof runoff compared to other urban surfaces, but sediment/particulates are present nonetheless (Charters et al., 2016; Charters et al., 2021). There are also organic surfaces, such as the periostracum, available as adsorption surfaces. Given the importance of Fe and clay oxides/hydroxides as adsorbing surfaces in the general environment, their potential presence in the shells themselves, and Cu's known preference for organic ligands (Flemming & Trevors, 1989), it is surprising that their potential roles in dissolved metal removal has not been explored in this context.

Therefore, dissolved Zn and Cu removal mechanisms should be investigated in the specific context of a Storminator™ system, i.e. a flow-through treatment column. The use of a geochemical model to predict these mechanisms should be evaluated for several reasons: to ensure predictions of metal speciation and retention are relevant to waters of low (but ecologically relevant) metal concentrations as found in roof runoff; to examine whether the predictions are relevant to the contact timescales available in the inline treatment; and to provide credible causal pathways to explain the mechanism predictions.

## 1.5 RESEARCH AIM AND OBJECTIVES

Although the inclusion of mussel shells into stormwater treatment systems has shown promise in reducing Cu and Zn to environmentally acceptable levels, the lack of verification of actual removal mechanisms for each metal in the inline downpipe treatment context so far restricts optimisation of the Storminator™. This is required to predict how the media preparation and lifespan may be optimised, as well as what regeneration options may be available.

The aims of this research were therefore: to identify the dominant mechanisms by which waste seashells remove dissolved Zn and Cu from roof runoff in a downpipe scale column filter such as the Storminator™; to evaluate the applicability of geochemical modelling, using PHREEQC, in predicting these mechanisms; and to provide recommendations for media or column operation to optimise its efficacy, based on the mechanisms of Zn and Cu retention in the column.

In order to meet those aims, the following hypotheses were formed: that the dominant Zn and Cu removal mechanism is either mineral precipitation, adsorption to HFO, or adsorption to organic matter; and that geochemical modelling can predict the degree, form, and longevity of metal removal in these systems, also allowing prediction of regeneration methods.

The following research objectives were therefore proposed:

1. To predict the solid metal speciation of Cu and Zn in stormwater within the mussel shell media of an inline downpipe stormwater treatment system using the PHREEQC geochemical modelling program; and,
2. To verify the validity of the model predictions after having metal contaminated stormwater passed through a Storminator™ based treatment system by using: wet chemical analysis of the treated effluent to evaluate predictions of changes to dissolved/solid metal partitioning; electron microscope and elemental imaging techniques to look for evidence of minerals and metal bearing solids on the mussel shells; and, wet chemical extractions to look for evidence of metal presence in specific chemical fractions of the mussel shells; and,
3. To infer, from the information gained above: how the media and column may be optimised; the lifespan estimated; and a feasible method of regeneration or re-use for the mussel shells proposed, in the context of the Storminator™ system.

# 2 METHODS

## 2.1 METHODOLOGY OVERVIEW

Table 2-1 identifies the methods used in this study which were expected to provide direct evidence of, or refute, the three $Zn_{diss}$ and/or $Cu_{diss}$ removal mechanisms proposed in this study's first hypothesis: mineral precipitation, adsorption to HFO, or adsorption to organic matter. Other methods or experiments were also needed in support of these methods, all of which are explained in sections below. All processes and analyses were carried out by the author unless stated.

**Table 2-1: Overview of key methods used in this study and the data expected from them, categorised by which removal mechanism they were expected to provide evidence of or refute.**

| Mechanism | Method | Expected evidence |
|---|---|---|
| **Precipitation** | Flow-through column experiments | Change in dissolved vs acid soluble Zn or Cu partitioning |
| | PHREEQC modelling | Prediction of $Zn_{diss}$ and $Cu_{diss}$ reductions possible due to precipitation of Zn or Cu containing minerals |
| | SEM-EDS with used shells | Visual identification of particulates and their elemental composition |
| **Adsorption to HFO** | PHREEQC modelling | Prediction of $Zn_{diss}$ and $Cu_{diss}$ reductions possible due to adsorption to HFO |
| | Sequential extraction (SEP) with used shells | Proportions of Zn or Cu associated with Fe oxides in the shells |
| | SEM-EDS with used shells | Visual identification of particulates, and spatial distribution of all identified elements on the used shells |
| **Adsorption to organic matter** | Metal content (hot acid digestions) with used shells | Proportions of Zn or Cu associated with the inorganic vs organic layers of the used shells |
| | Sequential extraction (SEP) with used shells | Proportions of Zn or Cu associated with the organic fraction in the shells |
| | SEM-EDS with used shells | Visual identification of particulates, and spatial distribution of all identified elements on the organic vs inorganic used shells surfaces |

## 2.2 EXPERIMENTAL COLUMN SETUP

Column experiments were required to allow collection of influent and effluent samples for three main reasons: to analyse the suite of parameters needed for solution chemistry input into PHREEQC modelling; provision of measured $Zn_{diss}$ and $Cu_{diss}$ reductions with which to compare model predictions; and to analyse how the solution chemistry changed following treatment in the column. This section describes the physical experimental setup, and the following section (2.3) describes the experiments run through the setup. Section 2.4 then describes the methods of analysis used for the samples gained in the column experiments.

### 2.2.1 THE COLUMNS

Figure 2-1 shows the arrangement of the three identical columns constructed of a type of standard domestic downpipe: PVC piping with an 80mm internal diameter, and cut to a length of 120mm. The bottom of the columns had PVC end caps with large holes drilled in them, overlaid with a coarse plastic mesh, to retain the shells within the column while allowing water to pass freely through (Figure 2-2). These end caps then had funnels attached to the bottom to facilitate effluent sampling. A trough was placed below the columns to collect the waste discharge, and this was piped directly to a nearby floor drain to allow continuous passive draining. Liquid effluent went into the municipal wastewater network as it was not classified as hazardous. This setup was constructed by staff at the Environmental laboratory in CNRE, University of Canterbury. All components were rinsed thoroughly with tap water prior to use.


**Figure 2-1: Front view of experimental column setup, showing dimensions, and the direction of flow through the column and to the drain.**

**Figure 2-2: Column end cap internal view.**

### 2.2.2 THE SHELLS

"Crushed Mussel Shell" sourced from Pearson's Landscape Supplies Ltd, Bromley, Christchurch was used as the column media. It was assumed the shells were weathered prior to purchase as there was no meat remaining on the shells. The shells were manually crushed within a plastic bag, then passed through a 10mm and a 2.36mm sieve to retain the 2.36-10mm fraction. A mechanical rock crusher was also trialled, but generated too many fines to be considered suitable for the remainder of the shells. The total volume of crushed shells was mixed in a cement mixer to create a more even distribution of size fractions from the different crushing methods prior to storage and use. Of note is that the final mix had fragments that were larger than 10mm along some axes (but would fit in one direction through the sieve), and bits of free organic material that appeared to have spilt off from the shells, see Figure 2-3. The columns were then filled to a depth of 1m from the end cap of the column with shell media, with no compaction. The columns were then flushed with very high volumes of tap water (>100L) to remove fines from the crushing process. It was noted that regardless of thorough flushing, after a period of no flushing the subsequent first flush of effluent contained fines. This aligned with observations from others in the research group so pre-experiment flushing was considered complete.

**Figure 2-3: Rinsed and crushed shells used to pack the experimental columns.**

### 2.2.3 HYDRAULIC CONDUCTIVITY

To assess comparability with other experimental or field column treatment devices, and to calculate a maximum flow rate that would not flood the system, the constant head saturated hydraulic conductivity was determined after the pre-experiment flushing. Tap water was directed into the column via a hose and the flow rate slowly increased until there was a constant head of water above the shells. The slow increase of flow should have avoided air pockets being trapped in the media, which could influence the measured conductivity. The head height was marked on the column for measurement, then the time taken to fill a 1L jug that was held at the outflow was recorded. This was repeated only twice for each column because results were concordant. The constant head saturated hydraulic conductivity ($K_{sat}$) was calculated using a derivation of Darcy's law:

$$K_{sat} = \frac{Q \times L}{A \times (L + P)} \times 3600$$

Where $K_{sat}$ = constant head saturated hydraulic conductivity (m/hr)

Q = flow through the substrate ($m^3/s$)

L = depth of substrate (m)

A = cross sectional area of the substrate ($m^2$)

P = depth of water overlying the substrate (m)

### 2.2.4 THE WATER FLOW

A variable speed peristaltic pump was used to pump water to the columns from the relevant feeder tank. The influent feeder hose outlet had multiple holes along its length and was placed transverse across the top of the column, to allow the water to contact the surface of the media in a spray rather than a jet. To enable consistency of flow rates between experiments they were carried out sequentially, using the same feeder hose and clamp combination. This was calibrated to the desired flow rate prior to each experiment. See Figure 2-4 for the rear view of the experimental setup with the pump and tubing arrangement. This arrangement was set up with assistance from staff in the Environmental laboratory, CNRE, University of Canterbury.

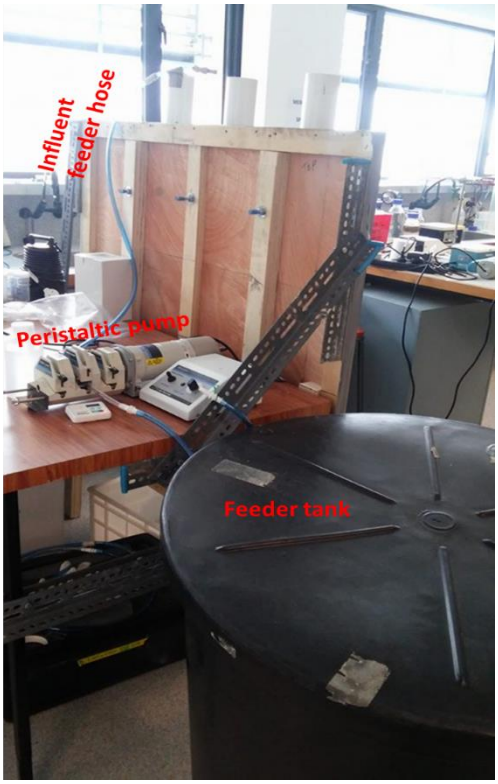


**Figure 2-4: Rear view of the experimental columns showing the pump and hose setup.**

The desired flow rate was calculated by downloading the previous 5 year's worth of 10min interval rainfall data from CliFlo (NIWA, 2019) for the Kyle St station (in Riccarton, close to the university campus, number 24120). It was sorted by 10min mm of rainfall, converted to a flow rate for a 100m$^2$ roof area (given by the Storminator™ developers as an ideal of one Storminator™ per 100m$^2$), and sorted by intensity to show proportion of 10 minute rainfall periods that would give rise to a particular flow rate. At 2 L/min this would encompass 64% of all 10min rainfall periods, and so was chosen for all experiments.

### 2.2.5 OTHER EQUIPMENT

Containers used for storage of water for the experiments were cleaned with detergent and hot water, then well rinsed with tap water before use. As tap water was to be used as the base for the synthetic roof runoff this was considered acceptable as a final rinse for all equipment.

## 2.3 THE COLUMN EXPERIMENTS

### 2.3.1 BASELINE EXPERIMENT

The baseline experiment was conducted to evaluate what impact the column media would have on water passing through which had had no additional chemicals added to it.

Synthetic roof runoff was preferred over real roof runoff largely due to the logistical constraints involved in collection of sufficient volumes and its use prior to potential changes in the chemistry of real roof runoff. The lack of particulates in synthetic roof runoff would also simplify modelling.

Synthetic roof runoff was to be based on the tap water (groundwater-sourced) freely available in the laboratory. Although groundwater was expected to have a different ionic makeup to rainwater, using tap water aligned with previous experiments within the research group. Also, sensitivity testing was carried out in the geochemical modelling to confirm that a different major ion balance would not

significantly impact modelling results. The tap water used already contained appreciable concentrations of Zn (a key analyte of interest, at 0.1 mg/L) and so the experiment could not be considered a true control experiment. However it could still be used as a comparison with experiments that had a metal artificially added to the tap water.

The baseline experiment was conducted in triplicate (once through each column) in order to establish the variability of results. Tap water was pumped at 2 L/min into the column (as per experimental setup described above) for 45 minutes, and samples were collected of the influent, the first flush effluent (the first 400mL of effluent) and the effluent at 5, 15, 30 and 45 min. A deionised (DI) water blank and a duplicate sample of the influent were also collected. Each sample was sub-sampled and preserved for analysis as per section 2.4.1.

The following parameters were measured in samples from the baseline experiment: pH, temperature, DO, conductivity, turbidity, dissolved and acid soluble major cations (sodium (Na), calcium (Ca), potassium (K), magnesium (Mg)), major anions (dissolved inorganic carbon, sulphate ($SO_4$), chloride (Cl)), nutrients (oxidised nitrogen ($NO_x$-N), ammoniacal nitrogen ($NH_4$-N), dissolved reactive phosphorus (DRP)), dissolved and acid soluble trace metals (Fe, Mn, Al, Zn, Cu, Pb, chromium (Cr), nickel (Ni), Cd).

### 2.3.2 EXPERIMENTS 1-3 (Zn RANGE EXPERIMENTS)

The Zn range experiments were conducted to provide data on the solution chemistry of the influent/effluent from the column with elevated influent Zn concentrations, and how they could change with changes in influent Zn concentrations.

Using tap water as a base, a stock solution of $ZnCl_2$ was made, then solutions of approximately 0.3, 1, and 3 mg/L Zn were made by serial dilution to make synthetic roof runoffs that could be typical of runoff from a Zn roof. This range encompassed the dissolved Zn ($Zn_{diss}$) concentrations reported in several published and unpublished New Zealand studies (Bilek, 2019; Charters et al., 2016; Good et al., 2012; Gregoire, 2018; Wicke et al., 2014; Williamson, 1985). As the baseline experiment showed so little variation between the three columns, these experiments were run only once and through the same column. Experiment 1 (0.3 mg/L Zn) was run through column 1 one afternoon, then the following morning experiment 2 (1 mg/L Zn) was run through column 1, and experiment 3 (3 mg/L Zn) was run through column 1 that afternoon. From the results of the baseline experiment it was evident that the most crucial timeframe, where results changed rapidly, was within the first 10 minutes. Therefore, experiments 1-3 were only run for 9 minutes at 2 L/min and samples were taken of the influent, the first flush effluent, and effluent at 3, 6 and 9 minutes along with two duplicates and a deionised (DI) water blank. All samples were prepared and preserved as per section 2.4.1.

Samples were analysed for: pH, temperature, DO, conductivity, dissolved and acid soluble major cations (Na, Ca, K, Mg), nutrients ($NO_x$-N, DRP), dissolved and acid soluble trace metals (Fe, Mn, Al, Zn, Cu, Pb, Cr, Ni, Cd). The baseline experiment results showed that major ions in the effluent return to influent concentrations within 5 minutes, and that ammonia was only present in very low concentrations throughout the experiment, therefore neither major anions nor ammonia were measured in these experiments. For modelling purposes these concentrations were based on the baseline experiment results. Major cation results were returned from the same analytical method run as the trace element concentrations, so results for these cations were included. Visual observations were made of the opacity of the samples.

### 2.3.3 EXPERIMENTS 4-6 (Cu RANGE EXPERIMENTS)

The Cu range experiments were conducted to provide data on the solution chemistry of the influent/effluent from the column with elevated influent Cu concentrations, and how they could change with changes in influent Cu concentrations.

Using tap water a base, a stock solution of $CuCl_2$ was made, then solutions of approximately 0.5, 5, and 10 mg/L Cu were made by serial dilution to make synthetic roof runoffs that could be typical of runoff from a Cu roof. This range was chosen to encompass dissolved Cu ($Cu_{diss}$) concentrations observed in several published and unpublished NZ studies (Bilek, 2019; Charters et al., 2016; Gregoire, 2018; Pennington, 2004; Pennington & Webster-Brown, 2008; Wicke et al., 2014). Experiment 4 was run through column 2 on the day all three synthetic roof runoff solutions were made, and experiments 5 and 6 were run through column 2 on the two subsequent days. The same experimental time (9min), flow rate (2L/min) and samples (influent, first flush effluent, effluent at 3, 6, and 9min) were taken as for the Zn range experiments, and this batch of samples included 1 triplicate, 1 duplicate and a DI blank.

By the day after the synthetic solutions were made, the 5 and 10 mg/L solutions had developed a layer of precipitate floating on the surface, and precipitate continued to form in the remaining solutions over the following weeks (Figure 2-5). Therefore it is important to note that the influent sample was taken immediately prior to running each experiment (not on the day the solution was made), and from below the surface layer, and so represents the elemental composition of the solution as-run through the column. To allow investigation of the composition of this floating layer, a further liquid/precipitate sample was taken from the very top floating layer and processed as a liquid sample. A glass fibre filter paper was also dropped lightly onto the surface to collect a sample of the precipitate, then air dried to allow for analysis by SEM-EDS. All liquid samples were prepared and preserved as per section 2.4.1.

**Figure 2-5: Precipitate formed in the feeder tank of 10 mg/L Cu solution. Precipitate floating on the water surface was present the day of the experiment, precipitate on the bottom of the barrel accumulated over the following weeks.**

Samples were analysed for the same range of parameters as in the Zn range experiments, and the same rationale applies to the inclusion or exclusion of a parameter for measurement: pH, temperature, DO, conductivity, dissolved and acid soluble major cations (Na, Ca, K, Mg), nutrients ($NO_x$-N, DRP), dissolved and acid soluble trace metals (Fe, Mn, Al, Zn, Cu, Pb, Cr, Ni, Cd). To confirm that the dissolved inorganic carbon, $SO_4$, and Cl concentrations were as would be expected from the baseline experiment, selected samples were also analysed for these parameters.

### 2.3.4 REAL ROOF RUNOFF SAMPLES

To provide an indication of how real roof runoff could differ from the synthetic roof runoff made with (groundwater-sourced) tap water, two samples of real roof runoff were analysed for the same suite of parameters as the baseline experiment samples.

Samples of real roof runoff were being routinely collected by other members of the Hydroeco research group during this study period, and a sub-sample from two of those were provided to the author: one from a Cu roof located at the University of Canterbury; the other from a Zn roof located at Hagley College, Christchurch.

## 2.4 ANALYSIS OF LIQUIDS

Column influent and effluent samples were analysed for standard physico-chemical and chemical parameters, most of which were required for input in the PHREEQC geochemical model, while the others gave general indications of water composition for comparison between experiments.

### 2.4.1 SAMPLING, SUB SAMPLING, PREPARATION AND PRESERVATION OF LIQUID SAMPLES

Water samples were collected in 400mL PET jars which had been acid washed for ≥24 hours, then rinsed 3x with tap water and 3x with DI water to remove any acid, and dried in a 40°C oven prior to use. Within 6 hours of sample collection, sub-samples had been poured and preserved as per Table 2-2 and pH, conductivity, DO and temperature had been measured. The acid used for preservation was PrimarPlus- Trace analysis grade >68% $HNO_3$.

**Table 2-2: Water sample preparation and preservation for specific analytes.**

| Sub-sample | Preparation and preservation | Analytes measured from this sub-sample |
|---|---|---|
| 1 | 25mL into a new polypropylene (PP) tube, acidified to pH <2, refrigerated at <4°C | Acid soluble elements: trace metals and major cations |
| 2 | 50mL into a new PP tube, filtered through a 0.45 µm syringe filter, acidified to pH<2, refrigerated at <4°C | Dissolved elements: trace metals and major cations |
| 3 | 10mL into a new PP tube, filtered through a 0.2µm syringe filter, refrigerated at <4°C | Chloride and sulphate |
| 4 and 5 | 50mL each into a new PP tube, filtered through a 0.45 µm syringe filter, frozen | Phosphate, nitrate, ammonia (two separate sub samples taken to allow testing of an analyte on the day of sub-sample defrosting) |
| 6 | 40mL filtered through a 0.45 µm syringe filter, into a hot washed, darkened glass vial with septum lid, refrigerated at <4°C | Dissolved inorganic carbon |
| Retention sample | Remainder of sample after discarding the sub-sample used for pH, DO, temperature and conductivity, into a new PET jar, refrigerated at <4°C | Turbidity, other if needed |

### 2.4.2 pH

pH was measured within 6 hours of sampling, by an EDT RE 357 TX pH meter which had been calibrated that day prior to use. Measurements were carried out after the same equilibration time and reported to 1 decimal place.

### 2.4.3 DISSOLVED OXYGEN (DO) AND TEMPERATURE

DO and temperature were measured with a YSI 550A portable meter, within 6 hours of sampling. The DO meter was calibrated in water saturated air the day of use prior to sample measurement. The instrument presented measurements to 2 decimal places, and results were considered accurate to 1 decimal place.

### 2.4.4 CONDUCTIVITY

Conductivity was measured within 6 hours of sampling, using a YSI 30 Conductivity/Salinity meter. The instrument presented measurements up to 5 significant figures, results have been presented with up to 4 significant figures. To allow comparison of results from solutions of different temperatures, conductivity results were converted to specific conductance using the equation below.

$$\text{Specific conductance (µs/cm)} = \frac{\text{Conductivity (µS/cm)}}{1 + 0.02 * (\text{temperature (°C)} - 25)}$$

### 2.4.5 TURBIDITY

The turbidity of samples were measured using a Hach 2100N Turbidimeter, using Hach Gelex secondary standards as a calibration check (+/- 5% considered acceptable), and DI water to check the cleanliness of the sample cell. The detection limit of the method was estimated at 0.05 NTU, and results have been presented with 2 significant figures.

### 2.4.6 ACID SOLUBLE CATIONS

To each acidified 25mL sub-sample, an aliquot of 5mL of PrimarPlus- Trace analysis grade >68% $HNO_3$ was added, then digested at 110°C for 1 hour prior to filtration through a 0.45 µm filter. Analysis was conducted by ICP-MS at the University of Canterbury by Chemistry department staff for the following elements (estimated detection limit in µg/L): Na (0.1), Ca (0.1), Mg (0.1), K (0.1), Fe (1), Mn (1), Al (1), Cu (1), Zn (10), Cd (1), Cr (1), Pb (1), Ni (1).

### 2.4.7 DISSOLVED CATIONS

Pre-filtered and acidified samples were analysed by ICP-MS at the University of Canterbury by Chemistry department staff for the following (estimated detection limit in µg/L): Na (0.1), Ca (0.1), Mg (0.1), K (0.1), Fe (1), Mn (1), Al (1), Cu (1), Zn (10), Cd (1), Cr (1), Pb (1), Ni (1).

### 2.4.8 DISSOLVED INORGANIC CARBON

Dissolved inorganic carbon was analysed within 48 hours of sampling on a Shimadzu TOC-L CSH analyser coupled with a Shimadzu ASI-L autosampler, and run by TOC-control L v1.01 software. Inorganic carbon is determined by acidification of the sample to pH < 3 to convert all inorganic carbon

to $CO_2$, which is then sparged from the sample to be detected by a nondispersive infrared gas analyser (NDIR). The detection limit was estimated at 5 mg/L C. The species of inorganic C present ($H_2CO_3$, $HCO_3$, or $CO_3$) is dependent on the solution pH, therefore, because the solution pHs measured were circum-neutral, results were reported as $HCO_3$.

### 2.4.9 CHLORIDE AND SULPHATE

Samples were analysed with assistance from Chemistry department staff at the University of Canterbury, by ion chromatography on a Metrohm ECO IC, coupled with a Metrohm Compact Autosampler and using MagIC Net 3.2 software for peak identification and quantification. A commercial multi-anion standard was used to create a calibration curve for each ion prior to each sample run. The detection limit of this method was estimated at 0.1 mg/L.

### 2.4.10 DISSOLVED REACTIVE PHOSPHORUS

A colorimetric method analogous to that described in APHA 4500-P (E) was used to measure DRP. This involved forming phosphomolybdic acid by reaction of ammonium molybdate, antimony potassium tartrate and the reactive phosphorus present in the sample, then reduction of this by ascorbic acid to form molybdenum blue. Absorbance was measured at 880nm and results reported as $PO_4$. The detection limit of this method was estimated at 0.015 mg/L $PO_4$.

### 2.4.11 NITRATE

A colorimetric method analogous to the cadmium reduction method described in APHA 4500-$NO_3^-$ (E) was used to measure nitrate and nitrite. Due to the samples being fully oxygenated the amount of nitrite likely to be present was considered very low, therefore results from this method were treated as nitrate. The sample was reacted with spongy cadmium to reduce all nitrate to nitrite, then with sulphanilamide and N-(1-naphthyl)-ethylenediamine dihydrochloride to form an azo dye. The intensity of the azo dye colour formed was measured at 543nm and results reported as $NO_3$. The detection limit of this method was estimated at 0.09 mg/L $NO_3$. Occasional assistance with analysis was provided by Waterways staff at Lincoln University.

### 2.4.12 AMMONIACAL-NITROGEN

A colorimetric method analogous to the phenate method described in APHA 4500-$NH_3$ (F) was used to measure ammoniacal nitrogen. The reaction of ammonia, phenol, and hypochlorite with the sample was catalysed by sodium nitroprusside to form the blue compound indophenol. The absorbance at 640nm was measured and results reported at $NH_4$. The detection limit for this method was estimated at 0.01 mg/L $NH_4$.

## 2.5 ANALYSIS OF SOLIDS

Analysis of shells that had been exposed to Zn and/or Cu in a Storminator™ or similar system was required to provide evidence for any mechanisms predicted by geochemical modelling, or suggested by the literature. Volatile solids concentration and XRD was carried out to describe key structural characteristics of the shells, and chemical digestions and SEM-EDS were used to identify the physical and/or chemical location and form of Zn or Cu on the shells.

### 2.5.1 SHELL SAMPLING AND PREPARATION

The experiments run for the present study were not deemed likely to have incurred enough accumulation of metal on the shells to provide meaningful results from analysis of the shells themselves. Therefore, shells for analysis were sourced from columns that had either been in the field for at least 1 year, or from previous accelerated loading laboratory experiments, run by other members of the research group at the University of Canterbury. See Table 2-3 for details of the laboratory column shells collected, all of which were crushed and sieved to 2.36 mm < x > 10mm prior to deployment.

**Table 2-3: Details of the origins of the laboratory column shells used for SEM-EDS and wet chemical analysis in this study.**

| Column and attribution | Key experimental information | Shell sample location in column | Key metal expected to be found |
|---|---|---|---|
| **n/a- blank**<br><br>(present study) | • Prepared for the present research.<br>• Not rinsed or used in an experiment.<br>• A "shell blank". | n/a | none |
| **Laboratory-synthetic roof runoff**<br><br>Heffernan and Howe (2019) | • Synthetic roof runoff.<br>• Approximately 1100L through a 1m depth 100mm internal diameter.<br>• Operationally saturated: $Zn_{diss}$ removal efficiency 15% at sampling.<br>• 27mg/L Zn, 0.4mg/L Cu in influent. | Top<br>Middle<br>Bottom | Zn |
| **Laboratory-real roof runoff**<br><br>Heffernan and Howe (2019) | • Real roof roof runoff.<br>• Approximately 1100L through a 1m depth 100mm internal diameter.<br>• $Zn_{diss}$ removal efficiency 80% at sampling: considered operationally saturated.<br>• 0.3mg/L Zn, 0.005mg/L Cu in influent. | Top<br>Middle<br>Bottom | Zn |

See Table 2-4 below for details of the field column shells collected, and Figure 2-6 below for photographs of the two field column samples showing the debris and size range of shells. After collection from the field or lab source the shells were dried in a 40°C oven and stored in clean plastic containers.

**Table 2-4: Details of the origins of the field column shells used for SEM-EDS and wet chemical analysis in this study.**

| Column and attribution | Key experimental information | Shell sample location in column | Key metal expected to be found |
|---|---|---|---|
| **Field- University of Canterbury E8 (Cu) roof.**<br><br>O'Sullivan, Cochrane, Charters, Bilek. | • Column installed 27/6/2018.<br>• Sampled 9/7/2019.<br>• Approximately 88m$^2$ drainage area to the column.<br>• 1m depth, 100mm internal diameter.<br>• Copper roof.<br>• Estimated influent means of 0.74 mg/L Cu, 0.29 mg/L Zn (estimated from Bilek, 2019).<br>• $Cu_{diss}$ removal efficiency estimated at 86% at sampling (estimated from Bilek, 2019). | Top<br><br>(1-2cm below the surface) | Cu |
| **Field- Hagley College Science block (Zn) roof.**<br><br>O'Sullivan, Cochrane, Charters, Bilek, Hansen. | • Column installed prior to 24/2/2019.<br>• Sampled 12/2/2020.<br>• Approximately 93m$^2$ drainage.<br>• 1.5m depth, 150mm internal diameter.<br>• Zincalume roof. | Top<br><br>(1-10cm below the surface) | Zn |


**Figure 2-6: Dried shell sample from the Cu roof column (left), and from the Zn roof column (right), showing the size variation of shell fragments and the debris attached to the shells. The blue tinge of the shells from the Cu roof may indicate a coating of a Cu hydroxycarbonate.**

### 2.5.2 VOLATILE SOLIDS

To estimate the weight of organic (volatile) matter in the shells, four sub-samples of approximately 10g were accurately weighed to 4 d.p. then ashed at 550°C for two hours. The samples were re-weighed after cooling and the difference calculated as the organic proportion of the shell mix.

### 2.5.3 XRD

To determine the main polymorph of calcium carbonate present in the shells prepared for the experimental columns, two samples were sent to Panda Geoscience for analysis by X-ray Diffraction (XRD). Different crystal structures produce different diffraction patterns when subjected to X-rays, and so can distinguish between polymorphs of the same chemical composition such as calcite and aragonite. It was suspected that there were two types of mussel shell in the mix (green lipped mussels, and blue mussels), so one sample sent was of shells that were visibly blue, the other of shells that were not visibly blue, all other sample preparation analysis was carried out by the third party laboratory. The samples were a mix from the top, middle and bottom of Heffernan & Howe's (2019) laboratory column.

### 2.5.4 METAL CONTENT

To quantify the presence of Zn or Cu and other trace metals on the used shells, hot acid digestions were performed on the shells. To evaluate any preferential attachment to the organic periostracum layer, compared to the inorganic $CaCO_3$ bulk of the shell, a second set of hot acid digestions was performed on the periostracum layer only. The results from these hot acid digestions are referred to as the metal content.

For the two sets of laboratory shell samples, no further preparation was carried out prior to digestion for metal content. For the two field column shell samples however, as the experiment was to determine what was attached to the shell, rather than what was in the debris, it was necessary to attempt to remove the debris stuck to the shell. Two different methods were trialled to achieve this. For the Cu roof shell sample, the debris was brushed off until the sample was visibly clean. For the Zn roof shell a sub-sample was rinsed in DI water, filtered and re-dried. The filtrate was kept and analysed to investigate how much of the shell, and potentially of adsorbed metals, were removed in this step.

One set of digestions was conducted with every shell sample using fragments of the full shell, for which each fragment included visibly present nacreous, bulk and organic layers. A sample of debris from the Cu roof shell sample was also analysed. A second set of digestions was carried out with a smaller group of samples using only the organic layer, which had been manually removed from the carbonate bulk of the shells.

For both sets of digestions, sub-sample sizes of 0.3-1g of dried shells (depending on shell fragment size) were weighed directly into acid washed Teflon beakers. Each sample was analysed in triplicate where possible, or less where sample size was not large enough: for example, where the lightweight nature of the organic layer meant that the original shell sample needed to be very large, and was not necessarily available.

An aliquot of 10 mL of trace analysis grade >69% nitric acid was then added to each beaker, as well as to 2 empty beakers to be used as method blanks, then heated under partial reflux until 'almost dry'. This digestion dissolved the entirety of the shell samples. To ensure any precipitates or residues from the rigorous digestion step were re-dissolved, 45 mL of 0.1 N nitric acid was added and the beaker was heated covered for a further hour. The beaker was then heated uncovered until the liquid volume was <10mL. Once cooled, the remaining liquid was poured into a pre-weighed tube, along with 0.1N nitric acid rinsings of the beaker, and the final weight of the tube and extract was taken.

Due to the high ionic content expected, the concentration of metals in the digestions were analysed by ICP-OES at Lincoln University by Agriculture and Life Sciences division staff, with the following detection limits (µg/L): Fe 0.4; Mn 0.05; Al 1; Cu 0.6; Zn 0.3; Pb 3; Cr 0.5; Ni 1.3; Cd 0.3. The highest method blank result (of two duplicates) per element was subtracted from all sample results for that element. Any blank adjusted results that were less than the instrument blank were discarded. Results in mg/kg of original sample were calculated by the equation below, and rounded to 3 significant figures, or to no more than 2 decimal places.

$$\text{concentration in sample} = \frac{\text{concentration in digested extract x final weight of extract}}{\text{Initial weight of sample}}$$

### 2.5.5 SEQUENTIAL EXTRACTION

To investigate which specific chemical phase the Zn or Cu was bound to in the used shells, a sequential extraction procedure was carried out with the shells. The sequential extraction procedure used was that described in Leleyter and Probst (1999), with minor modifications. This procedure allows for categorisation of what the metal was bound to into the following operational categories: water soluble; readily exchangeable; bound to carbonates, bound to manganese oxides; bound to amorphous Fe oxides; bound to crystalline Fe oxides; bound to organic matter.

The key procedural information is shown in Table 2-5. The main modifications to the method from that described in Leleyter and Probst (1999) are:

- In the bound to carbonate step, 20mL of reagent was used instead of 10mL. This was to account for the sample itself being almost entirely calcium carbonate (c.f. the samples this procedure was designed for were river sediments, no such procedures designed specifically for shell samples were known to the author), and the observations of Leleyter and Probst (1999) regarding the efficacy of this step with high carbonate content sediments;
- Both centrifugation and filtration were used to separate the residue from the leachate and rinsings. Centrifugation minimised the amount of fines that would otherwise be caught in the filter and therefore removed from further extraction steps;
- Volumes and concentrations of reagents were modified in the first part of step 7 (bound to organic matter) to allow for differences in available reagent concentrations.

**Table 2-5: The sequential extraction procedure used. Based on Leleyter and Probst (1999).**

| Category | Reagent | Reaction time | Temperature |
|---|---|---|---|
| 1. Water soluble | 10mL ultrapure water | 30 minutes | Ambient (≈20°C) |
| 2. Readily exchangeable | 10mL 1M magnesium nitrate | 2 hours | Ambient (≈20°C) |
| 3. Bound to carbonates | 20mL 1M sodium acetate at pH 4.5 | 5 hours | Ambient (≈20°C) |
| 4. Bound to manganese oxides | 10mL 0.1M hydroxylamine hydrochloride | 30 minutes | Ambient (≈20°C) |
| 5. Bound to amorphous iron oxides | 10mL [0.2M ammonium oxalate – 0.2M oxalic acid] | 4 hours (in darkness) | Ambient (≈20°C) |
| 6. Bound to crystalline iron oxides | 10mL [0.2M ammonium oxalate – 0.2M oxalic acid – 0.1M ascorbic acid] | 30 minutes | 80°C |
| 7. Bound to organic matter | a) 1.6mL 0.04M nitric acid + 9.3mL 30% hydrogen peroxide | a) 5 hours | a) 85°C |
| | b) 5mL 3.2M ammonium acetate in 20% v/v nitric acid | b) 30 minutes | b) 85°C |

### SAMPLE PREPARATION

Seven of the shell samples described above were selected for the sequential extraction procedure: Top and bottom samples from both laboratory experiments (4 samples), both top samples from field columns (2 samples), and the “shell blank” unused sample from the present study (1 sample). For the two field column samples, first the debris was manually removed from a sub-sample of each with a clean brush.

While this study is concerned with how metals are attached to the surface of the shells (rather than elements bound in the inner bulk layers of the shell), the heterogeneous nature of the samples meant that obtaining an as-is sample of the appropriate weight for analysis that was also representative was not feasible. Therefore, a sub-sample of between 2 and 5g (depending on the sample availability) of all seven samples were crushed and ground to a powder using an acid washed ceramic mortar and pestle. The powdered samples were re-dried overnight in a 40°C oven in case the powdering process had introduced any moisture. Approximately 1g of each dry sample was then accurately weighed into a new plastic tube for the extractions.

### RESIDUE MIXING, SEPARATION, AND RINSING

For all extractions carried out at ambient temperature all samples with added reagent, and a reagent only blank, were given an initial vigorous manual mix (to break up loosely bound aggregates), then mixed on a rotary mixer. The mixer was set to a speed high enough to ensure constant suspension of the sample within the liquid, and samples were mixed for the length of time specified in Table 2-5. For extractions that required heating, the residue was manually mixed with the reagent at the beginning, then left static in the heating block for the reaction time.

Samples were centrifuged for 10 minutes at 3000rpm to separate the residue from the leachate, then the leachate was filtered through a 0.45 µm PVDF filter. The residue was washed with 10mL of ultrapure water, the mixture centrifuged and filtered as before and the rinsings were added to the leachate. This rinsing process was carried out twice. The final volume of the leachate plus rinsings was recorded, and the sample acidified and stored at <4°C until analysis. The residues were then dried in a 40°C oven prior to the next extraction step, to avoid dilution of the next leaching solution.

### LEACHATE ANALYSIS

Each leachate was analysed for Ca, Mn, Al, Fe, Cu, Zn, Pb, Cr, Cd and Ni: Fractions 1 and 4-7 were analysed by ICP-MS at the University of Canterbury by Chemistry department staff (see section 2.4.7 for detection limits), while due to the high dissolved salt content of fractions 2 and 3 these were analysed by ICP-OES at Lincoln University by Agriculture and Life Sciences division staff, with detection limits of 0.01 for Ca µg/L and the others as per section 2.5.4.

In reflection of the required accuracy as well as the practical difficulties in retaining all of the residue during the separation and rinsing steps, results are presented to 3 significant figures, or to no more than 1 decimal place.

## 2.5.6 SEM-EDS

To look for visible particulates that Zn or Cu may be associated with, and to see spatial correlations of Zn or Cu with any particular surface or other element on the used shells, shell samples were analysed by SEM-EDS.

Sample fragments were stuck to a mounting block with tape, then coated in palladium to provide a conductive coating for scanning electron microscopy with electron dispersive spectroscopy (SEM-EDS) analysis. Most samples were analysed with a JEOL JSM-7000F coupled with the JED-2300 AnalysisStation software, the others with a JEOL JSM-IT300LV SEM-EDS machine coupled with the Aztec version 3.2 EDS software by Oxford Instruments, both at the University of Canterbury. On both instruments a 20kV accelerating voltage was used. The JSM-7000F machine was preferred due to its superior morphological imaging and more informative elemental reports. Preparation of the samples for, and operation of, the SEM-EDS was carried out by staff in the Mechanical Engineering department of the University of Canterbury, under supervision and guidance by the author.

Two main approaches to identifying metal bearing areas of the shell were used: elemental mapping, where the whole of an image was scanned and a map built for each element of its spatial location; and spot analyses, where a very small area was chosen and the elemental composition of that area was analysed, producing a report with relative elemental concentrations. While elemental maps can

be highly informative in showing where to conduct spot analyses they are also highly time consuming, so spot analyses were also carried out based on visual identification of shapes of interest from the SEM images, and based on the location on the shell.

## 2.6 PHREEQC MODELLING

PHREEQC is a geochemical equilibrium software program with a graphical user interface which simulates chemical interactions between the chemical species of a water as well as with solids and their associated adsorption sites (among other abilities) (Parkhurst & Appelo, 2017). It was written for, and continues to be maintained by, the USGS. This speciation modelling is based on balancing equilibrium equations for the formation of known chemical species, to predict the quantity of a given element that could be present as any of the known species that could exist in the defined system. The thermodynamic equilibrium equations and their constants are located in a database that is selected by the user from several that are supplied with the program. It has been used successfully in many contexts, though a few recent examples that align with the current study's use of the model are: prediction of metal leaching behaviour from soils (Jalali & Latifi, 2018); speciation of trace metals in river and wastewater (Magu et al., 2016); and prediction of groundwater quality after potable, desalinated, or urban stormwater injection into the aquifer (Antoniou et al., 2015). Given that it is maintained (unlike other geochemical speciation programs), that it has been used successfully in similar contexts to this proposal, and that expertise in its use was readily available to the researcher, PHREEQC was the model of choice for this research. Of particular use in this study was its ability to predict aqueous elemental speciation, mineral saturation in a solution, and adsorption of dissolved elements to surfaces such as hydrous ferric oxide (HFO). The PHREEQC version used in this study was 3.4.0-12927.

### 2.6.1 DISSOLVED SPECIATION AND SATURATION MODELLING

Saturation modelling allows the prediction of mineral compounds that would precipitate given thermodynamic equilibrium. This would reduce the concentration of a dissolved ion involved in forming the mineral. Therefore if a Zn or Cu mineral is predicted to be oversaturated in a solution chemistry representative of that in the treatment column, this may indicate a mechanism by which dissolved Zn or Cu could be removed from solution.

For each PHREEQC input chemistry, the following parameters were used to define the solution: pH, temperature, dissolved major cations (Na, Ca, K, Mg), dissolved major anions ($CO_3$, $SO_4$, Cl), dissolved nutrients ($NO_3$, $NH_4$, $PO_4$), and dissolved trace metals (Fe, Mn, Al, Zn, Cu, Pb, Cr, Ni, Cd). In addition to this the pe (a measure of redox potential) was set to 12 to model the solution as an oxygenated system, the validity of which was confirmed by the DO measurements being at or near saturation. As per section 2.3, where a parameter was not measured in a particular sample, the value used in modelling was taken from the baseline experiment (influent, or 5 minute effluent, for influents and effluents respectively). For sensitivity modelling selected parameters were artificially changed, and where this occurred the artificial change made is indicated in the results.

The MINTEQv4 database was used in this modelling, chosen over the other potentially relevant WATEQf database due its inclusion of more options for chemical parameter input. An addition was made to the Phase section of this database to include a means of fixing the pH at a given value for

some of the modelling (pH_Fix with an equation of H+ = H+ and log_k = 0). The method used for this pH fixing was as per the explanation of the Equilibrium Phases datablock in the PHREEQC user guide.

From among the standard output of data from speciation in PHREEQC, dissolved speciation of elements of interest and mineral saturation indices were extracted for particular focus. Where a mineral was predicted to be oversaturated, investigation was made into the likelihood of this being able to occur in a low temperature low pressure environment such as the Storminator™. This was necessary as PHREEQC does not take into account kinetic barriers to mineral formation, and so not all oversaturated minerals were likely to precipitate out of solution in the column system. Where a mineral was found to be likely to precipitate, the solution was then remodelled allowing that mineral to precipitate out of solution until it was no longer oversaturated, and the impact on the concentration of dissolved elements of interest was analysed.

### 2.6.2 HYDROUS FERRIC OXIDE (HFO) ADSORPTION MODELLING

Adsorption to a particulate is another mechanism by which dissolved Zn and Cu concentrations may be expected to decrease. Adsorption to HFO is the most well studied among naturally occurring adsorbing surfaces in the environment, owing to its importance in that context (Dzombak & Morel, 1990). It was also expected that Fe would be present in roof runoff, so HFO was chosen as the adsorbing surface to be used in modelling, to investigate whether it could explain any observed reductions in dissolved Zn and Cu concentrations in the column experiments.

The same parameters as described for speciation and saturation modelling above were used to define the solution that would come in contact with the HFO. To define the maximum concentration of HFO available for reaction the following were calculated: the particulate Fe concentration (acid soluble Fe – dissolved Fe), expressed as $Fe(OH)_3$; and the number of weak and strong sites on the HFO, which is calculated from Dzombak and Morel (1990) giving 1.87 x $10^{-3}$ mol weak sites/g HFO, and 4.68 x $10^{-5}$ mol strong sites/g HFO. The model uses a default area of 600$m^2$/g HFO (Dzombak & Morel, 1990). The default option employing the Dzombak & Morel Diffuse Double Layer surface complexation model was selected, and the standard parameters for the diffuse layer were allowed by selecting “No explicit diffuse layer”.

From among the standard output of data from running HFO adsorption modelling in PHREEQC the dissolved concentration of elements of interest, and the elements adsorbed to the strong and weak HFO sites, were extracted for particular focus

## 2.7 QUALITY CONTROL AND ERROR ANALYSIS

### 2.7.1 WATERS: REAL OR SYNTHETIC ROOF RUNOFF, COLUMN EFFLUENTS

With each batch of samples for analysis (16 experimental samples at most) a DI water blank, and one-two duplicate samples were collected and analysed as separate samples.

The DI water blanks showed that systematic contamination of some metals from sampling or testing may have occurred. While Cu and Ca concentrations were higher than might be expected from a DI water, they were well below concentrations seen in experimental samples so were not of concern Table 2-6, Table 2-7, Table 2-8, Table 2-9). However, Al and Fe concentrations in the blanks were in

the same order of magnitude as in experimental samples, so those results were treated as maxima which may have overstated the true amount (Table 2-6, Table 2-8, Table 2-9). The most likely source of contamination was the dispenser outlet/cap on the acid used for preservation and digestion.

**Table 2-6: Results for physico-chemical parameters and trace element concentrations in quality control (QC) DI water blanks run with each batch of liquid samples. Dissolved ion concentrations are in normal text, acid soluble concentrations are below the dissolved concentrations and in *italics*.**

| QC Sample | pH | Specific conductance (µS/cm) | Dissolved oxygen (mg/L) | Temperature (°C) | Fe (µg/L) | Mn (µg/L) | Al (µg/L) | Zn (µg/L) | Cu (µg/L) |
|---|---|---|---|---|---|---|---|---|---|
| Blank 1 | 5.6 | 2.4 | 8.6 | 20.4 | 1.1 | <1 | 5.8 | <10 | 1.3 |
| | | | | | *8.7* | *<1* | *110* | *<10* | *1.3* |
| Blank 2 | 6.0 | 1.9 | 8.0 | 23.0 | <1 | <1 | 4.7 | <10 | 1.8 |
| | | | | | *7.2* | *<1* | *94.4* | *<10* | *3.2* |
| Blank 3 | 5.0 | <0.0 | 8.7 | 20.4 | 1.9 | <1 | 10.0 | <10 | <1 |
| | | | | | *21.5* | *<1* | *121* | *<10* | *1.6* |

**Table 2-7: Results for major ions from quality control (QC) DI water blanks run with each batch of liquid samples. Dissolved ion concentrations are in normal text, acid soluble concentrations are below the dissolved concentrations and in *italics*. "-" not tested**

| QC Sample | Na (mg/L) | Ca (mg/L) | K (mg/L) | Mg (mg/L) | Cl (mg/L) | $SO_4$ (mg/l) | $NO_3$ (mg/L) | $NH_4$ (mg/L) | $PO_4$ (mg/L) | $HCO_3$ (mg/L) |
|---|---|---|---|---|---|---|---|---|---|---|
| Blank 1 | 0.004 | 0.03 | <0.0001 | 0.002 | <0.1 | <0.1 | 0.1 | 0.01 | <0.005 | 2.6 |
| | *0.1* | *0.5* | *<0.0001* | *<0.0001* | | | | | | |
| Blank 2 | <0.0001 | <0.0001 | <0.0001 | <0.0001 | - | - | <0.02 | - | 0.01 | - |
| | *<0.0001* | *0.6* | *<0.0001* | *<0.0001* | | | | | | |
| Blank 3 | <0.0001 | <0.0001 | <0.0001 | <0.0001 | 0.8 | <0.1 | <0.02 | - | 0.009 | - |
| | *0.4* | *0.7* | *<0.0001* | *<0.0001* | | | | | | |

The replicate results of physico-chemical parameters were in close agreement: pH varied by 0.2 at most; conductivities were within 3%; and DO varied by 0.1 mg/L at most (Table 2-8 and Table 2-9). The overall error in the dissolved ion concentrations for each solution was estimated at ≤10%, as the ion balances for most solutions entered into PHREEQC returned ion balance errors of ≤10%. The exceptions to this were the influents for 5/6 of the Cu and Zn range experiments, where ion balances were up to 23%. This was likely due to the high levels of Zn or Cu added to tap water to make the synthetic solutions, which were one to three orders of magnitude above the concentrations found in the tap water base, and also above the top calibration point used in the ICP-MS analyses. Some of the trace element concentrations in the samples run in replicate are >10% different, but these are where the concentrations are close to the detection limit which can make quantification difficult (Table 2-8 and Table 2-9). The acid soluble ion concentrations had a larger error, estimated at ≤20% from the replicates analysed (Table 2-8). While the samples were heated in capped tubes it was noted that after the 1 hour digestion time the liquid levels varied slightly between tubes, so this evaporation is likely the source of the higher error.

All dissolved inorganic carbon samples had been filtered through a 0.45 µm filter prior to analysis, therefore to ensure that the filtration process did not impact on the dissolved/particulate partitioning two samples were analysed unfiltered and compared to their filtered counterpart. Results showed no difference between filtered and unfiltered inorganic carbon results, and so results from filtered samples were deemed valid.

There were several anomalies in acid soluble vs dissolved Zn results, so explanations of how they were treated are provided here. In one influent the acid soluble Zn concentration was lower than the dissolved Zn concentration, which is not chemically possible. However, in this instance those results were processed in duplicate and showed good agreement, and the dissolved and acid soluble results were within the estimated uncertainty (10%) therefore were left as-is. There were a small number of other instances (5) throughout the experiments where again dissolved Zn concentrations appeared higher than acid soluble concentrations. When this occurred, if they were within 10% of each other the results were left as-is, if they were not then the first preference was to consider all Zn dissolved and the dissolved Zn concentration was reported as the acid soluble concentration (a lower error was assumed in the dissolved results as less sample preparation had gone into them). The second preference, of setting the acid soluble Zn concentration as the dissolved concentration, was only used where replicate results suggested the error was in the dissolved concentration. This issue had been noted by several members of the research group, and no adequate explanation had yet been found. However it had minimal impact on what these results could contribute to meeting the objectives of this research, therefore were not investigated in detail.

Where a numerical result was returned for a parameter which was subsequently determined to be below detection, the result that was returned was used as an estimate of the actual concentration for modelling and graphing purposes, but reported as below the appropriate detection limit. Identification of trends across experiments was a key part of interpretation of this dataset, and where these trends were seen this suggested that the results were sensible in spite of being below the estimated limit of detection, and so their inclusion was warranted.

**Table 2-8: Results from quality control (QC) replicate samples run with each batch of liquid samples in the baseline and experiments 1-3. Dissolved ion concentrations are in normal text, acid soluble concentrations are below the dissolved concentrations and in italics. "-" not tested. *Suspect result.**

| QC Sample | pH | Specific conductance (µS/cm) | Dissolved oxygen (mg/L) | Temperature (°C) | mg/L | | | | | | | | | µg/L | | | | |
|---|---|---|---|---|---|---|---|---|---|---|---|---|---|---|---|---|---|---|
| | | | | | Na | Ca | K | Mg | Cl | $SO_4$ | $NO_3$ | $PO_4$ | $HCO_3$ | Fe | Mn | Al | Zn | Cu |
| Baseline influent-1 | 7.0 | 117 | 8.6 | 19.8 | 8.2 | 10.7 | 0.8 | 2.4 | 4.4 | 3.4 | 2.4 | 0.03 | 52 | 2.0 | 2.3 | 1.6 | 116 | 4.6 |
| | | | | | *8.0* | *11.9* | *0.8* | *2.4* | | | | | | *31.8* | *2.5* | *40.7* | *96.8* | *5.2* |
| Baseline influent-2 | 7.2 | 114 | 8.6 | 20.5 | 8.2 | 10.9 | 0.8 | 2.4 | 4.4 | 3.5 | 0.4* | 0.04 | 51 | 5.9 | 2.3 | 4.5 | 117 | 4.7 |
| | | | | | *9.5* | *13.9* | *0.9* | *2.8* | | | | | | *35.5* | *2.9* | *39.9* | *114* | *6.3* |
| Exp. 1 6 minute effluent-1 | 7.6 | 173 | 8.4 | 22.6 | 6.7 | 22.8 | 0.7 | 1.6 | - | - | 29.1 | 0.135 | - | 4.3 | <1 | 3.0 | 14.4 | 1.7 |
| | | | | | *7.5* | *26.4* | *0.9* | *1.8* | | | | | | *30.0* | *1.1* | *96.4* | *16.8* | *2.7* |
| Exp. 1 6 minute effluent- 2 | 7.7 | 176 | 8.4 | 22.5 | 6.8 | 22.9 | 0.7 | 1.7 | - | - | 25.6 | 0.121 | 37 | 4.1 | <1 | 2.8 | 14.5 | 1.8 |
| | | | | | *7.0* | *25.4* | *0.9* | *1.8* | | | | | | *217** | *1.5* | *93.6* | *16.1* | *2.4* |
| Exp. 3 3 minute effluent-1 | 7.5 | 152 | 8.2 | 22.5 | 5.5 | 20.3 | 0.6 | 1.3 | - | - | 12.6 | 0.03 | - | 6.9 | <1 | 8.1 | 121 | 1.2 |
| | | | | | *6.6* | *24.1* | *0.8* | *1.6* | | | | | | *25.0* | *1.0* | *104* | *125* | *1.7* |
| Exp. 3 3 minute effluent- 2 | 7.5 | 149 | 8.2 | 22.4 | 5.7 | 20.4 | 0.6 | 1.4 | - | - | 12.0 | 0.03 | 27 | 2.7 | <1 | 6.8 | 124 | 1.0 |
| | | | | | *6.5* | *24.5* | *0.8* | *1.6* | | | | | | *26.7* | *1.1* | *104* | *129* | *2.5* |

**Table 2-9: Results from quality control (QC) replicate samples run with each batch of liquid samples in experiments 4–6. Dissolved ion concentrations are in normal text, acid soluble concentrations are below the dissolved concentrations and in italics. "-" not tested.**

| QC Sample | pH | Specific conductance (µS/cm) | Dissolved oxygen (mg/L) | Temperature (°C) | mg/L | | | | | | | | | µg/L | | | | |
|---|---|---|---|---|---|---|---|---|---|---|---|---|---|---|---|---|---|---|
| | | | | | Na | Ca | K | Mg | Cl | $SO_4$ | $NO_3$ | $PO_4$ | $HCO_3$ | Fe | Mn | Al | Zn | Cu |
| Exp. 4 9 minute effluent-1 | 7.8 | 183 | 8.9 | 20.7 | 8.6 | 22.5 | 0.8 | 2.3 | - | - | 29.0 | 0.111 | - | 3.9 | <1 | 12.3 | 15.0 | 201 |
| | | | | | *8.6* | *24.7* | *0.9* | *2.5* | | | | | | *31.2* | *<1* | *131* | *15.0* | *216* |
| Exp. 4 9 minute effluent- 2 | 7.9 | 178 | 9.0 | 20.8 | 8.7 | 23.0 | 0.9 | 2.3 | - | - | 32.4 | 0.115 | - | 4.5 | <1 | 19.6 | 14.5 | 206 |
| | | | | | *9.0* | *25.1* | *0.9* | *2.5* | | | | | | *25.1* | *<1* | *131* | *16.8* | *219* |
| Exp. 5 3 minute effluent- 1 | 7.4 | 205 | 8.8 | 20.0 | 8.7 | 26.6 | 0.8 | 2.1 | 9.5 | 5.0 | 38.3 | 0.109 | 50 | 2.5 | <1 | 5.0 | <10 | 462 |
| | | | | | *8.9* | *28.6* | *0.9* | *2.4* | | | | | | *22.8* | *1.3* | *104* | *<10* | *1360* |
| Exp. 5 3 minute effluent- 2 | 7.4 | 205 | 8.8 | 20.0 | 8.6 | 26.3 | 0.8 | 2.1 | - | - | 37.5 | 0.105 | 50 | 2.1 | <1 | 4.5 | <10 | 474 |
| | | | | | *8.7* | *27.8* | *0.9* | *2.3* | | | | | | *25.0* | *1.2* | *105* | *13.5* | *1310* |
| Exp. 5 3 minute effluent- 3 | 7.5 | 203 | 8.8 | 19.9 | 8.8 | 26.9 | 0.9 | 2.1 | - | - | 37.5 | 0.109 | - | 2.0 | <1 | 7.1 | <10 | 479 |
| | | | | | *8.7* | *27.4* | *0.9* | *2.3* | | | | | | *32.0* | *1.2* | *117* | *<10* | *1310* |

### 2.7.2 SHELLS: METAL CONTENT AND SEQUENTIAL EXTRACTION LEACHATES

#### METAL CONTENT

No relevant reference material to analyse with the samples was identified, so samples were processed in replicate where possible and results for each replicate interpreted separately. Where each replicate showed a similar result or trend the overall results were considered valid.

As noted in 2.5.4, method blanks were included with each digestion and used to correct all results. A shell blank was also analysed: a sample of the shells prepared for this study's column experiments, which had not been rinsed. There was some Fe, Mn, and Al present on the full shells, which could have been introduced by the sieving and mixing processes used to prepare them for the columns, during weathering prior to obtaining the shells for this experiment, or as traces naturally present in the shells (Table 2-10). They otherwise show no detection of the other metals tested for, with the exception of a small amount of Cu in one of the replicates (Table 2-10).

Zn was detected on the organic layer when this was analysed separately, though not on the full shell (Table 2-10). This was likely because in the full shell digestion the Zn concentration would have been diluted with low-Zn calcite/aragonite. Fe, Mn and Al were present on the blank in similar concentrations to those measured on the laboratory column shells, but very little Zn or Cu was observed (Table 2-10).

**Table 2-10:** Metal content results for the unused shell "blank" sample.

| | Element (mg/kg) | Fe | Mn | Al | Zn | Cu |
|---|---|---|---|---|---|---|
| Full shell | Replicate 1 | 40.4 | 6.15 | <1 | <0.3 | 0.74 |
| | Replicate 2 | 27.6 | 5.98 | 23.1 | <0.3 | <0.6 |
| | Replicate 3 | 12.3 | 3.28 | <1 | <0.3 | <0.6 |
| | *Mean* | *26.8* | *5.13* | *23.3* | *<0.3* | *0.74* |
| Organic layer only | Replicate 1 | 593 | 28.6 | 649 | 9.99 | 7.87 |
| | Replicate 2 | 455 | 24.7 | 432 | 7.89 | 9.72 |
| | Replicate 3 | 533 | 24.0 | 503 | 6.27 | 10.0 |
| | *Mean* | *527* | *25.7* | *528* | *8.05* | *9.2* |

#### SEQUENTIAL EXTRACTIONS

There are some well-known difficulties that arise in a sequential extraction procedure which make it less viable as a quantitative method (Bacon & Davidson, 2008). The selectivity of reagents, the efficiency of the reaction, re-adsorption of the target elements to other fractions, or formation of 'new' compounds during the reactions can all affect the quantitative precision and accuracy of the

procedure (Bacon & Davidson, 2008). Even the choice to dry and grind the samples can allow the target elements to redistribute into different fractions prior to the extraction procedure (Bacon & Davidson, 2008).

Therefore, to evaluate whether the Cu and Zn results from this method would be valid Ca, Mn, and Fe fractionation within the shells was also analysed to see if they were leached in the expected fraction. These analyses are presented in the results (section 3.8.1).

An unused shell "blank" was analysed with the experimental shells as an estimate of the trace element concentrations that would likely be present prior to being exposed to roof runoff. Cu was at/below detection in all fractions, but there were small concentrations of Zn in most fractions: the highest being 3.9 mg/kg in the carbonates fraction (Table 2-11). Low levels of Mn were present in most fractions (<6 mg/kg, Table 2-11). Higher concentrations of Fe and Al were measured in these blank shells, and the highest concentrations of both were in the 'crystalline Fe oxides' fraction: up to 253 mg/kg Fe and 94.5 mg/kg Al (Table 2-11).

**Table 2-11:** Sequential extraction analysis results for the unused shell "blank" sample.

| | Element (mg/kg) | Fe | Mn | Al | Zn | Cu | Ca |
|---|---|---|---|---|---|---|---|
| SEP | Water soluble | <0.4 | <0.05 | 1.1 | <0.3 | <0.6 | 442 |
| | Readily exchangeable | <0.4 | 3.4 | <1 | <0.3 | 0.7 | 2760 |
| | Bound to carbonates | 1.6 | 5.5 | 1.6 | 3.9 | <0.6 | 151000 |
| | Bound to Mn oxides | <0.4 | 0.6 | <1 | 0.3 | <0.6 | 6610 |
| | Bound to amorphous Fe oxides | 33.1 | 0.5 | 17.7 | 0.4 | <0.6 | 33.0 |
| | Bound to crystalline Fe oxides | 253 | 2.2 | 94.5 | 0.7 | <0.6 | 19.8 |
| | Bound to organics | 121 | 4.3 | 92.1 | 0.4 | <0.6 | 26300 |
| Calculated | Sum of all SEP fractions | 409 | 16.5 | 207 | 5.7 | 0.7 | 187000 |

Where a numerical result was returned for a parameter which was subsequently determined to be below detection, the result returned was used as an estimate of the actual concentration for graphing purposes, but reported as below the appropriate detection limit. In sum calculations results below detection were treated as zero. Identification of trends across experiments was a key part of interpretation of this dataset, and where these trends were seen this suggested that the results were sensible in spite of being below the estimated limit of detection, and so their inclusion was warranted.

# 3 RESULTS: EXPERIMENTAL

In this chapter first the experimental columns' hydraulic conductivity is reported, then physico-chemical results for the influents and effluents from the three sets of column experiments are presented. The real roof runoff sample compositions are then compared with the synthetic roof runoff composition used in the column experiments.

The results from investigations into the used shells are then provided. First, XRD and volatile solids results describing the make-up of the shells themselves are presented. Then results from hot acid digestions are given to show the amount of Zn and Cu found in the shells, and in some cases the distribution of them within a column, or between the organic and inorganic fractions of the shell. A finer distinction between phases that the Zn and Cu were bound to in the shells is then shown via the results from the sequential extractions performed. Finally, images and elemental analyses performed by SEM-EDS are presented to show any spatial and/or morphological characteristics of Zn and Cu seen on used shells.

## 3.1 COLUMN FUNCTION: $K_{SAT}$

The constant head saturated hydraulic conductivity ($K_{sat}$) varied slightly between the three columns from 37.2 to 40.7 m/hr. This correlated to a contact time between the shells and the runoff of ≈30 seconds. It was observed that this was also the time taken for the first flush of effluent to emerge following the start of runoff inflow, therefore it appeared that the degree of water saturation in the column made little difference to the contact time.

The $K_{sat}$ values from the present study are similar to those columns from which this study's used shell samples were taken (described in section 2.5.1): Heffernan and Howe (2019) measured 30–42 m/hr in their laboratory columns, and their shells had been prepared in the same manner as this study; and Bilek (2019) measured 28.1–35.2 m/hr for the two field columns, for which the shells had not been crushed or sieved (Figure 2-6). Therefore different hydraulic conductivities did not prevent comparison of the results between those studies, from which this study's used shells were collected, and this.

## 3.2 BASELINE COLUMN EXPERIMENT: SOLUTION ANALYSIS

This column experiment was run in triplicate columns using un-modified tap water. The main purpose was to examine the trends in water quality parameters that occurred due to the treatment system, but without augmented influent Zn or Cu concentrations. The secondary purpose was to assess the variability between columns. Therefore, results described are the mean of the triplicates (or duplicates for the influent), but the standard deviation is also presented.

The pH increased from 7.1 to 7.4 within 5 minutes of flow, reaching a maximum of 7.6 after 45 minutes (Table 3-1). DO concentrations in the influent indicated an oxygenated solution (8.6 mg/L). DO was slightly lower in the first flush effluent (8.2) than in the influent, but had returned to slightly above influent levels (8.7 mg/L) by 5 minutes of flow (Table 3-1). There was a spike in specific conductance and turbidity in the first flush effluent, ≈10x and 2000x the influent results respectively, but by 5 minutes of flow both had returned to close to influent levels (Table 3-1). The turbidity in the first flush

effluent was a beige sediment visible to the naked eye. Standard deviations indicate the results from each column were in close agreement, with the exception of the first flush effluents (Table 3-1).

**Table 3-1: Mean (n=3 for effluents, n=2 for influent) physico-chemical results from the baseline column experiments, standard deviation in *bracketed italics.***

| Sample | pH | Specific conductance (µS/cm) | Dissolved oxygen (mg/L) | Turbidity (NTU) |
|---|---|---|---|---|
| **Influent (tap water)** | 7.1 *(0.1)* | 115.6 *(1.6)* | 8.6 *(0)* | 0.15 *(0)* |
| **First flush effluent (30s)** | 7.1 *(0)* | 1128 *(36.7)* | 8.2 *(0.1)* | 300 *(82.7)* |
| **Effluent 5min** | 7.4 *(0.1)* | 142.5 *(1.8)* | 8.7 *(0)* | 0.41 *(0)* |
| **Effluent 15min** | 7.4 *(0.2)* | 131.1 *(1.9)* | 8.7 *(0)* | 0.22 *(0)* |
| **Effluent 30min** | 7.5 *(0.2)* | 127.6 *(1.0)* | 8.7 *(0)* | 0.22 *(0.1)* |
| **Effluent 45min** | 7.6 *(0.1)* | 126.6 *(1.4)* | 8.7 *(0.1)* | 0.26 *(0.1)* |

Most major ion concentrations in the effluent returned to close to influent concentrations within the first 5 minutes (Table 3-2). Ca and $HCO_3$ were the exceptions, remaining slightly elevated from influent concentrations throughout the 45 minutes, and could be expected due to some dissolution of the shells (Table 3-2). The first flush effluent had major ion concentrations 2–13x the influent concentrations (Table 3-2). Standard deviations were low, though higher in the first flush effluent (Table 3-2).

**Table 3-2: Mean (n=3 for effluents, n=2 for influent) (dissolved) major ion results from the baseline column experiments, standard deviation in *bracketed italics.***

| Sample | Na (mg/L) | Ca (mg/L) | K (mg/L) | Mg (mg/L) | Cl (mg/L) | $SO_4$ (mg/L) | $HCO_3$ (mg/L) |
|---|---|---|---|---|---|---|---|
| **Influent (tap water)** | 8.2 *(0)* | 10.8 *(0.1)* | 0.8 *(0)* | 2.4 *(0)* | 4.4 *(0)* | 3.5 *(0)* | 51 *(0.3)* |
| **First flush effluent (30s)** | 47.2 *(1.8)* | 149 *(8.1)* | 3.7 *(0.1)* | 11.5 *(1)* | 10.1 *(0.2)* | 41.7 *(3.5)* | 134 *(5.7)* |
| **Effluent 5min** | 9.4 *(0.5)* | 16.6 *(0.7)* | 0.9 *(0)* | 2.4 *(0.1)* | 4.4 *(0)* | 4.3 *(0)* | 56 *(0.1)* |
| **Effluent 15min** | 8.7 *(0.2)* | 14.3 *(0.2)* | 0.9 *(0)* | 2.4 *(0.1)* | 4.4 *(0)* | 3.9 *(0)* | 55 *(0.3)* |
| **Effluent 30min** | 8.0 *(0.6)* | 13.2 *(0.7)* | 0.8 *(0)* | 2.3 *(0.2)* | 4.4 *(0)* | 3.8 *(0)* | 55 *(0.3)* |
| **Effluent 45min** | 8.1 *(0.5)* | 13.1 *(0.7)* | 0.8 *(0)* | 2.3 *(0.2)* | 4.4 *(0)* | 3.8 *(0)* | 55 *(0.3)* |

Nitrate and phosphate concentrations remained elevated over 30–45 minutes of flow (Table 3-3). Both peaked in the first flush effluent (nitrate 184x, and phosphate 12x their influent concentrations), and at 45 minutes the effluent phosphate concentration was still double the influent concentration (Table 3-3). Nitrate had returned to below influent concentrations by 45 minutes of flow, and ammonia by 5 minutes (Table 3-3). Nutrient concentrations were higher than expected, but investigation into the their source was outside the scope of this study.

**Table 3-3: Mean (n=3 for effluents, n=2 for influent) (dissolved) nutrient results from the baseline column experiments, standard deviation in *bracketed italics.***

| Sample | $NO_3$ (mg/L) | $NH_4$ (mg/L) | $PO_4$ (mg/L) |
|---|---|---|---|
| **Influent (tap water)** | 2.4 *(0)* | 0.02 *(0)* | 0.034 *(0.001)* |
| **First flush effluent (30s)** | 441 *(42.6)* | 0.08 *(0.02)* | 0.40 *(0.03)* |
| **Effluent 5min** | 8.6 *(1)* | 0.02 *(0.004)* | 0.15 *(0.005)* |
| **Effluent 15min** | 4.8 *(1.2)* | 0.02 *(0.002)* | 0.10 *(0.002)* |
| **Effluent 30min** | 2.7 *(0.3)* | 0.02 *(0.002)* | 0.076 *(0.001)* |
| **Effluent 45min** | 2.1 *(0.1)* | 0.02 *(0.001)* | 0.070 *(0.005)* |

Fe, Mn and Al were assessed together as they all commonly form oxide/hydroxide based adsorbing surfaces in the environment (Müller & Sigg, 1990; Stumm & Morgan, 1995). The first flush concentrations were higher than the influent or other effluents (both dissolved and acid soluble) (Table 3-4). There was little to no dissolved Fe or Mn present (<3 µg//L), and low amounts of dissolved Al (<10 µg/L) which was comparable to the blanks (Table 3-4). Acid soluble concentrations (particulate + dissolved) were all higher than their dissolved counterparts, meaning that these elements were predominantly present in particulate form (Table 3-4). Al concentrations were the highest of these three elements (≈50–70 µg/L acid soluble Al in a non-first flush effluent), and were comparable to concentrations reported for the blanks (Table 3-4). Acid soluble Fe concentrations were slightly higher than in the blanks, ≈30–50 µg/L, and acid soluble Mn was <2 µg/L (not including first flush effluents) (Table 3-4). Standard deviations were higher in the acid soluble concentrations (up to 9 µg/L) (Table 3-4).

The unmodified tap water already had experimentally relevant amounts of an analyte of interest (117 µg/L Zn), and so the experiment could not strictly be considered a control (Table 3-5). It was therefore interpreted as a low Zn experiment in its own right. Because of the closeness in acid soluble and dissolved Zn concentrations, all Zn was assumed to be present in a dissolved form (Table 3-5). On the other hand, the difference between acid soluble and dissolved Cu concentrations suggests some Cu

was present as a particulate (Table 3-5). Unlike Fe, Mn and Al, neither Zn nor Cu were higher in the first flush effluent than in the influent, suggesting that any particles first flushed out did not contain Zn or Cu. Dissolved Zn ($Zn_{diss}$) was reduced in the column by a minimum of 89%, and $Cu_{diss}$ by 74% (of 4.6 µg/L) (Table 3-5). Standard deviations were low (Table 3-5).

**Table 3-4: Mean (n=3 for effluents, n=2 for influent) dissolved and acid soluble Fe, Mn and Al results from the baseline column experiments, standard deviation in *bracketed italics.***

| Sample | Dissolved (µg/L) | | | Acid soluble (µg/L) | | |
|---|---|---|---|---|---|---|
| | Fe | Mn | Al | Fe | Mn | Al |
| **Influent (tap water)** | <10 | 2.3 *(0)* | 3.0 *(1.4)* | 33.6 *(1.8)* | 2.7 *(0.2)* | 40.3 *(0.4)* |
| **First flush effluent (30s)** | <10 | 3.0 *(0.7)* | 8.7 *(1.4)* | 1150 *(161)* | 49.4 *(7.1)* | 1960 *(281)* |
| **Effluent 5min** | <10 | <1 | 7.5 *(2)* | 47.3 *(0.7)* | 1.6 *(0.1)* | 71.5 *(5.4)* |
| **Effluent 15min** | <10 | <1 | 7.9 *(1.5)* | 38.5 *(3.7)* | 1.5 *(0.1)* | 56.5 *(7.8)* |
| **Effluent 30min** | <10 | <1 | 5.8 *(2.6)* | 37.5 *(9.1)* | 1.6 *(0.1)* | 52.3 *(5.9)* |
| **Effluent 45min** | <10 | 1.1 *(0.1)* | 5.0 *(1.1)* | 32.9 *(4.2)* | 1.7 *(0.1)* | 49.4 *(8.5)* |

**Table 3-5: Mean (n=3 for effluents, n=2 for influent) dissolved and acid soluble Zn and Cu results from the baseline column experiments, standard deviation in *bracketed italics.* The acid soluble influent Zn concentration was lower than the dissolved concentration but within 10%, so the result was not altered.**

| Sample | Dissolved (µg/L) | | Acid soluble (µg/L) | |
|---|---|---|---|---|
| | Zn | Cu | Zn | Cu |
| **Influent (tap water)** | 117 *(0.4)* | 4.6 *(0.1)* | 105 *(8.5)* | 5.7 *(0.5)* |
| **First flush effluent (30s)** | 11.2 *(0.4)* | 3.0 *(0.1)* | 36.5 *(3.3)* | 5.9 *(0.3)* |
| **Effluent 5min** | <10 | 1.2 *(0.1)* | <10 | 2.0 *(0)* |
| **Effluent 15min** | <10 | 1.0 *(0.1)* | 11.5 *(0.8)* | 1.9 *(0.1)* |
| **Effluent 30min** | 12.0 *(2.7)* | <1 | 15.2 *(0.5)* | 1.9 *(0.2)* |
| **Effluent 45min** | 14.3 *(1.6)* | <1 | 18.4 *(1.5)* | 1.8 *(0.1)* |

### 3.2.1 KEY FINDINGS

- The first flush effluent had a very different composition to both the influent and subsequent effluents;
- Effluent pH increased as flow through the column continued over 45 minutes;
- The majority of major ions had returned to close to influent concentrations by 5 minutes;
- Raised Ca and $HCO_3$ concentrations suggested that dissolution of the shells was occurring during flow;
- There was slightly more Al than Fe present in both influent and effluents, and it was mostly in particulate form;
- There was ≈0.1 mg/L Zn already in the unmodified tap water;
- Dissolved Zn and Cu are reduced from influent concentrations right from the first volume of water through the column;
- Running experiments in triplicate was not necessary for future experiments, due to low standard deviations between triplicate results.

## 3.3 ELEVATED Zn COLUMN EXPERIMENTS: SOLUTION ANALYSIS

Synthetic roof runoff solutions of ≈ 0.3, 1 and 3 mg/L $Zn_{diss}$ were run once through a shell packed column in the same manner as the baseline experiment. The primary purpose of this was to provide full influent and effluent solution chemistries (Appendix 1: Full chemical solution datasets) to use in PHREEQC modelling (Chapter 4). The secondary purpose was to investigate how any of the parameters might change with an increase in $Zn_{diss}$ concentration.

Dissolved and acid soluble Zn concentrations were so close as to suggest that all Zn was present in the dissolved form (Table 3-6, Figure 3-1). Regardless of the influent Zn concentration, Zn was reduced even from the first volume of water to flush through the column (Table 3-6, Figure 3-1). However, the higher the influent Zn concentration the higher the Zn concentration remaining in the effluent (Table 3-6, Figure 3-1). The concentration of Zn remaining in the effluent also increased as flushing time increased from 0–9 minutes (Table 3-6, Figure 3-1)

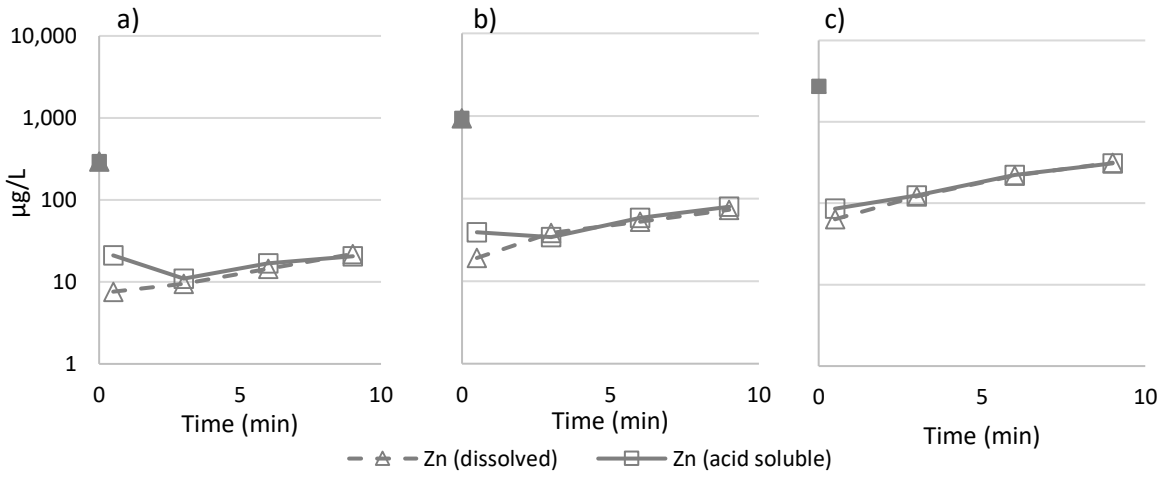


**Figure 3-1: Dissolved and acid soluble Zn (µg/L) across time in experiment 1 (chart a), experiment 2 (chart b) and experiment 3 (chart c). Log scale used for the concentration axis. Influent concentrations in filled markers, effluent concentrations in empty markers.**

**Table 3-6: Influent and effluent Zn concentrations (dissolved and acid soluble) in experiments 1-3. Each acid soluble influent Zn concentration was originally >10% lower than the dissolved concentration, so was set to the dissolved Zn concentration (see section 2.7.1). In the other three instances of acid soluble<dissolved concentrations, they were within the estimated method error and so were not modified.**

| Sample | Zn (µg/L) | | | | | |
|---|---|---|---|---|---|---|
| | Experiment 1 (≈ 0.3 mg/L Zn) | | Experiment 2 (≈ 1 mg/L Zn) | | Experiment 3 (≈ 3 mg/L Zn) | |
| | Dissolved | Acid soluble | Dissolved | Acid soluble | Dissolved | Acid soluble |
| **Influent** | 295 | 295 | 936 | 936 | 2740 | 2740 |
| **First flush effluent (30s)** | <10 | 21.0 | 19.1 | 39.2 | 63.6 | 85.8 |
| **Effluent 3min** | <10 | 11.0 | 38.4 | 34.1 | 121 | 125 |
| **Effluent 6min** | 14.4 | 16.8 | 52.2 | 58.3 | 218 | 223 |
| **Effluent 9min** | 21.9 | 20.5 | 73.1 | 79.5 | 315 | 309 |

Reductions of $Zn_{diss}$ as a percentage of the influent concentration varied from 97% at the highest to 73% at the lowest across all experiments performed (Figure 3-2). Between the highest and lowest reduction in each experiment the difference was ≤ 12%, and there were higher % reductions in higher influent Zn concentration solutions (Figure 3-2).

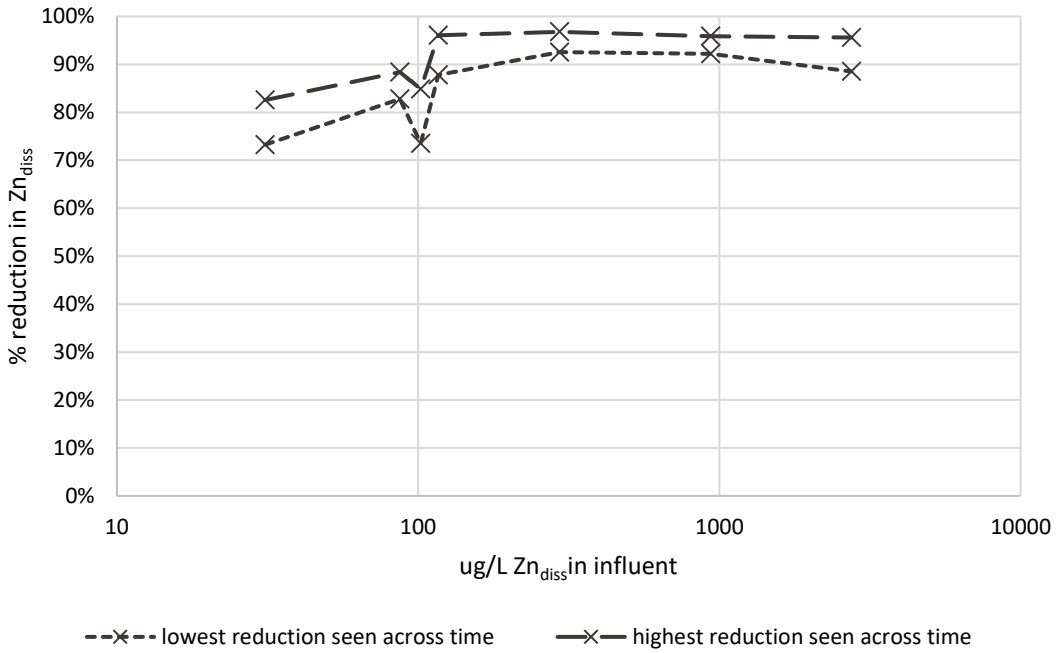


**Figure 3-2: The % reduction in effluent $Zn_{diss}$ concentrations for different influent $Zn_{diss}$ concentrations, shown for all experiments (baseline, elevated Zn, and elevated Cu experiments. Elevated Cu experimental data presented below). Both the lowest and highest reduction seen during each experiment are plotted.**

The maximum pH reached in an effluent in the three elevated Zn experiments varied between 7.6 and 7.8, and all increased across the time period sampled (9 minutes of flow) (Table 3-7).

**Table 3-7: Influent and effluent pHs in experiments 1-3.**

| Sample | pH | | |
|---|---|---|---|
| | Experiment 1 (≈ 0.3 mg/L Zn) | Experiment 2 (≈ 1 mg/L Zn) | Experiment 3 (≈ 3 mg/L Zn) |
| **Influent** | 6.7 | 6.7 | 6.9 |
| **First flush effluent (30s)** | 6.8 | 7.0 | 7.0 |
| **Effluent 3min** | 7.4 | 7.5 | 7.5 |
| **Effluent 6min** | 7.6 | 7.6 | 7.6 |
| **Effluent 9min** | 7.7 | 7.6 | 7.8 |

That the influent Zn concentration did not significantly impact the behaviour of pH, DO (Figure 3-3); major cations (Figure 3-4); nutrients (Figure 3-5); or dissolved and acid soluble Fe, Mn and Al (Figure 3-6) was suggested by the trends across time in each of these parameters being similar in each experiment. The peak in specific conductance in the first flush effluent did vary between experiments (by ≤1265 µS/cm), but the influent and subsequent effluents were comparable (≤60 µS/cm difference) and followed the same trends across time (Figure 3-3).

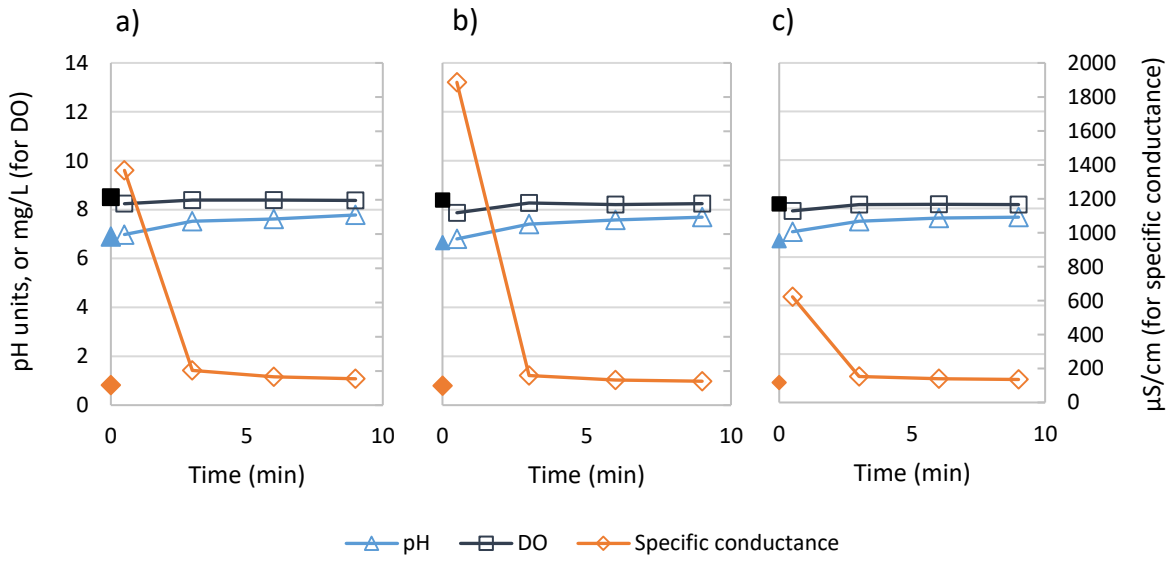


**Figure 3-3: pH, DO and specific conductance across time in experiment 1 (chart a), experiment 2 (chart b) and experiment 3 (chart c). Influent concentrations in filled markers, effluent concentrations in empty markers.**

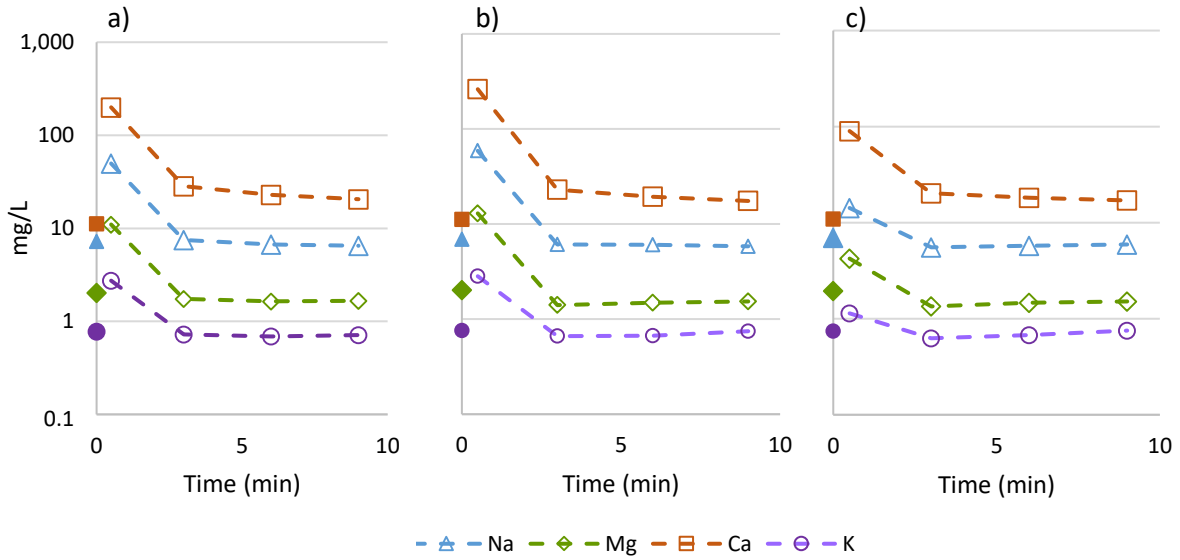


**Figure 3-4: Major cations (mg/L) across time in experiment 1 (chart a), experiment 2 (chart b) and experiment 3 (chart c). Log scale used for the concentration axis. Influent concentrations in filled markers, effluent concentrations in empty markers.**

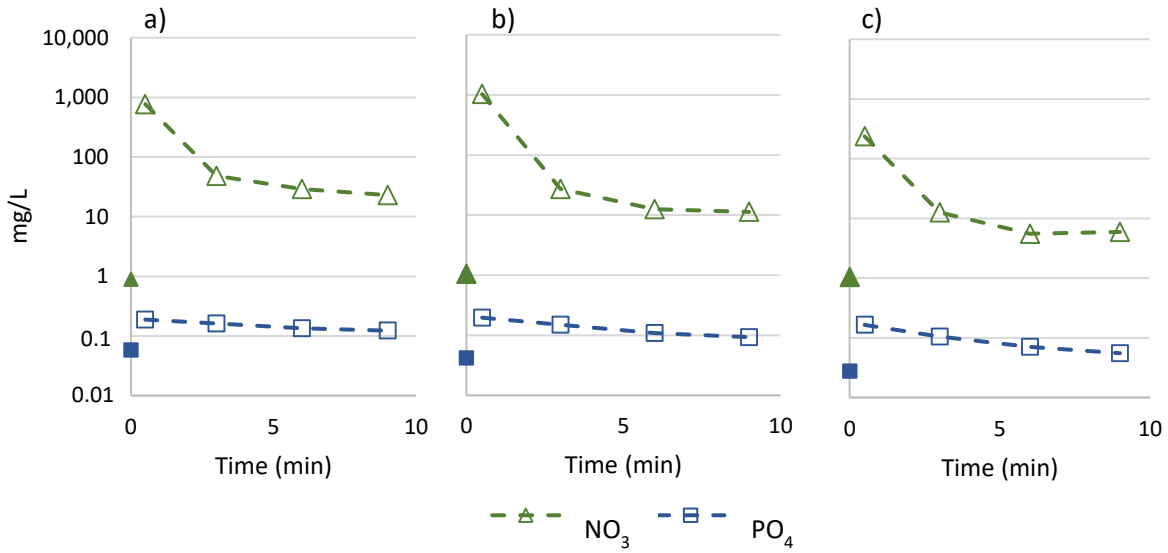


**Figure 3-5: Nitrate and phosphate (mg/L) across time in experiment 1 (chart a), experiment 2 (chart b) and experiment 3 (chart c). Log scale used for the concentration axis. Influent concentrations in filled markers, effluent concentrations in empty markers.**

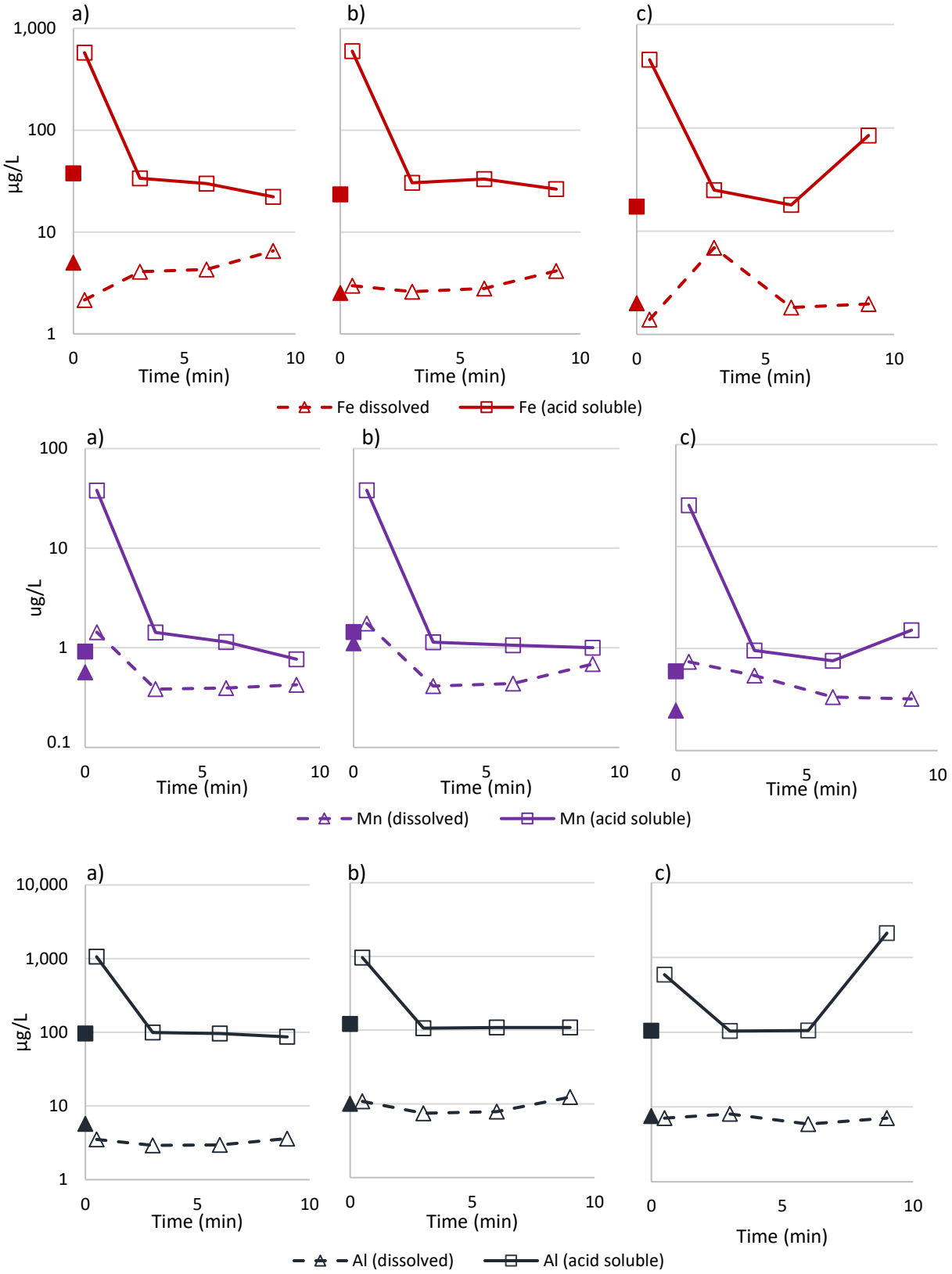


**Figure 3-6: Dissolved and acid soluble Fe (µg/L, top row, red), Mn (µg/L, middle row, purple) and Al (µg/L, bottom row, grey) across time in experiment 1 (chart a), experiment 2 (chart b) and experiment 3 (chart c). Log scale used for the concentration axis. Influent concentrations in filled markers, effluent concentrations in empty markers.**

Cu was present in very low initial concentrations (< 7µg/L, unmodified from the tap water base), and unlike Zn, up to ≈ 50% of the Cu was in particulate form (Figure 3-7). Nonetheless, both acid soluble and dissolved Cu were reduced from influent concentrations in the column (Figure 3-7).

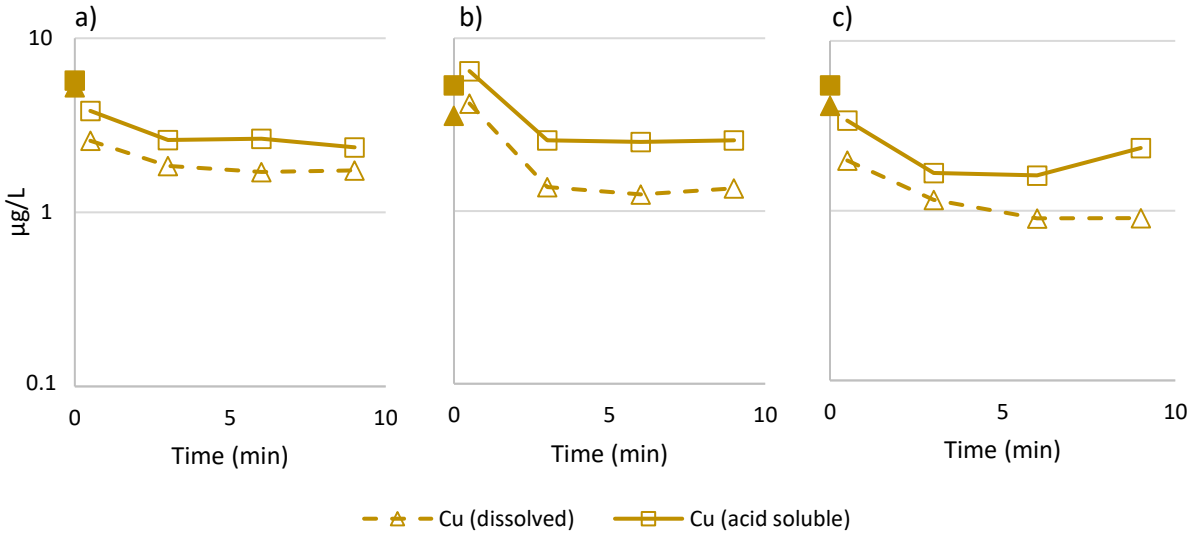


**Figure 3-7: Dissolved and acid soluble Cu (µg/L) across time in experiment 1 (chart a), experiment 2 (chart b) and experiment 3 (chart c). Log scale used for the concentration axis. Influent concentrations in filled markers, effluent concentrations in empty markers.**

Trends in each parameter measured for the elevated Zn experiments were the same as those in the baseline experiment, so trends in major anions and ammonia (not measured) were assumed to be comparable to the baseline experiment. As visually observed in the baseline experiment, a fine beige sediment was observed in each first flush effluent of these experiments, and not in the influents or subsequent effluents (turbidity not measured).

### 3.3.1 KEY FINDINGS

- Zn was almost exclusively present in the dissolved form;
- $Zn_{diss}$ was reduced in the column by 73%–97%;
- Initial Zn concentration did not influence any other parameter measured, so trends were the same as in the baseline experiment.

## 3.4 ELEVATED Cu COLUMN EXPERIMENTS: SOLUTION ANALYSIS

Synthetic roof runoff solutions of ≈ 0.5, 5 and 10 mg/L Cu were run once through a shell packed column in the same manner as the baseline and elevated Zn experiments. The primary purpose of this was to provide full influent and effluent solution chemistries (Appendix 1: Full chemical solution datasets) to use in PHREEQC modelling (Chapter 4). The secondary purpose was to investigate how any of the parameters might change with an increase in $Cu_{diss}$ concentration.

While all Cu was added in a dissolved form to make the synthetic roof runoff solutions, the particulate-dissolved partitioning changed prior to sampling/experimentation. The acid soluble concentrations were close to the concentration added (≈ 5 and 10 mg/L for experiments 5 and 6 respectively). In contrast, $Cu_{diss}$ concentrations were only ≈ 2 and 3 mg/L in these experiments (Table 3-8). Some

change in the Cu partitioning was expected, based on observed blue precipitation from the influent solutions (section 2.3.3). It was noted that both the influent and effluent samples from experiments 5 and 6 had a white opacity when the sample was mixed, which was visibly blue when settled out, showing that this precipitate was not (fully) removed in the column.

**Table 3-8: Influent and effluent Cu concentrations (dissolved and acid soluble) in experiments 4-6.**

| Sample | Cu (µg/L) | | | | | |
|---|---|---|---|---|---|---|
| | Experiment 4 (≈ 0.5 mg/L $Cu_{diss}$) | | Experiment 5 (≈ 2 mg/L $Cu_{diss}$) | | Experiment 6 (≈ 3 mg/L $Cu_{diss}$) | |
| | Dissolved | Acid soluble | Dissolved | Acid soluble | Dissolved | Acid soluble |
| **Influent** | 488 | 531 | 1990 | 4690 | 2900 | 9090 |
| **First flush effluent (30s)** | 105 | 114 | 698 | 1210 | 1380 | 3270 |
| **Effluent 3min** | 185 | 191 | 462 | 1360 | 774 | 3910 |
| **Effluent 6min** | 212 | 205 | 422 | 1100 | 728 | 3800 |
| **Effluent 9min** | 201 | 216 | 403 | 989 | 823 | 3820 |

In experiment 4 all Cu present in the effluent was dissolved, whereas in experiments 5 and 6 the higher concentration of acid soluble Cu was evidence of particulate Cu making it through the column (Table 3-8, Figure 3-8). This was consistent with the observation of a blue precipitate in those effluent samples. There was a reduction in both acid soluble and dissolved Cu concentrations in the effluent when compared to the influent, even in the first flush effluent (Table 3-8, Figure 3-8). This reduction stayed constant for the time period of the experiments (Table 3-8, Figure 3-8).

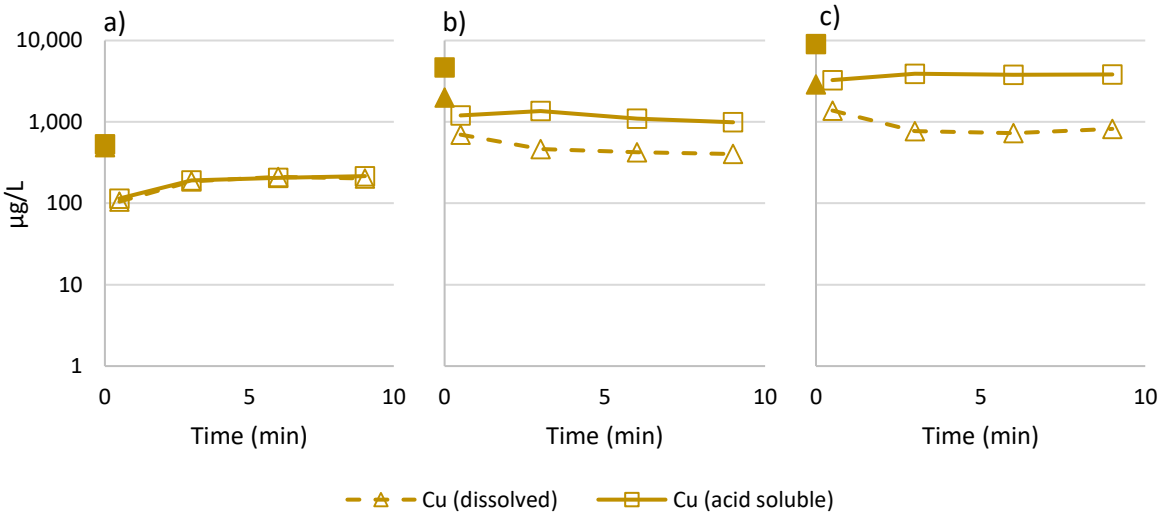


**Figure 3-8: Dissolved and acid soluble Cu (µg/L) across time in experiment 4 (chart a), experiment 5 (chart b) and experiment 6 (chart c). Log scale used for the concentration axis. Influent concentrations in filled markers, effluent concentrations in empty markers.**

The reduction in $Cu_{diss}$ as a percentage of the influent concentration ranged from 55% to 82% across all experiments performed, and the difference between the highest and lowest % reduction was only 6% at most (Figure 3-9). No clear trend can be discerned from the data about % removal and initial $Cu_{diss}$ concentration.

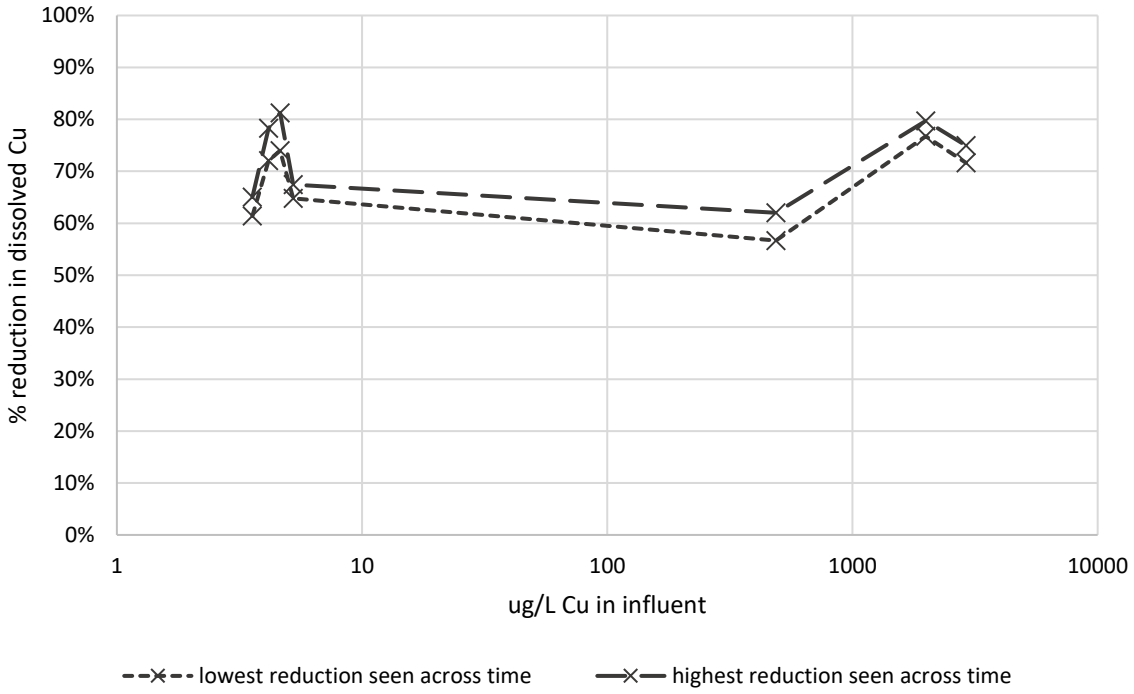


**Figure 3-9: The % reduction in effluent $Cu_{diss}$ concentrations for different influent $Cu_{diss}$ concentrations, shown for all experiments (baseline, elevated Zn, and elevated Cu experiments). Both the lowest and highest reduction seen during each experiment are plotted.**

The maximum pH reached in an effluent in the three elevated Cu experiments varied between 7.4 and 7.8, and all increased for at least the first 6 minutes. In experiments 5 and 6 the effluent pH plateaued after 6 minutes, while the pH of the 9 minute effluent in experiment 4 increased (Table 3-9).

**Table 3-9: Influent and effluent pHs in experiments 4-6.**

| Sample | pH | | |
|---|---|---|---|
| | Experiment 4 (≈ 0.5 mg/L $Cu_{diss}$) | Experiment 5 (≈ 2 mg/L $Cu_{diss}$) | Experiment 6 (≈ 3 mg/L $Cu_{diss}$) |
| **Influent** | 6.7 | 6.3 | 6.3 |
| **First flush effluent (30s)** | 7.0 | 6.7 | 6.7 |
| **Effluent 3min** | 7.5 | 7.4 | 7.2 |
| **Effluent 6min** | 7.7 | 7.6 | 7.4 |
| **Effluent 9min** | 7.8 | 7.6 | 7.4 |

pH, DO, specific conductance, nutrients and major cations (Figure 3-10); dissolved and acid soluble Fe, Mn and Al (Figure 3-11); and dissolved and acid soluble Zn (Figure 3-12) exhibit the same trends in these experiments as in the elevated Zn and baseline experiments. Therefore there was no evidence that different initial Cu concentrations influenced the other parameters measured.

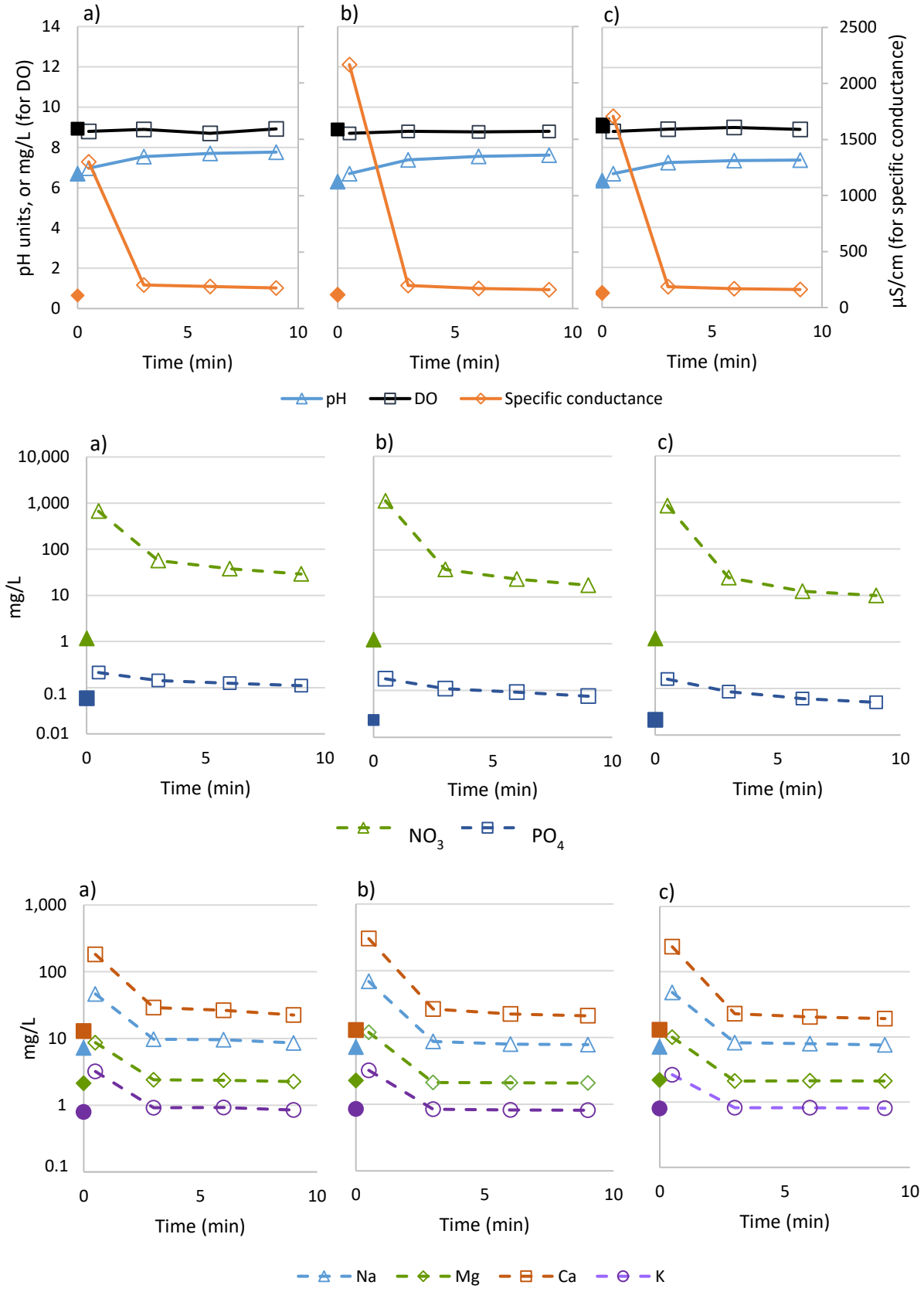


**Figure 3-10: pH, DO and specific conductance (top row), nitrate and phosphate (mg/L, middle row) and major cations (mg/L, bottom row) across time in experiment 4 (chart a), experiment 5 (chart b) and experiment 6 (chart c). Influent concentrations in filled markers, effluent concentrations in empty markers. Log scale used for the concentration axis in the middle and bottom row charts.**

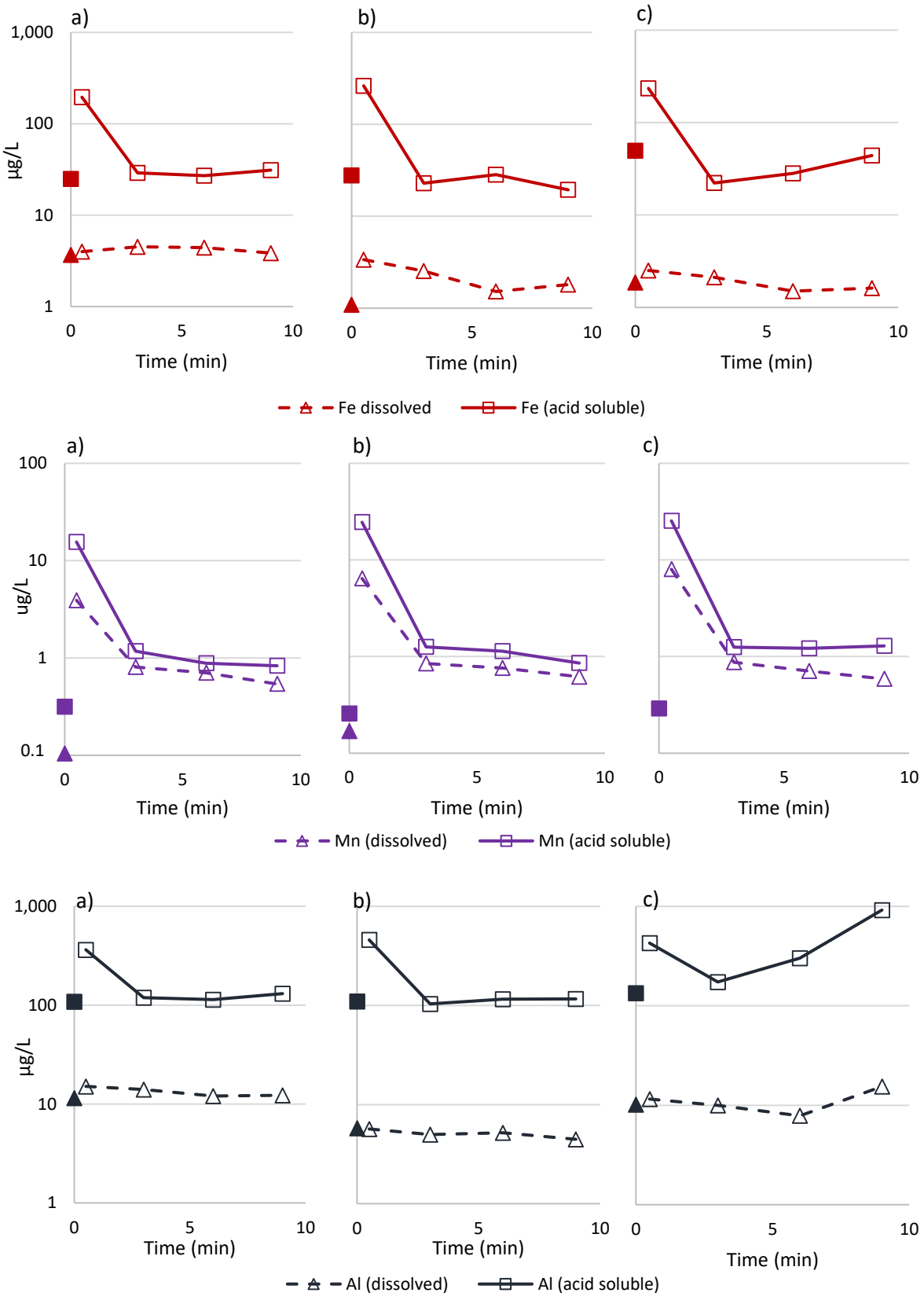


**Figure 3-11: Dissolved and acid soluble Fe (µg/L, top row, red), Mn (µg/L, middle row, purple) and Al (µg/L, bottom row, grey) across time in experiment 4 (chart a), experiment 5 (chart b) and experiment 6 (chart c). Log scale used for the concentration axis. Influent concentrations in filled markers, effluent concentrations in empty markers.**

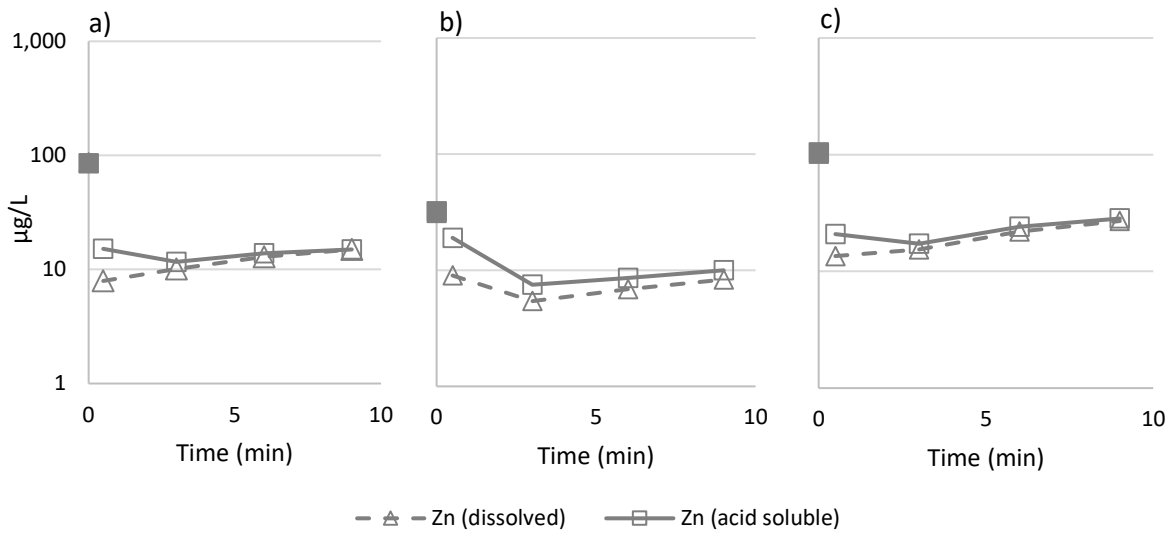


**Figure 3-12: Dissolved and acid soluble Zn (µg/L) across time in experiment 4 (chart a), experiment 5 (chart b) and experiment 6 (chart c). Log scale used for the concentration axis. Influent concentrations in filled markers, effluent concentrations in empty markers.**

As trends in each parameter measured for the elevated Cu experiments were the same as those in the baseline and elevated Zn experiments, the trends in major anions (not routinely measured) and ammonia (not measured) were assumed to be comparable to those experiments. Measurement of inorganic carbon, Cl and $SO_4$ in selected samples confirmed this assumption was valid (< 15% different from baseline values, Cl addition accounted for). Turbidity was not measured in these experiments, though as seen in the elevated Zn and baseline experiments the first flush effluents all showed a beige fine particulate.

Analysis of the top layer of the 5 mg/L synthetic roof runoff solution in the feeder tank, including the floating precipitate (analogous to that seen in Figure 2-5), showed the same composition as the bulk solution, with the exception of a very high nitrate concentration (32 mg/L) and a higher pH (7.9 vs 6.3 in the bulk solution). The origin of the nitrate is unclear, but the high pH and blue colour of the precipitate may indicate the presence of a Cu hydroxide/carbonate.

### 3.4.1 KEY FINDINGS

- Cu partitioned to the particulate phase when elevated ≥ 0.5 mg/L;
- Acid soluble and dissolved Cu were both reduced in the column, $Cu_{diss}$ by 55%–82%;
- Initial Cu concentration did not impact the behaviour of other parameters measured, so trends were the same as in the baseline and elevated Zn experiments.

## 3.5 REAL ROOF RUNOFF ANALYSIS

As an indication of how real roof runoff may differ from the synthetic roof runoff made with tap water (groundwater sourced), two samples of real roof runoff were analysed for the same suite of parameters as for synthetic roof runoff. One sample was from a Cu roof located at the University of Canterbury, the other was from a Zn roof located at Hagley College, Christchurch.

Comparisons of major ion and nutrient compositions with the tap water used in the laboratory experiments showed that no ions were consistently higher or lower, with the exception of ammonia which was higher in the real roof runoff (Table 3-10 and Table 3-11). DO concentrations in the roof runoff were indicative of a fully oxygenated water and pHs were similar to tap water (Table 3-10).

**Table 3-10: Physico-chemical and major ion results for two real roof runoff samples.**

| Sample | pH | DO (mg/L) | Na (mg/L) | Ca (mg/L) | K (mg/L) | Mg (mg/L) | Cl (mg/L) | $SO_4$ (mg/L) | $HCO_3$ (mg/L) |
|---|---|---|---|---|---|---|---|---|---|
| **Cu roof runoff** | 6.2 | 9.8 | 13.4 | 6.0 | 0.7 | 1.8 | 23.6 | <0.1 | 18 |
| **Zn roof runoff** | 6.4 | 9.9 | 4.2 | 3.2 | 0.5 | 0.8 | 6.0 | 9.8 | 10 |

**Table 3-11: Nutrient results for two real roof runoff samples.**

| Sample | $NO_3$ (mg/L) | $NH_4$ (mg/L) | $PO_4$ (mg/L) |
|---|---|---|---|
| **Cu roof runoff** | 0.5 | 0.2 | 0.01 |
| **Zn roof runoff** | 1.2 | 1.06 | 0.05 |

Dissolved Fe and Al was < 40 µg/L in both runoff samples, but both had much higher particulate concentrations. The acid soluble concentrations were approximately 400 and 700 µg/L for Fe and Al respectively in the Cu roof runoff, and approximately 2800 and 4700 µg/L respectively in the Zn roof runoff, placing them well above the concentrations seen in the blanks (Table 3-12). Overall Mn was in lower concentrations than Fe and Al (<47 µg/L acid soluble Mn) (Table 3-12). Fe, Mn and Al concentrations were all much higher (up to an order of magnitude) in the real roof runoff than in the tap water (Table 3-12).

The Cu roof runoff contained a Zn concentration (355 µg/L) that was almost 2/3 of the Cu concentration (540 µg/L), while the Zn roof runoff had very little Cu (2.4 µg/L) compared to Zn (260 µg/L) (Table 3-12). These concentrations were similar to the influents at the low end of the Zn and elevated Cu experiments.

**Table 3-12: Trace element results for two real roof runoff samples.**

| Sample | Dissolved (µg/L) | | | | | Acid Soluble (µg/L) | | | | |
|---|---|---|---|---|---|---|---|---|---|---|
| | Fe | Mn | Al | Zn | Cu | Fe | Mn | Al | Zn | Cu |
| **Cu roof runoff** | 8.1 | 19.8 | 38.7 | 355 | 540 | 405 | 25.8 | 763 | 355 | 759 |
| **Zn roof runoff** | 9.0 | 7.2 | 29.3 | 260 | 2.4 | 2870 | 46.3 | 4710 | 273 | 12.4 |

### 3.5.1 KEY FINDINGS

- No consistent differences in major ion concentrations were found between the roof runoff and tap water, with the exception of higher ammonia in the roof runoff;
- The roof runoff had Fe, Mn and Al concentrations up to an order of magnitude higher than in the tap water;
- Cu and Zn concentrations in the roof runoff were comparable to the lowest concentrations used in synthetic roof runoff experiments.

## 3.6 SHELL STRUCTURE

To clarify the form of $CaCO_3$ and quantify the presence of organic matter in the shell media used in experimental columns, two aspects of shell structure were investigated using sub-sampled whole shell fragments from the collection of shells used to pack this study's columns.

### 3.6.1 XRD RESULTS

XRD analysis confirmed that the two visibly different shell types in the shell mix supplied by the landscape gardening store had two different calcium carbonate structures. The blue shells were predominantly calcite, with minor amounts of aragonite, and this is consistent with the structure expected of *Mytilus edulis,* the common blue mussel (Cubillas et al., 2005). The non-blue shells were predominantly aragonite, with minor amounts of calcite, and this is consistent with the structure of *Perna canaliculus,* otherwise known as the New Zealand green-lipped mussel shell (Ben Shir et al., 2013). Therefore, a mix of aragonitic and calcitic calcium carbonate is assumed to be present in the shells packing the columns.

Though the samples were from a Zn loaded experimental column, it was not expected that XRD would detect any Zn minerals as they would be present in very low concentrations if at all. Indeed, no Zn minerals were found in XRD analysis.

### 3.6.2 VOLATILE SOLIDS

An estimate of the weight proportion of the organic periostracum layer in the shells is provided by the weight % of volatile solids. The four samples tested gave results ranging between 0.062 and 0.075 mg/g of volatile solids, so the weight % of the organic layer was estimated as 0.01%.

## 3.7 METAL CONTENT

To quantify the amount of Zn, Cu and other key metals (Fe, Al and Mn) present on Zn/Cu loaded shells, hot acid digestions were carried out on shell samples from other researcher's laboratory and field columns, as they had received higher Zn or Cu loads than the shells in this study and so were more likely to be in detectable concentrations (section 2.5.1). These digestions were performed on whole shell fragments sub-sampled from the collection of shells comprising the original sample. This meant that they were not homogenous replicates, and so results are presented as means as well as for each sub-sample.

### 3.7.1 FULL SHELL

Results for both the synthetic and real roof runoff of top/middle/bottom-of-the-column sample sets from Heffernan and Howe (2019)'s columns show that Zn concentrations decrease down the column, though in the real roof runoff samples the quantities measured in the middle and bottom were similar (Table 3-13). There was some variation between sub-samples from each location, but this did not negate the overall trend (Table 3-13).

**Table 3-13: Mean Zn concentrations (mg/kg) on shells from Zn loaded columns, standard deviation in bracketed italics, n provided for each mean. "-"not measured.**

| Sample location in column | Laboratory column: synthetic roof runoff (Zn spiked) | Laboratory column: real Zn roof runoff | Field column: Zn roof runoff |
|---|---|---|---|
| **Top** | 1450<br>*(186)*<br>*n=3* | 72.2<br>*(35.0)*<br>*n=2* | 93.7<br>*(18.3)*<br>*n=3* |
| **Middle** | 1140<br>*(147)*<br>*n=3* | 20.3<br>*(12.4)*<br>*n=3* | - |
| **Bottom** | 810<br>*(130)*<br>*n=3* | 17.6<br>*(14.9)*<br>*n=2* | - |

The mean Zn concentration of the samples from the synthetic laboratory column was 1,133 mg/kg, which was close to the concentration estimated by Heffernan and Howe (2019) of 1,040 mg/kg based on Zn loading and removal in their column. The top sample from the spent synthetic roof runoff laboratory column had a mean Zn concentration of 1450 mg/kg (Table 3-13), while top sample from the Zn roof field column had a mean Zn concentration of 93.7 mg/kg. The field column shell sample had been rinsed with DI water prior to acid digestion to remove excess debris from the shell (section 2.5.1), and analysis of the rinseate showed that 4.3 mg of Zn per kg of shell + debris was removed in this process. Therefore, the Zn concentration in this sample may have been underestimated. However, the field column had accumulated significantly less Zn than the spent laboratory column, and so could still be expected to be effective at Zn removal. Similarly, the real roof runoff laboratory column top sample had a mean Zn concentration of only 72.2 mg/kg, and the authors of that experiment (Heffernan & Howe, 2019) did confirm that the $Zn_{diss}$ removal efficiency at the time of sampling was still 80%.

The shell sample from the Cu roof field column had mean Cu concentration of 876 mg/kg Cu (n=3, standard deviation 203 mg/kg). The debris sampled from the same column had 19,400 mg/kg Cu, 33,800 mg/kg Fe, 17,400 mg/kg Al, and <2,000 mg/kg Zn, Pb, Cr, Ni, Cd and Mn.

Fe was highest in shells from the Cu roof field column, but not above the blank shell concentration in the Zn roof field column (Table 3-14). Al was consistently higher in experimental columns compared to the blank (by up to 58 mg/kg), as was Mn although concentrations were low (all <11 mg/kg) (Table 3-14).

**Table 3-14: Mean concentrations of Fe, Mn and Al (mg/kg) in shells from the top of five columns, standard deviation in bracketed italics.**

| Sample | Fe | Mn | Al |
|---|---|---|---|
| **Shell blank (n=3)** | 26.8 *(11.5)* | 5.1 *(1.3)* | 8.4 *(10.5)* |
| **Laboratory column: synthetic roof runoff (Zn spiked) (n=3)** | 66.2 *(18.0)* | 6.9 *(0.7)* | 66.4 *(32.9)* |
| **Laboratory column: real Zn roof runoff (n=2)** | 56.1 *(25.8)* | 10.7 *(1.2)* | 57.1 *(21.8)* |
| **Field column: Zn roof runoff (n=3)** | 14.5 *(3.9)* | 8.3 *(2.1)* | 17.9 *(2.1)* |
| **Field column: Cu roof runoff (n=3)** | 163 *(124)* | 10.0 *(2.2)* | 54.4 *(33.2)* |

Trace metal concentrations were transformed into mole proportions of the total amount of Al, Fe, Mn, Cu and Zn analysed in each sample. Those elements were chosen as they were found in every sample and sub-sample, and because Al, Fe and Mn are common adsorption surfaces for other trace elements such as Cu and Zn. If the Zn (or Cu) were associated with another particular trace metal, the relative proportions between the two could be expected to remain constant regardless of the actual concentration of Zn. However, the proportions of metals changed with changing shell Zn concentrations (Figure 3-13, Figure 3-15). Of particular interest was the mole ratio of Zn:Fe (see HFO modelling, section 4.4.7), and in most samples the amount of Zn far exceeded that of Fe (Figure 3-13, Figure 3-15). On the real runoff laboratory column shells however there was more Fe than Zn (Figure 3-13).

For shells used to treat Cu roof runoff, the amount of Cu far exceeds the amount of Fe in each sub-sample (Figure 3-14).

In almost all samples, Al was present in proportions of 0.03 up to 0.7 (Figure 3-13, Figure 3-15, Figure 3-14), showing its ubiquitous presence in roof runoff, Christchurch tap water (the base for the synthetic roof runoff), as well as the ease of introduction from the weathering and/or sieving process carried out with the shells prior to use. Small proportions of Mn were also seen in most samples, though in higher proportions in the shells exposed to real roof runoff than to synthetic roof runoff (Figure 3-13, Figure 3-15).

Full acid digestion results for each shell sample analysed, also including Pb, Cr, Cd and Ni concentrations are available in Appendix 2: Full chemical solids datasets.

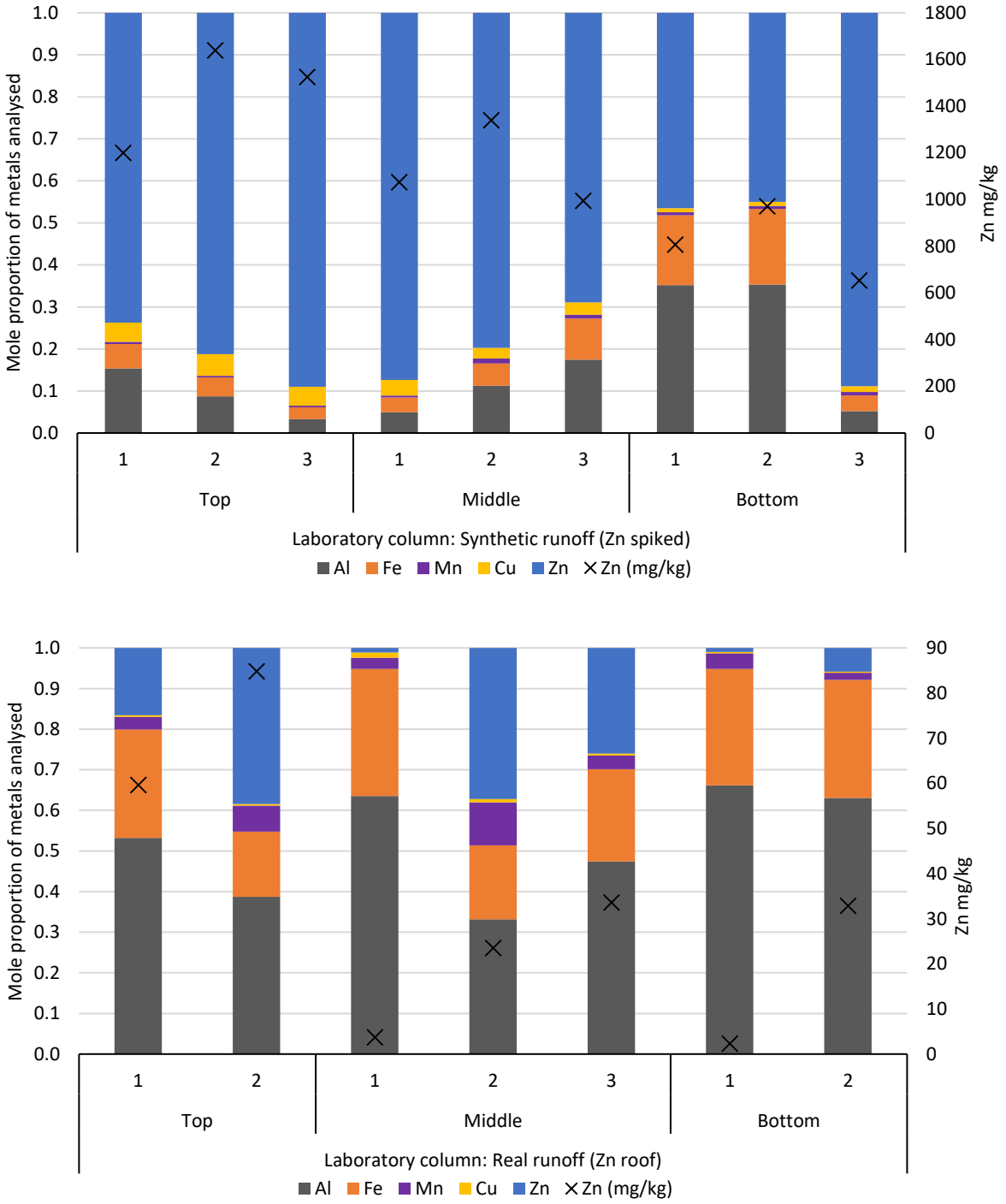


**Figure 3-13: Each trace metal as a mole proportion of the total amount of Al, Fe, Mn, Cu and Zn analysed, for the laboratory column samples loaded with synthetic Zn roof runoff (top chart), and laboratory column samples loaded with real runoff from a Zn roof (bottom chart). Top-Bottom denote where in the column the sample was from, and 1-3 denote the individual sub-samples tested from each location. Also showing the mean concentration of Zn in mg/kg on the secondary axis.**

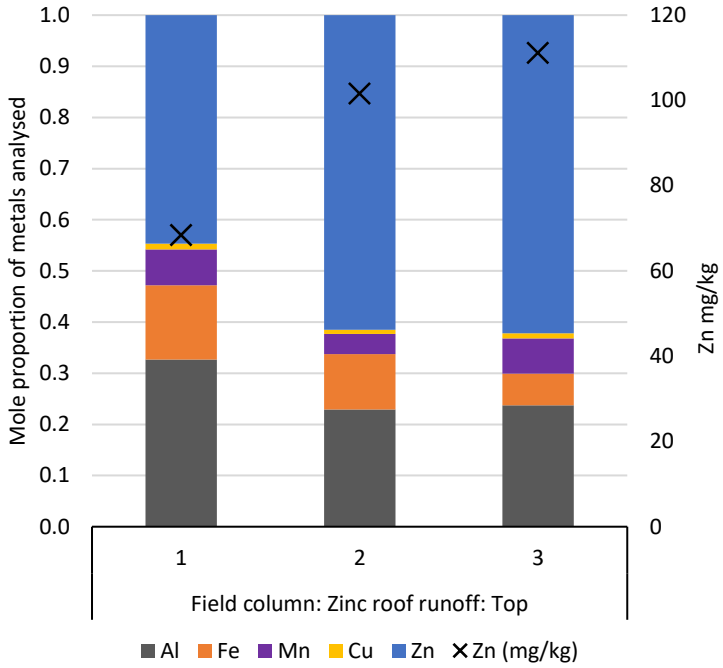


**Figure 3-14: Each trace metal as a mole proportion of the total amount of Al, Fe, Mn, Cu and Zn analysed, for the field column servicing a zinc roof. 1-3 denote the individual sub-samples tested, all of which were from the top of the column. Also showing the mean concentration of Zn in mg/kg on the secondary axis.**

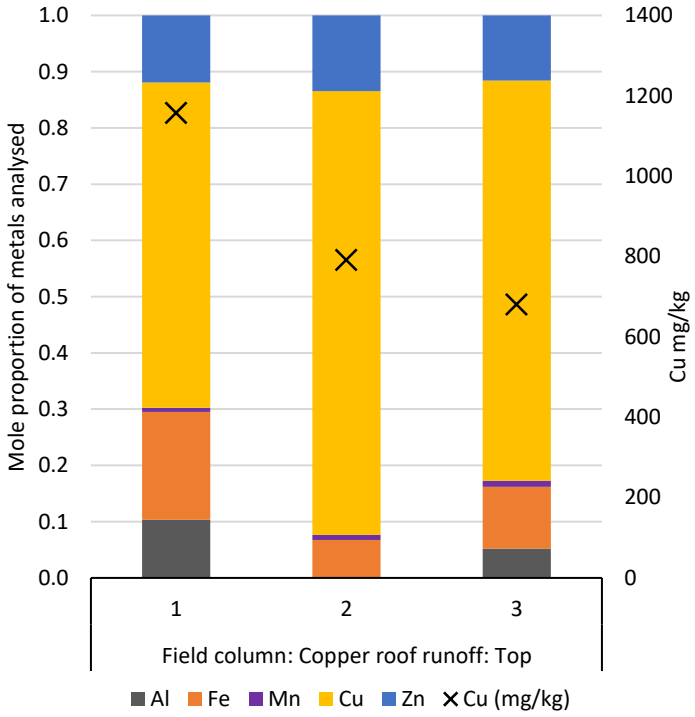


**Figure 3-15: Each trace metal as a mole proportion of the total amount of Al, Fe, Mn, Cu and Zn analysed, for the field column servicing a copper roof. 1-3 denote the individual sub-samples tested, all of which were from the top of the column. Also showing the mean concentration of Cu in mg/kg on the secondary axis.**

### 3.7.2 ORGANIC LAYER ONLY

Metal contents were also measured in the organic layer of shells from four different columns: the synthetic roof runoff laboratory column (top sample), the real runoff laboratory column (top sample), the Zn roof runoff field column (top sample), and the shell blank. Analysis of the organic layer from the Cu roof field column shells was not possible due to insufficient sample. On a weight/weight basis the organic layer had trace metal concentrations one to two orders of magnitude higher than those measured on the full shell (Table 3-15). The Fe, Mn and Al concentrations in the two laboratory column samples are close to or higher than those in the blank, while the field column had approximately twice as much Fe and Mn and ≈30% more Al (Table 3-15). Zn concentrations were 2-3 orders of magnitude higher in the experimental columns than in the blank, and the Cu concentrations were 2-100x higher than the blank (Table 3-15).

**Table 3-15: Mean trace element concentrations (mg/kg) in the organic layer of four column samples, standard deviation in bracketed italics.**

| Sample | Zn | Cu | Fe | Mn | Al |
|---|---|---|---|---|---|
| **Shell blank (n=3)** | 8.1 *(1.5)* | 9.2 *(1.0)* | 527 *(56.6)* | 25.7 *(2.0)* | 528 *(90.2)* |
| **Laboratory column: synthetic roof runoff (Zn spiked) (n=1)** | 6370 | 913 | 451 | 25.2 | 325 |
| **Laboratory column: real Zn roof runoff (n=2)** | 626 *(51.5)* | 19.3 *(0.6)* | 422 *(41.2)* | 32.7 *(0.9)* | 388 *(17.4)* |
| **Field column: Zn roof runoff (n=3)** | 509 *(29.5)* | 23.0 *(2.3)* | 1126 *(246)* | 51.9 *(4.4)* | 712 *(158)* |

The organic layer of the shell held a large weight/weight amount of the trace metals but itself made up only a small proportion of the total weight in a full shell sample (0.01%, section 3.6.2). To calculate the percentage contribution to the full shell, the element concentrations were multiplied by the weight % of the organic layer in the full shell. Results for the elements of interest (Al, Fe, Mn, Cu and Zn) are in Figure 3-16, which also shows the mean mg/kg concentration of each element in the full shell for context.

Overall the percentage of each trace metal attached to the organic layer of the shells was small, mostly <20%. In the Zn roof field column (Figure 3-16) all sub-samples had higher percentages (>30%) of Al and Fe attached to the organic layer, but comparison with the other samples shows that the proportion attached to the organic layer was not related to the whole shell concentration. Whole shell Zn concentrations for these samples ranged from 1450 to 72.2 mg/kg (Table 3-13), but regardless of the whole shell concentration <10% of Zn was found in the organic layer (Figure 3-16). The exception to this was in the shell blank, where Zn in the full shell was below detection (likely diluted by the comparatively large weight contribution of $CaCO_3$ to the sample size) and Zn in the organic layer was very low.

While Cu concentrations were not high in any of the samples analysed, in the 1–82 mg/kg Cu range seen in these samples the proportion attached to the organic layer was consistently slightly higher (10%-20%) than that for Zn.

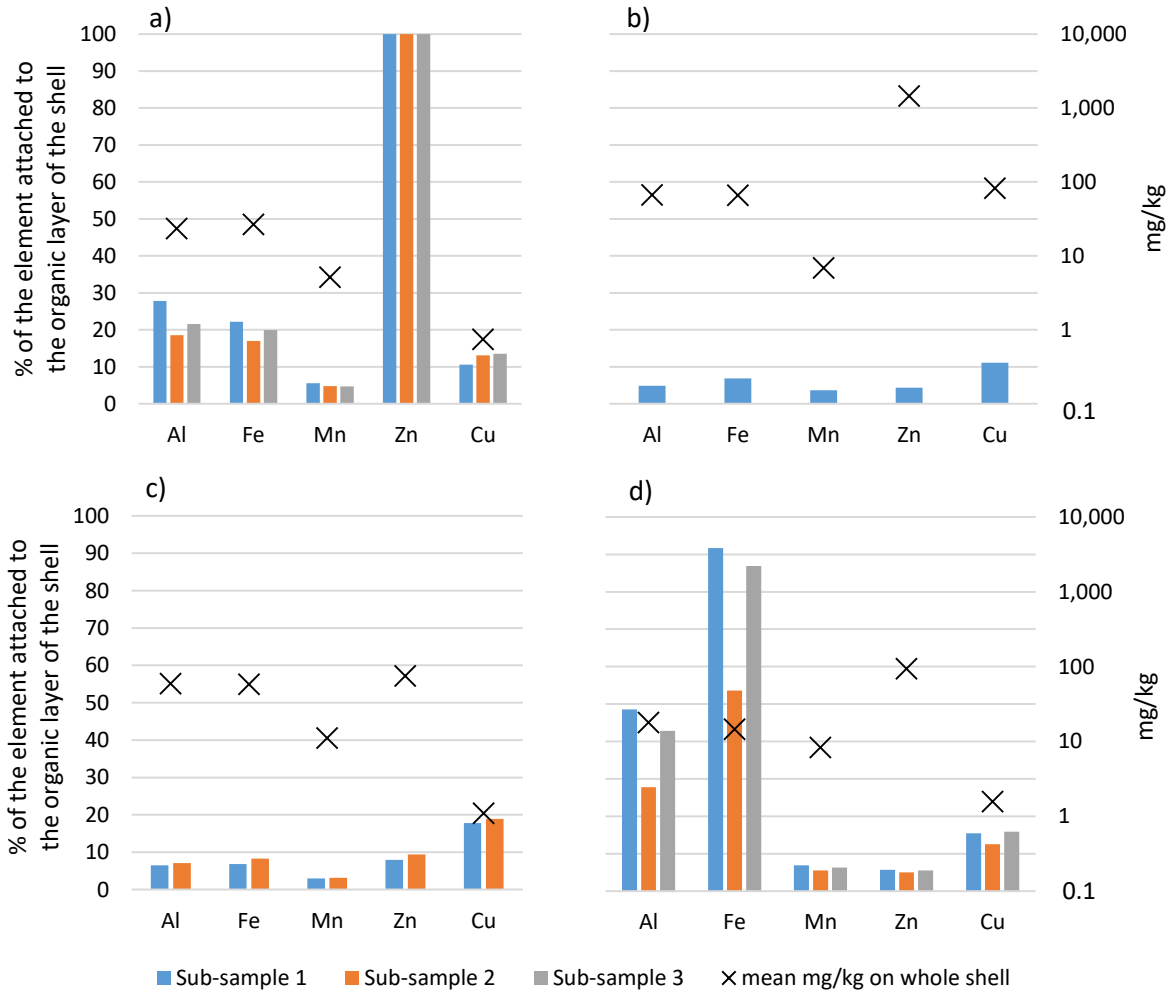


**Figure 3-16: The mass % of each element attached to the organic layer of the shell for A: the unused shell 'blank'; B: the synthetic runoff laboratory column; C: the real runoff laboratory column; and D: the Zn roof field column, shown for each sub-sample analysed. Also showing the mean amount of each element present on the whole shell in mg/kg, shown on a log scale.**

### 3.7.3 KEY FINDINGS

- Zn concentrations on the shells decreased down the column;
- The operationally saturated shells had a mean Zn concentration of 1,133 mg/kg;
- Zn and Cu mole concentrations were >> Fe mole concentrations;
- No relationship between the mole concentrations of Zn or Cu and Fe, Mn or Al was observed;
- On a weight/weight basis, Zn and Cu concentrations were 1–2 orders of magnitude higher on the organic layer than on the whole shell samples;
- Due to the organic layer comprising such a low proportion of the total shell weight, the proportion of whole shell Zn and Cu present on the organic layer was <20%.

## 3.8 SEQUENTIAL EXTRACTIONS

To provide a finer distinction of which phase any Zn or Cu was bound to in the shell sample, the shells were investigated by a sequential extraction procedure as described in Leleyter and Probst (1999). The full results for each sample are in Appendix 2: Full chemical solids datasets, and show the concentration of Fe, Mn, Al, Ca, Zn and Cu leached in each fraction, and the sum of the elements for all SEP fractions.

### 3.8.1 Ca, Fe, Mn, AND Al FRACTIONATION ON SHELLS

All of the elements Ca, Fe, Mn and Al were expected to be present as mineral phases on or within the shells, and could be expected to bind Zn or Cu to the shell. Therefore, as no relevant reference material was available and the procedure was not specifically designed for shells, the Ca, Mn and Fe leached in each fraction were measured to see if they were mainly extracted in the expected fraction. Ca was expected to leach in the "carbonates" fraction, Mn in the 'Mn oxides' fraction, and Fe in the "amorphous and crystalline Fe oxides" fraction, as the reagents were expected to dissolve the $CaCO_3$ and Mn and Fe oxides, not just to release ions bound to them (Chao, 1972; Leleyter & Probst, 1999).

Greater than 80% of the Ca was leached as expected in the "carbonates" fraction, while most of the remainder was released in the final "organics" fraction (Figure 3-17). After the "carbonates" extraction had been performed, in most samples some of the beige powder (assumed to be carbonate from the shells) remained clearly visible. This Ca would be released in the "organics" step which involved the addition of concentrated acid as well as heat, and would react with any remaining $CaCO_3$.

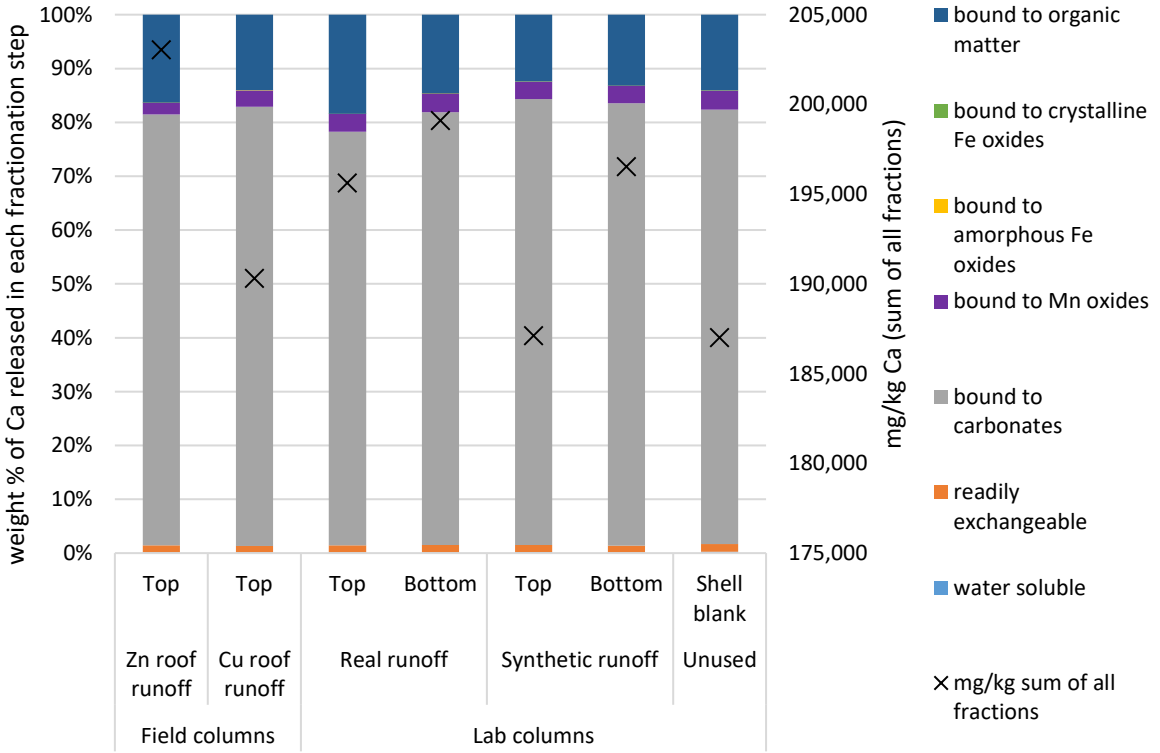


**Figure 3-17: Proportion of Ca released from shell samples in each fractionation step, and showing the sum of all fractions as mg/kg for each sample.**

For most samples Mn was released in the "readily exchangeable" and "carbonates" fractions, not the "Mn oxides" fraction as expected (Figure 3-18). However, the total amount of Mn was low (<20 mg/kg)

and mostly below the shell blank Mn concentration, so Mn oxides may not be present (Figure 3-18). Based on this, any proportions of Cu or Zn leaching in the "Mn oxides" step were treated with caution.

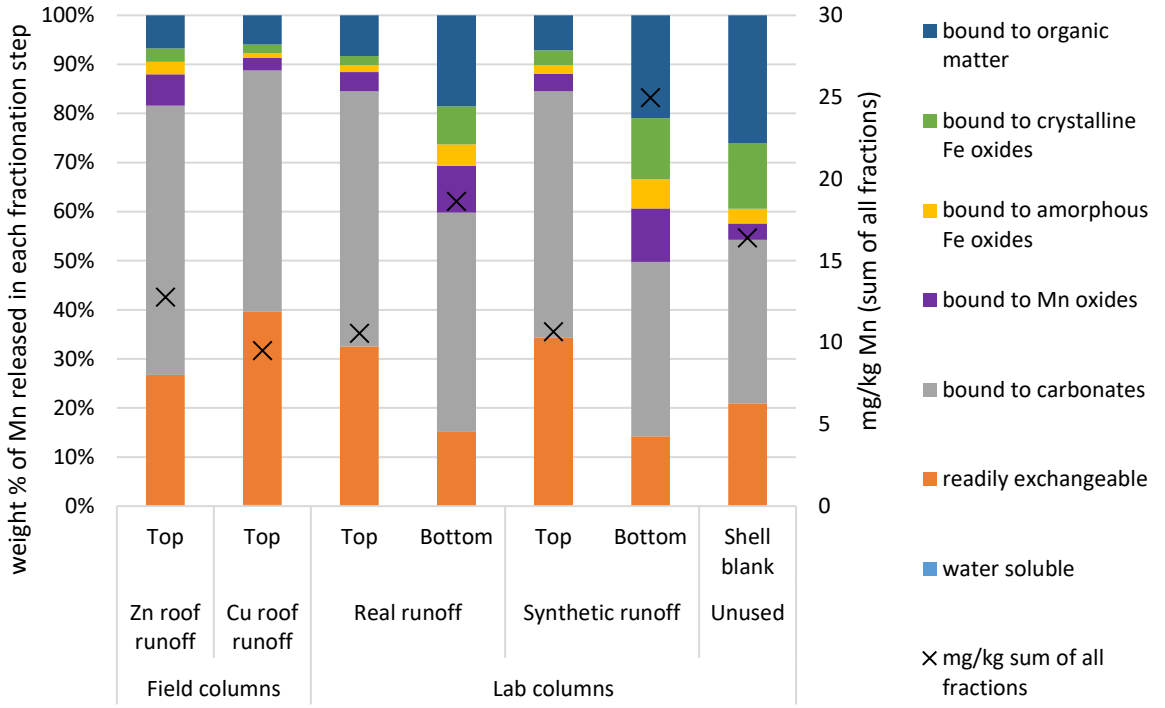


**Figure 3-18: Proportion of Mn released from shell samples in each fractionation step, and showing the sum of all fractions as mg/kg for each sample.**

More than 80% of the Fe was leached in the "amorphous Fe oxides" and "crystalline Fe oxides" steps as expected, and Fe concentrations were all above that measured in the shell blank (Figure 3-19).

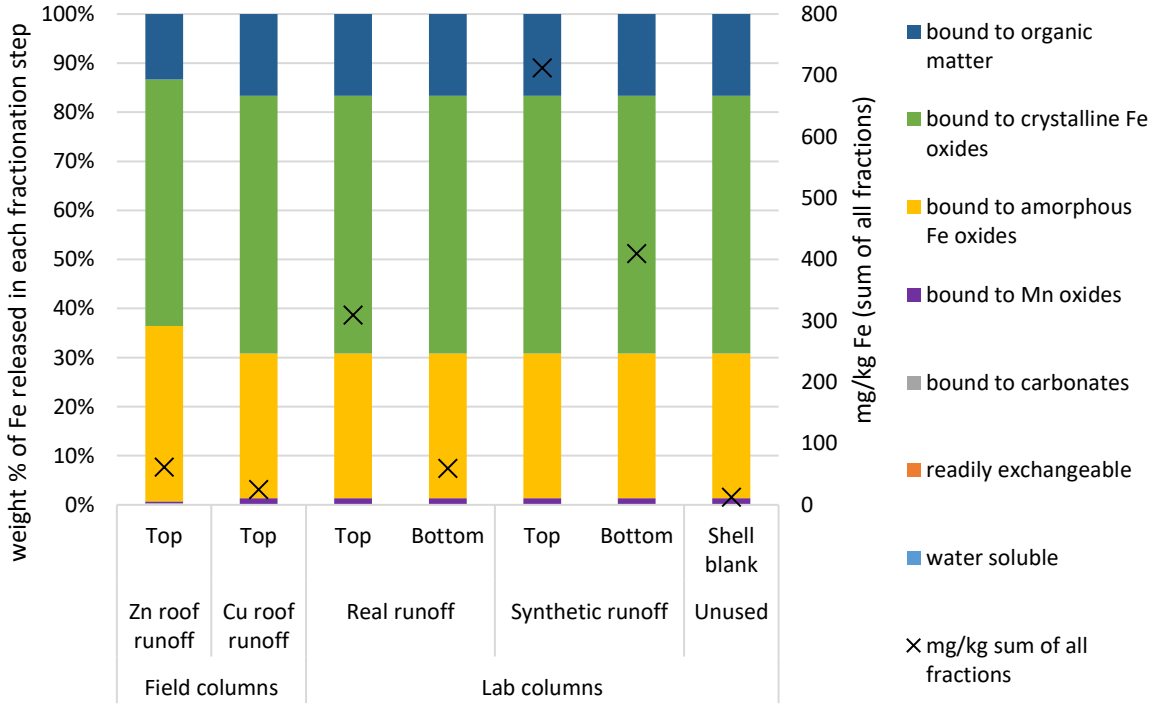


**Figure 3-19: Proportion of Fe released from shell samples in each fractionation step, and showing the sum of all fractions as mg/kg for each sample.**

The fractions in which Al was released was also investigated due to the presence of high amounts of Al (comparable to Fe concentrations, and above the shell blank concentrations), and the potential for oxide/hydroxides of Al to be an adsorbing surface similar to Fe or Mn oxides. Al was predominantly leached in the "amorphous and crystalline Fe oxides" and the "organics" fractions (Figure 3-20). Therefore, any amounts of Zn or Cu leaching in these steps could have been bound to an aluminium mineral, not just to a Fe oxide or organic surface.

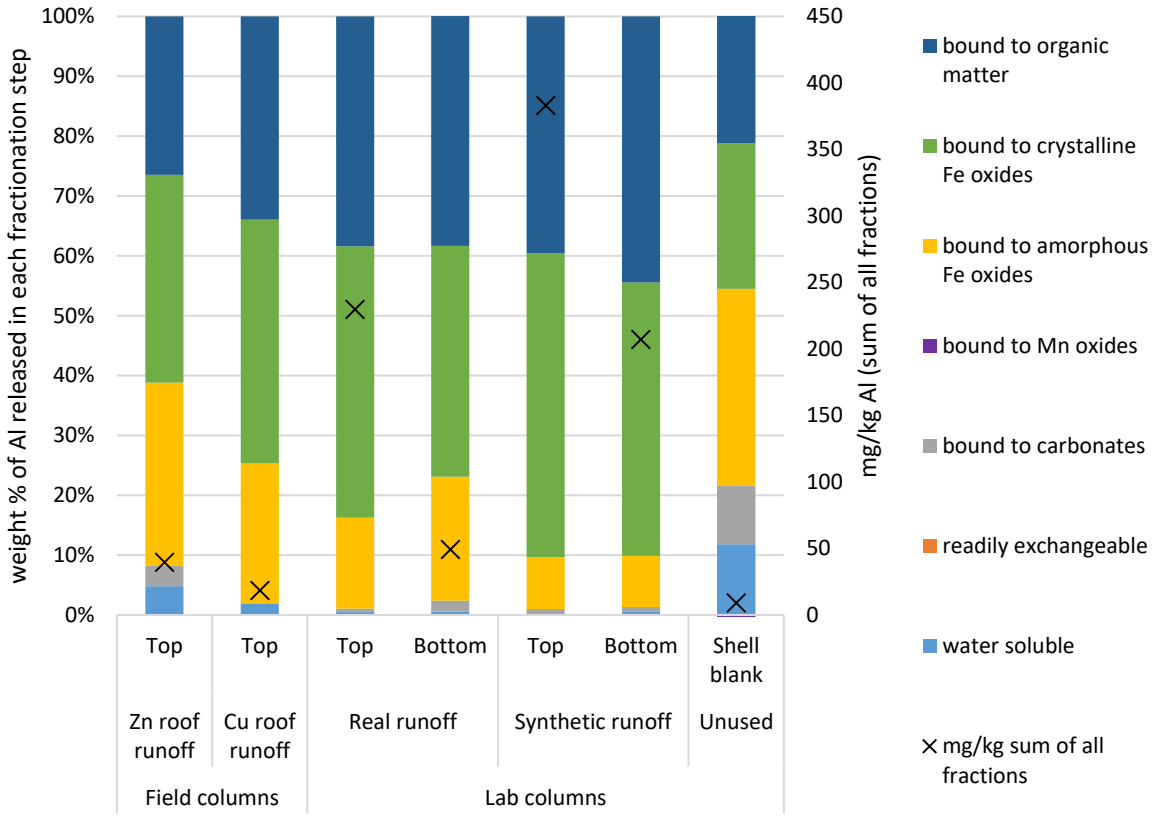


**Figure 3-20: Proportion of Al released from shell samples in each fractionation step, and showing the sum of all fractions as mg/kg for each sample.**

Even given these Mn and Al results, the distributions of Ca and Fe within the shells indicate that SEP should yield fractionation results for the target elements (Zn and Cu) that will be valuable.

### 3.8.2 Zn FRACTIONATION ON SHELLS

The majority (60%–90%) of Zn was leached from the "carbonates" fraction, regardless of the total amount of Zn measured across the extraction procedure, the location of the sample within the column, or the source of the Zn (real or synthetic roof runoff, or even the undetermined source contributing the Zn in the unused blank shells) (Figure 3-21). It is considered unlikely that significant quantities of Zn were in fact bound to Mn oxides (as these were also released in the carbonate step) due to there being close to, or far more Zn than Mn. In the columns with lower Zn concentrations, 10-30% of Zn leached in the "amorphous or crystalline Fe oxides" fractions (Figure 3-21). Zn adsorption to HFO, or Al, would be limited by the availability of HFO, or Al, in the system, so less would be present in this fraction when the Zn concentration were higher.

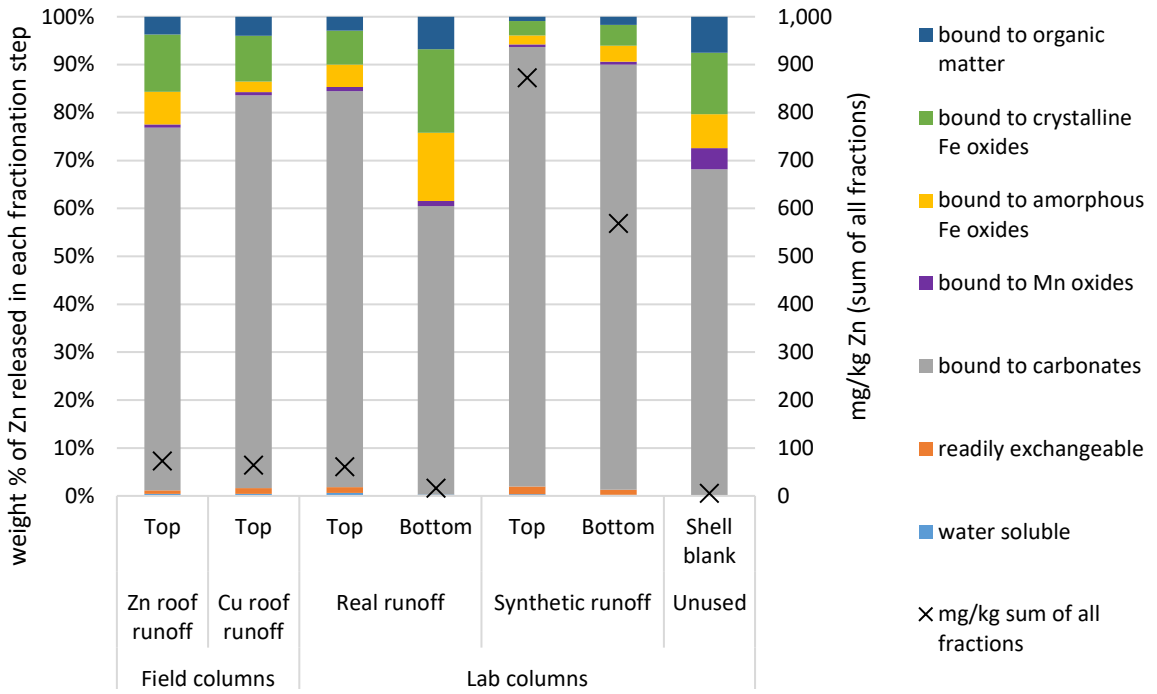


**Figure 3-21: Proportion of Zn released from shell samples in each fractionation step, and showing the sum of all fractions as mg/kg for each sample.**

### 3.8.3 Cu FRACTIONATION ON SHELLS

Cu showed a more variable fractionation than Zn, and it appears to be related to the amount of Cu present (Figure 3-22). The three columns with shell Cu concentrations of >2 mg/kg (up to 517 mg/kg) show 60%–85% of the Cu was leached in the "carbonates" step (Figure 3-22).

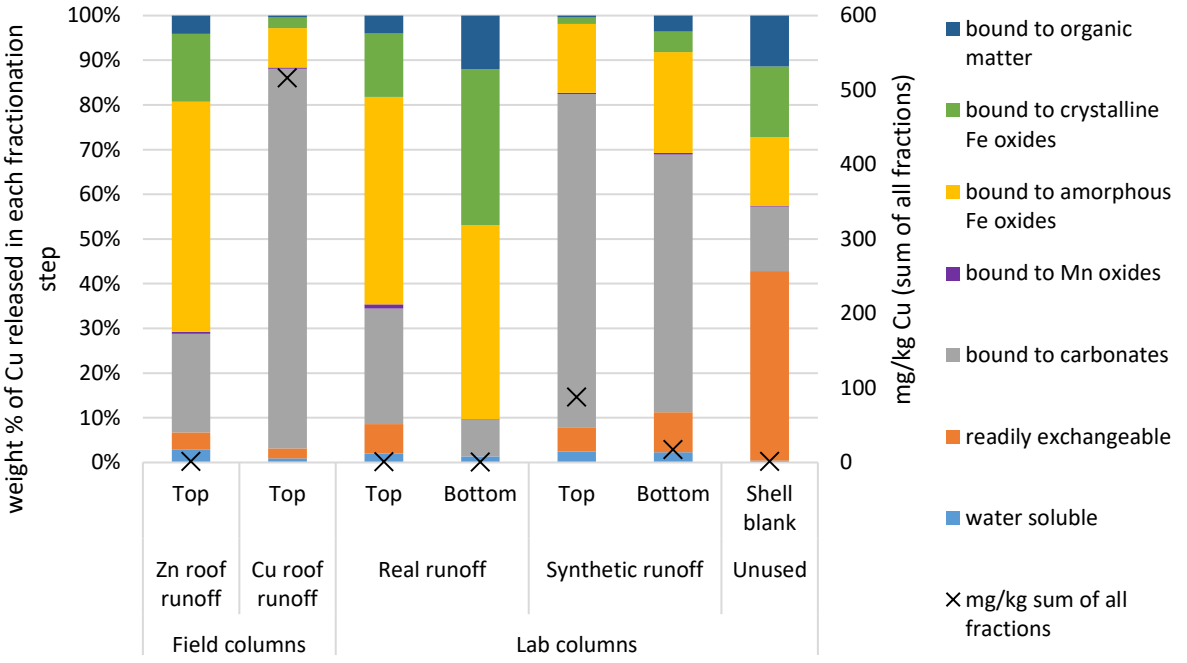


**Figure 3-22: Proportion of Cu released from shell samples in each fractionation step, and showing the sum of all fractions as mg/kg for each sample.**

These samples included shells exposed to both real roof runoff in a field column and synthetic roof runoff in a laboratory column so the source of the Cu did not seem to affect the fractionation. In the three used column shell samples with Cu concentrations around 1-2 mg/kg, the largest proportion of Cu was released in the "Fe oxides" steps (60%-80%). In the unused shell blank, which also had a shell Cu concentration of around 1-2 mg/kg the fractionation was more varied, with approximately 40% of the Cu was leached in the "readily exchangeable" step. The same as for Zn, it is likely that Cu adsorption to HFO or Al would be more important for low Cu concentrations.

### 3.8.4 KEY FINDINGS

- The sequential extraction procedure used was suitable for shell samples;
- The Fe oxides steps also released most of the Al present, so results from those steps should be treated as potentially related to Fe and/or Al;
- Zn was mostly released in the carbonates step, regardless of shell total Zn concentration, runoff source or the location of the shells in the column;
- Cu at higher shell total concentrations was mostly released in the carbonates step;
- At lower shell total concentrations of Zn or Cu, larger proportions of that concentration were released in the Fe oxides steps.

## 3.9 SEM-EDS

To investigate the micro-nano scale morphology of shell surfaces that the Zn and Cu may come into contact with in the column, and to search for evidence of precipitation and/or adsorption of Zn or Cu to any surface, SEM coupled with EDS was used for its imaging (SEM) and elemental analysis (EDS) capabilities.

### 3.9.1 SHELL MORPHOLOGY

Mussel shells, such as those used in this experiment, have a thin organic layer on their outside surface (the periostracum), and the bulk of the shell is comprised of $CaCO_3$ (Figure 3-23). In Figure 3-23 the periostracum had pulled away from the carbonate layers during the drying process.

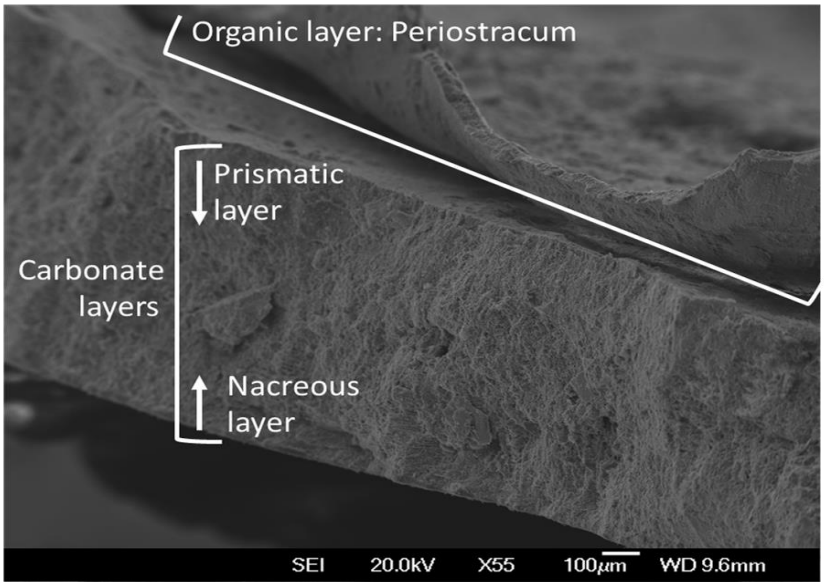


**Figure 3-23: Annotated SEM image of a shell cross-section.**

The carbonate bulk is formed of two layers of $CaCO_3$ in different orientations: the nacreous layer (nacre) forming the inside surface of the shell (visible to the naked eye as a pearly surface); and the prismatic layer in between the nacre and periostracum (Figure 3-23). The relative depths of each carbonate layer depends on the shellfish species the shell is from.

Figure 3-24 shows examples of the different surfaces of the shell available to interact with the runoff as it passes through the column.

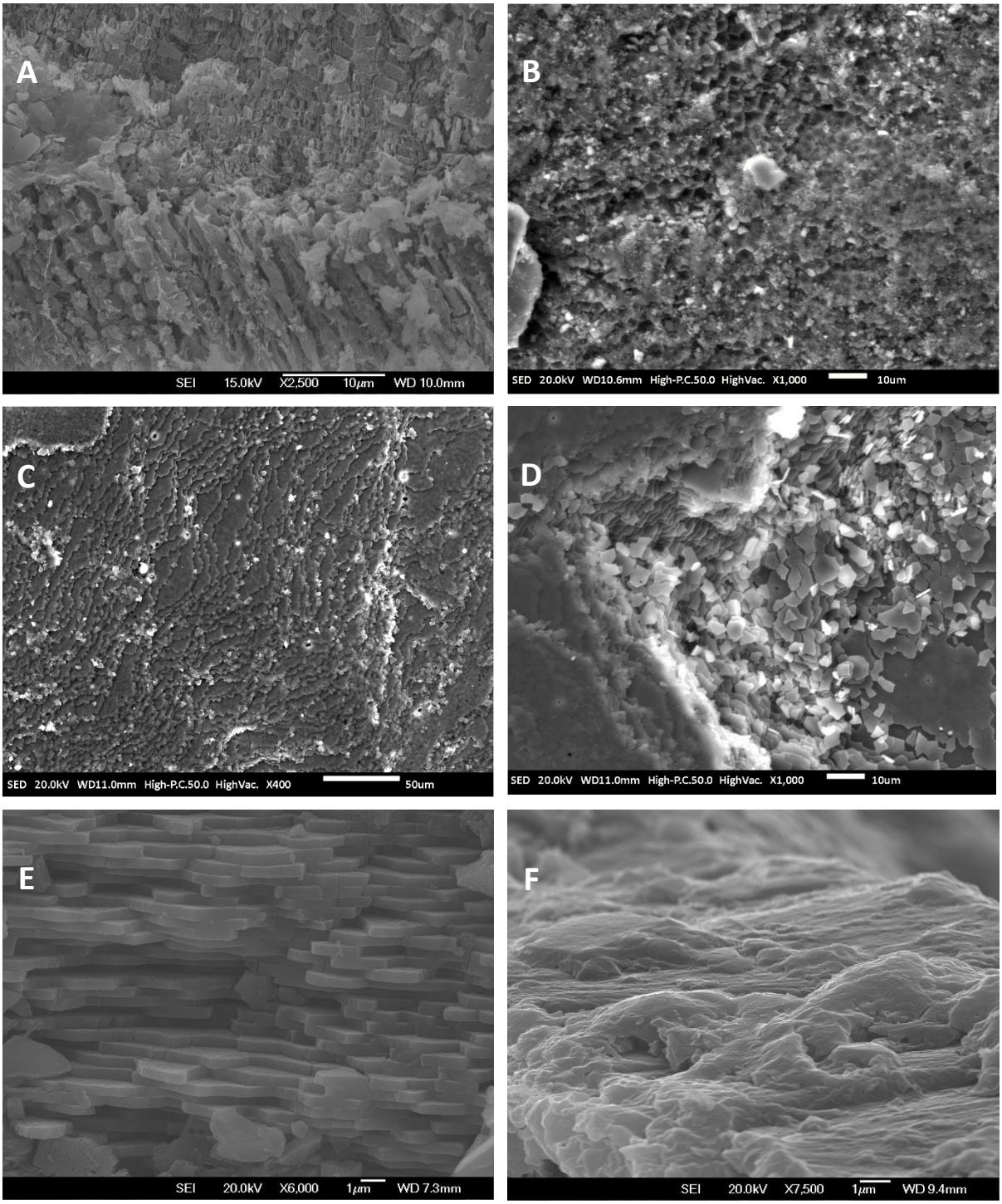


**Figure 3-24: Morphology of different layers of the shells as seen by SEM: A) cross-section of the prismatic layer; B) surface of the prismatic layer; C) surface of the nacreous layer; D) higher magnification of the surface of the nacreous layer; E) cross-section of the nacreous layer; F) cross section of the periostracum.**

Images A and B are a cross-section and surface view of the prismatic layer respectively, where the rough nature of the surface is clear in image B, and two different orientations of $CaCO_3$ are seen in image A. Feng et al. (2000) reported two distinct orientations of $CaCO_3$ in the prismatic layer, however it appeared that the nacre layer in these shells formed a much larger proportion of the shells analysed than the prismatic layer, and this would agree with Ben Shir et al.'s (2013) structural observations of *P. canaliculus* (the NZ green lipped mussel). It was reported in section 3.6 that the shells are a mix of common and green lipped mussels so these observations are unsurprising. Images C, D and E of Figure 3-24 are of the nacreous layer and show rough surfaces in spite of the smooth surface that is visible to the naked eye. Image D shows fragmentation of the lamellae into small plates in a dip in the surface, possibly from the crushing process, and from image E (the lamellae in cross-section) the lamellae are shown to be ≤ 1 µm thick. Image F shows the very smooth surface of the periostracum even in cross-section, in spite of its rough appearance to the naked eye.

### 3.9.2 Zn IN FIELD COLUMN SHELLS

The shells from a field column servicing a Zn roof had dust and debris present, as well as many rough surfaces for Zn to accumulate on or adsorb to. Figure 3-25 is an example of this on the prismatic shell surface, and also shows that the spatial distribution of (the very small amount of) Zn was quite uniform. Figure 3-26, taken on the nacreous surface, shows a little more Zn present and the majority appeared to correspond to the tissue-like fragment in the upper right corner of the image. Figure 3-27 presents a magnified view of that fragment, and based on its transparent (to electrons) and ordered pattern as well as the hair-like shards, it may be of biological origin. In Figure 3-28 debris is seen on a section of the periostracum, and appears to include a Zn rich particle.

Overall, it was difficult to locate areas of higher Zn concentration on these shells, and where it was located it was in low concentrations (≤ 0.2 atomic (at)%) and likely to correlate spatially with debris.

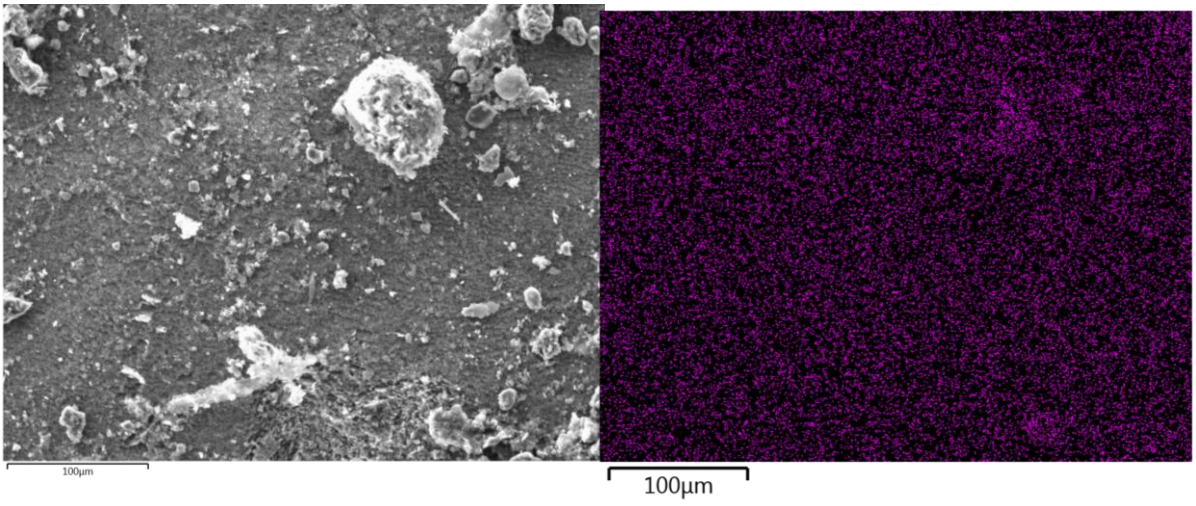


| Element | C | O | Zn | Ca | Al | Si | Fe | Mg | Na | Sum |
|---|---|---|---|---|---|---|---|---|---|---|
| At %: Sum | 30 | 51 | n.d. | 15 | 0.8 | 1.7 | 0.3 | 0.1 | 0.5 | 99.4 |

**Figure 3-25: SEM image (top left: shell flat, perpendicular to the probe), Zn spatial distribution (top right), and elemental composition of the whole image (bottom) on a section of the prismatic layer of a shell from a field column servicing a Zn roof.**

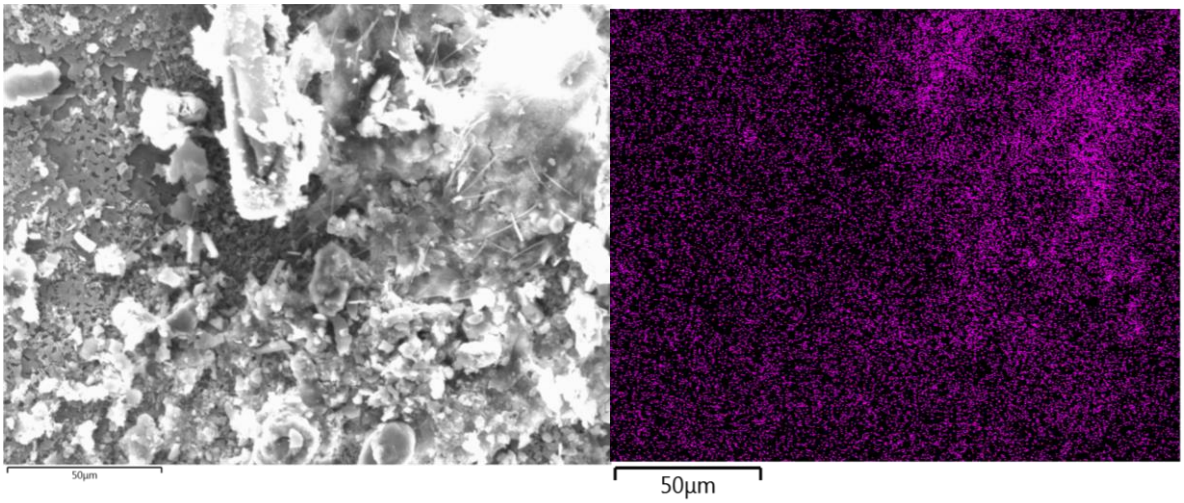


| Element | C | O | Zn | Ca | Al | Si | Fe | Mg | Na | Sum |
|---|---|---|---|---|---|---|---|---|---|---|
| At %: Sum | 46 | 38 | 0.2 | 10 | 1.4 | 3.2 | 0.4 | 0.2 | 0.5 | 99.9 |

**Figure 3-26: SEM image (top left: shell flat, perpendicular to the probe), Zn spatial distribution (top right), and elemental composition of the whole image (bottom) on a section of the nacreous layer of a shell from a field column servicing a Zn roof.**

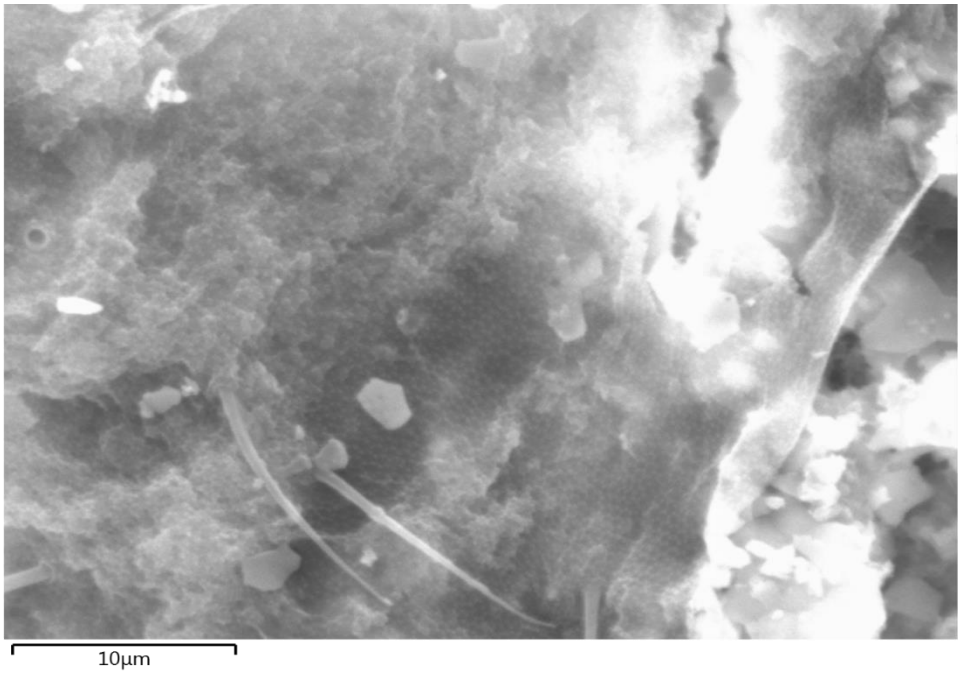


**Figure 3-27: Magnified image of the tissue-like fragment seen in Figure 3-26.**

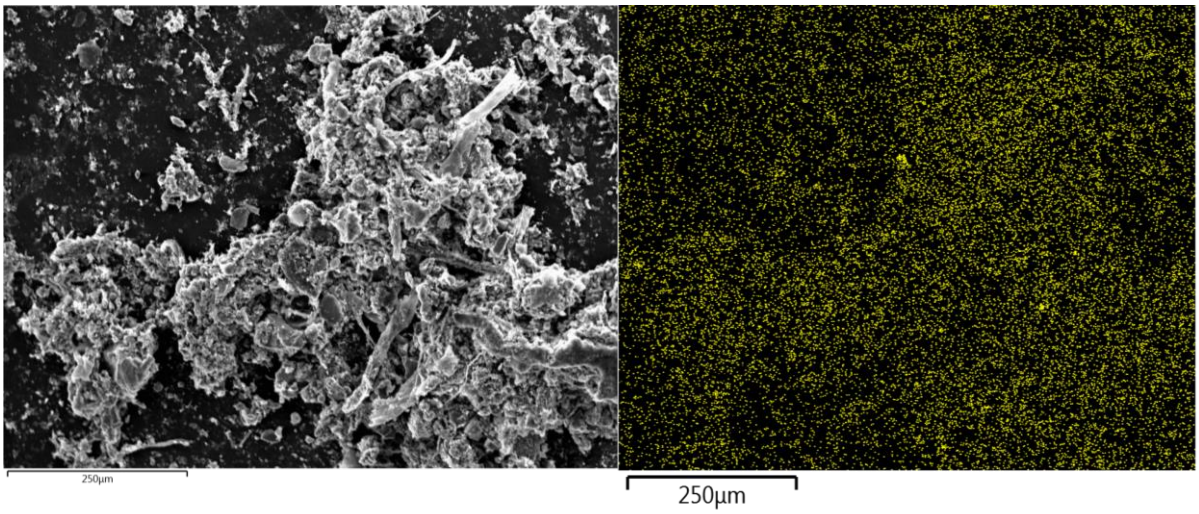


| Element | C | O | Zn | Ca | Al | Si | Fe | Mg | Na | Ti | Sum |
|---|---|---|---|---|---|---|---|---|---|---|---|
| At %: Sum | 60 | 31 | 0.1 | 1.8 | 1.4 | 3.6 | 0.6 | 0.2 | 0.3 | 0.1 | 100.1 |

**Figure 3-28: SEM image (top left: shell flat, perpendicular to the probe), Zn spatial distribution (top right), and elemental composition of the whole image (bottom) on a section of the periostracum layer of a shell from a field column servicing a Zn roof.**

Some spot EDS analyses were undertaken on various objects seen on the nacreous surface of a Zn roof servicing shell (Figure 3-29, Table 3-16). The background shell surface did not show any significant quantity of Zn, and the two fragments that did show some Zn still had only very small concentrations (<0.2 at%).

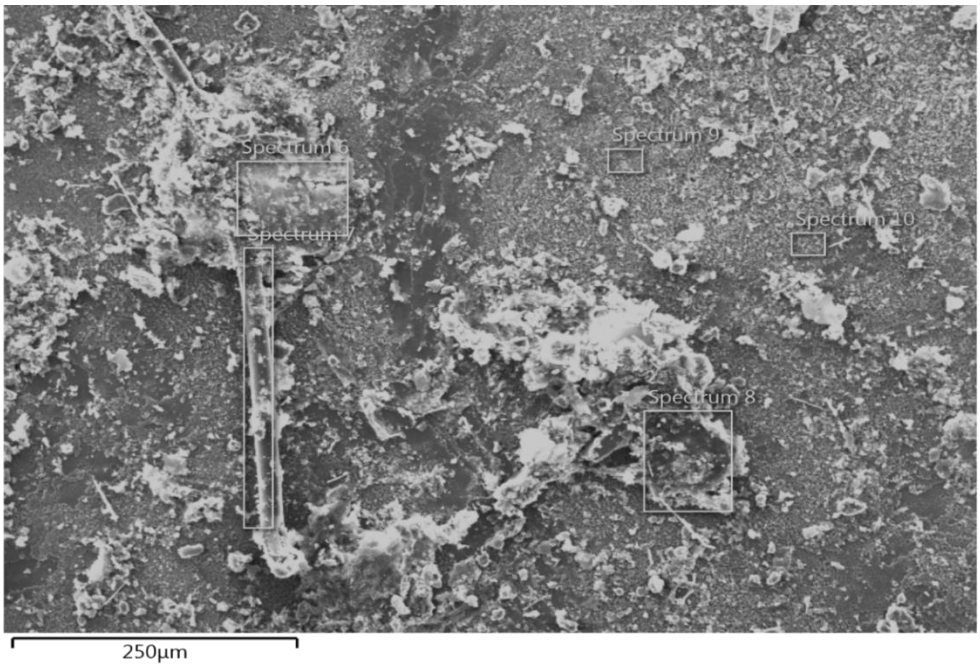


**Figure 3-29: SEM image of a section of the nacreous surface of a shell from a field column servicing a Zn roof, showing areas analysed by EDS- see Table 3-16 for elemental composition of the areas marked in white.**

**Table 3-16: Elemental composition as reported by EDS analysis, of the areas marked in Figure 3-29.**

| Element | Spectrum 6 | Spectrum 7 | Spectrum 8 | Spectrum 9 | Spectrum 10 |
|---|---|---|---|---|---|
| C | 56 | 58 | 52 | 52 | 53 |
| O | 34 | 32 | 37 | 26 | 26 |
| Ca | 6.4 | 7.9 | 4.9 | 19 | 21 |
| Al | 0.8 | 0.4 | 2.2 | 0.8 | 0.1 |
| Si | 2.2 | 1.2 | 2.9 | 1 | 0.1 |
| Na | 0.3 | 0.2 | 0.3 | 0.3 | 0.4 |
| Fe | 0.3 | 0.2 | 0.5 | 0.1 | *n.d.* |
| Mg | 0.2 | 0.1 | 0.2 | 0.1 | *n.d.* |
| Zn | 0.1 | 0.0 | 0.2 | 0.0 | *n.d.* |
| Sum | 100.3 | 100 | 100.2 | 99.3 | 100.6 |

### 3.9.3 Zn IN LABORATORY COLUMN SHELLS SATURATED WITH SYNTHETIC ROOF RUNOFF

SEM and EDS analysis was conducted on a sample of shells which were taken from the top section of the operationally saturated laboratory column, which had been loaded with synthetic roof runoff very high in Zn (27 mg/L). At the time of sampling the column removal efficiency for $Zn_{diss}$ had reduced from 45% to 15% (Heffernan & Howe, 2019), therefore the column was considered saturated. It was anticipated that if any Zn precipitates had formed, they would be visible in the SEM-EDS investigation of these shells.

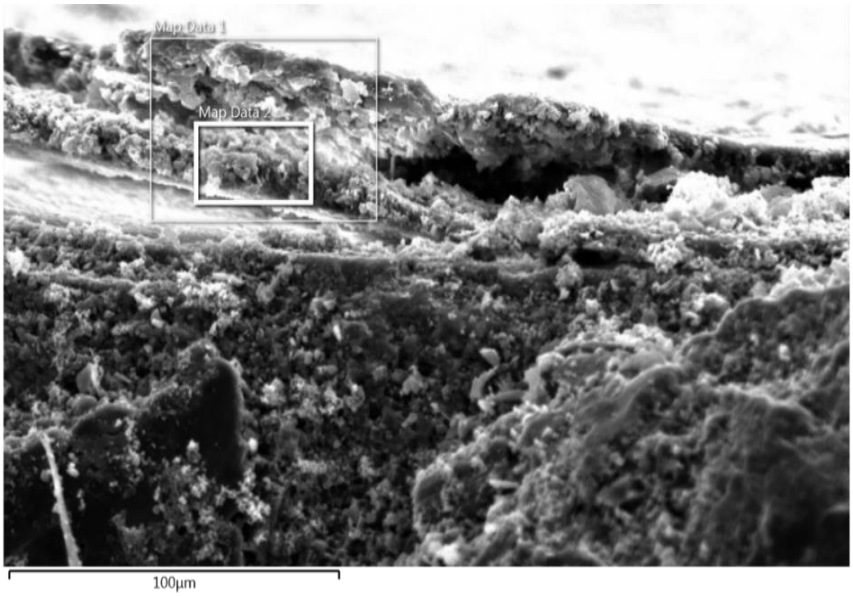


**Figure 3-30: SEM image of where the periostracum (top layer) meets the carbonate layer (bottom of image) of the Zn loaded shell from a laboratory column. The inner square shown on the periostracum shows the area analysed by EDS- spatial maps of this are in Figure 3-31.**

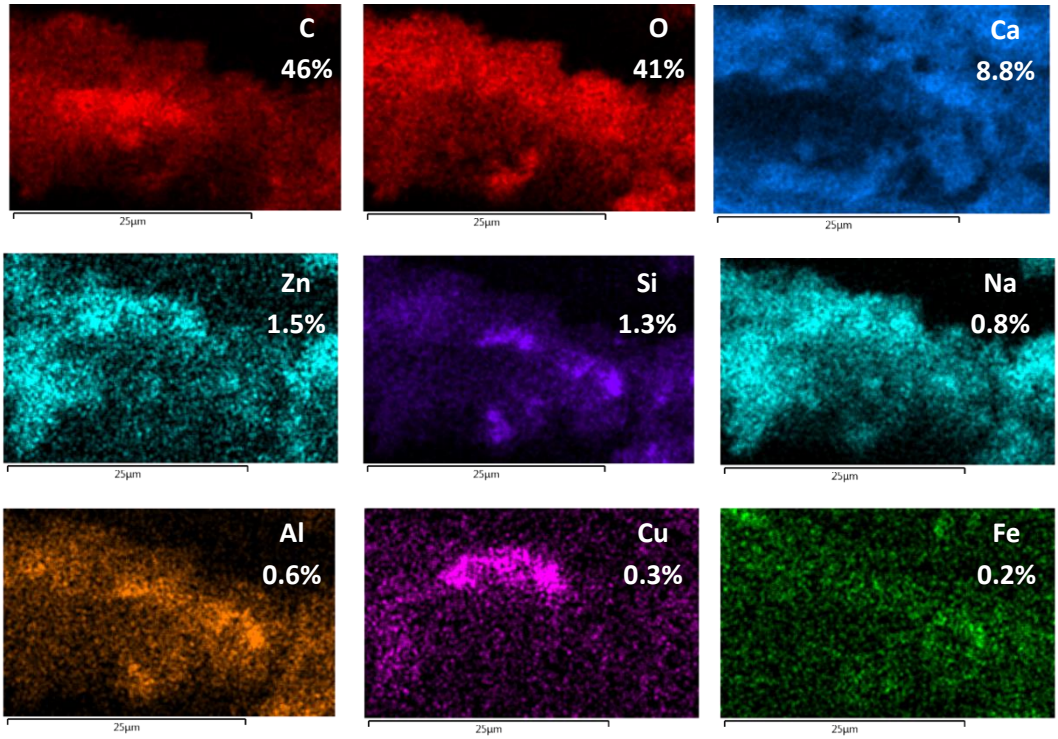


**Figure 3-31: EDS maps of a Zn hotspot on the periostracum of a Zn loaded shell from a laboratory column, showing the atomic % of the element in the image area. All scale bars show 25µm. The area analysed is shown in the SEM image in Figure 3-30.**

Figure 3-31 shows the spatial distribution and at% of all detected elements in the area shown in the smaller white box in Figure 3-30, located on the periostracum layer of the shell. There appears to be a close correlation between the spatial distributions of Zn and Na.

Figure 3-33 shows EDS maps and the at% of each element identified in a Zn "hotspot" on the carbonate layer of a shell, and shown in the SEM image in Figure 3-32.

Both rounded and conglomerates of fine flakes are seen in Figure 3-32, and have relatively high concentrations of Zn (4 at% Zn in the whole image area, Figure 3-33). As in Figure 3-31, Na shows a close spatial correlation with Zn, and this time so does Si. Figure 3-34 also shows similar conglomerates of fine flakes, and EDS mapping (Figure 3-35) again locates Na with Zn, and Cu also overlaps Zn in some areas.

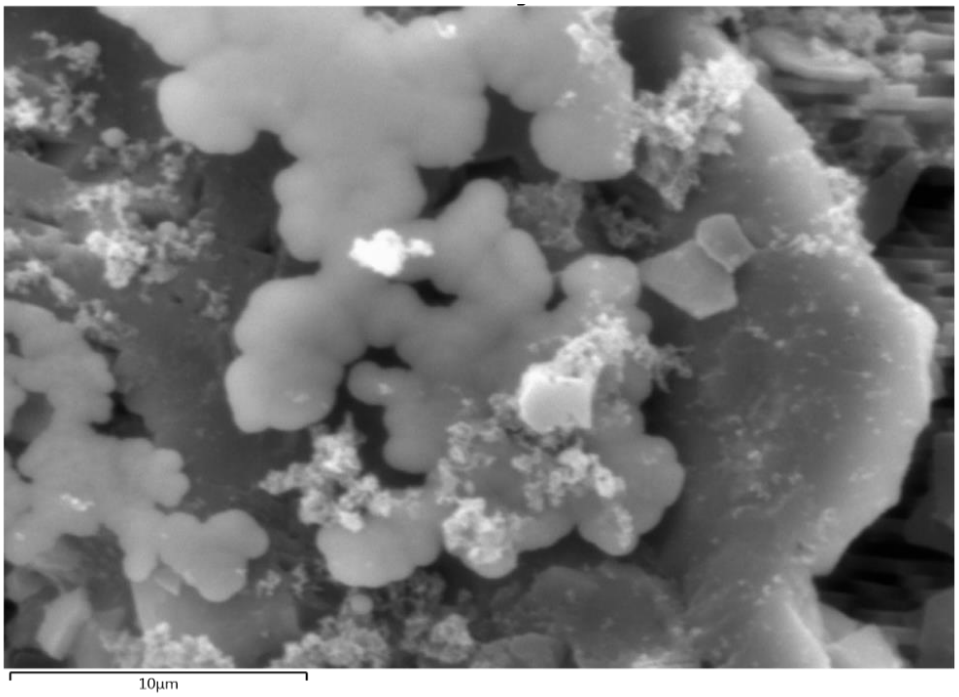


**Figure 3-32: SEM image of the Zn hotspots located on the carbonate layer of a Zn loaded shell from a laboratory column. Corresponding EDS spatial maps for all elements identified are in Figure 3-33.**

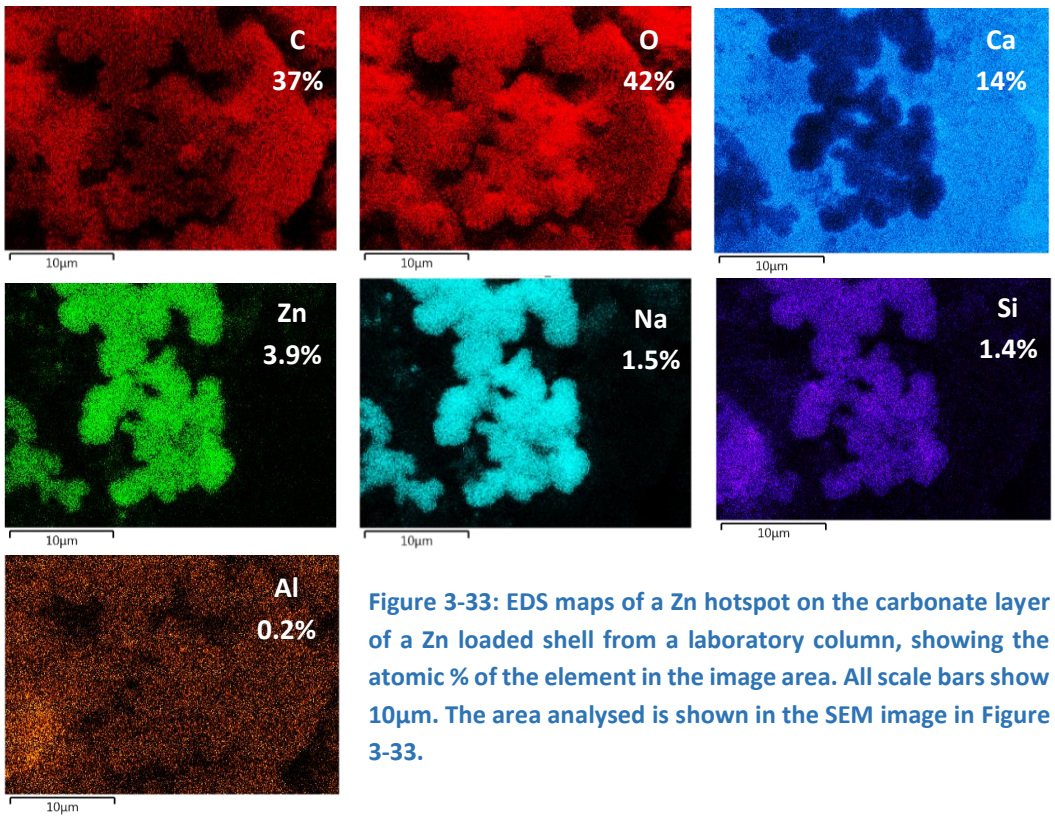


**Figure 3-33: EDS maps of a Zn hotspot on the carbonate layer of a Zn loaded shell from a laboratory column, showing the atomic % of the element in the image area. All scale bars show 10µm. The area analysed is shown in the SEM image in Figure 3-33.**

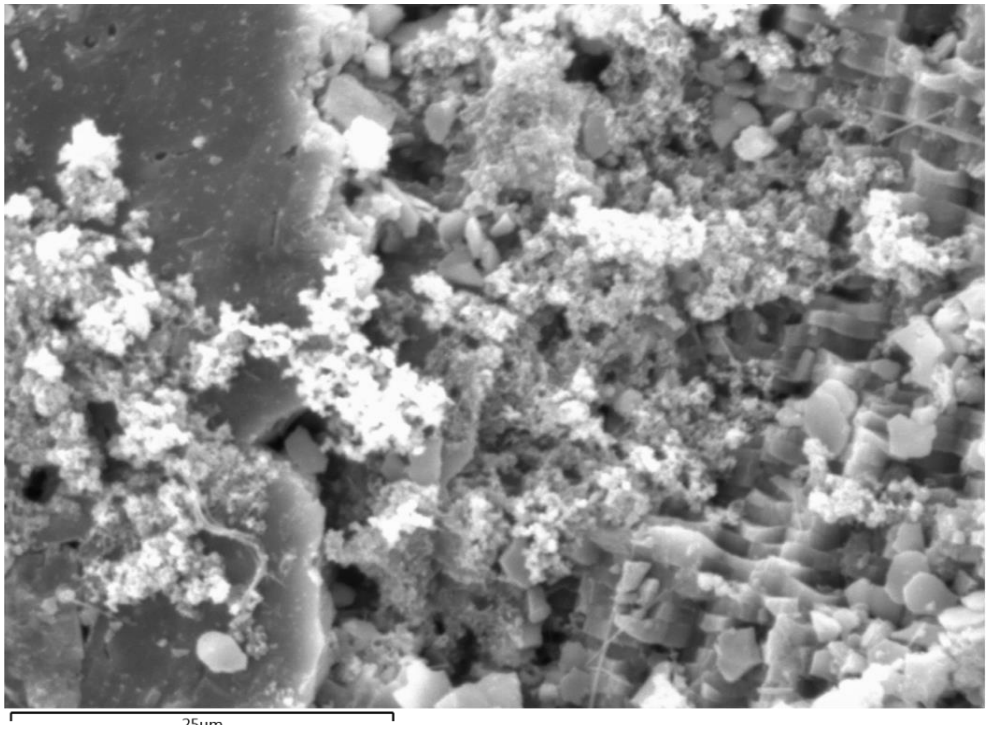

Figure 3-34: SEM image of Zn hotspots (flaky compounds on the surface of the lamellae) on the carbonate layer of a Zn loaded shell from a laboratory column. Elemental maps shown in Figure 3-35.

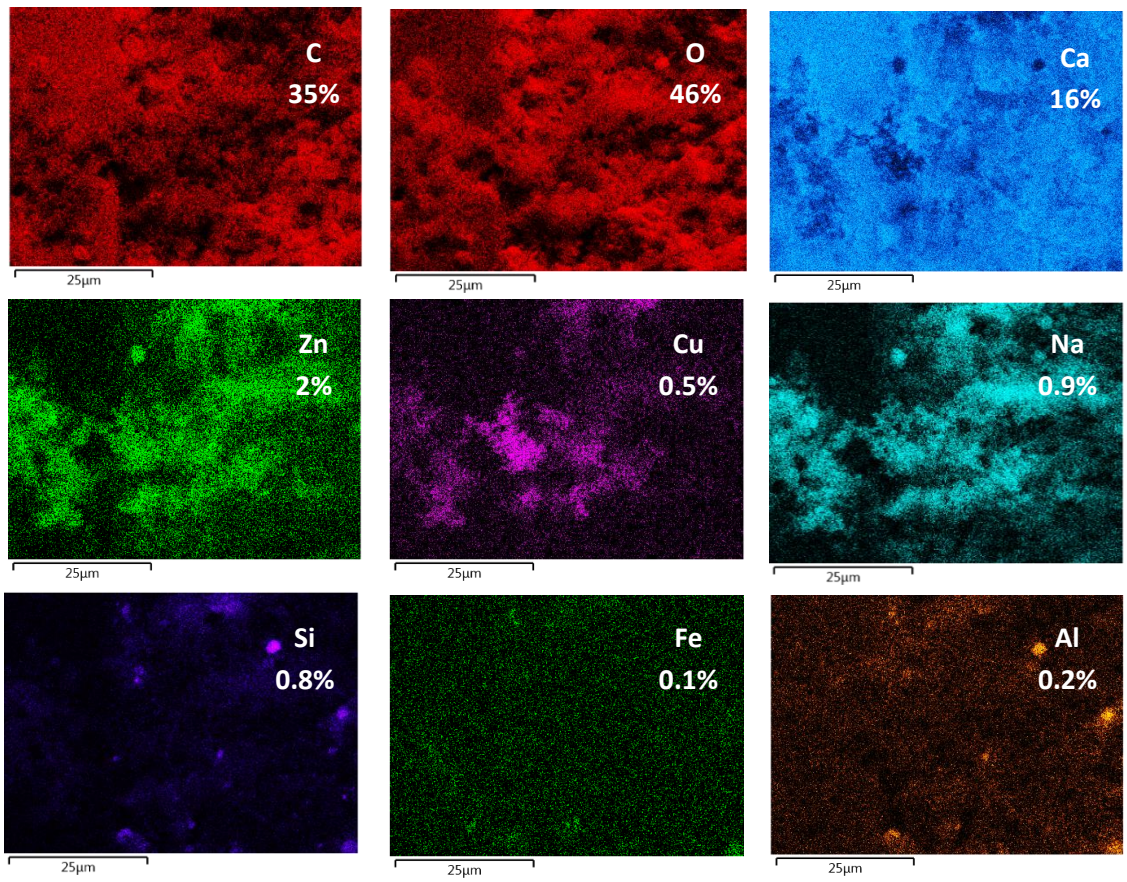


Figure 3-35: EDS maps showing Zn hotspots on the carbonate layer of a Zn loaded shell from a laboratory column, showing the at% of the element in the image area. All scale bars show 25µm. The area analysed is shown in the SEM image in Figure 3-34.

### 3.9.4 Cu IN FIELD COLUMN SAMPLES

Imaging and spot EDS analyses were conducted to investigate fragments and areas of potential interest on shells that had been exposed to Cu roof runoff in a field column. Figure 3-36 is an SEM image of the periostracum and prismatic layers of a Cu roof field column shell, and the areas on each layer analysed by EDS (Table 3-17). EDS analysis showed a very small difference in Cu concentrations between the periostracum (2 at%) and the prismatic (1 at%) layers.

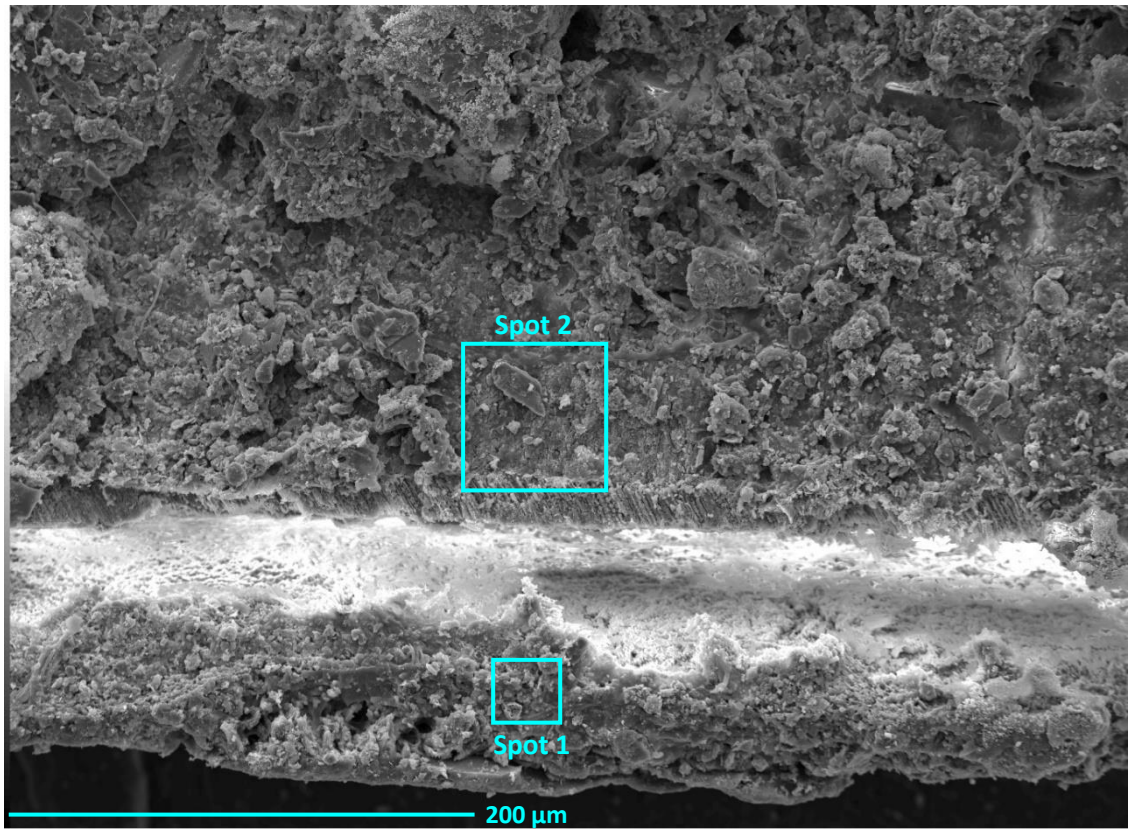


**Figure 3-36: Cross-sectional SEM image of a shell from a field column servicing a copper roof. The periostracum is at the bottom of the image and prismatic layer in the upper part, with a strip of poor resolution where the periostracum had separated from the prismatic layer creating a gap. Spot 1 and spot 2 show the areas analysed by EDS, results in Table 3-17.**

**Table 3-17: The atomic % of each element identified by EDS in spots shown on Figure 3-36. "n.d." = no detection. Sum figures vary from 100% due to rounding to a maximum of 1 decimal place.**

| Element | Spot 1 (periostracum) | Spot 2 (prismatic layer) |
|---|---|---|
| C | 55 | 30 |
| O | 32 | 46 |
| Ca | 4 | 19 |
| Cu | 2 | 1 |
| Al | 2 | 1 |
| Si | 4 | 3 |
| Fe | 1 | n.d. |
| S | 0.3 | n.d. |
| Sum | 100.3 | 100 |

Figure 3-37 shows an area of the prismatic surface of a shell exposed to Cu roof runoff in a field column.

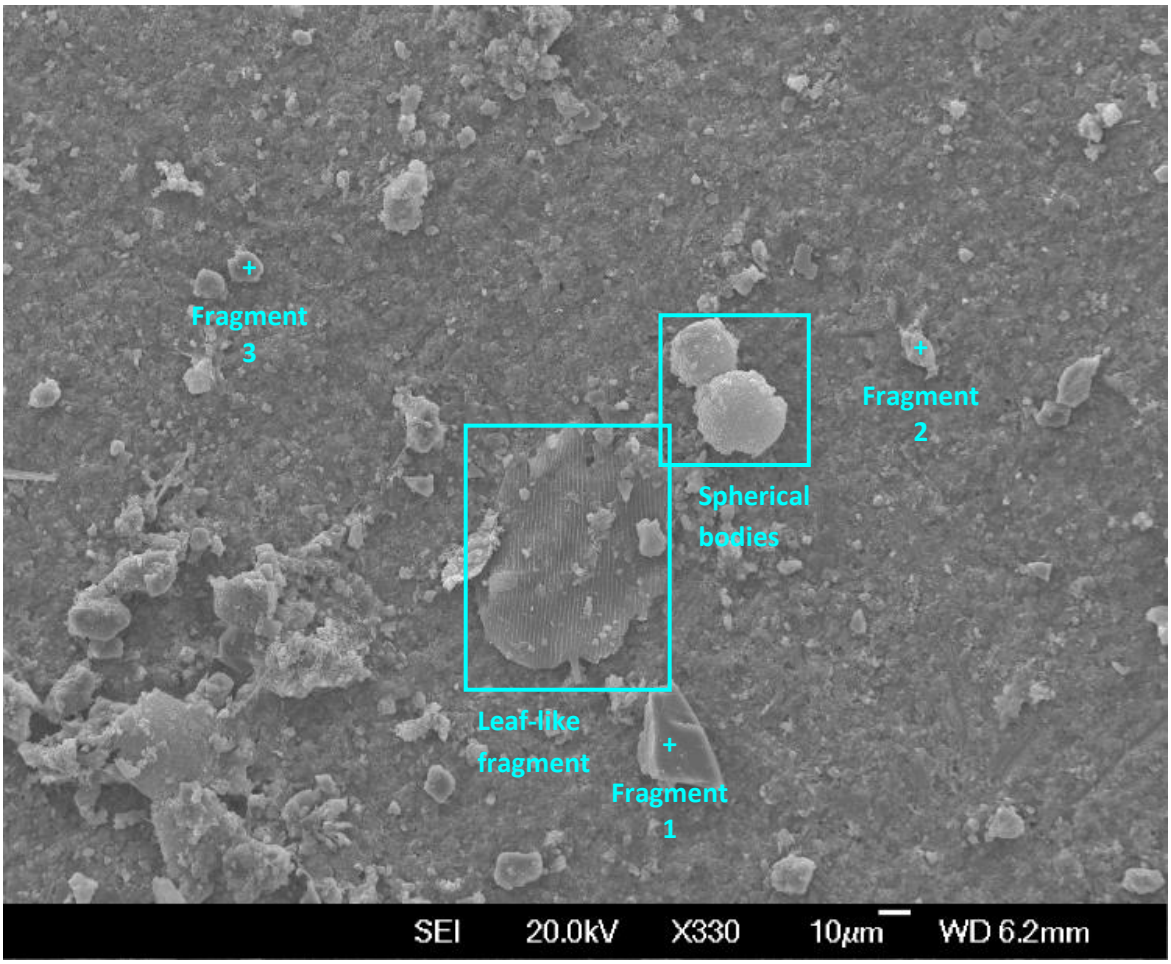


**Figure 3-37: SEM image of a section of the nacreous layer of a shell from a field column servicing a Cu roof. Areas analysed by EDS are noted in blue.**

The rough surface of the carbonate is visible, along with many angular fragments, some rounded or spherical bodies, and an intriguing but unidentified leaf-like structure likely of biological origin. There was no Cu detected in the background, but the spherical bodies, leaf-like fragment, and fragment 2 contained minor concentrations of 2, 1, and 6 at% Cu respectively (Table 3-18). Rounded particles were observed in several images, like the ones in Figure 3-37, and these contained very minor amounts Cu (<2 at%). The presence of P and its rounded shape suggests an organic particle like pollen, and small amounts of Al and Si suggest some clay mineral bound to it. Based on the relatively high amounts of Al and Si, and the ubiquitous presence of windblown dust/dirt/loess in Christchurch, fragment 2 is likely a particle of clay with Cu adsorbed to it. No Cu was detected on the angular fragment 1 or rounded fragment 3.

**Table 3-18: The atomic % of each element identified by EDS in areas noted in Figure 3-37. Sum figures vary from 100% due to rounding to a maximum of 1 decimal place. * the numbers presented are an average of 2 analyses in different areas of the object. *n.d.* = no detection.**

| Element | Leaf-like fragment* | Spherical bodies* | Background, no fragment* | Fragment 1 | Fragment 2 | Fragment 3 |
|---|---|---|---|---|---|---|
| C | 61 | 79 | 42 | 67 | *n.d.* | 47 |
| O | 24 | 16 | 31 | 9 | 36 | 30 |
| Ca | 14 | 2 | 28 | 0.4 | 7 | 0.5 |
| Cu | 1 | 2 | *n.d.* | *n.d.* | 6 | *n.d.* |
| Al | *n.d.* | 0.3 | *n.d.* | *n.d.* | 11 | 5 |
| Si | 1 | 1 | 0.5 | 23 | 26 | 14 |
| P | *n.d.* | 0.4 | *n.d.* | *n.d.* | *n.d.* | *n.d.* |
| Fe | *n.d.* | *n.d.* | *n.d.* | *n.d.* | 4 | 0.3 |
| S | *n.d.* | *n.d.* | *n.d.* | *n.d.* | 11 | *n.d.* |
| Na | *n.d.* | *n.d.* | *n.d.* | *n.d.* | *n.d.* | 3 |
| Sum | 101 | 101 | 102 | 99 | 101 | 100 |

EDS spatial maps were also recorded, and showed that Cu was not generally concentrated into hotspots relating to visible (or not visible) fragments. Figure 3-38, Figure 3-39 and Figure 3-40 show typical SEM images of the nacreous, prismatic and periostracum layers respectively, typical spatial Cu distributions within the image area, and the elemental composition of the image area as determined by EDS.

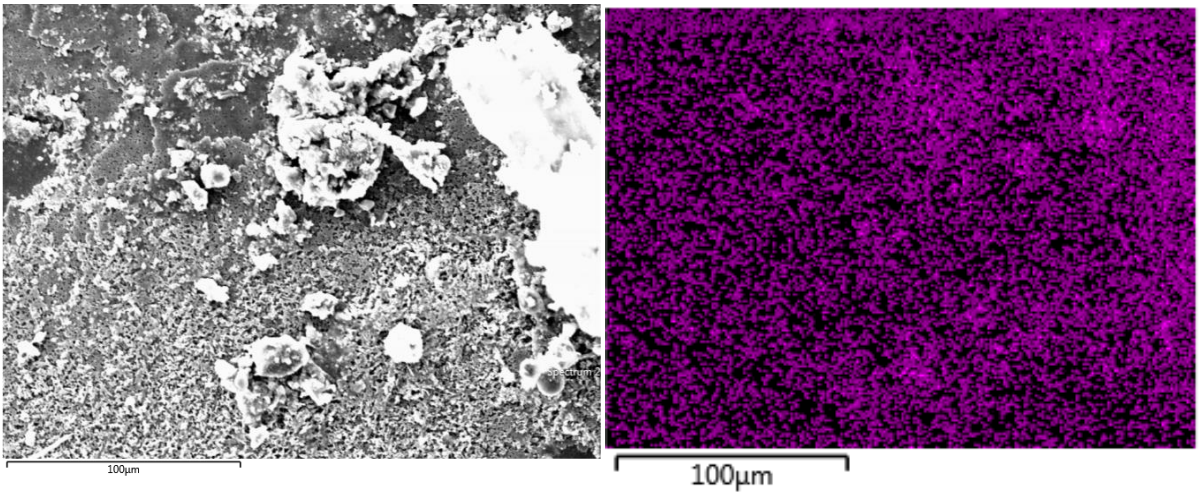


| Element | C | O | Cu | Ca | Al | Si | Fe | S | Na | Sum |
|---|---|---|---|---|---|---|---|---|---|---|
| At %: Sum | 40 | 38 | 0.5 | 17 | 1 | 2 | 0.4 | 0.1 | 0.3 | 99.3 |

**Figure 3-38: SEM image (top left: shell surface), spatial distribution of Cu (top right), and elemental composition of the whole image (bottom) on a section of the nacreous layer of a shell from a field column servicing a Cu roof.**

Although there were numerous fragments and rough surfaces that promote nucleation of Cu minerals, the spatial distribution maps show a mostly uniform Cu distribution. The exception to this was where the spot analysis of the Cu hotspot suggested it was a Cu metal fragment. There were no obvious mineral precipitates seen at this scale, nor any correlation with Fe, or any other element, to suggest adsorption to HFO or to another particulate.

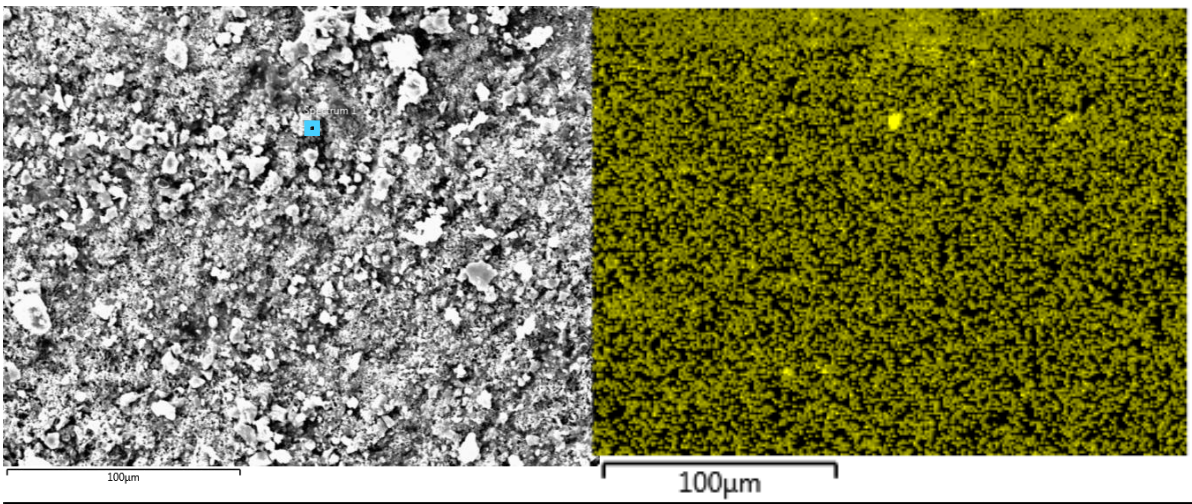


| Element | C | O | Cu | Ca | Al | Si | Fe | S | Na | Sum |
|---|---|---|---|---|---|---|---|---|---|---|
| At %: Sum | 37 | 38 | 1 | 20 | 1 | 2 | 0.3 | n.d. | 0.4 | 99.7 |
| At %: Spot | n.d. | n.d. | 67 | 12 | n.d. | 8 | n.d. | 13 | n.d. | 100 |

**Figure 3-39: SEM image (top left: shell flat, perpendicular to the probe), spatial distribution of Cu (top right), and elemental composition of the whole image and of the Cu hotspot (bottom) (in the blue square on the SEM image) on a section of the prismatic area of a shell from a field column servicing a Cu roof.**

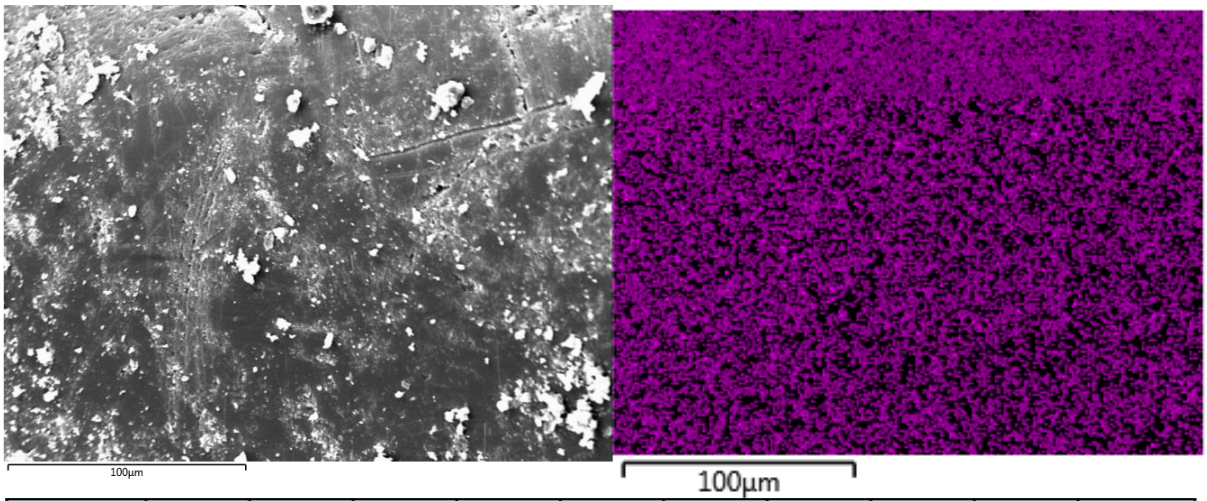


| Element | C | O | Cu | Ca | Al | Si | Fe | S | Na | Sum |
|---|---|---|---|---|---|---|---|---|---|---|
| At %: Sum | 81 | 16 | 1 | n.d. | 0.3 | 1 | 0.1 | 1 | n.d. | 100.4 |

**Figure 3-40: SEM image (top left: shell flat, perpendicular to the probe), Cu spatial distribution (top right), and elemental composition of the whole image (bottom) on a section of the periostracum of a shell from a field column servicing a Cu roof.**

### 3.9.5 Cu SOLUTION PRECIPITATE

A sample of the floating blue precipitate that formed on the surface of the 10 mg/L Cu synthetic roof runoff solution was collected onto a glass fibre filter membrane, and analysed by SEM.

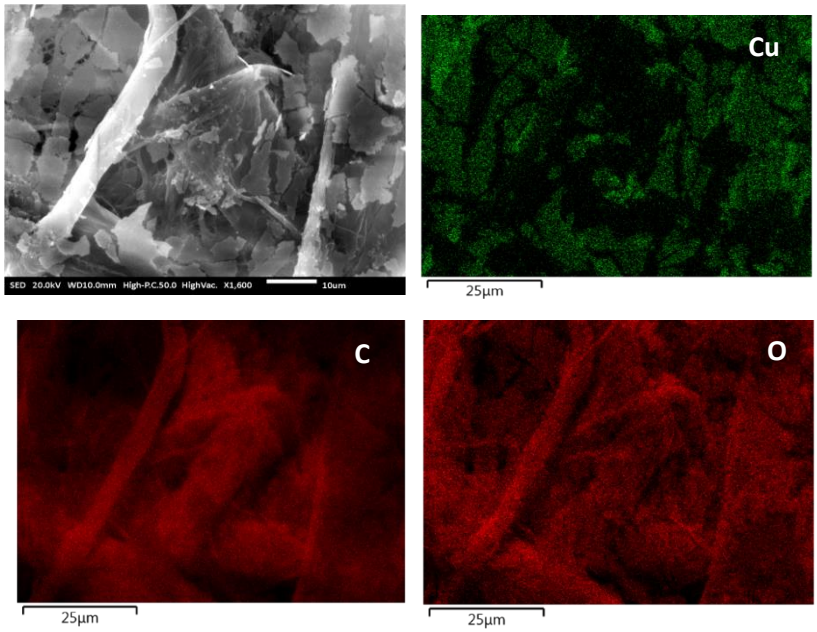


**Figure 3-41: SEM image (left), and EDS map of the spatial distribution of Cu (right) on a filter paper soaked with the precipitate floating on the 10 mg/L Cu synthetic stormwater solution.**

The Cu precipitate nested in the $SiO_2$ fibres appears flake-like (top left in Figure 3-41), and the EDS spectrum of the whole image area recorded Cu at 0.8 at%. The only other two elements detected were C and O (72 and 27 at% respectively, Figure 3-41), so the precipitate was likely composed of Cu and C, O and/or elements lighter than O (which EDS does not easily identify).

### 3.9.6 FIRST FLUSH EFFLUENT PARTICLES

The morphology of the particles making the first flush effluent turbid could indicate whether they were newly formed precipitates, likely to be amorphous in shape, or fine shell particles generated by the weathering/crushing process, which may look similar to other parts of the shell.

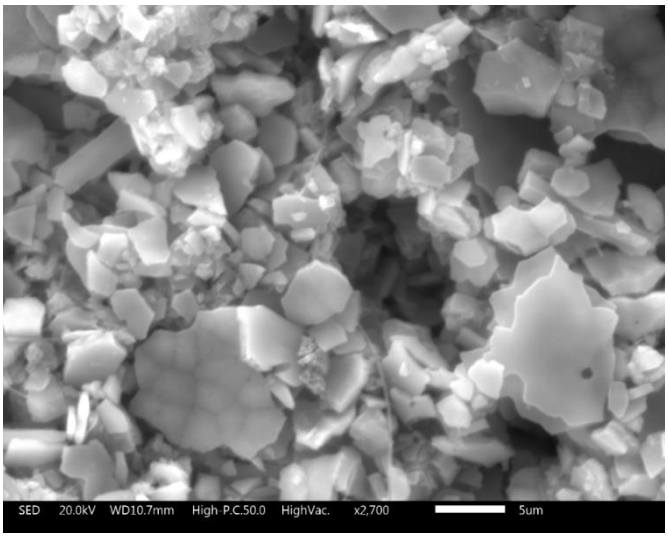


**Figure 3-42: Particles filtered from the first flush effluent of one of this study's experimental columns.**

As seen in Figure 3-42, the first flush particles were plate-like and similar to fragments (Figure 3-24), which suggest they were not newly formed precipitates, but fines broken from the shells.

### 3.9.7 KEY FINDINGS

- The shells contained an abundance of rough surfaces, and a morphology typical of mussel shells;
- Zn on field column shells (exposed to lower influent Zn concentrations) typically showed a uniform spatial distribution on each shell surface (periostracum, prismatic and nacreous), with a slight accumulation related to debris observed in some instances;
- Zn on laboratory column shells (exposed to higher influent Zn concentrations) showed some evidence of surface precipitates containing Zn: hydrozincite, and a Zn/Na compound;
- Cu on field column shells typically showed a uniform spatial distribution on each shell surface, with some slightly higher concentrations detected on organic or aluminosilicate debris;
- The Cu precipitate that formed in the synthetic roof runoff was flake like, and comprised of Cu, C, O (and potentially elements lighter than O):
- The morphology of particles in the first flush effluent was consistent with shell fragments.

# 4 RESULTS: MODELLING

## 4.1 SOLUTION SPECIATION MODELLING

The solution speciation was modelled using PHREEQC for the chemistry of each influent and effluent sampled in the baseline and experiments 1-6. Where anions were not measured in all experiments (Cl, $SO_4$, $HCO_3$, $NH_4$) they have been assumed to be the same as those measured in the baseline experiment (the influent value for the influents, and the 5 minute effluent value for all effluent samples). Justification for using the baseline values can be seen in the ion balance errors being acceptable, ie. ≤10%, for the majority of the chemistries analysed.

### 4.1.1 DISSOLVED Zn SPECIATION

The dominant Zn species for every input chemistry was the free $Zn^{2+}$ ion (>86 mole % for all input chemistries), with smaller percentages present as a carbonate or hydroxide species, and minor amounts of sulphate or nitrate species (Figure 4-1). The model did predict an increase in carbonate and/or hydroxide species between the influent and the effluent (Figure 4-1). As water continues to flow through the column the relative amount of carbonate and hydroxide species was predicted to increase, though they reached a maximum of only 12% of the total dissolved species in any of the experiments (Figure 4-1). The same trend was predicted regardless of Zn or Cu concentrations in the influent (Figure 4-1).

### 4.1.2 DISSOLVED Cu SPECIATION

Cu speciation was predicted to include high proportions of carbonate and hydroxide species for all input chemistries, and low proportions of the free $Cu^{2+}$ ion (Figure 4-1). The proportion of $CuCO_3^0$ increases and displaces the $Cu^{2+}$ species over time in each experiment, reaching a maximum of 80% of the dissolved species and a minimum of 69% (Figure 4-1). As seen in the speciation for experiments 4-6, as the influent $Cu_{diss}$ concentration increased so did the proportion of the $Cu^{2+}$ species. And, while this $Cu^{2+}$ proportion was always reduced after flowing through the column, $Cu^{2+}$ remained in higher proportions in the effluent of the higher Cu concentration solutions. The presence of higher concentrations of Zn also appears to increase the proportion of Cu present as $Cu^{2+}$ (Figure 4-1). However after flowing through the column, the $Cu^{2+}$ proportion reduces to <11% and this appears to occur regardless of the Zn concentration (Figure 4-1).

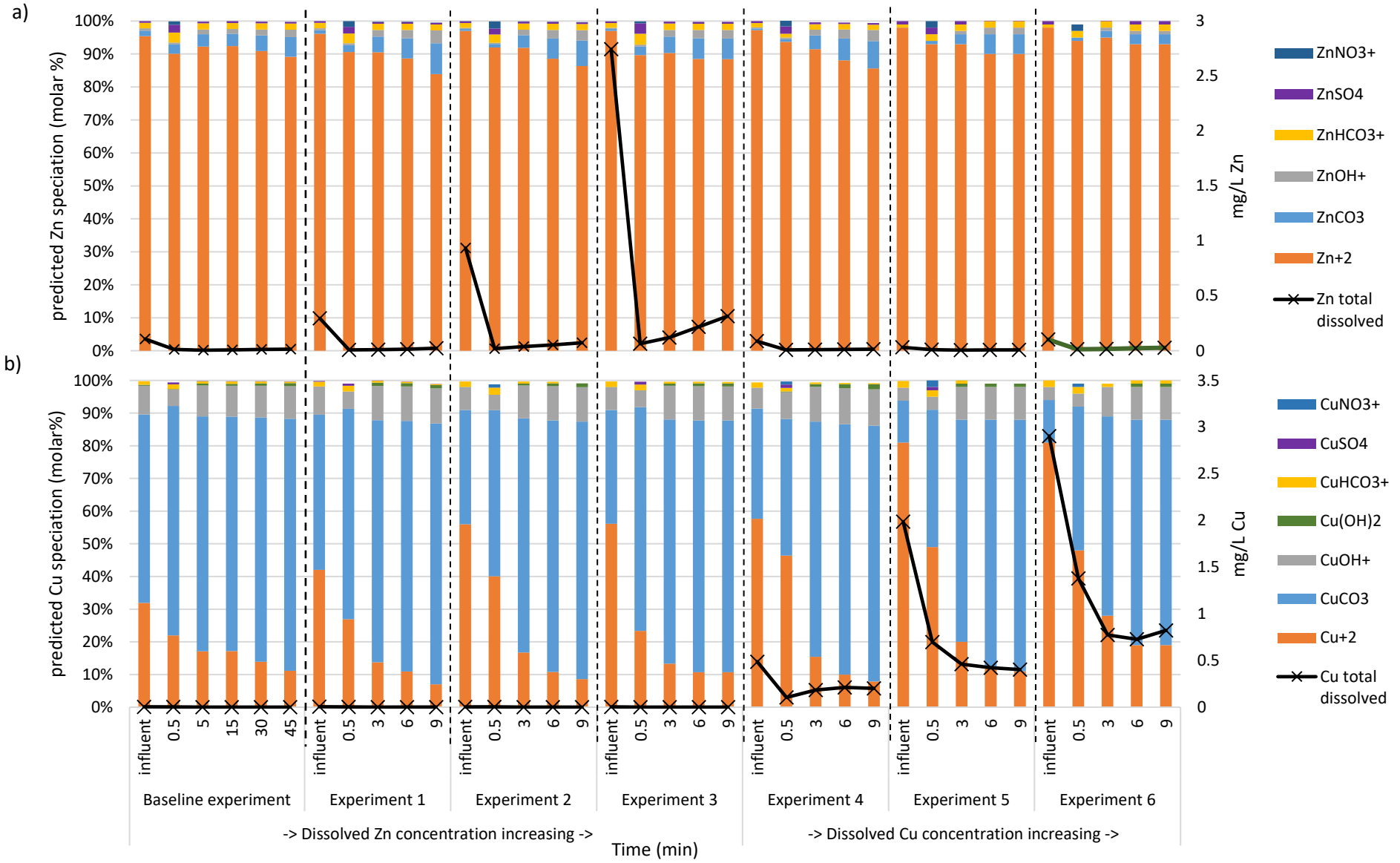


**Figure 4-1: The dissolved speciation of Zn (top panel) and Cu (bottom panel) predicted by PHREEQC for all experiments. Stacked columns are plotted against the left hand axis and present the predicted molar % of the dissolved species, while the crossed lines are plotted against the right hand axis and show the total dissolved concentration of all Zn (top panel) or Cu (bottom panel) species.**

## 4.2 PRECIPITATION MODELLING: COMMONLY OVERSATURATED MINERALS

### 4.2.1 Fe, Mn, Al, P AND Ca

Speciation modelling in PHREEQC predicts almost all of the same Fe, Al, Mn, P and Ca minerals to be oversaturated for all input chemistries, these are all oxides or hydroxides, with the exception of a calcium phosphate hydroxide (for a representative list of oversaturated minerals see Appendix 3: Commonly oversaturated minerals).

The oversaturation of the Fe and Mn minerals could suggest that the water chemistries as input into the model were not quite at equilibrium. This is likely an artefact of Fe- and Mn- particles that were small enough to pass through the 0.45 µm filter as newly formed HFO particles can be nano-sized (Dzombak & Morel, 1990). Calcite and aragonite in the effluent chemistries come very close to being oversaturated, which confirms that this chemistry reflects a nearly saturated system with respect to the mussel shells.

As PHREEQC is an equilibrium model the list in the Appendix shows the minerals that could form if at thermodynamic equilibrium, and does not take into account any kinetic barriers to mineral formation. As such, many of the minerals listed are not likely to form in the temperatures and pressures likely to exist in the treatment device. Also, though there are several minerals that potentially could exist in the treatment system environment, it is unreasonable to include all of these minerals in precipitation modelling because it is most likely that only the most common minerals will form. Therefore, only the following Fe, Mn, Al, Ca and P based minerals were allowed to precipitate out of solution (if oversaturated) in all precipitation modelling:

**Table 4-1: The minerals chosen as representative for each of the elements that may precipitate, and the molecular formula used by PHREEQC when allowing precipitation of that element to occur.**

| Element | Representative precipitating mineral used in modelling | Formula used by PHREEQC in precipitation modelling |
|---|---|---|
| Fe | Ferrihydrite, also known as hydrous ferric oxide (HFO).<br>(Dzombak & Morel, 1990; Stumm & Morgan, 1995) | $Fe(OH)_3$ |
| Mn | Pyrolusite<br>(Howe et al., 2004) | $MnO_2$ |
| Al | Gibbsite<br>(Sparks, 2003) | $Al(OH)_3$ |
| P | Hydroxylapatite<br>(the only P mineral predicted to be oversaturated in the modelling) | $Ca_5(PO_4)_3OH$ |
| Ca | Calcite<br>(Stumm & Morgan, 1995) | $CaCO_3$ |

### 4.2.2 Zn

The following Zn minerals were commonly predicted to form in the solutions modelled: ZnO (zincite), ZnO (active), $ZnCO_3.H_2O$ (no mineral name), $ZnCO_3$ (smithsonite), $Zn_3(PO_4)_2.4H_2O$ (no mineral name), and in higher Zn concentration solutions $Zn(OH)_2$ (no specifier) (epsilon) (gamma) (beta) and (am) were also predicted to be close to or oversaturated.

ZnO (zincite) is unlikely to form in the temperatures and pressures of the treatment system as it is a rare mineral (Frost et al., 2008). The other ZnO that PHREEQC (using the MINTEQv4 database) lists is ZnO (active), though it is unclear what "active" means in this context. However, it was assumed to be a precipitate that is likely to form in the column environment, due to ZnO being a common corrosion product of zinc metal (Bouchard & Smith, 2001; Del Angel et al., 2015). Two zinc carbonates are included in the mineral saturation calculations: $ZnCO_3.H_2O$ (no mineral name), and $ZnCO_3$ (Smithsonite). Both have very similar solubilities, and so the choice between them was somewhat arbitrary. As $ZnCO_3.H_2O$ has a slightly lower solubility it represents the 'best' case scenario for Zn removal via precipitation of a zinc carbonate, and so was chosen for use in precipitation modelling here. Hydrated zinc phosphate, $Zn_3(PO_4)_2.4H_2O$, could potentially form in a low temperature, low pressure system and so has also been allowed to precipitate if oversaturated (Bach et al., 2015). $Zn(OH)_2$ can form as a corrosion product of Zn (Mouanga et al., 2010), and given the numerous choices between polymorphs of $ZnOH_2$, the amorphous (am) polymorph is the most likely to form in the short timescales present in the experiment. Of note is that hydrozincite ($Zn_5(CO_3)_2(OH)_6$) is not included in the MINTEQv4, WATEQ4f, or PHREEQC databases and so its oversaturation is not predicted, though it is also a common corrosion product of Zn (Del Angel et al., 2015; Frost et al., 2008).

Therefore, the following Zn phases were allowed to precipitate out of solution where oversaturated, thus reducing the concentration of $Zn_{diss}$ left in solution: ZnO (active), $ZnCO_3.1H_2O$, $Zn(OH)_2$ (am) and $Zn_3(PO_4)_2.4H_2O$. Only one of these minerals was principally responsible for Zn reductions in any given solution chemistry, such that in allowing all four to precipitate if required, only one actually did.

### 4.2.3 Cu

The Cu minerals predicted to form in the lower Cu concentration solution chemistries were: cupricferrite $CuFe_2O_4$, cuprousferrite $CuFeO_2$, malachite $Cu_2(OH)_2CO_3$, azurite $Cu_3(OH)_2(CO_3)_2$, tenorite CuO, and $Cu(OH)_2$.

Neither cupric nor cuprous ferrite are known to form at low temperatures so were not included in precipitation modelling. Both malachite and azurite are copper hydroxide carbonates, so for modelling purposes malachite was chosen as it is more likely to form at the pHs in the column system and is a common mineral formed in copper weathering, therefore it could form at the temperatures/pressures in the column system (Vink, 1986). Tenorite was the only CuO listed, and this reacts rapidly to form more stable compounds so was not included as a likely precipitation product (Leygraf et al., 2016). It should be possible to form $Cu(OH)_2$ at the temperatures and pressures of the column system, though where possible it will form a copper hydroxide carbonate instead and so was not included in modelling (Schmutzler et al., 2017). Also, malachite had a consistently higher oversaturation than copper hydroxide, and so $Cu(OH)_2$ was not oversaturated by the time malachite had been allowed to precipitate. Hence of the minerals above, malachite was the only Cu mineral allowed to precipitate in modelling.

At higher Cu concentrations, brochantite $Cu_4(OH)_6SO_4$, and langite $Cu_4(OH)_6SO_4{:}H_2O$, atacamite $Cu_2(OH)_3Cl$ and antlerite $Cu_3(OH)_4SO_4$ were also predicted to form. According to Leygraf et al. (2016) they are all observed as copper corrosion products, the dominant mineral depending on the sulphate or chloride dominance in the system and time. They all begin via $Cu_2O$ formation, which according to PHREEQC predictions was far below saturation so would not form in this system. However, the formation of malachite dominated the precipitation of Cu minerals, such that inclusion of these other Cu minerals as potential precipitates (in addition to malachite) made no difference to the amount of $Cu_{diss}$ removed from solution.

### 4.2.4 KEY FINDINGS

- Each solution chemistry modelled had a similar list of minerals that were oversaturated. Therefore in each solution chemistry modelled the following minerals were allowed to precipitate if oversaturated: ferrihydrite ($Fe(OH)_3$); pyrolusite ($MnO_2$); gibbsite ($Al(OH)_3$); hydroxylapatite ($Ca_5(PO_4)_3OH$); calcite ($CaCO_3$).
- Zn minerals that were allowed to precipitate if oversaturated were: ZnO (active); $ZnCO_3.1H_2O$ (no mineral name); $Zn(OH)_2$ (am); $Zn_3(PO_4)_2.4H_2O$ (no mineral name), but typically only one of them did precipitate in a given solution chemistry;
- Malachite ($Cu_2(OH)_2CO_3$) was the only Cu mineral allowed to precipitate if oversaturated, because it is common and the addition of other minerals to the list made no difference to predicted $Cu_{diss}$ reductions.

## 4.3 Zn PRECIPITATION MODELLING: PREDICTED $Zn_{DISS}$ REDUCTIONS

$Zn_{diss}$ reductions due to Zn mineral formation were not predicted in any of the following solutions: the influents and effluents from this study's column experiments; two of three approaches to estimating the chemistry within this study's columns (section 4.3.1); real runoff from a Zn and a Cu roof, both as measured, and when modified to the chemistry expected of the column's effluent (section 4.3.2); an effluent of this study's column with the major ion composition substituted for that of a real runoff (section 4.3.3) (Table 4-2).

The only scenario where Zn mineral precipitation was predicted was when aragonite was allowed to dissolve until saturation, without restricting the pH to that observed experimentally (section 4.3.1). This resulted in $Zn_{diss}$ reductions of up to 67%, but also a final pH of 8.4 (*cf.* the experimental maximum of 7.7) (Table 4-2).

**Table 4-2: Summary of Zn mineral precipitation PHREEQC modelling results for the baseline and Zn range experiments, and including Cu range experiment data in the un-modified influent and effluent results. "SI" refers to the saturation index.**

| Input solution chemistry | Number of solution chemistries modelled | Zn concentration (range) used in solution chemistry (mg/L) | Zn mineral formation predicted? | Mineral predicted to be oversaturated *(or close, SI > -3)* | % reduction in $Zn_{diss}$ predicted |
|---|---|---|---|---|---|
| Influent and effluent from every column experiment sample | 36 | 0.046–2.74 | No | n/a *($ZnCO_3.H_2O$ close in most solutions)* | n/a |
| Column solution estimation approach *a* (section 4.3.1) | 4 | 0.117–2.74 | No | n/a *($ZnCO_3.H_2O$ close in some solutions, $Zn_3(PO_4)_2.4H_2O$ close in 2.74 mg/L Zn solution)* | n/a |
| Column solution estimation approach *b* (section 4.3.1) | 4 | 0.117–2.74 | No | n/a *($ZnCO_3.H_2O$, ZnO (active) close in some solutions)* | n/a |
| Column solution estimation approach *b*- pH unrestricted (section 4.3.1) | 3 | 0.295<br>0.936<br>2.74 | No<br>Yes<br>Yes | n/a *($ZnCO_3.H_2O$ close)*<br>ZnO (active)<br>$ZnCO_3.H_2O$ | n/a<br>47%<br>67% |
| Real roof runoff, un-modified (section 4.3.2) | 2 | 0.26–0.355 | No | n/a | n/a |
| Real roof runoff, modified to effluent (section 4.3.2) | 2 | 0.26–0.355 | No | n/a *($ZnCO_3.H_2O$, ZnO (active) close in both solutions)* | n/a |
| Column solution estimation approach *a*, with real runoff major ions (section 4.3.3) | 1 | 2.74 | No | n/a *($ZnCO_3.H_2O$, ZnO (Active), $Zn(OH)_2$(am), $Zn_3(PO_4)_2.4H_2O$ close)* | n/a |

### 4.3.1 ESTIMATION OF CHEMISTRY WITHIN THE COLUMN

None of the measured influent or effluent chemistries could accurately define what was likely to be going on inside the treatment device, where speciation was expected to change and precipitation to occur if it will. So, the chemistry within the column was estimated via two approaches and modelled.

#### APPROACH *a*

For each experiment the 3 minute effluent chemistry was used as the basis for the solution chemistry, but the $Zn_{diss}$ concentration was changed to that of the influent. In none of these chemistries were any Zn minerals predicted to be oversaturated. $ZnCO_3.H_2O$ was close in most solutions and closer in the higher Zn concentration ones, while $Zn_3(PO_4)_2.4H_2O$ was close to oversaturation in the 2.74 mg/L Zn solution.

#### APPROACH *b*

A second method of estimating the chemistry within the device was carried out to evaluate whether the method of modelling had an impact on the results. The dissolution of aragonite in the column was the expected reason for the pH increase seen in the effluents, so this approach used the influent chemistries to define the initial solution, then required sufficient aragonite to dissolve to obtain the maximum pH observed in the effluents. This did not result in any Zn minerals becoming oversaturated, though $ZnCO_3.H_2O$ and ZnO (active) were close in most solutions.

When the influent chemistries of experiments 2 and 3 are allowed to equilibrate with aragonite dissolution without restriction on pH, this did predict the formation of Zn minerals ZnO(active) (experiment 2), and $ZnCO_3.1H_2O$ (experiment 3) and a reduction in $Zn_{diss}$ of up to 67% (experiment 3). Nevertheless it did also predict a final solution pH of up to 8.4, which was higher than the observed maximum effluent pH of 7.7. In spite of a predicted pH increase to 8.5 by allowing aragonite dissolution in experiment 1's influent, no Zn minerals become oversaturated.

### 4.3.2 REAL ROOF RUNOFF

Speciation and saturation modelling was carried out using 2 real roof runoff chemistries, one from a Cu roof and another from a Zn roof. Neither sample had been through a treatment system. Both chemistries were predicted to be oversaturated with the same minerals as those predicted to form from laboratory experiment chemistries, neither of which included a likely Zn or Cu mineral.

To estimate how the chemistry would change if it went through the treatment system (and became an 'effluent'), the pH was raised to 7.5 and the Ca concentration doubled to be in approximate alignment with the results seen in the laboratory experiments. The carbonate concentration was raised by the amount that would result from the dissolution of $CaCO_3$ to provide the extra Ca added.

In neither the Cu roof nor the Zn roof estimated effluent chemistry did this result in any likely Cu or Zn mineral becoming oversaturated.

### 4.3.3 GROUNDWATER VS ROOF RUNOFF BASED MAJOR ION COMPOSITION

To validate the use of groundwater as a base for making synthetic roof runoff, the major ion composition of one of the experimental chemistries was replaced with that from a real roof runoff

sample. In experiment 3's 3 minute effluent with the influent Zn concentration, the following ion concentrations were replaced with those from the real Zn roof runoff sample: Na, K, Mg, Cl, $SO_4$, $NO_3$, and $NH_4$. Ca and $CO_3$ concentrations were left as per the experimental results as these would be expected change in treatment system. This change of major ion composition made very little difference to the saturation indices of likely Zn minerals, none of which reached oversaturation though $ZnCO_3.H_2O$, $Zn(OH)_2$ (am), $Zn_3(PO_4)_2$:$4H_2O$ and ZnO (active) were close.

### 4.3.4 SENSITIVITY TESTING: INITIAL Zn CONCENTRATION

To test the impact of the initial Zn concentration on predicted Zn mineral formation, the Zn concentration was increased in the PHREEQC solution composition up to an order of magnitude above the highest laboratory experiment. The rest of the parameters used for the modelling were that of the 3 minute effluent from experiment 3, at a pH of 7.5. At the Zn concentrations used in the laboratory experiments, no $Zn_{diss}$ was expected to precipitate so % reduction remains at 0 (Figure 4-2). At 5 mg/L a sharp increase in $Zn_{diss}$ reduction was predicted, and this flattens out above 10 mg/L, reaching only a 29% reduction at 30 mg/L Zn (Figure 4-2). The most oversaturated Zn mineral predicted to precipitate was $Zn_3(PO_4)_2.4H_2O$, and $ZnCO_3.H_2O$ precipitation was also predicted. ZnO (active) was predicted to form only at 30 mg/L initial Zn concentration.

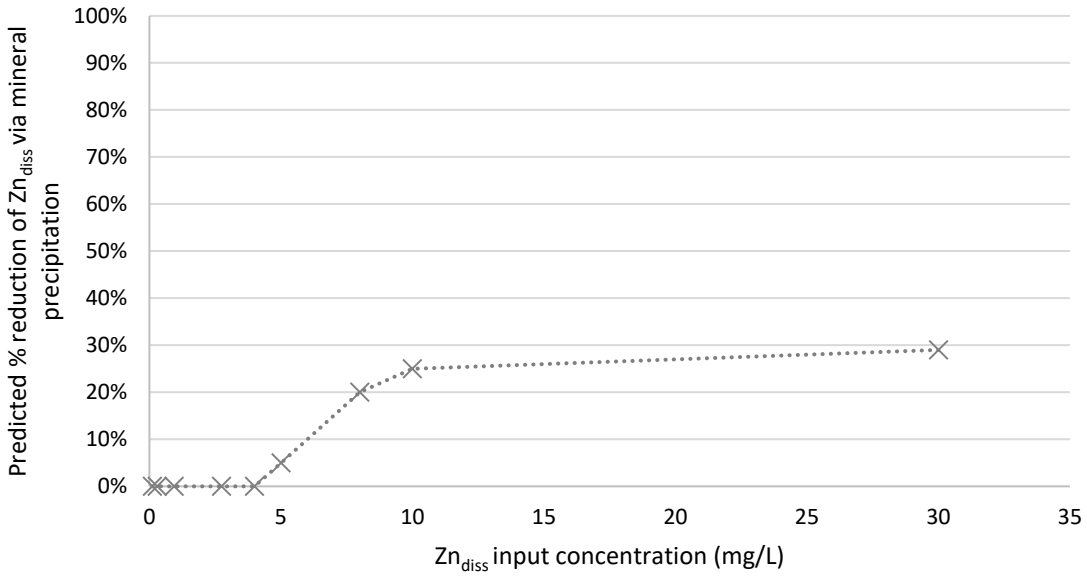


**Figure 4-2: Predicted % reduction of $Zn_{diss}$ due to Zn mineral formation, at different initial Zn concentrations and an initial pH of 7.5.**

### 4.3.5 SENSITIVITY TESTING: pH

The sensitivity of Zn mineral formation to pH in this system was also investigated via modelling experiments. For each experiment's 3 minute effluent/influent Zn chemistries, the pH was incrementally increased from its original value using the dissolution of aragonite to fix the pH at the desired value, as this was the only likely mechanism of pH increase in the system. The pH was increased until the model returned error results, suggesting that the dissolution of aragonite could not create the pH requested. Precipitation of likely minerals was allowed, and the resulting % reduction in $Zn_{diss}$ was calculated.

An increase in pH made no difference in solutions with 0.3 mg/L Zn or less (Figure 4-3). At 1 mg/L the pH would need to increase above 8, while at 3 mg/L the pH would only need to increase above 7.5 before Zn minerals are predicted to precipitate (Figure 4-3). The mineral predicted to form below pH 8 was $ZnCO_3.1H_2O$, and above pH 8 was ZnO (active).

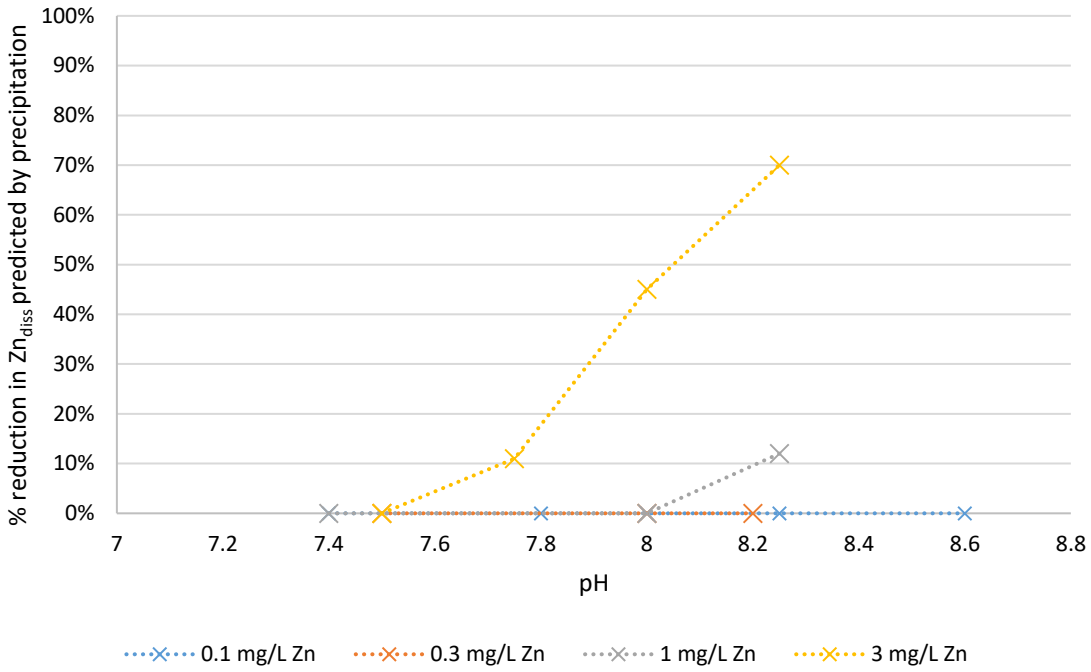


**Figure 4-3: Predicted % reduction in $Zn_{diss}$ due to Zn mineral formation, as a function of pH and for different initial Zn concentrations.**

### 4.3.6 SENSITIVITY TESTING: CARBONATE CONCENTRATION

The sensitivity of Zn mineral saturation in this system to an increase in carbonate concentration was modelled. The carbonate concentration was doubled, and the charge balanced with Ca ($CaCO_3$ dissolution being the expected reason for an increase in carbonate). Aragonite remained undersaturated at this increased carbonate (and Ca) concentration, confirming that this was not an unrealistic scenario. No increase to the pH was entered as these and previous experiments by Heffernan and Howe (2019) did not show a positive relationship between pH and alkalinity in the ranges studied. The rest of the parameters were modelled with each experiment's 3 minute effluent/influent Zn concentrations as a basis.

For solutions with a Zn concentration ranging from 0.1 to 1 mg/L (baseline experiment and experiments 1 and 2), none of these changes resulted in a Zn mineral being precipitated. However, in experiment 3 the increased carbonate concentration resulted in an 8% reduction in $Zn_{diss}$, via precipitation of $ZnCO_3.1H_2O$.

### 4.3.7 KEY FINDINGS

- No Zn mineral was predicted to precipitate in any of the influent or effluent chemistries, whether as-is, modified to an estimate of the composition inside the column, or with major ion concentrations modified to that of real runoff;

- ZnO and $ZnCO_3.1H_2O$ were predicted to precipitate when aragonite was set to dissolve to saturation, but this raised the pH to above that measured experimentally;
- Of the initial Zn concentration, the pH, and the carbonate concentration, $Zn_{diss}$ reductions via mineral precipitation were most sensitive to changes in pH (pH > 7.7), but only when there was also a higher influent Zn concentration (> 1 mg/L).
- No $Zn_{diss}$ reduction predictions reached reductions seen in the column experiments.

## 4.4 Cu PRECIPITATION MODELLING: PREDICTED $Cu_{DISS}$ REDUCTIONS

Reductions in $Cu_{diss}$ of >70% from the formation of malachite were predicted in almost all solution chemistries modelled (Table 4-3). Only where the $Cu_{diss}$ concentration was <0.01 mg/L was there no oversaturation of malachite predicted (Table 4-3).

**Table 4-3: Summary of Cu mineral precipitation PHREEQC modelling results for the baseline and Cu range experiments, and including Zn range experiment data in the un-modified influents and effluent results. * one data point removed from analysis as an outlier: a first flush effluent with a reduction of 19% predicted.**

| Input solution chemistry | Number of solution chemistries modelled | Cu concentration (range) used in solution chemistry (mg/L) | Malachite formation predicted? | % reduction in $Cu_{diss}$ predicted |
|---|---|---|---|---|
| Un-modified influent (as prepared) from experiments 4–6 (section 4.4.1) | 3 | 0.531–9.09 | Yes | 74%–80% |
| Un-modified influent (as-run) and effluent from every column experiment sample (section 4.4.2) | 36 | 0.0009–0.0052<br>0.105–2.90 | No *(close in some solutions)*<br>Yes | n/a<br>71%*–96% |
| Column solution estimation approach *a* (section 4.4.3) | 3 | 0.488–2.90 | Yes | 93%–98% |
| Column solution estimation approach *b* (section 4.4.3) | 3 | 0.488–2.90 | Yes | 96%–99% |
| Real roof runoff, un-modified (section 4.4.4) | 1 | 2.90 | Yes | 98% |

### 4.4.1 INFLUENT (AS PREPARED) CHEMISTRY MODELLING

It was noted during the 3 days of experiments that precipitation was occurring in the 5 and 10 mg/L Cu influents prepared, and that further precipitation continued to occur over the following weeks.

Therefore, as all Cu was added in a dissolved form to begin with, the influents were modelled in PHREEQC using the acid soluble Cu concentration (and all other parameters dissolved).The ion balances for these solutions were up to 26%, and it was thought that the source of error was most likely the high Cu concentrations compared to the other analytes.

Malachite was the most oversaturated Cu mineral (likely to form) in each influent, azurite and tenorite were also oversaturated in all three influents, and brochantite was oversaturated in the 5 and 10 mg/L Cu influents. Based on the previous discussion of likely copper minerals to precipitate (section 4.2.3), the influents were remodelled with malachite formation allowed. This resulted in predicted $Cu_{diss}$ concentrations reducing to 0.14, 0.94, and 2.1 mg/L from initial concentrations of 0.53, 4.7, and 9.1 mg/L respectively.

### 4.4.2 INFLUENT (AS RUN) AND EFFLUENT CHEMISTRY MODELLING

The influents were also modelled as-run in the column experiments, using the $Cu_{diss}$ concentration from the influent sample taken at the beginning of each experiment. The impact of malachite precipitation on the influent $Cu_{diss}$ concentration predicted by PHREEQC was a reduction to 0.138–0.687 mg/L, from the 0.488–2.9 mg/L concentrations respectively measured in the influents.

Mineral oversaturation in the effluents was modelled, and an example of the common trend can be seen in the 3 minute effluents. In these solutions the $Cu_{diss}$ concentrations were predicted to be between 0.03 and 0.05 mg/L after the precipitation of malachite, which was lower than the measured 3 minute effluent concentrations of between 0.18–0.77 mg/L in the three experiments.

### 4.4.3 ESTIMATION OF CHEMISTRY WITHIN THE COLUMN

The same two approaches as described in section 4.3.1 were used to estimate the chemistry within the column in the Cu experiments.

#### APPROACH *a*

The 3 minute effluent with the influent $Cu_{diss}$ concentration was modelled, and similarly to the 3 minute effluents, the final $Cu_{diss}$ concentrations predicted were between 0.03 and 0.06 mg/L, reduced from 0.488–2.9 mg/L via the formation of malachite. The final pH was predicted to decrease slightly in experiments 5 and 6, by up to 0.2 pH units.

#### APPROACH *b*

Very similar results to those gained in approach *a* were predicted by approach *b*. Using aragonite dissolution to raise the pH (to 7.8) predicted final $Cu_{diss}$ concentrations were between 0.02 and 0.035 mg/L, down from 0.488–2.9 mg/L, by the formation of malachite.

### 4.4.4 GROUNDWATER VS ROOF RUNOFF BASED MAJOR ION COMPOSITION

An analogous approach to that described in section 4.3.3 was used to replace the major ion composition of experiment 6's 3 minute effluent with that from Cu roof runoff. This replacement made minimal difference to the amount of Cu expected to remain dissolved.

### 4.4.5 SENSITIVITY TESTING: INITIAL Cu CONCENTRATION

To evaluate the impact of the initial $Cu_{diss}$ concentration on the final predicted $Cu_{diss}$ concentration via formation of malachite, precipitation modelling was carried out with increasing initial Cu concentrations (from 0.005 to 2.9 mg/L) and using the 3 minute effluent chemistry from experiment 6 for all other parameters. All usual minerals were allowed to precipitate (section 4.2.1), and the initial pH of this solution was 7.2.

Above an initial $Cu_{diss}$ concentration of 0.25 mg/L >80% of the $Cu_{diss}$ was predicted to be removed from solution by the formation of malachite, and the increase in reduction was steep between initial concentrations between 0.005 and 0.25 mg/L (Figure 4-4). From the final $Cu_{diss}$ concentrations predicted throughout these modelling exercises, the concentration at which Cu was saturated with respect to malachite in these solution compositions was approximately 0.03–0.06 mg/L, which explains this steep increase in % reduction. The final pH predicted dropped very slightly to 7.1 in the higher initial Cu concentration modelling.

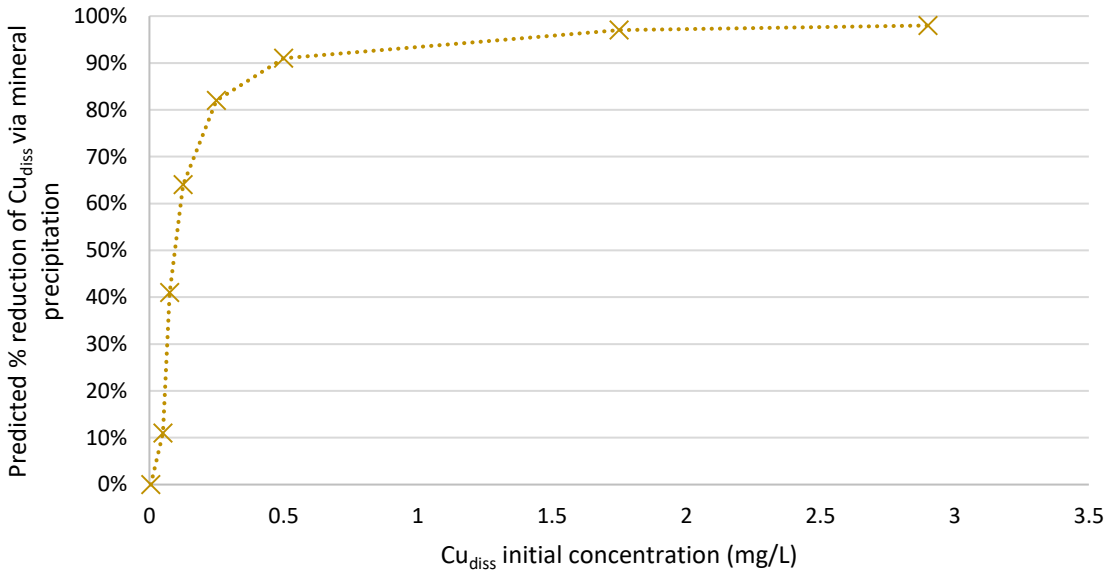


**Figure 4-4: Predicted % reduction of $Cu_{diss}$ due to malachite mineral formation, at different initial Cu concentrations and an initial pH of 7.2.**

### 4.4.6 SENSITIVITY TESTING: COMPETITION BETWEEN Cu AND Zn

To investigate the impact of a competing ion being present, precipitation modelling was carried out with increasing amounts of Cu, using experiment 3's 3 minute effluent with influent Zn and pH 8 as the basis for all other parameters. The pH of 8 was chosen as at this pH an appreciable amount of Zn was predicted to precipitate out of solution (predicted reduction of 40%), whereas below that pH predicted Zn precipitation was much less.

When the proportion of Cu present was low compared to Zn, there was little change in how much Zn was likely to be reduced by, in spite of a steep increase in the amount of Cu removed from solution by formation of malachite (Figure 4-5). When the Cu concentration reaches 1000 mg/L (just over a third of the Zn concentration) >97% of Cu was predicted to be removed by the formation of malachite, and

predicted $Zn_{diss}$ reductions lowered to approximately 20% (Figure 4-5). When the molar Cu concentration equals that of Zn, Zn mineral precipitation was reduced to <10% while the Cu reduction reaches 99% (Figure 4-5).

The final pH was predicted to decrease from the initial pH of 8, to a minimum of 7.7 (when the initial Cu was around 3 mg/L). This decrease in pH could itself have an impact on the amount of Zn precipitating out of solution (section 4.3.5).

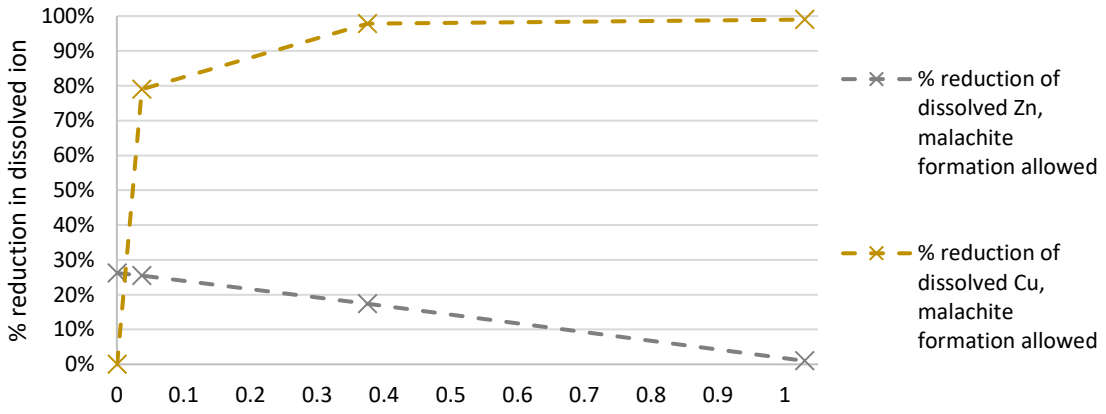


**Figure 4-5: Predicted % reduction in dissolved Cu or Zn due to precipitation of likely minerals, shown for different ratios of Cu to Zn (where 1 = 2.744 mg/L) at an initial solution pH of 8.**

### 4.4.7 KEY FINDINGS

- $Cu_{diss}$ reductions predicted by malachite precipitation exceeded reductions measured in the column experiments for all chemistries modelled;
- $Cu_{diss}$ reductions from malachite precipitation were also predicted in the influents, i.e. in solutions not impacted by the column system;
- Predicted reductions in $Cu_{diss}$ from malachite formation increased sharply in solutions with influent concentrations of 0.005 mg/L up to 0.25 mg/L, above which predicted reductions remained >80%;
- When there were comparable concentrations of $Cu_{diss}$ and $Zn_{diss}$ in the same solution chemistry, a decrease in Zn mineral precipitation was predicted compared to when $Cu_{diss}$ << $Zn_{diss}$. This was likely due to a reduction in pH caused by the precipitation of malachite.

## 4.5 Zn HFO ADSORPTION MODELLING: PREDICTED $Zn_{DISS}$ REDUCTIONS

### 4.5.1 MEASURED INFLUENT/EFFLUENT CHEMISTRIES

Predicted Zn adsorption to HFO was insignificant where the amount of $Zn_{diss}$ was greater than the amount of HFO (Zn:HFO molar ratios >1), which was the case for most of the influents and some of the effluents in the high Zn concentration experiments (first two rows of Table 4-4). Where there was more HFO than $Zn_{diss}$ (Zn:HFO molar ratio <1), as in most of the effluents, appreciable amounts of Zn are predicted to adsorb to the HFO and the effect was larger where the pH was higher (second two

rows of Table 4-4). However, the % reduction in $Zn_{diss}$ concentration predicted via HFO adsorption (at most <10%, Table 4-4) was much lower than the reduction observed in the experiments (>70%, Figure 3-2). In the column experiment samples >60% of the adsorbed Zn was predicted to be adsorbed to the weak sites on HFO. In the Zn roof runoff 88% of the adsorbed Zn was predicted to be adsorbed to a strong site.

**Table 4-4: Selected chemistries modelled in PHREEQC for Zn adsorption to HFO, showing the key parameters of pH, Zn and HFO concentration, and the amount of Zn predicted to adsorb to HFO.**

| Input chemistry | pH (initial) | Zn mg/L (initial) | $Fe(OH)_3$ mg/L (initial) | Predicted % Zn adsorbed to HFO (molar) |
|---|---|---|---|---|
| Baseline experiment: influent | 7.1 | 0.117 | 0.057 | 0.2 |
| Experiment 3: influent | 6.7 | 2.74 | 0.029 | 0.01 |
| Baseline experiment: 0 min effluent | 7.1 | 0.011 | 2.2 | 9.0 |
| Zn roof runoff | 6.4 | 0.26 | 5.5 | 4.4 |

### 4.5.2 SENSITIVITY MODELLING: INCREASED pH

To investigate the effect of a higher pH on Zn adsorption to HFO, sensitivity modelling was carried out at different pHs for different Zn:HFO molar ratios, using experimental data as a start point. Where the amount of Zn far exceeds that of HFO (as was likely to be seen in the influents), the pH makes no discernible difference to the amount of Zn adsorbed to HFO (Figure 4-6). When the ratio of Zn:HFO was smaller, which was more likely to represent the effluent samples, an increase in pH predicts an increase in adsorption to HFO. The maximum reduction of $Zn_{diss}$ was only 27% in the pH range seen experimentally (Figure 4-6).

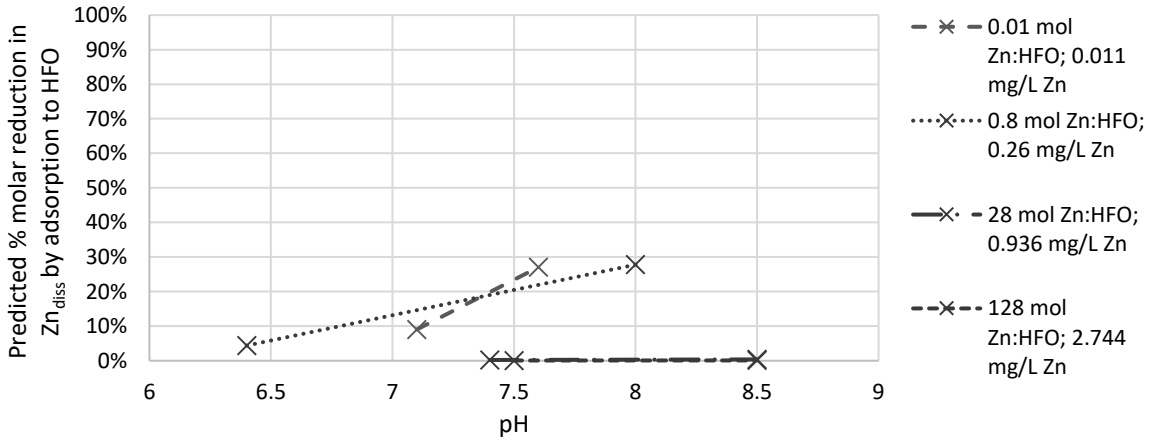


**Figure 4-6: The % reduction in $Zn_{diss}$ predicted by PHREEQC via adsorption to HFO, at different pHs and for different ratios of Zn:HFO, with the actual $Zn_{diss}$ concentration also noted in the legend.**

### 4.5.3 SENSITIVITY MODELLING: INCREASED AMOUNT OF HFO

To investigate the impact of higher amounts of HFO on Zn adsorption, different molar ratios of Zn:HFO were modelled for two different initial Zn concentrations. Experimental Zn and Fe concentrations were used as the starting point, and the pH was set at 7.5 (a common effluent pH).

The reduction predicted by adsorption to HFO did not reach >50% until the proportion of Zn:HFO was <0.1 regardless of the initial Zn concentration (Figure 4-7). The molar ratio of ≤0.1 Zn:HFO was not seen in influents or effluents (other than the first flush effluent) in any of the experiments, and at a Zn concentration of 2.744 mg/L this would equate to requiring an Fe concentration of 21 mg/L (present as HFO).

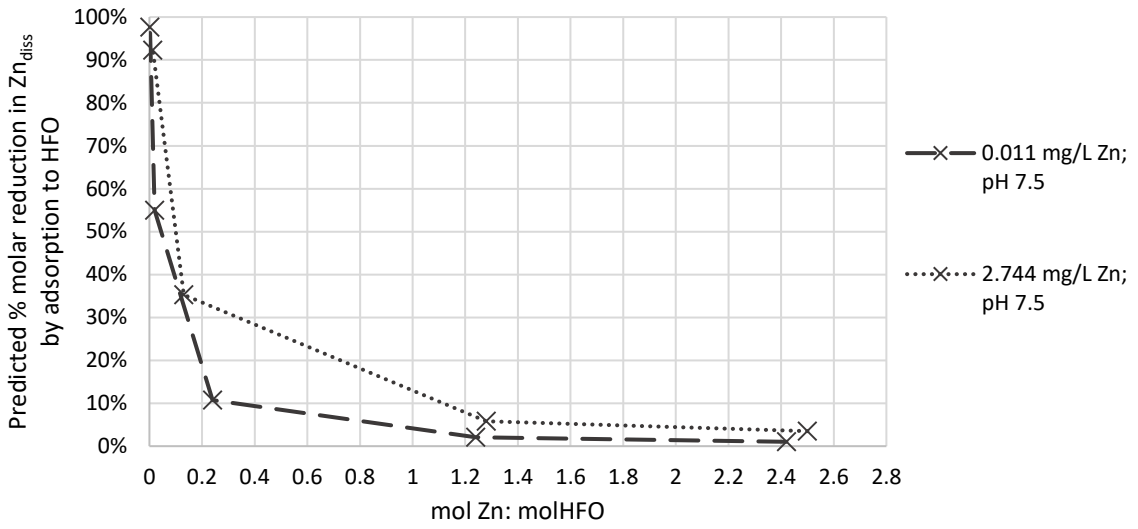


**Figure 4-7: The % reduction in $Zn_{diss}$ predicted by PHREEQC via adsorption to HFO at different ratios of Zn:HFO for two initial $Zn_{diss}$ concentrations, with the pH set constant (at 7.5).**

### 4.5.4 KEY FINDINGS

- Modelling of Zn adsorption to HFO predicted $Zn_{diss}$ reductions an order of magnitude lower than reductions seen in the column experiments;
- Predicted $Zn_{diss}$ reductions were more sensitive to changes in HFO concentrations than pH;
- To predict a $Zn_{diss}$ reduction of >50% at pH 7.5 with the highest $Zn_{diss}$ concentration used in column experiments (2.744 mg/L), an HFO concentration of 21 mg/L would be required.

## 4.6 Cu HFO ADSORPTION MODELLING: PREDICTED $Cu_{DISS}$ REDUCTIONS

### 4.6.1 MEASURED INFLUENT/EFFLUENT CHEMISTRIES

Appreciable amounts of Cu are predicted to adsorb to HFO where the amount of HFO far exceeds that of Cu (Table 4-5). As the amount of HFO remained in the same range throughout all experiments, the Cu:HFO ratio in the baseline influent results was common for the baseline and Zn range experiment influents and effluents. In these solutions the amount of Cu was in the 0.001–0.01 mg/L range and the Cu:HFO molar ratio ranges between 0.01 and 0.24. Therefore Cu adsorption to HFO in these experiments could be expected to be <50%. The only solutions where Cu adsorption could be expected to reach around 90% are the other first flush effluents, where the Cu:HFO molar ratios are 0.002–0.006.

In spite of a lower pH, a small amount of Cu was predicted to adsorb to HFO where the amounts of both are similar (Table 4-5), though this scenario was rare in the experiments conducted.

Adsorption was insignificant where there was far more Cu than HFO (Cu:HFO molar ratios >5), in spite of a similar pH as in the baseline experiment results (Table 4-5). This scenario represents most of the solutions measured in the Cu range experiments, so this indicates that adsorption to HFO was not predicted solely to account for the reductions in $Cu_{diss}$ seen in the experiments. Where any Cu adsorption to HFO took place in these solutions, >87% of it was predicted to be to weak sites.

**Table 4-5: Selected chemistries modelled in PHREEQC for Cu adsorption to HFO, showing the key parameters of pH, Cu and HFO concentration, and the amount of Cu predicted to adsorb to HFO.**

| Input chemistry | pH (initial) | Cu mg/L (initial) | $Fe(OH)_3$ mg/L (initial) | Predicted % Cu adsorbed to HFO (molar) |
|---|---|---|---|---|
| Baseline experiment: influent | 7.1 | 0.005 | 0.06 | 16 |
| Baseline experiment: 0 min effluent | 7.1 | 0.003 | 2.2 | 87 |
| Cu roof runoff | 6.2 | 0.54 | 0.76 | 3 |
| Experiment 6: 3 minute effluent | 7.2 | 0.77 | 0.04 | 0.4 |

### 4.6.2 SENSITIVITY MODELLING: INCREASED pH

Analogous to section 4.5.2, several solutions were modelled with both their original pH and one higher to investigate the effect of pH on Cu adsorption to HFO.

An increase in pH makes little-no difference to the amount of Cu predicted to adsorb to HFO (Figure 4-8). The adsorption predicted in a solution with a 1.2:1 mol ratio of Cu:HFO (based on the Cu roof runoff) was higher than that predicted for a solution with a 0.5:1 mol ratio (based on the experiment 4 first flush influent) (Figure 4-8). It was likely therefore that there was some other key parameter influencing Cu adsorption predictions for the Cu roof runoff that was neither pH nor the Cu:HFO ratio.

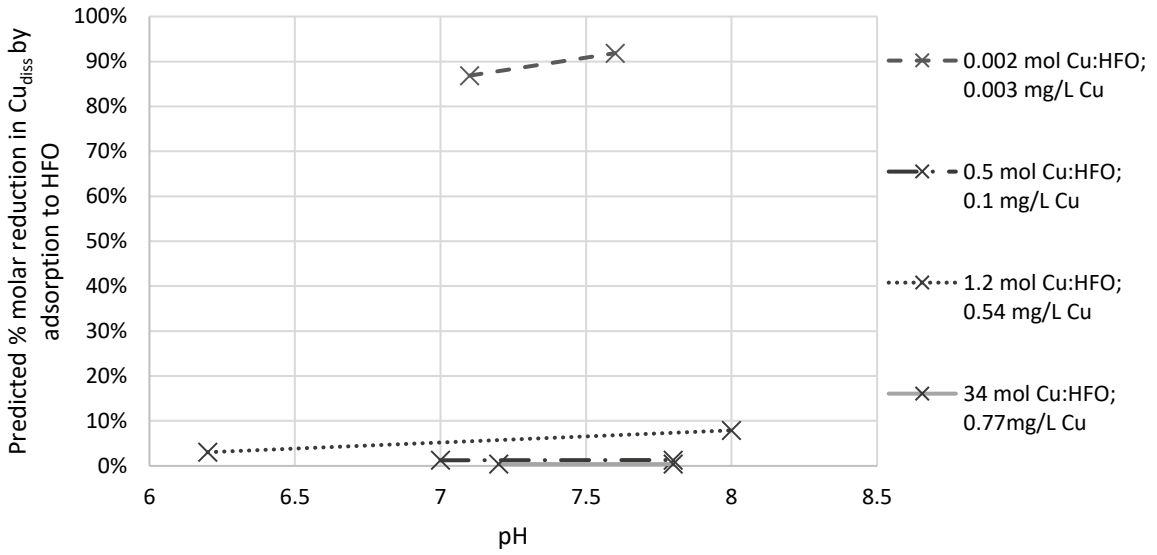


**Figure 4-8: The % reduction in $Cu_{diss}$ predicted by PHREEQC via adsorption to HFO, at different pHs and for different ratios of Cu:HFO, with the actual $Cu_{diss}$ concentration also noted in the legend.**

### 4.6.3 SENSITIVITY MODELLING: INCREASED AMOUNT OF HFO

An analogous approach to section 4.5.3 was used to evaluate how predicted $Cu_{diss}$ adsorption would change with a change in Cu:HFO molar ratio. Where there are higher initial amounts of $Cu_{diss}$, more of it was predicted to adsorb to HFO (Figure 4-9). Adsorption to HFO could account for a reduction in Cu concentrations of >50% (the magnitude of reductions seen in the column experiments, Figure 3-9) where the molar ratio of Cu:HFO was <0.3 and the initial Cu concentration was close to 1 mg/L, or <<0.1 when the initial concentration of Cu was close to 0.001 mg/L. This would equate to Fe (present as HFO) concentrations of close to 5 mg/L, and more than 0.008 mg/L Fe respectively, required to adsorb significant amounts of Cu.

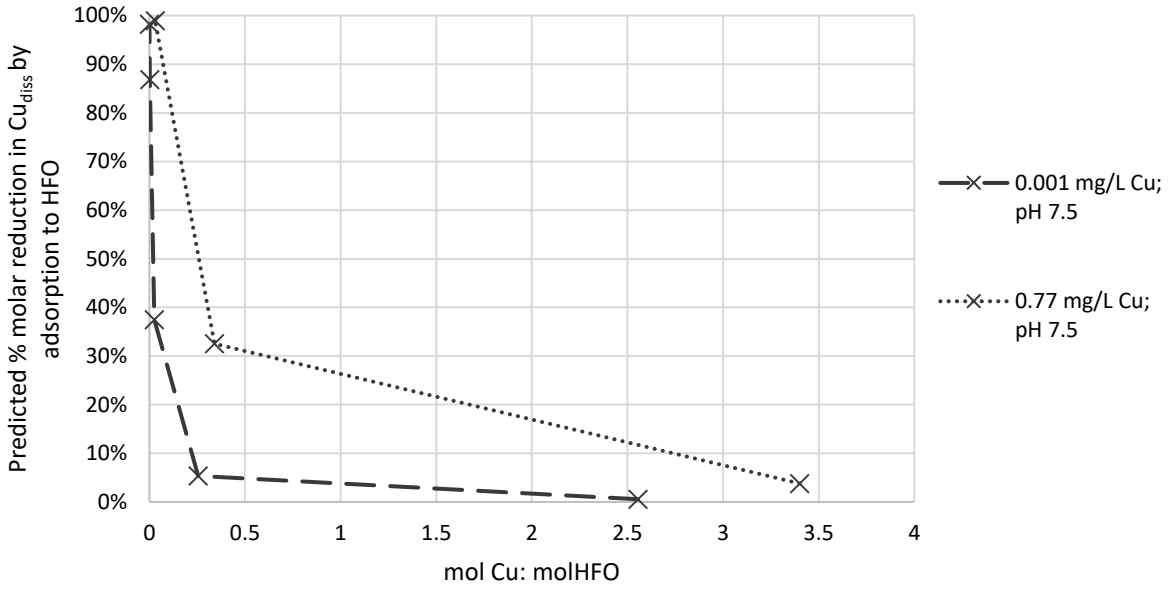


**Figure 4-9: The % reduction in $Cu_{diss}$ predicted by PHREEQC via adsorption to HFO at different ratios of Cu:HFO for two initial $Cu_{diss}$ concentrations, with the pH set constant (at 7.5).**

### 4.6.4 KEY FINDINGS

- In solutions with higher $Cu_{diss}$ concentrations, such as Cu roof runoff or from elevated Cu experiments, adsorption to HFO was not predicted to produce reductions in $Cu_{diss}$ comparable to those measured experimentally;
- Where the concentration of HFO was much greater than the concentration of $Cu_{diss}$, such as in the solutions without artificially increased Cu concentrations, significant amounts of Cu were predicted to adsorb to HFO.
- Predicted $Cu_{diss}$ reductions were more sensitive to changes in HFO concentrations than pH;
- To predict a $Cu_{diss}$ reduction of >50% at pH 7.5 and a $Cu_{diss}$ concentration of 0.77 mg/L (the mid-range influent concentration in the elevated Cu experiments), an HFO concentration of 5 mg/L would be required.

# 5 DISCUSSION

## 5.1 POTENTIAL MECHANISMS OF Zn AND Cu RETENTION BY WASTE SEASHELLS

The removal of dissolved Zn and Cu from solution by shells is likely to involve several mechanisms, and the dominant mechanism may differ between metals. Evidence for the three mechanisms specifically investigated in this research: mineral precipitation; adsorption to hydrous ferric oxide (HFO); and adsorption to organic matter, are discussed first. Following this, evidence from this research is discussed in relation to two other proposed mechanisms suggested by other authors: adsorption to $CaCO_3$; and adsorption to Al, Si and Na compounds. Finally, the most likely mechanisms of Zn and Cu removal in the flow-through column system are proposed, and implications for optimisation of a Storminator™ type flow-through treatment device are discussed.

### 5.1.1 MINERAL PRECIPITATION

Mineral precipitation involves dissolved ions combining to form a mineral compound, and when the concentration of that compound exceeds its solubility in the solvent (becomes oversaturated), it precipitates as a solid. This process therefore describes a way that free cations, such as dissolved $Zn^{2+}$ or $Cu^{2+}$, can combine with free anions, such as $CO_3^{2-}$ or $OH^-$, and so partition from the dissolved to the particulate (solid) phase, thereby reducing the concentration of those dissolved ions. For example, the aqueous precipitation of malachite (a Cu mineral) is controlled by the equation below:

$$2Cu^{2+}_{(aq)} + CO_3^{2-}{}_{(aq)} + 2OH^-_{(aq)} \leftrightarrow Cu_2(OH)_2CO_{3\,(s)}$$

This process occurs in the aqueous phase, so in the context of the treatment system under investigation, this process describes a mechanism that does not specifically include the solid shell media. Rather, the link between the shells and potential mineral precipitation is made through the shells' (partial) dissolution and their resulting contribution of dissolved species, such as Ca and $CO_3$, to the aqueous solution. The shells may subsequently function as a physical filter, retaining any precipitates formed.

Evidence to support Zn or Cu mineral precipitation occurring in the treatment column could be an increase in the effluent concentration of acid soluble metal relative to the dissolved concentration, the PHREEQC prediction of a Zn- or Cu-containing mineral being oversaturated, or by visual identification of a particle via SEM and subsequent confirmation of its composition by EDS. Another way that the shells could contribute to mineral precipitation is by providing nucleation sites for precipitates to build on. This is not accounted for in thermodynamic modelling, but visual identification of particles, or of rough surfaces on the shells, via SEM, regardless of whether EDS identifies a metal presence on them, could indicate an abundance of nucleation sites. Sequential extraction procedures indicate an association but do not usually specify whether a metal is present as a precipitate, or adsorbed to a surface, or associated through some other mechanism.

### Zn

Almost all Zn in the column experiment influents and effluents was present in a dissolved form, and speciation modelling predicted a dominance of the free $Zn^{2+}$ ion. Saturation modelling did not predict any probable Zn mineral to be oversaturated in any of the influents or effluents, so none of these results suggested that Zn was forming a mineral precipitate in the column. However, sensitivity modelling suggested that for higher Zn concentrations (>1 mg/L) the precipitation of $ZnCO_3.H_2O$ or ZnO could become feasible at pH > 7.5. Concentrations of that magnitude are not uncommon in roof runoff (Charters et al., 2017; Charters et al., 2021), and so pH would appear to be the crucial factor in relating this study's column results to field systems.

Gregoire (2018) and Vijayaraghavan et al. (2010) were the only previous studies found that investigated non pH-adjusted column systems (like the current study's), and who reported the effluent pHs: maxima of 8.9 and 8.1 respectively. These pHs are closer to the effluent pH predicted in PHREEQC if aragonite was allowed to dissolve to equilibrium (pH 8.4). In a column system the solution entering the column is undersaturated with respect to aragonite/calcite, and is allowed a limited contact time with the media, so the thermodynamic drive will continue to be in the direction of aragonite/calcite dissolution down the length of the column. However, the amount of aragonite/calcite given the opportunity to dissolve will be limited by the contact time, as well as by the shell surface area available. While the effluent pHs in this study could be considered low in comparison to those two other column studies, this could be explained by the higher flow rate used in this study (2 L/min (present study) vs 0.01 L/min (Vijayaraghavan et al., 2010)), and/or the smaller shell surface area available due to the larger shell size packing the column (2.36–10 mm (present study) vs 1.18–2.36 mm (Gregoire, 2018) vs 0.5–1 mm (Vijayaraghavan et al., 2010). Therefore, the potential for precipitation of a Zn mineral in a column system should not be discounted, although based on the PHREEQC modelling it is unlikely to account for a large proportion of the 73%–97% $Zn_{diss}$ reductions observed in the column effluent.

Sequential extraction results suggested that the majority of Zn was bound to a "carbonate". This would include any Zn present as $ZnCO_3$ that was attached to the shells, but cannot separately identify a Zn mineral precipitate from Zn adsorbed directly onto a carbonate surface. However, the lack of significant Zn carbonate precipitates predicted would suggest it is the latter.

SEM images of a shell with a high concentration of Zn show two distinct morphologies associated with Zn hotspots as identified by EDS. One morphology was a conglomerate of flaky particles (Figure 3-34), and this has been described as characteristic of hydrozincite ($Zn_5(CO_3)_2(OH)_6$) (Du et al., 2011). Du et al. (2011) also conducted saturation modelling, using the geochemical model MINTEQ, for aqueous solutions of Pb, Cd, and Zn at equilibrium with aragonite and calcite mollusc shells, but at much higher concentrations than used in this study (up to 300 mg/L Zn). They reported that hydrozincite was not predicted to be oversaturated, but found flaky precipitates using SEM that they attributed to hydrozincite. PHREEQC databases (WATEQ, PHREEQC, and MINTEQ) did not include hydrozincite and so this mineral was not included in this study's modelling.

The other Zn-rich morphology identified by SEM-EDS was clumps of rounded particles (Figure 3-32). Given the rounded amorphous shape of the particles, and their spatial association with Na and Si, they could be freshly formed precipitates of Zn/Na/Si mineral, or of a sodium silicate precipitate with Zn

adsorbed to its surface (Qomariyah et al., 2019). The MINTEQ database used in modelling did not include any Zn silicate minerals, and Si was not measured in the influents/effluents, and so could not have predicted its formation. To further investigate the potential significance of this mechanism for $Zn_{diss}$ removal, inclusion of Si in influent/effluent analyses, and Zn/Na/Si minerals in the geochemical model database would be recommended in future study.

#### Cu

The precipitation of a Cu mineral was observed in two out of three synthetic roof runoff influents, suggesting that interaction of the synthetic roof runoff with the shells was not necessary to promote precipitate formation. The dominant $Cu_{diss}$ species predicted was $CuCO_3^0$ in most effluents, and Cu minerals were predicted to be oversaturated in almost all solutions. The precipitation of malachite alone was predicted to account for a $Cu_{diss}$ reduction of at least >70%, and commonly >90%. This suggests that the precipitation of a Cu mineral such as malachite is likely, and in amounts that could explain the $Cu_{diss}$ reductions observed in the effluents (55%–80%). This may not necessarily have required interaction with the shell media, though the media's impact on the solution composition and provision of nucleation sites could help speed up precipitate formation in the short contact time available.

In shells with higher concentrations of Cu, most of it was released from the "carbonate" fraction during the sequential extraction. As with the Zn results, this could indicate that it was bound either as a carbonate mineral, or directly to the shell's carbonate surface.

SEM-EDS analysis however did not find conclusive evidence of a Cu mineral precipitate. The few fragments found and identified as having higher Cu concentrations either had morphologies and other elements typical of aluminosilicates, or were particles of biological origin with Cu adsorbed to their surface. The presence of such particles could be expected, since the shells examined by SEM were from a column servicing a real roof, and so windblown dusts and organic matter would be washed off the roof into the column. Given that the areas observed under SEM are typically micro- to nano-scale, it is possible that views of such precipitates were missed. Also, there was no opportunity to analyse high Cu shells analogous to those high in Zn (from the operationally saturated column), to search for deposited or adsorbed precipitates on shells where they would be more likely to have occurred. Therefore, the absence of evidence for Cu mineral precipitation from this study's SEM-EDS analysis cannot rule out their potential as a $Cu_{diss}$ removal mechanism in this context, and analysis of a wider range of Cu loaded shells would be recommended to investigate this.

### 5.1.2 ADSORPTION TO HFO

Hydrous ferric oxide (HFO, ferrihydrite) is one of the most common adsorbing surfaces in the environment, so data on its adsorption properties have been well studied (Dzombak & Morel, 1990). When in an aqueous matrix it acquires surface OH groups in which the O can act as a Lewis base (electron donor) and the metal acts as a Lewis acid (electron acceptor), and thereby complexes (i.e. adsorbs) the metal according to the equation below (Stumm & Morgan, 1995).

$$\equiv Fe\text{-}OH + M^{2+} \leftrightarrow \equiv Fe\text{-}OM^{+} + H^{+}$$

While assuming that HFO is the only adsorption surface available will underestimate the adsorption sites likely to be available in a complex natural media such as the shells (with windblown dust and organic matter also present, section 2.2.2), it is worth investigating whether adsorption to HFO could contribute to the reductions in dissolved Zn and Cu observed.

Evidence of Cu or Zn adsorption to HFO could come from PHREEQC modelling using the HFO adsorption module, the metals being released from the "amorphous or crystalline iron oxides" fractions during sequential extraction, or from a spatial correlation between Fe and Zn or Cu in particles analysed by SEM-EDS.

### Zn

Modelling of Zn adsorption to HFO predicted that this was not likely to be a significant removal mechanism for $Zn_{diss}$. In all influents and effluents the predicted $Zn_{diss}$ removal was <10%, and sensitivity modelling showed that much higher concentrations of HFO (relative to Zn) would be required to obtain the $Zn_{diss}$ reductions seen experimentally. For example 2.7mg/L Zn would require a particulate Fe concentration of 21mg/L (present as HFO) to adsorb >50% of the $Zn_{diss}$, c.f. the majority of Fe concentrations recorded in the influents/effluents of <0.1mg/L. Fe concentrations (stoichiometrically equivalent to HFO) on the shells from field columns, and from synthetic roof runoff laboratory columns, were also much smaller than Zn concentrations (Fe typically <100mg/kg vs Zn typically >100mg/kg). In the real roof runoff laboratory column shells however, where Zn concentrations were lower (<60mg/kg), the Fe concentrations were higher and closer to or greater than Zn concentrations, showing a potential limitation in the use of a synthetic roof runoff for laboratory experiments. Adsorption of significant quantities of Zn to HFO could be more likely in that system.

The sequential extraction of the shells also hinted that, at very low concentrations of Zn, the relative concentration of Fe could be high enough to adsorb larger proportions of Zn (31% of 16.5 mg/kg Zn released in an Fe oxide fraction), though this scenario was not common. It should be noted that gross debris was brushed off the field column samples with a clean dry brush before analysis by sequential extraction, so this may have removed larger Fe-based particulates and any Zn bound to them. However, smaller (still visible) particles remained embedded in shell crevices so some Fe particulates may have remained, and dry brushing should have avoided a redistribution of Zn between phases more closely attached to or part of the shell (the surfaces of interest).

SEM-EDS analysis did not show any evidence of Zn adsorption to a Fe containing particle, though at such low concentrations it may be likely that they were too difficult to locate.

Adsorption to HFO is also a competitive process, and so the presence of other metal ions could impede Zn from adsorbing to HFO. Real roof runoff contains numerous dissolved metals. For example, the Cu roof runoff sample analysed in this study had Zn concentrations approaching the Cu concentrations (0.355 mg/L $Zn_{diss}$ vs 0.540 mg/L Cu). In such cases Zn may not adsorb to HFO in any significant amount, even if there were enough HFO present, because Cu will bind preferentially, as indicated by the relative positions of the $Cu^{2+}$ and $Zn^{2+}$ adsorption edges (Figure 5-1).

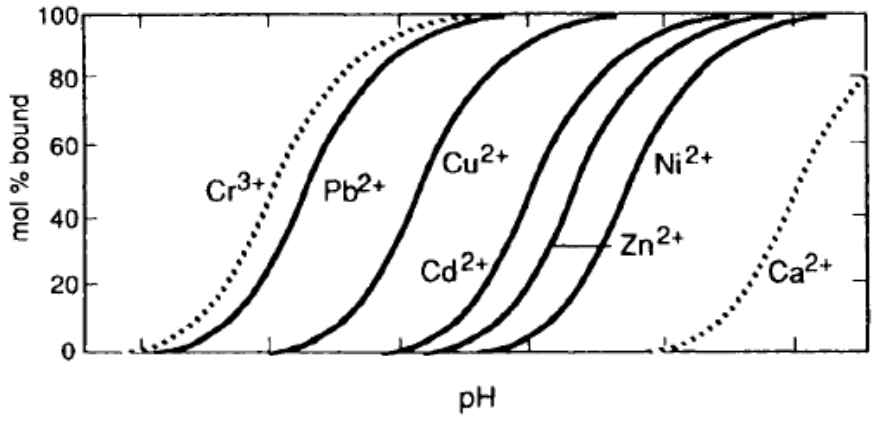


**Figure 5-1: Relative adsorption of metal ions to HFO at varying pH. Adapted from Stumm and Morgan (1995).**

### Cu

Cu adsorption to HFO appears to follow a similar pattern to that described for Zn, but there was a greater representation of low Cu concentrations (relative to Fe) in both aqueous and shell matrices. This provided some evidence to support the hypothesis that, at very low Cu concentrations (<10 mg/kg), adsorption to HFO could be a significant $Cu_{diss}$ removal mechanism. This is supported by sequential extraction results (Figure 3-22). However at higher Cu concentrations, such as those recorded for shells from a Cu roof field column or from a synthetic roof runoff laboratory column, the relative concentration of Fe on the shells and sequential extraction results suggest that HFO adsorption did not play a significant part in $Cu_{diss}$ removal.

## 5.1.3 ADSORPTION TO ORGANIC MATERIAL

While seashells are predominantly comprised of $CaCO_3$ they also contain organic matter. The two main forms of this are the polysaccharide chitin, which forms the 'mortar' between the carbonate 'bricks' in the body of the shell, and proteins which both complex with the chitin and form the outer periostracum layer of the shell (Jacob et al., 2008; Martínez-García et al., 2017; Roberts, 1992). These organic compounds provide oxygen and nitrogen containing reactive surface functional groups such as carboxyl, hydroxyl, amine and amide groups, which can complex the metal ions or adsorb metal micro-precipitates formed near the surface (Richards et al., 2019; Roberts, 1992; Stumm & Morgan, 1995; Vijayaraghavan et al., 2010). An example of such a complexation reaction (to an amine surface group) is given in the equation below.

$$\equiv R\text{-}\ddot{N}H_2 + M^{2+} \leftrightarrow \equiv R\text{-}NMH_2$$

While the weight of the organic proportion of the shell is very small compared to the carbonate portion (estimated in this study at 0.01 wt% of the total shell), it would be expected to provide approximately half of the surface area available for metals to adsorb to as it coats the outer half of the shell. In addition to this, Cu in particular is known to favour organic ligands over inorganic, so it is worthwhile looking for evidence of adsorption of Cu or Zn specifically to the organic fraction of the shells (Flemming & Trevors, 1989).

Acid digestions of the periostracum compared with full shell reveal that typically <10% of the Zn was located on the periostracum. Cu proportions in the periostracum were slightly higher, but still only making up 10%–20% of the Cu bound to the shell as a whole. The sequential extractions were in agreement with this, showing that at most 12% of the Zn or Cu was bound in an "organic" phase, and the larger percentages bound in this phase were for shells with lower total Zn or Cu concentrations (<20mg/kg). EDS analysis of shells from a Cu roof field column suggested there could be slightly more Cu on the periostracum than on the carbonate surfaces, though concentrations were very low (0.5–2 at%) so differences of 0.5–1 at% may not be significant. EDS analyses showed that Zn was equally likely to be found on the periostracum as a carbonate surface, whether present in a very low concentration uniform distribution, or as part of defined particles. That there was Cu or Zn found on the periostracum via acid digestion, in the organic phase in the sequential extractions, and in a uniform spatial distribution by EDS, does however suggest that adsorption to the organic surface had taken place.

Modelling of metal adsorption to organic matter is possible in PHREEQC (Example 19 of the User Guide (Parkhurst & Appelo, 2017)), however, compilation of the data required to do this was outside the scope of this study. Shell analyses suggest that while adsorption to organic matter was likely to play a small part, this was not the dominant mechanism for metal removal in this system. Similar conclusions were drawn by Du et al. (2011) for Zn in batch adsorption studies using solutions of a much higher metal concentration than the present study (up to 300mg/L Zn). It would therefore appear that investing in modelling to organic surfaces may not return a benefit significant enough to warrant the effort to compile the necessary data.

### 5.1.4 ADSORPTION TO CALCIUM CARBONATE

Dissolved metals can form metal carbonates both when the carbonate is in solution (as discussed above as mineral precipitation) and when the carbonate is a functional group on a surface (adsorption). In the latter case the carbonate can become available when the $CaCO_3$ partially dissolves, and ion exchange of the $Ca^{2+}$ ion with the dissolved metal ion can then occur (equations below).

$$\equiv CO_3Ca \leftrightarrow \equiv CO_3^{2-} + Ca^{2+}$$

$$\equiv CO_3^{2-} + M^{2+} \leftrightarrow \equiv CO_3M$$

Small increases in $Ca_{diss}$, and smaller increases in $CO_{3\ diss}$, were observed in the effluents relative to the influents in the current study's column experiments, which supports the hypothesis of partial $CaCO_3$ dissolution and ion exchange. Other authors have also confirmed that Ca was leached from shell media in contact with metal-loaded synthetic roof runoff, in experiments involving longer contact times or higher metal concentrations than the present study (Richards et al., 2019; Vijayaraghavan et al., 2010). These authors attributed the first steps of metal removal they observed to the dissolution of $CaCO_3$ and ion exchange between Ca and the metal. It would be reasonable to expect that this could still occur under the conditions of the present study, though perhaps to a lesser extent given the shorter contact time and lower thermodynamic drive provided by lower metal concentrations.

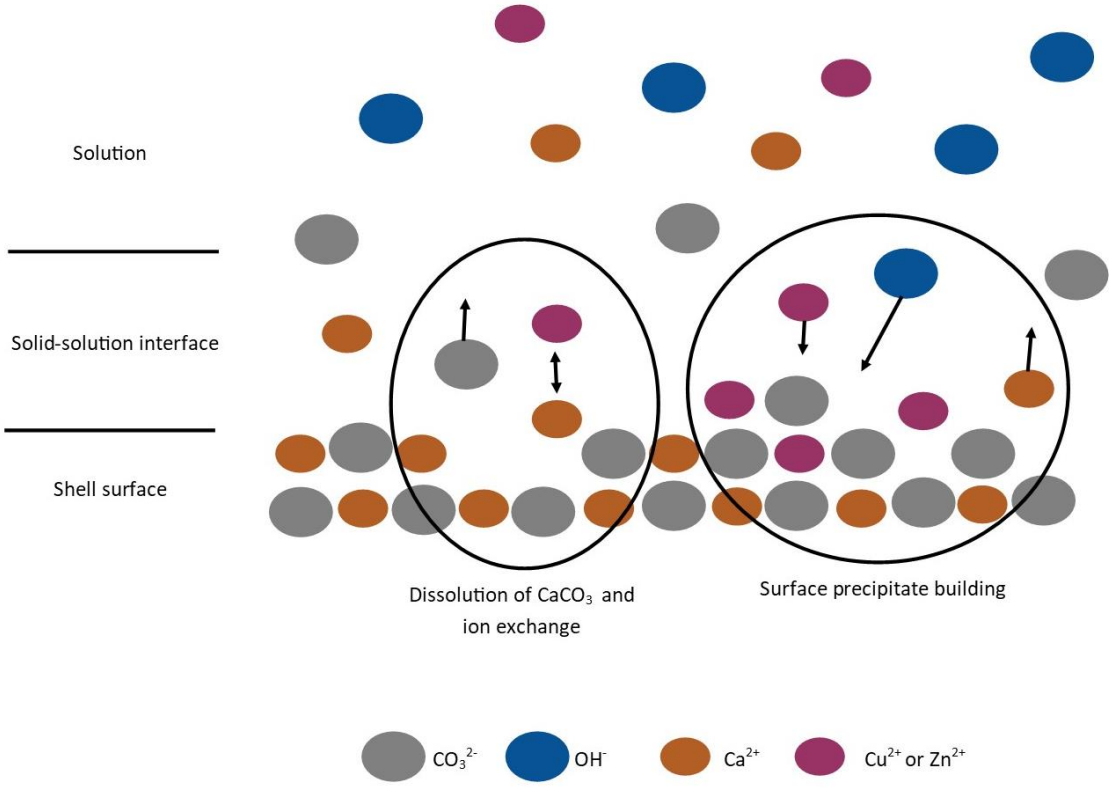


**Figure 5-2:** Diagram of potential adsorption mechanisms of Cu and Zn, including: partial $CaCO_3$ dissolution; ion exchange; and the formation of a surface precipitate from continued adsorption and incorporation of other dissolved ions.

Indeed where enough of this dissolution and ion exchange occurs in the same location, a surface precipitate may form as the abundance of the surface complex increases (Figure 5-2). The surface complex may even incorporate other dissolved ions such as $OH^-$, and so lead to the formation of an [adsorption based] mineral such as hydrozincite or malachite (Figure 5-2). Several authors note an initial rapid adsorption of a metal to a shell, followed by a slower approach to equilibrium (Belova et al., 2014; Bozbaş & Boz, 2016; Vijayaraghavan et al., 2010). This can be explained by the incorporation of a few more metal ions during the slow recrystallization phase (Belova et al., 2014). In the present context, recrystallization and the formation of a surface precipitate from adsorbed species may occur during the drying/dry phase after column flushing, as some solution would remain in contact with the surface, but the process would not be disturbed by continued flow of runoff across the surface.

Evidence of adsorption to the carbonate surfaces in the current study would be expected to come primarily from the sequential extractions and SEM-EDS analyses of used shells, but observations and analyses of aqueous components could help to distinguish between adsorption and aqueous-based precipitation.

### Zn

The sequential extraction of Zn from the used shells showed that the majority was released in the "carbonates" fraction. Given that aqueous precipitation modelling did not predict significant formation of Zn minerals, the sequential extraction results are more likely to support the hypothesis that Zn was adsorbed directly to the carbonate surface. Further evidence of this is provided by the uniform spatial distribution of Zn across carbonate surfaces, as seen in several EDS maps of shells that had lower Zn metal contents.

SEM-EDS also identified some particulate Zn compounds on the surface of shells that had higher Zn concentrations, and which had been considered operationally saturated with respect to metal adsorption. However, this does not discount their presence being due to adsorption rather than deposition of a precipitate. A difference between the crystal lattice structure of a mineral and a substrate encourages the growth of mineral precipitates in randomly oriented three-dimensional structures, as opposed to forming a thin film that coats the surface (Du et al., 2011). In this context, the substrate is either calcite or aragonite, with trigonal or orthorhombic crystal structures respectively, whereas the mineral identified by SEM-EDS as hydrozincite has a monoclinic structure (Du et al., 2011; McLaren, 2011a, 2011b). Therefore, three-dimensional growth would be expected, which leaves space and charge available on the surface to encourage continued adsorption of Zn. Based on this it could be expected that, given continued contact of the shells with Zn loaded water, Zn carbonates would grow into visible (under SEM) surface precipitates on the shell surface, but whose origins are based on adsorption to the carbonate surface.

### Cu

In similar results to Zn, where >17 mg/kg Cu was present on a shell (up to 517 mg/kg), the majority of it was released in the "carbonates" fraction of the sequential extraction. Unlike Zn however, saturation modelling did predict the oversaturation of Cu carbonate hydroxides, and aqueous precipitation was observed in the influents and effluents. Any of these mineral precipitates would have been dissolved in the carbonate extraction, along with the carbonate shell, and so the results of the sequential extraction cannot differentiate between the two possibilities.

SEM-EDS analysis of a Cu roof field column used shell showed that the spatial distribution of Cu on it was largely uniform. Some exceptions were observed, where there were slightly higher concentrations of Cu on visible (by SEM) fragments, however their morphologies and elemental compositions did not suggest that they were a Cu precipitate such as malachite. The uniform distribution of Cu suggests that adsorption of Cu to the carbonate surface is likely. Given high enough concentrations of Cu together with the low solubility of Cu carbonate hydroxide minerals, surface precipitates could be expected to form in a similar (three-dimensional) manner to hydrozincite, as both malachite and azurite belong to the monoclinic crystal system, which is different to the calcite and aragonite crystal systems (see above).

### COMPETITION

Adsorption is a competitive process due to there being a finite number of adsorption sites available on a given quantity of media. Several authors, who (unlike the present study) conducted batch experiments and/or used solutions of much higher metal concentrations, observed a reduction in

dissolved metal removal when there were competing ions present (Kim, 2003; Reddy et al., 2014; Wu et al., 2014; Xu et al., 2019). In the present study, only one metal at a time was increased in the influent to the columns, so the effects of competition were not expected to be obvious from the effluent compositions. However, the sample of Cu roof runoff analysed showed that Zn and Cu may be found in comparable concentrations in a single source of roof runoff, therefore there may be trace metal ion competition for adsorption sites in the column. This would be in addition to the potential competition from major cations such as Ca and Mg. The relative proportions of Cu and Zn on shells from the column servicing that same Cu roof hints that competition for sites may be occurring. There was ≈ 6 times the amount of Cu, compared to Zn on the shells, compared to Cu concentrations in the runoff sample of only ≈ 1.5 times that of Zn. However, further evidence would be required to augment these observations before definite conclusions could be drawn regarding the rapid flow column system under investigation. Experiments targeting mixed Zn and Cu influents, run to saturation (chemical or operational, whichever occurred first), and subsequent analysis of shells representative of the whole column could help to investigate the potential impact of competition.

### 5.1.5 ADSORPTION TO Al, Si, Na COMPOUNDS

Si and Al are abundant in the natural environment, and Na containing clays are common in the Christchurch area, so their presence on the shells could be expected as even the laboratory column shells had been exposed to the outdoor environment prior to packing the column (Raeside, 1964; Stumm & Morgan, 1995). In an analogous manner to HFO (section 5.1.2), these aluminosilicates and/or Si and Al oxyhydroxides contain surface OH groups which encourage metal adsorption to the particulate surface (Stumm & Morgan, 1995). Indeed zeolite is comprised of aluminosilicate minerals and is commonly used as an adsorbent for metal removal (Köhler et al., 2007; Reddy et al., 2021; Shin et al., 2014). Therefore, the potential for Cu or Zn adsorption to Si, Al and Na compounds is worthwhile investigating.

The analyses of real roof runoff in the present study indicate that it contained high concentrations of Al (>700 µg/L), >95% of which was particulate. Acid digestions of the used shells released ≈ 17–66 mg/kg Al (comparable to Fe concentrations), and the sample of debris from a Cu roof analysed confirmed that there were large quantities of particulate Al in the runoff (17,400 mg/kg Al, comparable to the Cu concentration in the debris of 19,400 mg/kg). In the sequential extractions Al was released in the “iron oxides” and “organic” fractions (Figure 3-20). While the amount of Cu or Zn released in those fractions was relatively small (Figure 3-21, Figure 3-22), based on the above finding it should be considered that what was released in those fractions could have in fact been bound to an Al compound, rather than the iron oxide or organic phase as labelled by the procedure. While particulate Si and Na were not measured in the roof runoff or shell digestions, SEM-EDS analyses showed that Al, Si and/or Na were present in low concentrations on all used shells studied, regardless of whether they were from a field or a laboratory column. In several instances, these elements coincided spatially with higher concentration areas of Cu or Zn, and some angular or plate-like fragment morphologies suggested clay type particles, while others were rounded in shape (for example Figure 3-32 from the Zn saturated laboratory shells).

These results suggest that Al, Si, and/or Na compounds may play a minor role in removing dissolved Cu and Zn from this system. Detailed investigation into the specifics of this potential mechanism was

outside the scope of the current study, but results indicate that further investigation could prove insightful, particularly for runoff with high concentrations of Zn.

### 5.1.6 MOST LIKELY MECHANISMS OF REMOVAL FOR Zn AND FOR Cu

The dominant mechanism of $Zn_{diss}$ removal in this flow-through column system is most likely to be adsorption to $CaCO_3$, leading to the formation of micro scale Zn (hydroxy)carbonate precipitates on the surface of the shell where it is exposed to very high concentrations of Zn. Minor contributions to the total amount of $Zn_{diss}$ removed likely comes from adsorption to the organic material in the shell, and from adsorption to or formation of Zn incorporated Na/Si/Al compounds. At very low Zn concentrations, where the concentration of Fe (as HFO) greatly exceeds that of Zn (for example by an order of magnitude), adsorption to HFO may also play a minor role in removing $Zn_{diss}$.

For Cu, the dominant mechanism is likely to be formation of Cu hydroxycarbonate precipitates, whether by aqueous precipitation or via surface precipitation following adsorption to $CaCO_3$ on the shell surface. However, although aqueous precipitation of a Cu hydroxycarbonate mineral in roof runoff may be possible in the timescales involved between the roof and exit from the column, such precipitates may not (all) be retained in the column. Adsorption to an organic phase in or deposited on the shell is likely to play a minor role, though perhaps a slightly larger role than for Zn. Similarly to Zn, adsorption to HFO, or to Na/Si/Al compounds is also likely to play a minor role in reducing $Cu_{diss}$, particularly where HFO>>$Cu_{diss}$.

Overall, for both elements the dominance of each mechanism appears to depend on the concentration of the metal relative to the adsorbing surfaces available. Where the metal concentration is low compared to the availability of HFO, Na/Si/Al compounds, or organic material, significant proportions (up to 90%, Figure 3-21, Figure 3-22) of the metal may be adsorbed to these surfaces. However as metal concentrations increase, for example to Cu and Zn concentrations commonly seen in roof runoff, adsorption to the more abundant $CaCO_3$ surface may dominate (accounting for >60%) the removal mechanisms for Zn (Figure 3-21), or $CaCO_3$ adsorption as well as mineral formation may dominate for Cu (Figure 3-22).

Wu et al. (2014) and Du et al. (2011) conducted batch adsorption experiments to $CaCO_3$ at high metal concentrations (up to 100 mg/L Cu and 300 mg/L Zn respectively), and proposed that adsorption to $CaCO_3$ [without SEM-visible surface precipitates] is likely at lower metal concentrations (<30 mg/L), while [adsorption driven] surface precipitation is likely where metal concentrations are higher (>30 mg/L). In spite of the differences in experimental conditions, their conclusions support the conclusions drawn for this low contact time flow-through column system.

While adsorption to organic matter appears to play a minor role, it could be enough to promote the dissolved metal removal efficacy of a biogenic $CaCO_3$ (such as a seashell) above a geogenic one (such as limestone) (Belova et al., 2014; Zhou et al., 2017). Zhou et al. (2017, regarding Pb) attribute some of the biogenic $CaCO_3$'s efficacy to adsorption of the metal to the organic surface, but mostly to the porous $CaCO_3$ structure created by the inclusion of organic material as the 'mortar' in the shell's carbonate 'brick and mortar' (prismatic and nacreous) layers. This contrasts with the compact crystalline $CaCO_3$ structure as found in geogenic materials, leaving a lower surface area of $CaCO_3$

exposed and available as an adsorbing surface, as neatly shown in Zhou et al.'s (2017) graphical abstract below.

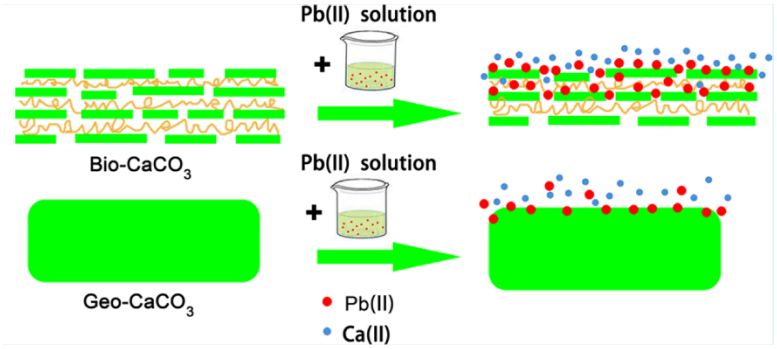


**Figure 5-3: Graphical abstract from Zhou et al. (2017), showing the difference between biogenic and geogenic $CaCO_3$ with respect to adsorption of Pb.**

Belova et al. (2014, regarding Ni) also identify the presence of organic material as a differentiating factor between efficacies of biogenic and synthetic calcite, but also attribute the presence of clay nanoparticles to some of the increased efficacy observed. The current study's results, combined with these authors' observations, suggest that while organic matter, HFO, and/or Na/Si/Al compounds play a minor role in the removal of dissolved metal when compared to adsorption to $CaCO_3$, their role can be nonetheless important. It is unclear from this research whether adsorption to the different surfaces is additive, where the addition of more of the alternative surfaces would cause a larger decrease in dissolved metal removal, or competitive, where dissolved metal concentrations would only decrease further given an increase in the most preferred adsorbing surface. Reddy et al. (2021) report that for the removal of heavy metals in a batch-fed column, mixed media (zeolite, calcite, sand and iron fillings) performed similarly to or better than the individual media (reported in Reddy et al., 2014). This suggests there may be additive effects of additional adsorbing surfaces, and so could warrant further investigation in the Storminator™ context.

## 5.2 IMPLICATIONS FOR OPTIMISATION, LIFESPAN, AND REGENERATION

Understanding the mechanisms that retain the metals on the shells can provide insight into how best to prepare the shells, how long they are likely to work, and if/how they might be regenerated once saturated. Therefore, some implications for the design and operation of a shell-based column system are presented.

### 5.2.1 SHELL OPTIMISATION

As the dominant retention mechanism is likely to be adsorption to the $CaCO_3$ surface following partial dissolution of this surface, preparation of the shells should expose as much $CaCO_3$ surface as possible, for example by crushing. This would allow more of the surface to dissolve and provide a greater surface area for adsorption to take place on. It would also expose more of the prismatic layer (normally sandwiched between the nacreous and periostracum layers), which Wu et al. (2014) reported can adsorb more Cu than the nacreous layer due to its increased porosity. The minimum shell fragment size should be guided by hydraulic conductivity, however, as there will be a diminishing return on

surface area gains provided by crushing given that the shell morphology is thin to begin with. A greater proportion of aragonitic shells (such as NZ green lipped mussel shells) would also be preferable to calcitic shells (such as blue mussel or oyster shells), as aragonite dissolves more easily in water. It is still likely to be beneficial to have calcitic shells in the media mix however, as different metals may adsorb preferentially to different $CaCO_3$ polymorphs (Egerić et al., 2018). Targeted experiments for Zn and Cu adsorption to calcite-only and aragonite-only shells could help to determine adsorption surface preferences for these two elements of key concern in roof runoff, and may contribute some explanation of the lower retention of Cu compared to Zn observed in this study.

Organic material in the shell appears to play a role that ameliorates the efficacy of biogenic compared to geogenic $CaCO_3$. It can adsorb very high concentrations of metal on a weight/weight basis, but the periostracum is prone to separating from the shell bulk when dried, and easily flies away during media handling as it is very light. Therefore, care should be taken to retain it throughout the shell preparation process. Its inclusion in the [mostly] $CaCO_3$ layers of the shell, leading to a porous structure (Figure 5-3), also highlights that the use of a biogenic product such as seashells not only makes use of an abundant waste product, but is likely to be more effective than a mined geogenic $CaCO_3$ product such as limestone.

As adsorption to HFO and Na/Si/Al compounds also appears to play a role in Cu and Zn retention in the shells, allowing the shells to weather outdoors prior to use is likely to improve them by allowing windblown dust and dirt to settle on them (and so be included in the column media). Some fines appear to remain in the shell media in spite of pre-operation flushing (section 2.2.2), so flushing to optimise the hydraulic conductivity of the column should not totally remove the benefit of outdoor weathering.

By providing some variety of adsorption surfaces it is more likely that multiple metals at varying concentrations, as is present in roof runoff, will be more able to be retained in the media. A wider variety of adsorption sites may be possible to obtain even within the shells themselves: Liu et al. (2009) reported that acid pre-treatment of shells revealed a greater amount and variety of surface sites, and these were then involved in removing Cu from industrial wastewater in batch experiments. For roofs expected to have particularly high Zn or Cu concentrations in their runoff, pre-treatment, such as in Liu et al. (2009), may be beneficial enough to outweigh the added costs of the treatment. This could prove particularly beneficial for the removal of Cu, as removal in the current study was only 55%–82%, and effluent $Cu_{diss}$ concentrations were 185–823 µg/L. This is considerably higher than the ANZG (2019) trigger value for 95% protection of aquatic species of 1.4 µg/L, even considering that the roof runoff will be diluted by mixing with other runoff and then again instream.

### 5.2.2 COLUMN OPTIMISATION

The current study used an influent flow rate of 2 L/min, and the retention (contact) time within the column resulting from that flow rate and the column size and packing was approximately 30 seconds. This length of contact time was sufficient to remove >73% and >55% of Zn and Cu respectively. Several authors have reported that removal of dissolved metals by shells occurs in two phases: a rapid initial stage, then a slow uptake until it reached equilibrium (Belova et al., 2014; Bozbaş & Boz, 2016; Vijayaraghavan et al., 2010). While it appears that Belova et al. (2014) consider “rapid” to be in hours

for their solution of 52 µg/L Ni, Bozbaş and Boz (2016) report the rapid stage as involving 2.5–7.5 minutes of contact time for their solution of 20 mg/L Cu. Vijayaraghavan et al. (2010) found that the rapid uptake phase lasted for a few minutes for their mixed metal solutions including Zn and Cu at 4.4 and 5.1 mg/L. From this it could be expected that increasing the retention time in the column system to 1–2 minutes could maximise the time the runoff is in contact with the media during the rapid adsorption stage, while minimising the impact on the system's capacity to cope with the flows it is required to treat. Further investigation into the impact of retention time in a column system would be useful to test this hypothesis.

### 5.2.3 COLUMN LIFESPAN

One of the shell sample sets analysed in the current study was from a column that was considered saturated from an operational perspective (its removal efficiency had fallen below 15%), and at this point they had between 810 and 1450 mg/kg Zn bound to them. The rest of the shells analysed had lower concentrations of Zn or Cu. Maximum adsorption capacities reported for shells in similar (batch) experiments, where shell modification was confined to washing, drying and grinding/crushing, were generally >7,500 mg/kg and often >100,000 mg/kg, which suggests that the shells analysed in this study were not nearing chemical saturation (Bozbaş & Boz, 2016; Du et al., 2011; Liu et al., 2009; Vijayaraghavan et al., 2010; Wu et al., 2014). The shells in the aforementioned experiments had much smaller grain sizes (<1 mm) than the shells analysed in the present study (>2.36 mm), so the smaller surface area available for adsorption may have decreased the total adsorption capacity of the shells. However, it is more likely that the column design and operation was the limiting factor in adsorption capacity, making it difficult to compare removal capacities between batch and column experiments. The column is required to function as a flow-through system with limited retention time, thus reducing the contact time between the shells and the metal loaded solution. The static nature of the shells in the column also introduces the potential for preferential flow paths through the column, which could become saturated while adsorption capacity remains in other areas.

In this study, only the shells that had a high Zn concentration applied to them (27mg/L), and which also had the highest Zn concentration on the shell, showed evidence of Zn-based surface precipitation. If the formation of surface precipitates were only feasible where influent Zn concentrations were high (section 5.1.4), then the lifespan of a column servicing a degraded Zn roof (high influent Zn) may be longer than, rather than [proportionally] less than, one servicing a less degraded roof with lower influent Zn concentrations but the same cumulative Zn load. This could be explained by the surface precipitates leaving more adsorption sites available (section 5.1.4), as well as themselves seeding further crystal growth which captures the Zn that passes by. However, this study's used shell sample set was not sufficient to verify this hypothesis, so further study, focused on analysing shell samples from a wider range of influent concentrations vs cumulative loads in a column system, could provide insight into lifespan expectations on different roof types.

Another key contributing factor to the useful lifespan of a shell column servicing a roof is the build-up of debris between the shells, which eventually clogs the column. While the column can be shielded from gross debris such as leaves, finer debris builds up predominantly in the top section of field columns. The debris is likely to contain Fe and Al oxides and aluminosilicates, which can provide more adsorbing surfaces, so may aid in removing dissolved metals up until the point they physically clog the

column. As the debris may be beneficial, it could be worthwhile investigating the impact of mixing up the column contents and associated debris once the top layer begins to clog, thus redistributing the debris throughout the column and potentially restoring some of the lost hydraulic conductivity. This would also remove any preferential flow paths that had formed, and so potentially expose more available sites on the $CaCO_3$ surface.

Based on these hypotheses, it is expected that a field column will reach operational saturation (metal removal efficiency drops to an unacceptable level) before it reaches chemical saturation (of adsorption sites). So, estimation of its potential lifespan should be based on experiments using real roof runoff, or columns servicing roofs in the field.

### 5.2.4 COLUMN REGENERATION

To extend the lifespan of the column media, and to prevent unnecessary creation of potentially hazardous solid waste, it would be desirable to be able to desorb the metals bound to the shells, i.e. to regenerate them, when they are nearing saturation.

The sequential extraction procedure carried out in the present study could be considered a type of desorption study, and this showed that neither water (circum-neutral pH, low ionic strength) nor a high ionic strength salt solution would be successful in desorbing significant quantities of Cu or Zn. That the majority of Zn and Cu was removed by a weak acid at pH 4.5 indicates that this could be used as a regenerating solution, however it was also observed to dissolve the shells themselves to a greater or lesser extent depending on the contact time, and to generate gas. This was predictable, as the reaction of a carbonate with an acid will dissolve the carbonate and produce $CO_2$. Vijayaraghavan et al. (2010) conducted a desorption test with their metal loaded (including Zn and Cu) crab shells and their findings mirrored the present study's. They quantified the weight loss of the media after 1 hour shaking with 0.1 M HCl at 17%, and reported increased concentrations of dissolved Ca and Mg in the desorbing solution, both confirming partial dissolution of the shells.

As the dominant mechanism of retention by the shells is proposed to be adsorption to $CaCO_3$ and formation of metal carbonate surface precipitates, reaction with an acid is the logical choice for a desorption/regeneration solution. It could also provide the benefits of more varied adsorption sites as observed by Liu et al. (2009) in their acid pre-treated shells. Ideally the regeneration solution should be able to be applied *in situ*, and the effluent collected for appropriate disposal, removing the need to move the column from the field site and to reduce manual handling of the media. However the evolution of gas that will occur when acid is poured into a column full of $CaCO_3$ shells could make *in situ* regeneration impractical or potentially even dangerous. It should also be remembered that there will be inorganic and organic debris present in the column as well as the shells, and reaction of those with an acid may produce unintended or hazardous consequences.

Liu et al. (2009) also carried out a desorption study, and found they could remove up to 99% of Cu bound to their shells using 0.5 mM EDTA. The use of EDTA would mitigate several potential hazards that come with using an acid and so should be considered. The concentration and/or dose required may vary significantly depending on how much debris is present contributing ions that EDTA can complex. Its efficacy may also depend on how much of the Zn or Cu is present as a surface precipitate

compared to adsorbed only, as EDTA would not be expected to dissolve a precipitate but it could potentially complex an adsorbed ion.

Further investigation into potential regeneration solutions would be highly useful in understanding the practical lifespan of a shell media based column system. Starting areas of focus could include the use of EDTA, a low concentration weak acid, and a comparison with any benefits gained by re-mixing the debris and shells.

If regeneration were found not to be practical, the shells would need to be disposed of once they were no longer effective, for example in a landfill. In New Zealand landfills can be divided into two categories, depending on whether they do (Class A) or do not (Class B) meet the Centre for Advanced Engineering's Landfill Guidelines (2000) (Ministry for the Environment, 2004). Each landfill type has screening criteria for toxic metal concentrations in solid waste which indicate whether that landfill can accept that waste. The concentration of Zn on the used shells was mostly above the screening criteria for disposal in Class B landfills (20 mg/kg), and in some cases above the screening criteria for Class A landfills (200 mg/kg) (Ministry for the Environment, 2004). The concentration of Cu on the used shells was above the Class B criteria (10 mg/kg), and (given the standard deviation in results) potentially above the Class A criteria (100 mg/kg) (Ministry for the Environment, 2004). Where the screening criteria are exceeded, a leaching procedure can be performed, and results from this compared to leachate concentration criteria. Based on the concentrations reported for the shells in this study, it is likely to be necessary to conduct the leaching procedure to determine whether used shells could be disposed of in a Class A or B landfill. If leaching results exceeded the leachate criteria, the used shells may need to be disposed of via a specialist hazardous waste company.

# 6 CONCLUSIONS AND RECOMMENDATIONS

The aims of this research were: to identify the dominant mechanisms by which waste seashells remove dissolved Zn and Cu from roof runoff in a downpipe scale column filter such as the Storminator™; to evaluate the applicability of geochemical modelling, using PHREEQC, in predicting these mechanisms; and to provide recommendations for media or column operation to optimise its efficacy, based on the mechanisms of Zn and Cu retention in the column. This study has met those aims, and provided a sound basis for numerous recommendations for future work in optimising the Storminator™, and analysing its efficacy.

## 6.1 CONCLUSIONS

### 6.1.1 REMOVAL MECHANISMS

#### Zn

For influent Zn concentrations typical of roof runoff, the dominant mechanism by which $Zn_{diss}$ was removed by seashells in a Storminator™ style device was most likely to be adsorption to $CaCO_3$, and subsequent precipitation of a Zn (hydroxy)carbonate mineral on the shell surface if the Zn concentration in the influent was high enough (for example 27 mg/L). Minor mechanisms included adsorption to organic material in the shell, and incorporation into or adsorption to aluminosilicate compounds. Adsorption to HFO was not observed to play a significant role in $Zn_{diss}$ removal, with the possible exception of (uncommon) solutions with concentrations of HFO>>>Zn. Aqueous precipitation of Zn minerals did not appear to be likely.

#### Cu

For influent Cu concentrations typical of roof runoff, the dominant mechanism appeared to be the formation of Cu-hydroxycarbonates, but it was unclear whether aqueous precipitation or adsorption to the $CaCO_3$ surface (which can lead to surface precipitation) would be more prevalent: aqueous precipitation was likely in synthetic roof runoff even without interaction with the shell media, but precipitation was not all retained in the column; the influence of the shell media would have increased the thermodynamic drive for aqueous precipitation to occur, but the (limited) SEM-EDS evidence from used shells did not show any deposited precipitates, instead pointing towards adsorption to the $CaCO_3$ surface. Adsorption to organic matter and aluminosilicates played a minor role in $Cu_{diss}$ removal, as did adsorption to HFO in (uncommon) solutions where concentrations of HFO>>>Cu.

#### INFLUENCE OF Zn OR Cu INFLUENT CONCENTRATION

At lower Zn or Cu concentrations on the used shells (<20 mg/kg), the influence of the minor retention mechanisms increased. Therefore, at the low end of expected roof runoff Zn and Cu concentrations, the adsorbing surfaces of organic matter, aluminosilicates, and HFO may be expected to play a more dominant role in removing dissolved Zn and Cu.

### 6.1.2 GEOCHEMICAL MODELLING

The geochemical model PHREEQC was used to model speciation and saturation in the solutions, and to model adsorption to HFO, to investigate whether this modelling could predict the mechanism of Zn and Cu retention on the shells. On its own the modelling carried out did not predict the mechanisms, but nonetheless formed an key part of the evidence set as a whole, and provided invaluable guidance in interpretation of evidence provided by other (chemical) methods. Geochemical modelling is carried out stepwise as the modeller tests the predictions of a selected geochemical reaction, and the modelling conducted in this study represents the first steps in that process.

### 6.1.3 RECOMMENDATIONS FOR STORMINATOR™ OPTIMISATION

Based on the evidence gathered in this study, and hypotheses arising from that evidence and the literature, the following recommendations can be made to optimise the operation and lifespan in a Storminator™ runoff treatment system.

The shells should be:

- Predominantly (but not exclusively) aragonitic;
- Allowed to weather outdoors prior to use to allow incorporation of a variety of windblown dirt and dusts;
- Crushed to the minimum size possible while retaining the required hydraulic conductivity in the column; and,
- Organic material on the shell should be retained as much as possible in the preparation process.

The column should:

- Be designed to allow a longer retention time than present designs, for example 1–2 minutes;
- Not be expected to reach chemical saturation of all adsorption sites, because its lifespan will be limited by operational factors (clogging, preferential flow paths). Lifespan should therefore be estimated by field trials;
- Be decanted, mixed, and repacked to prolong the lifespan of the shell media;
- Be able to be regenerated by a low concentration solution of a weak acid.

## 6.2 RECOMMENDATIONS FOR FURTHER STUDY

There are several avenues for further study that are recommended to address the limitations of this research, and to test the suggestions arising from it. Recommendations in each section are offered in order of priority for usefulness in advancing the Storminator™ design.

### 6.2.1 GEOCHEMICAL MODELLING

The geochemical modelling conducted in this study was limited to speciation/saturation and adsorption to HFO due to time constraints. As the other (chemical) evidence from this study suggests that adsorption to $CaCO_3$ is a dominant mechanism, this should be modelled (for example in PHREEQC) to see if such modelling supports that hypothesis. A start point for this could be taken from Xu et al. (2019) who provide a dissociation constant ($K_d$) for adsorption of Cu to calcite at several initial Cu

concentrations, which can be used to define an adsorbing surface in PHREEQC. A thorough search of the literature would also be beneficial, searching specifically for $K_d$s reported for Cu and Zn adsorption to aragonite and calcite. If insufficient data were already available then these values would need to be experimentally determined.

The main limitation of the saturation modelling conducted in this study was the absence of hydrozincite, or any Zn hydroxycarbonate mineral, in the databases used by PHREEQC. As other evidence points to hydrozincite being likely to have formed, inclusion of this mineral in the geochemical database would be key to further saturation modelling. A solubility product ($K_{sp}$) for hydrozincite is provided by Du et al. (2011), and this could form the start point for this further modelling.

To predict the influence of aluminosilicates and organic matter as adsorbing surfaces in this context, these should be modelled as such. This is possible in PHREEQC, and Karamalidis and Dzombak (2010) may provide some data with which to start modelling adsorption to aluminium oxides. To facilitate modelling of interaction with Si-based species, further column experiments should include Si in their solution compositions, and be included in geochemical modelling. The MINTEQ database available with PHREEQC includes a variety of organic ligands available for inclusion in aqueous speciation, and may form a start point for modelling adsorption to organic matter (a similar process to aqueous complexation). Example 19 in the PHREEQC User Guide could also be of help in modelling adsorption to organic matter. If insufficient data were already available then these values would need to be experimentally determined, though a cost-benefit analysis would be beneficial before committing to the work required to determine this data.

### 6.2.2 COLUMN EXPERIMENTS

Evidence from this study and the literature suggests that increasing the retention time of water in the column to just 1–2 minutes may be enough to capitalise on the fast initial stage of metal adsorption to the shell media. The impact of retention time on metal removal efficacy should be investigated, and any efficacy gains weighed against the reduction in operational capacity to treat the rates required in a real world context.

Two experiments that may be expected to extend the lifespan of current columns should be carried out for efficacy analysis and comparison: decanting, mixing, and repacking the column to expose more of the remaining adsorption sites, by changing the flow paths and redistributing the other adsorbing surfaces throughout the column; and regeneration of the shells using a low concentration of a weak acid, or EDTA, to remove the adsorbed metals and so freeing previously occupied adsorption sites.

The main limitation of using synthetic roof runoff, as in the current study, is that the potential role of particulates and other elements commonly present in roof runoff (eg. Fe, Al) is ignored. While sensitivity modelling can go some way to predicting their likely importance, ideally future column experiments should use real roof runoff if conducted in the laboratory, or be based on field columns servicing actual roofs, to provide more real world inputs into analysis.

Evidence for additive or competitive effects from different adsorbing surfaces was not available from this research, but has the potential to provide important guidance on whether a mixed media would

be more effective than a single media in reducing dissolved Zn and Cu concentrations. Media mixes containing particulate Fe and aluminosilicates are recommended for investigation.

That the used shells analysed in this study were obtained on an opportunistic basis was the main limitation of that data set. While for Zn shell samples were available from 3 different experimental contexts, for Cu shells were only available from one experimental context. This limited the opportunity to observe evidence for predicted mechanisms, and how they may change in different circumstances. Therefore, it is recommended that a study focused on producing Zn- and Cu-laden shells in a wider range of influent concentrations be carried out, from the low to the high end of typical roof runoff concentrations, and run until they have reached the same cumulative load, allowing inference of the impact of influent concentration on removal mechanism and lifespan. The influent and effluent compositions could be used in conjunction with shell samples to attempt a mass balance of each metal. This could be particularly helpful in differentiating between adsorbed and precipitated Cu, and the impact of the shell media in facilitating precipitation. The whole columns would need to be sacrificed for analysis to allow representative and location based sampling, and should be analysed in a similar manner to this study. This would also entail the determination of a standardised method of removing or accounting for the attached debris that comes with shells exposed to real runoff. These sets of Zn- and Cu-laden shells should include a column exposed to a mixed metal influent to investigate the influence of competition.

### 6.2.3 METHODS FOR MECHANISM DETERMINATION

Geochemical modelling predictions did require chemical evidence to support (or refute) them. The sequential extractions were particularly helpful, and so would be recommended in analysis of further shell sets. The use of one ground sample per shell media sample, from which to sub-sample for both metal content and the SEP analyses is also recommended to allow comparison between the metal content and the sum of SEP fractions. Images and elemental maps from SEM-EDS were invaluable, so should also be included in future shell analyses.

Several other authors used FTIR to support their conclusions that metals were adsorbed to the $CO_3$ group on the shell surface. In advance of committing to shell analysis by FTIR, investigation into whether this method (on its own or in combination with other methods) could differentiate between adsorbed metals and deposited metal-carbonate precipitates would be beneficial.

# REFERENCES


Abdulaziz, M., & Musayev, S. (2017). Multicomponent Biosorption of Heavy Metals from Aqueous Solutions: A Review. *Polish Journal of Environmental Studies, 26*(4), 1433-1441.

Andral, M. C., Roger, S., Montréjaud-Vignoles, M., & Herremans, L. (1999). Particle Size Distribution and Hydrodynamic Characteristics of Solid Matter Carried by Runoff from Motorways. *Water Environment Research, 71*(4), 398-407.

Antoniou, E. A., van Breukelen, B. M., & Stuyfzand, P. J. (2015). Optimizing aquifer storage and recovery performance through reactive transport modeling. *Applied Geochemistry, 61*, 29-40.

ANZG. (2019). Australian and New Zealand Guidelines for Fresh and Marine Water Quality (Online database). Australian and New Zealand Governments and Australian state and territory governments, Canberra ACT, Australia. www.waterquality.gov.au/anz-guidelines

Asahi, H. (2014). Crystalline alloys: plain carbon and low alloy steels, (pp. 22). In L. H. Hihara, R. P. I. Adler, & R. M. Latanision (Eds.), *Environmental degradation of advanced and traditional engineering materials*. Boca Raton: CRC Press, Taylor & Francis Group.

Athanasiadis, K., Helmreich, B., & Wilderer, P. A. (2004). Elimination of Zinc from Roof Runoff through Geotextile and Clinoptilolite Filters. *Acta hydrochimica et hydrobiologica, 32*(6), 419-428.

Australian and New Zealand Environment and Conservation Council, & Agriculture and Resource Management Council of Australia and New Zealand. (2000). *Australian and New Zealand Guidelines for Fresh and Marine Water Quality: Volume 1-The Guidelines*.

Bach, S., Celinski, V. R., Dietzsch, M., Panthöfer, M., Bienert, R., Emmerling, F., . . . Tremel, W. (2015). Thermally Highly Stable Amorphous Zinc Phosphate Intermediates during the Formation of Zinc Phosphate Hydrate. *Journal of the American Chemical Society, 137*(6), 2285-2294.

Bacon, J. R., & Davidson, C. M. (2008). Is there a future for sequential chemical extraction? *Analyst, 133*(1), 25-46.

Belova, D. A., Lakshtanov, L. Z., Carneiro, J. F., & Stipp, S. L. S. (2014). Nickel adsorption on chalk and calcite. *Journal of Contaminant Hydrology, 170*, 1-9.

Ben Shir, I., Kababya, S., Katz, I., Pokroy, B., & Schmidt, A. (2013). Exposed and Buried Biomineral Interfaces in the Aragonitic Shell of Perna canaliculus Revealed by Solid-State NMR. *Chemistry of Materials, 25*(22), 4595-4602.

Bilek, F. (2019). *Storminator results*. Unpublished dataset.

Bouchard, M., & Smith, D. (2001). Evaluating Raman Microscopy for the non-destructive archaeometry of of corroded coins: a powerful technique for conservation studies. *Asian Chemistry Letters, 5*(3), 157-170.

Bozbaş, S. K., & Boz, Y. (2016). Low-cost biosorbent: Anadara inaequivalvis shells for removal of Pb(II) and Cu(II) from aqueous solution. *Process Safety and Environmental Protection, 103*, 144-152.

Brown, J. N., & Peake, B. M. (2006). Sources of heavy metals and polycyclic aromatic hydrocarbons in urban stormwater runoff. *Science of the Total Environment, 359*(1), 145-155.

Carpenter, J. F., Vallet, B., Pelletier, G., Lessard, P., & Vanrolleghem, P. A. (2014). Pollutant removal efficiency of a retrofitted stormwater detention pond. *Water Quality Research Journal of Canada, 49*(2), 124-134.

Chao, T. T. (1972). Selective Dissolution of Manganese Oxides from Soils and Sediments with Acidified Hydroxylamine Hydrochloride. *Soil Science Society of America Journal, 36*(5), 764-768.

Charters, F. J., Cochrane, T. A., & O'Sullivan, A. D. (2016). Untreated runoff quality from roof and road surfaces in a low intensity rainfall climate. *Science of the Total Environment, 550*, 265-272.

Charters, F. J., Cochrane, T. A., & O'Sullivan, A. D. (2017). Characterising urban zinc generation to identify surface pollutant hotspots in a low intensity rainfall climate. *Water Science and Technology, 76*(6), 1370-1377.

Charters, F. J., Cochrane, T. A., & O'Sullivan, A. D. (2021). The influence of urban surface type and characteristics on runoff water quality. *Science of the Total Environment, 755*(142470), 9pp.

Christchurch City Council. (2012). Stormwater treatment systems. *Waterways, wetlands and drainage guide: Part B Design* (pp. 46), Retrieved from https://ccc.govt.nz/environment/water/water-policy-and-strategy/waterways-wetlands-and-drainage-guide/.

Clark, S. E., & Pitt, R. (2012). Targeting treatment technologies to address specific stormwater pollutants and numeric discharge limits. *Water Research, 46*(20), 6715-6730.

Craggs, R. J., Cooke, J., Mathieson, T., & Park, J. (2010). *Potential of mussel shell as a biosorbent for stormwater treatment* (Auckland Regional Council Technical Report 2010/046, pp.57). Report prepared by NIWA for Auckland Regional Council.

Cubillas, P., Köhler, S., Prieto, M., Chaïrat, C., & Oelkers, E. H. (2005). Experimental determination of the dissolution rates of calcite, aragonite, and bivalves. *Chemical Geology, 216*(1), 59-77.

Dahiya, S., Tripathi, R. M., & Hegde, A. G. (2008). Biosorption of lead and copper from aqueous solutions by pre-treated crab and arca shell biomass. *Bioresource Technology, 99*(1), 179-187.

Davies, P. J., Wright, I. A., Jonasson, O. J., & Findlay, S. J. (2010). Impact of concrete and PVC pipes on urban water chemistry. *Urban Water Journal, 7*(4), 233-241.

Davis, A. P., Shokouhian, M., & Ni, S. (2001). Loading estimates of lead, copper, cadmium, and zinc in urban runoff from specific sources. *Chemosphere, 44*(5), 997-1009.

Del Angel, E., Vera, R., & Corvo, F. (2015). Atmospheric Corrosion of Galvanised Steel in Different Environments in Chile and Mexico. *International journal of electrochemical science, 10*, 7985-8004.

Demirbas, A. (2008). Heavy metal adsorption onto agro-based waste materials: A review. *Journal of Hazardous Materials, 157*(2), 220-229.

Dierkes, C., Göbel, P., Lohmann, M., & Coldewey, W. G. (2006). Development and investigation of a pollution control pit for treatment of stormwater from metal roofs and traffic areas. *Water Science and Technology, 54*(6-7), 291-298.

DiLoreto, Z. A., Weber, P. A., Olds, W., Pope, J., Trumm, D., Chaganti, S. R., . . . Weisener, C. G. (2016). Novel cost effective full scale mussel shell bioreactors for metal removal and acid neutralization. *Journal of Environmental Management, 183*, 601-612.

Du, Y., Lian, F., & Zhu, L. (2011). Biosorption of divalent Pb, Cd and Zn on aragonite and calcite mollusk shells. *Environmental Pollution, 159*(7), 1763-1768.

Dzombak, D. A., & Morel, F. (1990). *Surface complexation modeling: hydrous ferric oxide*. (pp. 393), New York, NY: Wiley.

Egerić, M., Smičiklas, I., Mraković, A., Jović, M., Šljivić-Ivanović, M., Antanasijević, D., & Ristić, M. (2018). Experimental and theoretical consideration of the factors influencing cationic pollutants retention by seashell waste. *Journal of Chemical Technology & Biotechnology, 93*(5), 1477-1487.

Egodawatta, P., Ziyath, A. M., & Goonetilleke, A. (2013). Characterising metal build-up on urban road surfaces. *Environmental Pollution, 176*, 87-91.

Environment Canterbury. (2019). Canterbury Land and Water Regional Plan Volume 1 (pp. 606), Retrieved from https://www.ecan.govt.nz/your-region/plans-strategies-and-bylaws/canterbury-land-and-water-regional-plan/canterbury-land-and-water-regional-plan/.

Feng, Q. L., Li, H. B., Pu, G., Zhang, D. M., Cui, F. Z., Li, H. D., & Kim, T. N. (2000). Crystallographic alignment of calcite prisms in the oblique prismatic layer of Mytilus edulis shell. *Journal of Materials Science, 35*(13), 3337-3340.

Flemming, C. A., & Trevors, J. T. (1989). Copper toxicity and chemistry in the environment: a review. *Water, Air, and Soil Pollution, 44*(1), 143-158.

Fletcher, T. D., Andrieu, H., & Hamel, P. (2013). Understanding, management and modelling of urban hydrology and its consequences for receiving waters: A state of the art. *Advances in Water Resources, 51*, 261-279.

Frost, R. L., Hales, M. C., & Wain, D. L. (2008). Raman spectroscopy of smithsonite. *Journal of Raman Spectroscopy, 39*(1), 108-114.

Gnecco, I., Sansalone, J. J., & Lanza, L. G. (2008). Speciation of Zinc and Copper in Stormwater Pavement Runoff from Airside and Landside Aviation Land Uses. *Water, Air, and Soil Pollution, 192*(1), 321-336.

Göbel, P., Dierkes, C., & Coldewey, W. G. (2007). Storm water runoff concentration matrix for urban areas. *Journal of Contaminant Hydrology, 91*(1), 26-42.

Good, J. F., O'Sullivan, A. D., Wicke, D., & Cochrane, T. A. (2012). Contaminant removal and hydraulic conductivity of laboratory rain garden systems for stormwater treatment. *Water Science and Technology, 65*(12), 2154-2161.

Good, J. F., O'Sullivan, A. D., Wicke, D., & Cochrane, T. A. (2014). pH Buffering in Stormwater Infiltration Systems—Sustainable Contaminant Removal with Waste Mussel Shells. *Water, Air, & Soil Pollution, 225*, 11pp.

Gregoire, N. (2018). *The removal of dissolved zinc and copper from roof runoff: a downpipe treatment system.* (Unpublished thesis for Master of Water Resource Management, pp.95), The University of Canterbury, Christchurch.

Guéguen, C., & Dominik, J. (2003). Partitioning of trace metals between particulate, colloidal and truly dissolved fractions in a polluted river: the Upper Vistula River (Poland). *Applied Geochemistry, 18*(3), 457-470.

Gunawardana, C., Egodawatta, P., & Goonetilleke, A. (2014). Role of particle size and composition in metal adsorption by solids deposited on urban road surfaces. *Environmental Pollution, 184*, 44-53.

Heffernan, W., & Howe, E. (2019). *Treatment media lifespan and long-term removal effects of dissolved zinc in a downpipe treatement system.* (Unpublished research paper for BE(Hons), pp. 8), University of Canterbury.

Herngren, L., Goonetilleke, A., & Ayoko, G. A. (2006). Analysis of heavy metals in road-deposited sediments. *Analytica Chimica Acta, 571*(2), 270-278.

Ho, S.-H., Chen, Y.-d., Yang, Z.-k., Nagarajan, D., Chang, J.-S., & Ren, N.-q. (2017). High-efficiency removal of lead from wastewater by biochar derived from anaerobic digestion sludge. *Bioresource Technology, 246*, 142-149.

Hossain, A., & Aditya, G. (2015). Biosorption of cadmium from aqueous solution by shell dust of the fresh water snail Melanoides tuberculata. *Bioremediation Journal, 19*(1), 80-91.

Howe, P. D., Malcolm, H. M., & Dobson, S. (2004). *Manganese and its compounds : environmental aspects.* M. Sheffer (Ed.) Retrieved from http://www.inchem.org/documents/cicads/cicads/cicad63.htm#5.3

Jacob, D. E., Soldati, A. L., Wirth, R., Huth, J., Wehrmeister, U., & Hofmeister, W. (2008). Nanostructure, composition and mechanisms of bivalve shell growth. *Geochimica et Cosmochimica Acta, 72*(22), 5401-5415.

Jalali, M., & Latifi, Z. (2018). Measuring and simulating effect of organic residues on the transport of cadmium, nickel, and zinc in a calcareous soil. *Journal of Geochemical Exploration, 184*, 372-380.

Kajimura, H. (2014). Crystalline alloys: stainless steels, (pp. 7). In L. H. Hihara, R. P. I. Adler, & R. M. Latanision (Eds.), *Environmental degradation of advanced and traditional engineering materials*. Boca Raton: CRC Press, Taylor & Francis Group.

Kammerer, J., Carle, R., & Kammerer, D. R. (2011). Adsorption and Ion Exchange: Basic Principles and Their Application in Food Processing. *Journal of Agricultural and Food Chemistry, 59*(1), 22-42.

Karamalidis, A., K, & Dzombak, D. (2010). *Surface Complexation Modeling: Gibbsite*. (pp. 293), Hoboken, NJ: John Wiley & Sons.

Kim, D. S. (2003). The removal by crab shell of mixed heavy metal ions in aqueous solution. *Bioresource Technology, 87*(3), 355-357.

Köhler, S. J., Cubillas, P., Rodríguez-Blanco, J. D., Bauer, C., & Prieto, M. (2007). Removal of Cadmium from Wastewaters by Aragonite Shells and the Influence of Other Divalent Cations. *Environmental Science & Technology, 41*(1), 112-118.

Leleyter, L., & Probst, J.-L. (1999). A New Sequential Extraction Procedure for the Speciation of Particulate Trace Elements in River Sediments. *International Journal of Environmental Analytical Chemistry, 73*(2), 109-128.

Levi-Kalisman, Y., Falini, G., Addadi, L., & Weiner, S. (2001). Structure of the Nacreous Organic Matrix of a Bivalve Mollusk Shell Examined in the Hydrated State Using Cryo-TEM. *Journal of Structural Biology, 135*(1), 8-17.

Leygraf, C., Wallinder, I. O., Tidblad, J., & Graedel, T. (2016). *Atmospheric Corrosion: Second Edition*. (pp. 400), Hoboken, NJ: John Wiley & Sons.

Liu, A., Goonetilleke, A., & Egodawatta, P. (2015a). Stormwater Treatment Design. In *Role of Rainfall and Catchment Characteristics on Urban Stormwater Quality* (pp. 15-30). Singapore: Springer Singapore.

Liu, A., Goonetilleke, A., & Egodawatta, P. (2015b). Urbanisation and Stormwater Quality. In *Role of Rainfall and Catchment Characteristics on Urban Stormwater Quality* (pp. 1-14). Singapore: Springer Singapore.

Liu, C.-C., Wang, M.-K., Chiou, C.-S., Li, Y.-S., Yang, C.-Y., & Lin, Y.-A. (2009). Biosorption of chromium, copper and zinc by wine-processing waste sludge: Single and multi-component system study. *Journal of Hazardous Materials, 171*(1), 386-392.

Londono-Zuluaga, C., Jameel, H., Gonzalez, R. W., & Lucia, L. (2019). Crustacean shell-based biosorption water remediation platforms: Status and perspectives. *Journal of Environmental Management, 231*, 757-762.

Magu, M. M., Govender, P. P., & Ngila, J. C. (2016). Geochemical modelling and speciation studies of metal pollutants present in selected water systems in South Africa. *Physics and Chemistry of the Earth, 92*, 44-51.

Makepeace, D., Smith, D., & Stanley, S. (1995). Urban stormwater quality: Summary of contaminant data. *Critical Reviews in Environmental Science and Technology, 25*(2), 93-139.

Mancinelli, E., Baltrėnaitė, E., Baltrėnas, P., Paliulis, D., Passerini, G., & Almås, Å. R. (2015). Trace metal concentration and speciation in storm water runoff on impervious surfaces. *Journal of Environmental Engineering and Landscape Management, 23*(1), 15-27.

Martínez-García, C., González-Fonteboa, B., Martínez-Abella, F., & Carro- López, D. (2017). Performance of mussel shell as aggregate in plain concrete. *Construction and Building Materials, 139*, 570-583.

McCauley, C. A., O'Sullivan, A. D., Milke, M. W., Weber, P. A., & Trumm, D. A. (2009). Sulfate and metal removal in bioreactors treating acid mine drainage dominated with iron and aluminum. *Water Research, 43*(4), 961-970.

McIntyre, J. K., Winters, N., Rozmyn, L., Haskins, T., & Stark, J. D. (2019). Metals leaching from common residential and commercial roofing materials across four years of weathering and implications for environmental loading. *Environmental Pollution, 255*, 8pp.

McLaren, S. J. (2011a). Aragonite. In D. Hopley (Ed.), *Encyclopedia of Modern Coral Reefs: Structure, Form and Process* (pp. 47-47). Dordrecht: Springer Netherlands.

McLaren, S. J. (2011b). Calcite. In D. Hopley (Ed.), *Encyclopedia of Modern Coral Reefs: Structure, Form and Process* (pp. 179-179). Dordrecht: Springer Netherlands.

Ministry for the Environment. (2004). Module 2 – Hazardous waste guidelines: Landfill waste acceptance criteria and landfill classification (pp. 37), Retrieved from https://www.mfe.govt.nz/publications/waste/module-2-%E2%80%93-hazardous-waste-guidelines-landfill-waste-acceptance-criteria-and-3.

Mouanga, M., Berçot, P., & Rauch, J. Y. (2010). Comparison of corrosion behaviour of zinc in NaCl and in NaOH solutions. Part I: Corrosion layer characterization. *Corrosion Science, 52*(12), 3984-3992.

Müller, B., & Sigg, L. (1990). Interaction of trace metals with natural particle surfaces: Comparison between adsorption experiments and field measurements. *Aquatic Sciences, 52*(1), 75-92.

National Policy Statement for Freshwater Management. (2020). Retrieved from https://www.mfe.govt.nz/publications/fresh-water/national-policy-statement-freshwater-management-2020.

NIWA. (2019). CliFlo: The national climate database. Retrieved 26 June 2019 from https://cliflo.niwa.co.nz/

Papadimitriou, C. A., Krey, G., Stamatis, N., & Kallianiotis, A. (2017). The use of waste mussel shells for the adsorption of dyes and heavy metals. *Journal of Chemical Technology & Biotechnology, 92*(8), 1943-1947.

Parkhurst, D., & Appelo, C. (2017). PHREEQC (Version Version 3.4.0.12927). Colorado, USA: US Geological Survey (USGS).

Pennington, S. L. (2004). *Roof runoff. A potential source of trace metals to the urban stormwater system.* (Unpublished thesis for Master of Science, pp. 123), The University of Auckland, Auckland.

Pennington, S. L., & Webster-Brown, J. G. (2008). Stormwater runoff quality from copper roofing, Auckland, New Zealand. *New Zealand Journal of Marine and Freshwater Research, 42*(1), 99-108.

Plassard, F., Winiarski, T., & Petit-Ramel, M. (2000). Retention and distribution of three heavy metals in a carbonated soil: comparison between batch and unsaturated column studies. *Journal of Contaminant Hydrology, 42*(2), 99-111.

Qomariyah, L., Widiyastuti, W., Winardi, S., Kusdianto, K., & Ogi, T. (2019). Volume Fraction Dependent Morphological Transition of Silica Particles Derived from Sodium Silicate. *International Journal of Technology, 10*(3), 603-612.

Raeside, J. D. (1964). Loess deposits of the South Island, New Zealand, and soils formed on them. *New Zealand Journal of Geology and Geophysics, 7*(4), 811-838.

Reddy, K. R., Dastgheibi, S., & Cameselle, C. (2021). Mixed versus layered multi-media filter for simultaneous removal of nutrients and heavy metals from urban stormwater runoff. *Environmental Science and Pollution Research, 28*(6), 7574-7585.

Reddy, K. R., Xie, T., & Dastgheibi, S. (2014). Adsorption of mixtures of nutrients and heavy metals in simulated urban stormwater by different filter materials. *Journal of Environmental Science and Health, Part A, 49*(5), 524-539.

Reed, B. E., Arunachalam, S., & Thomas, B. (1994). Removal of lead and cadmium from aqueous waste streams using granular activated carbon (GAC) columns. *Environmental Progress, 13*(1), 60-64.

Richards, S., Dawson, J., & Stutter, M. (2019). The potential use of natural vs commercial biosorbent material to remediate stream waters by removing heavy metal contaminants. *Journal of Environmental Management, 231*, 275-281.

Robalds, A., Naja, G. M., & Klavins, M. (2016). Highlighting inconsistencies regarding metal biosorption. *Journal of Hazardous Materials, 304*, 553-556.

Roberts, G. (1992). *Chitin chemistry*. (pp. 350), London, England: The Macmillan Press.

Sansalone, J., & Buchberger, S. (1997). Partitioning and First Flush of Metals in Urban Roadway Storm Water. *Journal of Environmental Engineering, 123*(2), 134-143.

Schmutzler, B., Eggert, G., & Kuhn-Wawrzinek, C. F. (2017). Copper(II) hydroxide on artefacts: Corrosion, conservation, colourants. *Studies in conservation, 62*(2), 61-67.

Shim, J.-W., Park, S.-J., & Ryu, S.-K. (2001). Effect of modification with HNO3 and NaOH on metal adsorption by pitch-based activated carbon fibers. *Carbon, 39*(11), 1635-1642.

Shin, W.-S., Kang, K., & Kim, Y.-K. (2014). Adsorption Characteristics of Multi-Metal Ions by Red Mud, Zeolite, Limestone, and Oyster Shell. *Environmental Engineering Research, 19*(1), 15-22.

Simon, T. (Ed.) (2002). *Biological Response Signatures: Indicator Patterns Using Aquatic Communities*. (pp 600), Boca Raton: CRC Press.

Sparks, D. L. (2003). 2 - Inorganic Soil Components. In D. L. Sparks (Ed.), *Environmental Soil Chemistry (Second Edition)* (pp. 43-73). Burlington: Academic Press.

Stumm, & Morgan, J. J. (1995). Aquatic Chemistry: Chemical Equilibria and Rates in Natural Waters. (pp. 1042), Somerset, NJ: John Wiley & Sons.

Uster, B. (2015). *The use of waste mussel shell in sulfate-reducing bioreactors treating mine-influenced waters.* (Unpublished thesis for Doctor of Philosophy, pp. 300), University of Canterbury, Christchurch.

Uster, B., O'Sullivan, A. D., Ko, S. Y., Evans, A., Pope, J., Trumm, D., & Caruso, B. (2015). The Use of Mussel Shells in Upward-Flow Sulfate-Reducing Bioreactors Treating Acid Mine Drainage. *Mine Water and the Environment, 34*(4), 442-454.

Vijayaraghavan, K., Joshi, U. M., & Balasubramanian, R. (2010). Removal of Metal Ions from Storm-Water Runoff by Low-Cost Sorbents: Batch and Column Studies. *Journal of Environmental Engineering, 136*(10), 1113-1118.

Vink, B. W. (1986). Stability relations of malachite and azurite. *Mineralogical magazine, 50*(1), 41-47.

Volesky, B. (2001). Detoxification of metal-bearing effluents: biosorption for the next century. *Hydrometallurgy, 59*(2), 203-216.

Weiss, J., Hondzo, M., Biesboer, D., & Semmens, M. (2006). Laboratory study of heavy metal phytoremediation by three wetland macrophytes. *Internation Journal of Phytoremediation, 8*(3), 245-259.

Wicke, D., Cochrane, T. A., & O'Sullivan, A. (2012). Build-up dynamics of heavy metals deposited on impermeable urban surfaces. *Journal of Environmental Management, 113*, 347-354.

Wicke, D., Cochrane, T. A., O'Sullivan, A. D., Cave, S., & Derksen, M. (2014). Effect of age and rainfall pH on contaminant yields from metal roofs. *Water Science and Technology, 69*(10), 2166-2173.

Williamson, R. B. (1985). Urban stormwater quality I. Hillcrest, Hamilton, New Zealand. *New Zealand Journal of Marine and Freshwater Research, 19*(3), 413-427.

Wu, P., & Zhou, Y. s. (2009). Simultaneous removal of coexistent heavy metals from simulated urban stormwater using four sorbents: A porous iron sorbent and its mixtures with zeolite and crystal gravel. *Journal of Hazardous Materials, 168*(2-3), 674-680.

Wu, Q., Chen, J., Clark, M., & Yu, Y. (2014). Adsorption of copper to different biogenic oyster shell structures. *Applied Surface Science, 311*, 264-272.

Xu, X., Liu, X., Oh, M., & Park, J. (2019). Oyster shell as a low-cost adsorbent for removing heavy metal ions from wastewater. *Polish Journal of Environmental Studies, 28*(4), 2949-2959.

Zhao, H., & Waite, J. H. (2005). Coating proteins: structure and cross-linking in fp-1 from the green shell mussel Perna canaliculus. *Biochemistry, 44*(48), 15915-15923.

Zhou, X., Liu, W., Zhang, J., Wu, C., Ou, X., Tian, C., . . . Dang, Z. (2017). Biogenic Calcium Carbonate with Hierarchical Organic-Inorganic Composite Structure Enhancing the Removal of Pb(II) from Wastewater. *ACS Applied Materials and Interfaces, 9*(41), 35785-35793.

# APPENDIX 1: FULL CHEMICAL SOLUTION DATASETS

**Table A1-1:** Physico-chemical, major ion, and trace metal results for the baseline column flow-through experiment. All values are the mean of the results across the three experimental columns (n=3). Dissolved ion concentrations are in normal text, acid soluble concentrations, where measured, are below the dissolved concentrations and in *italics*.

| Sample | pH | Specific conductance (µS/cm) | Dissolved oxygen (mg/L) | Temperature (°C) | Turbidity (NTU) | mg/L | | | | | | | | | | µg/L | | | | | | | | |
|---|---|---|---|---|---|---|---|---|---|---|---|---|---|---|---|---|---|---|---|---|---|---|---|---|
| | | | | | | Na | Ca | K | Mg | Cl | $SO_4$ | $NO_3$ | $NH_4$ | $PO_4$ | $HCO_3$ | Fe | Mn | Al | Zn | Cu | Pb | Cr | Ni | Cd |
| **Influent (tap water)** | 7.1 | 115.6 | 8.6 | 20.2 | 0.15 | 8.2 | 10.8 | 0.8 | 2.4 | 4.4 | 3.5 | 2.4 | 0.02 | 0.034 | 51 | 4.0 | 2.3 | 3.0 | 117 | 4.6 | <1 | <1 | <1 | <1 |
| | | | | | | *8.8* | *12.9* | *0.9* | *2.6* | | | | | | | *33.6* | *2.7* | *40.3* | *105* | *5.7* | *2.4* | *<1* | *<1* | *<1* |
| **First flush effluent (0min)** | 7.1 | 1128 | 8.2 | 20.7 | 300 | 47.2 | 149 | 3.7 | 11.5 | 10.1 | 41.7 | 441 | 0.08 | 0.40 | 134 | 5.8 | 3.0 | 8.7 | 11.2 | 3.0 | <1 | <1 | <1 | <1 |
| | | | | | | *56.5* | *262* | *4.6* | *13.9* | | | | | | | *1150* | *49.4* | *1960* | *36.5* | *5.9* | *3.5* | *1.7* | *1.2* | *<1* |
| **Effluent 5min** | 7.4 | 142.5 | 8.7 | 20.4 | 0.41 | 9.4 | 16.6 | 0.9 | 2.4 | 4.4 | 4.3 | 8.6 | 0.02 | 0.15 | 56 | 6.0 | <1 | 7.5 | <10 | 1.2 | <1 | <1 | <1 | <1 |
| | | | | | | *10.8* | *21.2* | *1.1* | *2.8* | | | | | | | *47.3* | *1.6* | *71.5* | <10 | *2.0* | *1.7* | *<1* | *<1* | *<1* |
| **Effluent 15min** | 7.4 | 131.1 | 8.7 | 20.3 | 0.22 | 8.7 | 14.3 | 0.9 | 2.4 | 4.4 | 3.9 | 4.8 | 0.02 | 0.10 | 55 | 6.7 | <1 | 7.9 | <10 | 1.0 | <1 | <1 | <1 | <1 |
| | | | | | | *10.5* | *19.1* | *1.0* | *2.9* | | | | | | | *38.5* | *1.5* | *56.5* | *11.5* | *1.9* | *1.6* | *<1* | *<1* | *<1* |
| **Effluent 30min** | 7.5 | 127.6 | 8.7 | 20.3 | 0.22 | 8.0 | 13.2 | 0.8 | 2.3 | 4.4 | 3.8 | 2.7 | 0.02 | 0.076 | 55 | 3.4 | <1 | 5.8 | 12.0 | <1 | <1 | <1 | <1 | <1 |
| | | | | | | *10.0* | *18.0* | *1.0* | *2.9* | | | | | | | *37.5* | *1.6* | *52.3* | *15.2* | *1.9* | *1.5* | *<1* | *<1* | *<1* |
| **Effluent 45min** | 7.6 | 126.6 | 8.7 | 20.5 | 0.26 | 8.1 | 13.1 | 0.8 | 2.3 | 4.4 | 3.8 | 2.1 | 0.02 | 0.070 | 55 | 2.8 | 1.1 | 5.0 | 14.3 | <1 | <1 | <1 | <1 | <1 |
| | | | | | | *9.6* | *17.0* | *0.9* | *2.7* | | | | | | | *32.9* | *1.7* | *49.4* | *18.4* | *1.8* | *1.9* | *<1* | *<1* | *<1* |

**Table A1-2:** Physico-chemical, major ion, and trace metal results for experiment 1 (influent Zn ≈0.1 mg/L). Dissolved ion concentrations are in normal text, acid soluble concentrations, where measured, are below the dissolved concentrations and in *italics*. " - " not measured, " * " calculated (see text body for explanation).

| Sample | pH | Specific conductance (µS/cm) | Dissolved oxygen (mg/L) | Temperature (°C) | mg/L | | | | | | | µg/L | | | | | | | | |
|---|---|---|---|---|---|---|---|---|---|---|---|---|---|---|---|---|---|---|---|---|
| | | | | | Na | Ca | K | Mg | Cl | $NO_3$ | $PO_4$ | Fe | Mn | Al | Zn | Cu | Pb | Cr | Ni | Cd |
| **Influent (≈0.3 mg/L Zn)** | 6.9 | 116.2 | 8.5 | 23.2 | 7.2 | 11.3 | 0.8 | 2.0 | 4.7* | 0.9 | 0.58 | 5.0 | <1 | 5.7 | 295 | 5.2 | <1 | <1 | 3.6 | <1 |
| | | | | | *7.4* | *11.8* | *0.9* | *2.2* | | | | *37.8* | *<1* | *96.3* | *295* | *5.7* | *<1* | *<1* | *3.9* | *<1* |
| **First flush effluent (0min)** | 7.0 | 1414 | 8.2 | 23.5 | 49.8 | 200 | 2.7 | 11.0 | - | 769 | 0.188 | 2.2 | 1.4 | 3.5 | <10 | 2.6 | <1 | <1 | <1 | <1 |
| | | | | | *51.9* | *244* | *3.1* | *11.4* | | | | *578* | *38.0* | *1060* | *21.0* | *3.8* | *1.3* | *1.2* | *<1* | *1.3* |
| **Effluent 3min** | 7.5 | 212.3 | 8.4 | 22.8 | 7.5 | 28.4 | 0.7 | 1.7 | - | 48.3 | 0.162 | 4.1 | <1 | 2.9 | <10 | 1.8 | <1 | <1 | <1 | <1 |
| | | | | | *7.8* | *32.1* | *0.9* | *1.8* | | | | *33.7* | *1.4* | *99.1* | *11.0* | *2.6* | *<1* | *<1* | *<1* | *<1* |
| **Effluent 6min** | 7.6 | 173.3 | 8.4 | 22.6 | 6.7 | 22.8 | 0.7 | 1.6 | - | 29.1 | 0.135 | 4.3 | <1 | 3.0 | 14.4 | 1.7 | <1 | <1 | <1 | <1 |
| | | | | | *7.5* | *26.4* | *0.9* | *1.8* | | | | *30.0* | *1.1* | *96.4* | *16.8* | *2.7* | *<1* | *1.4* | *<1* | *<1* |
| **Effluent 9min** | 7.8 | 161.4 | 8.4 | 22.7 | 6.5 | 20.6 | 0.7 | 1.7 | - | 23.0 | 0.123 | 6.5 | <1 | 3.6 | 21.9 | 1.7 | <1 | <1 | <1 | <1 |
| | | | | | *6.9* | *22.8* | *0.8* | *1.7* | | | | *22.2* | *<1* | *86.7* | *20.5* | *2.4* | *<1* | *<1* | *<1* | *<1* |

**Table A1-3:** Physico-chemical, major ion, and trace metal results for experiment 2 (influent Zn ≈1 mg/L). Dissolved ion concentrations are in normal text, acid soluble concentrations, where measured, are below the dissolved concentrations and in *italics*. " - " not measured, " * " calculated (see text body for explanation).

| Sample | pH | Specific conductance (µS/cm) | Dissolved oxygen (mg/L) | Temperature (°C) | mg/L | | | | | | | µg/L | | | | | | | | |
|---|---|---|---|---|---|---|---|---|---|---|---|---|---|---|---|---|---|---|---|---|
| | | | | | Na | Ca | K | Mg | Cl | $NO_3$ | $PO_4$ | Fe | Mn | Al | Zn | Cu | Pb | Cr | Ni | Cd |
| Influent (≈1 mg/L Zn) | 6.7 | 112.6 | 8.4 | 22.5 | 6.9 | 11.2 | 0.8 | 2.0 | 5.4* | 1.0 | 0.042 | 2.5 | 1.1 | 10.0 | 936 | 3.6 | <1 | <1 | <1 | <1 |
| | | | | | *7.4* | *13.2* | *1.0* | *2.1* | | | | *23.6* | *1.4* | *121* | *936* | *5.3* | *<1* | *<1* | *<1* | *<1* |
| First flush effluent (0min) | 6.8 | 1887 | 7.9 | 23.1 | 59.0 | 262 | 2.8 | 13.0 | - | 1030 | 0.196 | 3.0 | 1.8 | 10.8 | 19.1 | 4.2 | <1 | <1 | <1 | <1 |
| | | | | | *59.0* | *318* | *3.4* | *13.2* | | | | *601* | *38.1* | *964* | *39.2* | *6.5* | *1.3* | *1.2* | *1.3* | *1.3* |
| Effluent 3min | 7.4 | 173.8 | 8.3 | 22.3 | 6.1 | 22.9 | 0.7 | 1.4 | - | 27.0 | 0.149 | 2.6 | <1 | 7.5 | 38.4 | 1.4 | <1 | <1 | <1 | <1 |
| | | | | | *7.1* | *27.2* | *0.8* | *1.6* | | | | *30.6* | *1.1* | *106* | *34.1* | *2.6* | *<1* | *<1* | *<1* | *<1* |
| Effluent 6min | 7.6 | 146.3 | 8.2 | 22.5 | 6.1 | 19.4 | 0.7 | 1.5 | - | 12.5 | 0.108 | 2.8 | <1 | 7.8 | 52.2 | 1.2 | <1 | <1 | <1 | <1 |
| | | | | | *7.0* | *23.3* | *0.9* | *1.7* | | | | *33.3* | *1.1* | *109* | *58.3* | *2.5* | *<1* | *1.0* | *<1* | *<1* |
| Effluent 9min | 7.7 | 139.9 | 8.3 | 22.5 | 5.8 | 17.5 | 0.7 | 1.5 | - | 11.3 | 0.093 | 4.2 | <1 | 12.3 | 73.1 | 1.4 | <1 | <1 | <1 | <1 |
| | | | | | *6.8* | *20.3* | *0.9* | *1.7* | | | | *26.5* | *1.0* | *109* | *79.5* | *2.6* | *<1* | *<1* | *<1* | *<1* |

**Table A1-4:** Physico-chemical, major ion, and trace metal results for experiment 3 (influent Zn ≈3 mg/L). Dissolved ion concentrations are in normal text, acid soluble concentrations, where measured, are below the dissolved concentrations and in *italics*. " - " not measured, " * " calculated (see text body for explanation)," ~ " suspect result not reported.

| Sample | pH | Specific conductance (µS/cm) | Dissolved oxygen (mg/L) | Temperature (°C) | mg/L | | | | | | | µg/L | | | | | | | | |
|---|---|---|---|---|---|---|---|---|---|---|---|---|---|---|---|---|---|---|---|---|
| | | | | | Na | Ca | K | Mg | Cl | $NO_3$ | $PO_4$ | Fe | Mn | Al | Zn | Cu | Pb | Cr | Ni | Cd |
| **Influent (≈3 mg/L Zn)** | 6.7 | 117.9 | 8.2 | 22.5 | 7.0 | 10.9 | 0.7 | 1.9 | 7.6* | 1.0 | 0.028 | 2.0 | <1 | 7.5 | 2740 | 4.2 | <1 | <1 | <1 | <1 |
| | | | | | *7.2* | *12.8* | *1.0* | *2.0* | | | | *17.3* | *<1* | *105* | *2740* | *5.5* | *<1* | *<1* | *<1* | *<1* |
| **First flush effluent (0min)** | 7.0 | 622.4 | 7.9 | 23.2 | 14.2 | 89.9 | 1.1 | 4.2 | - | 237 | 0.164 | 1.4 | <1 | 7.1 | 63.6 | 2.0 | <1 | <1 | <1 | <1 |
| | | | | | *14.7* | *120* | *1.4* | *4.5* | | | | *457* | *25.4* | *590* | *85.8* | *3.4* | *1.0* | *1.0* | *<1* | *<1* |
| **Effluent 3min** | 7.5 | 152.1 | 8.2 | 22.5 | 5.5 | 20.3 | 0.6 | 1.3 | - | 12.6 | 0.104 | 6.9 | <1 | 8.1 | 121 | 1.2 | <1 | <1 | <1 | <1 |
| | | | | | *6.5* | *24.1* | *0.8* | *1.6* | | | | *25.0* | *1.0* | *104* | *125* | *1.7* | *<1* | *<1* | *<1* | *<1* |
| **Effluent 6min** | 7.6 | 139.0 | 8.2 | 22.4 | 5.7 | 18.2 | 0.7 | 1.5 | - | 5.5 | 0.070 | 1.8 | <1 | 5.9 | 218 | <1 | <1 | <1 | <1 | <1 |
| | | | | | *6.5* | *21.4* | *0.9* | *1.6* | | | | *17.9* | *<1* | *106* | *223* | *1.6* | *<1* | *<1* | *<1* | *<1* |
| **Effluent 9min** | 7.6 | 135.4 | 8.2 | 22.5 | 5.9 | 17.0 | 0.8 | 1.5 | - | 5.9 | 0.055 | 2.0 | <1 | 7.1 | 315 | <1 | <1 | <1 | <1 | <1 |
| | | | | | *6.9* | *23.5* | *1.0* | *1.8* | | | | *84.3* | *1.5* | *~* | *309* | *2.3* | *1.9* | *2.0* | *<1* | *<1* |

**Table A1-5:** Physico-chemical, major ion, and trace metal results for experiment 4 (influent ≈0.5 mg/L Cu). Dissolved ion concentrations are in normal text, acid soluble concentrations, where measured, are below the dissolved concentrations and in *italics*. " - " not measured.

| Sample | pH | Specific conductance (µS/cm) | Dissolved oxygen (mg/L) | Temperature (°C) | mg/L | | | | | | | | µg/L | | | | | | | | |
|---|---|---|---|---|---|---|---|---|---|---|---|---|---|---|---|---|---|---|---|---|---|
| | | | | | Na | Ca | K | Mg | Cl | $SO_4$ | $NO_3$ | $PO_4$ | Fe | Mn | Al | Zn | Cu | Pb | Cr | Ni | Cd |
| **Influent (≈ 0.5 mg/L Cu)** | 6.7 | 116.0 | 8.9 | 20.5 | 7.2 | 12.9 | 0.8 | 2.1 | 4.9 | 3.9 | 1.2 | 0.059 | 3.7 | <1 | 11.5 | 86.9 | 488 | <1 | <1 | <1 | <1 |
| | | | | | *7.3* | *14.4* | *0.8* | *2.3* | | | | | *24.9* | *<1* | *108* | *85.1* | *531* | *<1* | *1.7* | *<1* | *<1* |
| **First flush effluent (0min)** | 7.0 | 1300 | 8.8 | 21.1 | 46.5 | 182 | 3.2 | 8.7 | - | - | 667 | 0.213 | 4.0 | 3.9 | 15.1 | <10 | 105 | <1 | <1 | <1 | <1 |
| | | | | | *46.5* | *207* | *3.4* | *9.4* | | | | | *196* | *15.5* | *364* | *15.2* | *114* | *<1* | *2.1* | *<1* | *<1* |
| **Effluent 3min** | 7.5 | 209.8 | 8.9 | 20.9 | 9.8 | 29.1 | 0.9 | 2.4 | 5.0 | 5.0 | 56.6 | 0.142 | 4.5 | <1 | 14.0 | 10.1 | 185 | <1 | <1 | <1 | <1 |
| | | | | | *9.9* | *31.3* | *1.0* | *2.7* | | | | | *29.1* | *1.2* | *119* | *11.7* | *191* | *<1* | *1.8* | *<1* | *<1* |
| **Effluent 6min** | 7.7 | 194.9 | 8.7 | 20.8 | 9.6 | 26.4 | 0.9 | 2.4 | - | - | 38.0 | 0.125 | 4.4 | <1 | 12.1 | 12.9 | 212 | <1 | <1 | <1 | <1 |
| | | | | | *9.1* | *26.5* | *0.9* | *2.6* | | | | | *27.1* | *<1* | *114* | *13.9* | *205* | *<1* | *1.8* | *<1* | *<1* |
| **Effluent 9min** | 7.8 | 182.7 | 8.9 | 20.7 | 8.6 | 22.5 | 0.8 | 2.3 | - | - | 29.0 | 0.111 | 3.9 | <1 | 12.3 | 15.0 | 201 | <1 | <1 | <1 | <1 |
| | | | | | *8.6* | *24.7* | *0.9* | *2.5* | | | | | *31.2* | *<1* | *131* | *15.0* | *216* | *<1* | *3.2* | *<1* | *<1* |

**Table A1-6:** Physico-chemical, major ion, and trace metal results for experiment 5 (influent ≈5 mg/L Cu). Dissolved ion concentrations are in normal text, acid soluble concentrations, where measured, are below the dissolved concentrations and in *italics.* " - " not measured.

| Sample | pH | Specific conductance (µS/cm) | Dissolved oxygen (mg/L) | Temperature (°C) | mg/L | | | | | | | | µg/L | | | | | | | | |
|---|---|---|---|---|---|---|---|---|---|---|---|---|---|---|---|---|---|---|---|---|---|
| | | | | | Na | Ca | K | Mg | Cl | $SO_4$ | $NO_3$ | $PO_4$ | Fe | Mn | Al | Zn | Cu | Pb | Cr | Ni | Cd |
| **Influent (≈ 5 mg/L Cu)** | 6.3 | 123.0 | 8.9 | 20.2 | 7.1 | 12.9 | 0.8 | 2.3 | 9.5 | 3.9 | 1.2 | 0.023 | 1.1 | <1 | 5.8 | 31.1 | 1990 | <1 | <1 | <1 | <1 |
| | | | | | *7.2* | *13.9* | *0.9* | *2.2* | | | | | *27.8* | *<1* | *110* | *32.1* | *4690* | *<1* | *1.8* | *<1* | *<1* |
| **First flush effluent (0min)** | 6.7 | 2163 | 8.7 | 20.2 | 69.1 | 303 | 3.2 | 11.9 | - | - | 1120 | 0.178 | 3.4 | 6.4 | 5.7 | <10 | 698 | <1 | <1 | <1 | <1 |
| | | | | | *72.1* | *331* | *3.4* | *12.9* | | | | | *262* | *24.6* | *459* | *19.0* | *1210* | *<1* | *1.9* | *<1* | *<1* |
| **Effluent 3min** | 7.4 | 204.6 | 8.8 | 20.0 | 8.7 | 26.6 | 0.8 | 2.1 | 9.5 | 5.0 | 38.3 | 0.109 | 2.5 | <1 | 5.0 | <10 | 462 | <1 | <1 | <1 | <1 |
| | | | | | *8.9* | *28.6* | *0.9* | *2.4* | | | | | *22.8* | *1.3* | *104* | <10 | *1360* | *<1* | *1.7* | *<1* | *<1* |
| **Effluent 6min** | 7.6 | 178.2 | 8.8 | 19.9 | 7.9 | 22.4 | 0.8 | 2.1 | - | - | 23.9 | 0.092 | 1.5 | <1 | 5.2 | <10 | 422 | <1 | <1 | <1 | <1 |
| | | | | | *8.0* | *23.6* | *0.9* | *2.3* | | | | | *28.4* | *1.1* | *116* | <10 | *1100* | *<1* | *1.5* | *<1* | *<1* |
| **Effluent 9min** | 7.6 | 167.7 | 8.8 | 20.0 | 7.8 | 21.1 | 0.8 | 2.1 | - | - | 17.7 | 0.075 | 1.8 | <1 | 4.5 | <10 | 403 | <1 | <1 | <1 | <1 |
| | | | | | *7.8* | *22.1* | *0.9* | *2.2* | | | | | *19.4* | *<1* | *116* | *10.0* | *989* | *<1* | *1.6* | *<1* | *<1* |

**Table A1-7:** Physico-chemical, major ion, and trace metal results for experiment 6 (influent ≈10 mg/L Cu). Dissolved ion concentrations are in normal text, acid soluble concentrations, where measured, are below the dissolved concentrations and in *italics*. " - " not measured.

| Sample | pH | Specific conductance (µS/cm) | Dissolved oxygen (mg/L) | Temperature (°C) | mg/L | | | | | | | | µg/L | | | | | | | | |
|---|---|---|---|---|---|---|---|---|---|---|---|---|---|---|---|---|---|---|---|---|---|
| | | | | | Na | Ca | K | Mg | Cl | $SO_4$ | $NO_3$ | $PO_4$ | Fe | Mn | Al | Zn | Cu | Pb | Cr | Ni | Cd |
| **Influent (≈ 10 mg/L Cu)** | 6.3 | 129.3 | 9.1 | 19.9 | 7.0 | 12.9 | 0.8 | 2.2 | 15.3 | 3.8 | 1.2 | 0.021 | 1.9 | <1 | 10.1 | 102 | 2900 | <1 | <1 | <1 | <1 |
| | | | | | *7.3* | *13.6* | *0.9* | *2.2* | | | | | *49.5* | *<1* | *134* | *104* | *9090* | *1* | *1.7* | *<1* | *<1* |
| **First flush effluent (0min)** | 6.7 | 1707 | 8.8 | 19.6 | 48.2 | 241 | 2.6 | 9.9 | - | - | 855 | 0.159 | 2.5 | 8.0 | 11.5 | 13.5 | 1380 | <1 | <1 | <1 | <1 |
| | | | | | *50.8* | *277* | *2.9* | *10.9* | | | | | *234* | *25.4* | *428* | *20.8* | *3270* | *<1* | *1.9* | *<1* | *<1* |
| **Effluent 3min** | 7.2 | 186.1 | 8.9 | 19.6 | 8.1 | 22.6 | 0.8 | 2.1 | 15.1 | 4.9 | 24.0 | 0.086 | 2.1 | <1 | 10.0 | 15.4 | 774 | <1 | <1 | <1 | <1 |
| | | | | | *7.9* | *24.5* | *0.9* | *2.2* | | | | | *22.2* | *1.3* | *174* | *17.3* | *3910* | *<1* | *1.3* | *<1* | *<1* |
| **Effluent 6min** | 7.4 | 166.7 | 9.0 | 19.5 | 7.9 | 20.3 | 0.8 | 2.1 | - | - | 12.3 | 0.061 | 1.5 | <1 | 7.8 | 21.9 | 728 | <1 | <1 | <1 | <1 |
| | | | | | *7.6* | *22.5* | *0.9* | *2.3* | | | | | *28.1* | *1.2* | *302* | *24.1* | *3800* | *<1* | *1.7* | *<1* | *<1* |
| **Effluent 9min** | 7.4 | 160.6 | 8.9 | 19.7 | 7.5 | 19.1 | 0.8 | 2.1 | 15.1 | 4.4 | 10.0 | 0.050 | 1.6 | <1 | 15.4 | 27.0 | 823 | <1 | <1 | <1 | <1 |
| | | | | | *7.7* | *23.7* | *0.9* | *2.2* | | | | | *43.9* | *1.3* | *918* | *28.4* | *3820* | *1.6* | *1.9* | *1.8* | *<1* |

**Table A1-8:** Physico-chemical, major ion, and trace metal results for two real roof runoff samples. Dissolved ion concentrations are in normal text, acid soluble concentrations, where measured, are below the dissolved concentrations and in *italics*. " - " not measured.

| Sample | pH | Dissolved oxygen (mg/L) | Temperature (°C) | mg/L | | | | | | | | | | µg/L | | | | | | | | |
|---|---|---|---|---|---|---|---|---|---|---|---|---|---|---|---|---|---|---|---|---|---|---|
| | | | | Na | Ca | K | Mg | Cl | $SO_4$ | $NO_3$ | $NH_4$ | $PO_4$ | $HCO_3$ | Fe | Mn | Al | Zn | Cu | Pb | Cr | Ni | Cd |
| **Cu roof runoff** | 6.2 | 9.8 | 20.2 | 13.4 | 6.0 | 0.7 | 1.8 | 23.6 | <1 | 0.5 | 0.2 | 0.01 | 18 | 8.1 | 19.8 | 38.7 | 355 | 540 | <1 | <1 | 1.1 | <1 |
| | | | | - | - | - | - | | | | | | | *405* | *25.8* | *763* | *355* | *759* | *3.3* | *2.8* | *1.8* | *<1* |
| **Zn roof runoff** | 6.4 | 9.9 | 19.7 | 4.2 | 3.2 | 0.5 | 0.8 | 6.0 | 9.8 | 1.2 | 1.06 | 0.05 | 10 | 9.0 | 7.2 | 29.3 | 260 | 2.4 | <1 | <1 | <1 | <1 |
| | | | | - | - | - | - | | | | | | | *2870* | *46.3* | *4710* | *273* | *12.4* | *7.7* | *6.1* | *3.7* | *<1* |

# APPENDIX 2: FULL CHEMICAL SOLIDS DATASETS

**Table A2-1:** Wet chemical analysis results for the laboratory column, synthetic runoff, top of the column shell sample. "-" not measured.

| Sample | | | Element (mg/kg) | Fe | Mn | Al | Zn | Cu | Pb | Cr | Ni | Cd | Ca |
|---|---|---|---|---|---|---|---|---|---|---|---|---|---|
| **Laboratory column, synthetic roof runoff, top of column shell sample** | Acid digests | Full shell | Sub-sample 1 | 80.2 | 7.91 | 103 | 1200 | 71.6 | <3 | <0.5 | <1.3 | <0.3 | - |
| | | | Sub-sample 2 | 77.6 | 6.28 | 72.5 | 1640 | 101 | <3 | <0.5 | <1.3 | <0.3 | - |
| | | | Sub-sample 3 | 40.8 | 6.41 | 23.4 | 1520 | 74.2 | <3 | <0.5 | <1.3 | <0.3 | - |
| | | | *Mean* | *66.2* | *6.87* | *66.4* | *1450* | *82.4* | *<3* | *<0.5* | *<1.3* | *<0.3* | - |
| | | Organic layer only | Sub-sample 1 | 451 | 25.2 | 325 | 6370 | 913 | <3 | 0.56 | 0.72 | <0.3 | - |
| | SEP | | Water soluble | <1 | <1 | <1 | <10 | 2.2 | - | - | - | - | 333 |
| | | | Readily exchangeable | <0.4 | 3.7 | <1 | 14.2 | 4.8 | - | - | - | - | 2470 |
| | | | Bound to carbonates | 0.4 | 5.4 | <1 | 801 | 65.8 | - | - | - | - | 155000 |
| | | | Bound to Mn oxides | <0.4 | 0.4 | <1 | 4.8 | <0.6 | - | - | - | - | 6040 |
| | | | Bound to amorphous Fe oxides | 13.0 | 0.2 | 10.2 | 16.0 | 13.6 | - | - | - | - | 29.4 |
| | | | Bound to crystalline Fe oxides | 31.9 | 0.3 | 19.0 | 26.2 | 1.3 | - | - | - | - | 18.1 |
| | | | Bound to organics | 14.2 | 0.8 | 18.9 | 8.0 | <0.6 | - | - | - | - | 23300 |
| | Calculated | | Sum of all SEP fractions | 59.5 | 10.8 | 48.1 | 870 | 87.7 | - | - | - | - | 187000 |

**Table A2-2:** Wet chemical analysis results for the laboratory column, synthetic runoff, middle of the column shell sample.

| Sample | | | Element (mg/kg) | Fe | Mn | Al | Zn | Cu | Pb | Cr | Ni | Cd |
|---|---|---|---|---|---|---|---|---|---|---|---|---|
| **Laboratory column, synthetic runoff, middle of column shell sample** | Acid digests | Full shell | Sub-sample 1 | 37.0 | 5.0 | 25.1 | 1080 | 43.7 | <3 | <0.5 | <1.3 | <0.3 |
| | | | Sub-sample 2 | 75.7 | 16.2 | 78.3 | 1340 | 41.2 | <3 | <0.5 | <1.3 | <0.3 |
| | | | Sub-sample 3 | 120 | 10.7 | 104 | 995 | 41.5 | <3 | <0.5 | <1.3 | <0.3 |
| | | | *Mean* | *77.7* | *10.6* | *69.2* | *1140* | *42.1* | *<3* | *<0.5* | *<1.3* | *<0.3* |

**Table A2-3:** Wet chemical analysis results for the laboratory column, real runoff, middle of the column shell sample.

| Sample | | | Element (mg/kg) | Fe | Mn | Al | Zn | Cu | Pb | Cr | Ni | Cd |
|---|---|---|---|---|---|---|---|---|---|---|---|---|
| **Laboratory column, real runoff, middle of column shell sample** | Acid digests | Full shell | Sub-sample 1 | 91.1 | 8.0 | 89.4 | 3.7 | 4.3 | <3 | <0.5 | <1.3 | <0.3 |
| | | | Sub-sample 2 | 9.8 | 5.6 | 8.6 | 23.5 | <0.6 | <3 | <0.5 | <1.3 | <0.3 |
| | | | Sub-sample 3 | 25.1 | 3.7 | 25.2 | 33.6 | <0.6 | <3 | <0.5 | <1.3 | <0.3 |
| | | | *Mean* | *42.0* | *5.8* | *41.1* | *20.3* | *1.4* | *<3* | *<0.5* | *<1.3* | *<0.3* |

**Table A2-4:** Wet chemical analysis results for the laboratory column, synthetic runoff, bottom of the column shell sample. "-" not measured.

| Sample | | | Element (mg/kg) | Fe | Mn | Al | Zn | Cu | Pb | Cr | Ni | Cd | Ca |
|---|---|---|---|---|---|---|---|---|---|---|---|---|---|
| **Laboratory column, synthetic runoff, bottom of column shell sample** | Acid digests | Full shell | Sub-sample 1 | 246 | 10.4 | 252 | 807 | 16.9 | <3 | <0.5 | <1.3 | <0.3 | - |
| | | | Sub-sample 2 | 331 | 13.7 | 315 | 972 | 19.4 | <3 | <0.5 | <1.3 | <0.3 | - |
| | | | Sub-sample 3 | 23.4 | 5.0 | 15.8 | 653 | 10.1 | <3 | <0.5 | <1.3 | <0.3 | - |
| | | | *Mean* | *200* | *9.7* | *194* | *810* | *15.5* | *<3* | *<0.5* | *<1.3* | *<0.3* | - |
| | SEP | | Water soluble | <1 | <1 | <1 | <10 | <1 | - | - | - | - | 281 |
| | | | Readily exchangeable | <0.4 | 3.5 | <1 | 6.3 | 1.6 | - | - | - | - | 2500 |
| | | | Bound to carbonates | 1.5 | 8.9 | 3.2 | 504 | 10.1 | - | - | - | - | 161000 |
| | | | Bound to Mn oxides | <0.4 | 2.7 | <1 | 3.5 | <0.6 | - | - | - | - | 6410 |
| | | | Bound to amorphous Fe oxides | 69.0 | 1.5 | 33.3 | 19.2 | 4.0 | - | - | - | - | 32.1 |
| | | | Bound to crystalline Fe oxides | 492 | 3.1 | 194 | 24.8 | 0.8 | - | - | - | - | 22.2 |
| | | | Bound to organics | 149 | 5.2 | 152 | 9.5 | 0.6 | - | - | - | - | 25900 |
| | Calculated | | Sum of all SEP fractions | 712 | 24.9 | 383 | 567 | 17.1 | - | - | - | - | 197000 |

**Table A2-5:** Wet chemical analysis results for the laboratory column, real runoff, top of the column shell sample. "-" not measured.

| Sample | | | Element (mg/kg) | Fe | Mn | Al | Zn | Cu | Pb | Cr | Ni | Cd | Ca |
|---|---|---|---|---|---|---|---|---|---|---|---|---|---|
| **Laboratory column, real runoff, top of column shell sample** | Acid digests | Full shell | Sub-sample 1 | 81.9 | 9.4 | 78.9 | 59.6 | 1.3 | <3 | <0.5 | <1.3 | <0.3 | - |
| | | | Sub-sample 2 | 30.3 | 11.9 | 35.3 | 84.8 | 0.8 | <3 | <0.5 | <1.3 | <0.3 | - |
| | | | *Mean* | *56.1* | *10.7* | *57.1* | *72.2* | *1.1* | *<3* | *<0.5* | *<1.3* | *<0.3* | - |
| | | Organic layer only | Sub-sample 1 | 381 | 31.8 | 371 | 575 | 18.8 | <3 | 0.8 | 4.1 | <0.3 | - |
| | | | Sub-sample 2 | 463 | 33.6 | 406 | 678 | 19.9 | <3 | 0.9 | 4.9 | <0.3 | - |
| | | | *Mean* | *422* | *32.7* | *388* | *626* | *19.3* | *<3* | *0.8* | *4.5* | *<0.3* | - |
| | SEP | | Water soluble | <1 | <1 | <1 | <10 | <1 | - | - | - | - | 261 |
| | | | Readily exchangeable | <0.4 | 3.4 | <1 | 0.8 | <0.6 | - | - | - | - | 2530 |
| | | | Bound to carbonates | <0.4 | 5.5 | <1 | 50.4 | <0.6 | - | - | - | - | 150000 |
| | | | Bound to Mn oxides | <0.4 | 0.4 | <1 | 0.5 | <0.6 | - | - | - | - | 6470 |
| | | | Bound to amorphous Fe oxides | 7.4 | 0.1 | 4.3 | 2.9 | 0.6 | - | - | - | - | 27.6 |
| | | | Bound to crystalline Fe oxides | 13.1 | 0.2 | 7.5 | 4.3 | <0.6 | - | - | - | - | 17.2 |
| | | | Bound to organics | 4.2 | 0.9 | 6.3 | 1.8 | <0.6 | - | - | - | - | 36000 |
| | Calculated | | Sum of all SEP fractions | 24.7 | 10.5 | 18.1 | 60.7 | 0.6 | - | - | - | - | 196000 |

**Table A2-6:** Wet chemical analysis results for the laboratory column, real runoff, bottom of the column shell sample. "-" not measured.

| Sample | | | Element (mg/kg) | Fe | Mn | Al | Zn | Cu | Pb | Cr | Ni | Cd | Ca |
|---|---|---|---|---|---|---|---|---|---|---|---|---|---|
| **Laboratory column, real runoff, bottom of column shell sample** | Acid digests | Full shell | Sub-sample 1 | 54.9 | 7.3 | 61.4 | 2.3 | 0.6 | <3 | <0.5 | <1.3 | <0.3 | - |
| | | | Sub-sample 2 | 139 | 8.0 | 146 | 32.8 | 1.4 | <3 | <0.5 | <1.3 | <0.3 | - |
| | | | *Mean* | *96.9* | *7.7* | *104* | *17.7* | *1.0* | *<3* | *<0.5* | *<1.3* | *<0.3* | - |
| | SEP | | Water soluble | <1 | <1 | <1 | <10 | <1 | - | - | - | - | 318 |
| | | | Readily exchangeable | <0.4 | 2.8 | <1 | <0.3 | <0.6 | - | - | - | - | 2630 |
| | | | Bound to carbonates | <0.4 | 8.3 | 1.3 | 9.9 | <0.6 | - | - | - | - | 160000 |
| | | | Bound to Mn oxides | <0.4 | 1.8 | <1 | <0.3 | <0.6 | - | - | - | - | 6940 |
| | | | Bound to amorphous Fe oxides | 29.9 | 0.8 | 34.9 | 2.3 | <0.6 | - | - | - | - | 26.8 |
| | | | Bound to crystalline Fe oxides | 214 | 1.5 | 104 | 2.9 | <0.6 | - | - | - | - | 14.1 |
| | | | Bound to organics | 65.1 | 3.5 | 88.3 | 1.1 | <0.6 | - | - | - | - | 29100 |
| | Calculated | | Sum of all SEP fractions | 309 | 18.7 | 229 | 16.2 | <1 | - | - | - | - | 199000 |

**Table A2-7:** Wet chemical analysis results for the field column, copper roof runoff, top of the column shell sample. "-" not measured.

| Sample | | | Element (mg/kg) | Fe | Mn | Al | Zn | Cu | Pb | Cr | Ni | Cd | Ca |
|---|---|---|---|---|---|---|---|---|---|---|---|---|---|
| **Field column, copper roof runoff, top of column shell sample** | Acid digests | Full shell | Sub-sample 1 | 338 | 13.2 | 87.8 | 246 | 1160 | 6.1 | 1.0 | <1.3 | <0.3 | - |
| | | | Sub-sample 2 | 59.4 | 7.9 | <1 | 139 | 791 | <3 | 1.2 | <1.3 | <0.3 | - |
| | | | Sub-sample 3 | 91.9 | 9.0 | 21.3 | 114 | 681 | <3 | <0.5 | <1.3 | <0.3 | - |
| | | | *Mean* | *163* | *10.0* | *54.5* | *166* | *876* | *6.1* | *1.1* | *<1.3* | *<0.3* | - |
| | SEP | | Water soluble | <1 | <1 | 1.1 | <10 | 4.7 | - | - | - | - | 289 |
| | | | Readily exchangeable | <0.4 | 3.7 | <1 | 0.8 | 11.5 | - | - | - | - | 2220 |
| | | | Bound to carbonates | <0.4 | 4.7 | <1 | 52.6 | 439 | - | - | - | - | 155000 |
| | | | Bound to Mn oxides | <0.4 | 0.2 | <1 | 0.4 | 1.5 | - | - | - | - | 5860 |
| | | | Bound to amorphous Fe oxides | 6.1 | 0.1 | 3.0 | 1.4 | 45.8 | - | - | - | - | 20.9 |
| | | | Bound to crystalline Fe oxides | 4.8 | 0.2 | 2.2 | 6.1 | 12.2 | - | - | - | - | 21.5 |
| | | | Bound to organics | 1.2 | 0.6 | 2.0 | 2.6 | 2.1 | - | - | - | - | 26700 |
| | Calculated | | Sum of all SEP fractions | 12.1 | 9.5 | 8.3 | 63.9 | 517 | - | - | - | - | 190000 |

**Table A2-8:** Wet chemical analysis results for the field column, zinc roof runoff, top of the column shell sample. "-" not measured.

| Sample | | | Element (mg/kg) | Fe | Mn | Al | Zn | Cu | Pb | Cr | Ni | Cd | Ca |
|---|---|---|---|---|---|---|---|---|---|---|---|---|---|
| **Field column, zinc roof runoff, top of column shell sample** | Acid digests | Full shell | Sub-sample 1 | 19.0 | 9.0 | 20.7 | 68.4 | 1.7 | <3 | <0.5 | <1.3 | <0.3 | - |
| | | | Sub-sample 2 | 15.2 | 5.5 | 15.7 | 102 | 1.3 | <3 | <0.5 | <1.3 | <0.3 | - |
| | | | Sub-sample 3 | 9.5 | 10.4 | 17.5 | 111 | 1.7 | <3 | <0.5 | <1.3 | <0.3 | - |
| | | | *Mean* | *14.5* | *8.3* | *17.9* | *93.7* | *1.6* | *<3* | *<0.5* | *<1.3* | *<0.3* | - |
| | | Organic layer only | Sub-sample 1 | 1330 | 56.9 | 871 | 537 | 24.3 | 5.0 | 2.2 | 3.7 | 0.7 | - |
| | | | Sub-sample 2 | 780 | 46.2 | 498 | 468 | 19.7 | 3.6 | 1.4 | 3.1 | <0.3 | - |
| | | | Sub-sample 3 | 1260 | 52.5 | 768 | 521 | 24.9 | 4.7 | 1.9 | 3.4 | 0.4 | - |
| | | | *Mean* | *1130* | *51.9* | *712* | *509* | *23.0* | *4.4* | *1.8* | *3.4* | *0.4* | - |
| | SEP | Water soluble | | <1 | <1 | 1.9 | <10 | <1 | - | - | - | - | 234 |
| | | Readily exchangeable | | <0.4 | 3.4 | <1 | 0.6 | <0.6 | - | - | - | - | 2660 |
| | | Bound to carbonates | | <0.4 | 7.0 | 1.4 | 55.1 | <0.6 | - | - | - | - | 163000 |
| | | Bound to Mn oxides | | <0.4 | 0.8 | <1 | 0.5 | <0.6 | - | - | - | - | 4410 |
| | | Bound to amorphous Fe oxides | | 22.1 | 0.3 | 12.1 | 5.0 | 0.8 | - | - | - | - | 24.1 |
| | | Bound to crystalline Fe oxides | | 31.0 | 0.4 | 13.8 | 8.7 | <0.6 | - | - | - | - | 20.6 |
| | | Bound to organics | | 8.2 | 0.9 | 10.5 | 2.7 | <0.6 | - | - | - | - | 33100 |
| | Calculated | Sum of all SEP fractions | | 61.3 | 12.8 | 39.7 | 72.6 | 0.8 | - | - | - | - | 203000 |

# APPENDIX 3: COMMONLY OVERSATURATED MINERALS

**Table A3-1:** Fe, Mn, Al, P and Ca minerals that were commonly oversaturated, or very close to oversaturated, in the solution chemistries modelled in PHREEQC.

| **Fe minerals** | | **Mn minerals** | | **Al minerals** | | **P minerals** | | **Ca minerals** | |
|---|---|---|---|---|---|---|---|---|---|
| Hematite | $Fe_2O_3$ | Pyrolusite | $MnO_2$ | Diaspore | AlOOH | Hydroxylapatite | $Ca_5(PO_4)_3OH$ | Calcite | $CaCO_3$ |
| Maghemite | $Fe_2O_3$ | Nsutite | $MnO_2$ | Boehmite | AlOOH | | | Aragonite | $CaCO_3$ |
| Magnetite | $Fe_3O_4$ | Birnessite | $MnO_2$ | Gibbsite | $Al(OH)_3$ | | | | |
| Magnesioferrite | $Fe_2MgO_4$ | Bixbyite | $Mn_2O_3$ | | | | | | |
| *(no name)* | $Fe(OH)_{2.7}Cl_3$ | Manganite | MnOOH | | | | | | |
| Goethite | FeOOH | | | | | | | | |
| Lepidocrocite | FeOOH | | | | | | | | |
| Ferrihydrite | $Fe(OH)_3$ | | | | | | | | |